

RESEARCH INVESTIGATION RI97-021

## **PRECAST I-GIRDER CRACKING: CAUSES AND DESIGN DETAILS**

PREPARED FOR THE  
MISSOURI DEPARTMENT OF TRANSPORTATION

IN COOPERATION WITH THE  
U.S. DEPARTMENT OF TRANSPORTATION  
FEDERAL HIGHWAY ADMINISTRATION

Written By:

***University of Missouri-Rolla***

John J. Myers, Associate Professor  
Antonio Nanni, V. & M. Jones Professor  
Danielle Stone, M.S. Candidate

***University of Missouri – Columbia***

Vellore Gopalaratnam, Professor  
T. Patrick Earney, M.S. Candidate

CENTER FOR INFRASTRUCTURE ENGINEERING STUDIES  
UNIVERSITY OF MISSOURI-ROLLA

Submitted  
June 2001

The opinions, findings and conclusions expressed in this report are those of the principle investigators and the Missouri Department of Transportation. They are not necessarily those of the U.S. Department of Transportation, Federal Highway Administration. This report does not constitute a standard, specification or regulation.

### **Acknowledgements**

The researchers at the University of Missouri-Columbia and the University of Missouri-Rolla would like to express their appreciation to the Missouri Department of Transportation (MoDOT), the University Transportation Center (UTC) at the University of Missouri - Rolla, and the University of Missouri Research Board for funding this research project. The authors would also like to acknowledge Chris Criswell, Jeffery Ger, and Shyam Gupta of the MoDOT Bridge Division, Patricia Brake-Lemongelli of the MoDOT Research, Development, and Technology Division and Roger Schwartze of the MoDOT Maintenance Division for their

active interest and contributions to the discussions about the project. We would also like to thank Gale Barnhill at Nebraska DOR, Fred Conway at Alabama DOT, and Richard Miller at University of Cincinnati for the information that they have provided.

## **EXECutive summary**

This project was a collaborative effort of the University of Missouri – Columbia (UMC) and University of Missouri – Rolla (UMR) researchers in close connection with MoDOT RDT, Bridge, and Bridge Maintenance Divisions, and MoDOT District 9. Outlined herein are the objectives and conclusions of the research performed to determine the causes of cracking in continuous prestressed concrete I-girder bridges.

Three research tasks were undertaken by UMC. They were (1) to study early-age cracking due to heat of hydration, steam curing, and restraint provided by the form, (2) to study diaphragm detailing with respect to continuity provided and resultant implications, and (3) to study the potential for diagonal tension cracking due to shear stresses.

Early-age cracking at girder-ends was studied in Task 1 using a combination of analytical and numerical models. An analytical model developed earlier for calculation of girder-end tensile stress during prestress transfer was modified in light of experimental observations from a companion project dealing with monitoring of early-age strains. A finite element model of the girder cross-section for three types of MoDOT girders (Types II, III and VI) was developed to analyze distribution of residual stress due to early-age differential thermal loading caused by steam curing and hydration. It was concluded that the combined effect of residual stresses due to differential thermal loading at early-age and tensile stress at girder-ends due to prestress transfer is adequate to cause the horizontal web cracks and diagonal cracks in the reverse shear direction observed in the vicinity of the bottom and top flanges, respectively.

The effects of continuity provided at the diaphragms on cracking of the girder-ends and diaphragms were studied as a part of Task II. Vertical cracks in the girders near the end, spalling of diaphragms and girders pulling out of diaphragms were attributed to service temperature loading and continuity detailing used. Design detailing at the bents used by a few other states were reviewed in light of the problems encountered in Missouri with a view to offer several alternate designs for consideration.

Diagonal tension stresses were computed in Task III using uncracked elastic analysis. It was observed that when combined with residual tensile stresses due to early-age differential thermal loading and restraints provided by forms, the diagonal tensile stress might be adequate to cause girder-end cracking. However using ultimate analysis it was shown that the shear reinforcement provided in the MoDOT design is more than adequate to ensure that these cracks do not precipitate a catastrophic shear failure.

Four research tasks were undertaken by UMR. They were (1) to develop, statistically analyze, and draw conclusions regarding the causes of cracking from a database of bridge information, (2) to monitor temperature and temperature-induced movements at two existing bridges, (3) to determine the magnitude and distribution of thermal stress that could be expected in Missouri bridges, and (4) to propose a design modification to prevent this type of cracking in future construction.

For Task I, a database of bridge information was compiled and analyzed to determine potential causes of cracking. The database contained 150 cracked and uncracked bridges and extensive information regarding the location, geometry, and construction

of the bridges. A model was developed that has the ability to predict the cracked status of a bridge with 77% accuracy, based on certain bridge parameters.

In Task II, two existing bridges, one cracked and one uncracked, were monitored to determine accurate temperature profiles and the magnitude of thermal deflections experienced by these typical bridges. The AASHTO recommended thermal gradients were compared to the measured thermal gradients and were found to be in good agreement.

For Task III, a finite element analysis (FEA), using a commercially available FEA software package, and a numerical analysis using elastic theory, were performed on typical bridge cross sections. The numerical analysis was used to perform a parametric study to determine the magnitude and distribution of stresses that can be induced by the AASHTO positive and negative thermal gradients. The thermal stresses ranged from 500 psi (3.44 MPa) in tension to 1000 psi (6.89 MPa) in compression, which are on the order of 0.3 to 1.3 times the stress due to dead load, live load and prestressing.

Ultimately, the objective of this study was to effectively eliminate this type of cracking in the prestressed concrete I-girders. Therefore, in conjunction with Task IV, UMR has recommended to MoDOT that thermal stress calculations be incorporated into the current design procedure for prestressed concrete I-girder bridges. A design example was conducted to illustrate the incorporation of the thermal stresses into the design process and a number of design detail modifications were suggested.

## Table of contents

<b>LIST OF FIGURES .....</b>	<b>viii</b>
<b>LIST OF TABLES .....</b>	<b>xiii</b>
<b>LIST OF SYMBOLS .....</b>	<b>xv</b>
<b>1 INTRODUCTION .....</b>	<b>1</b>
1.1 PROJECT OVERVIEW .....	1
1.2 BACKGROUND INFORMATION .....	1
1.3 OBJECTIVE .....	4
1.4 PREVIOUS RESEARCH .....	4
<b>2 TECHNICAL APPROACH .....</b>	<b>11</b>
<b>3 COMPLETION OF THE DATABASE.....</b>	<b>12</b>
3.1 PRELIMINARY DATABASE.....	12
3.2 DEVELOPMENT OF THE REVISED DATABASE.....	17
3.3 STATISTICAL ANALYSIS OF THE REVISED DATABASE.....	19
3.3.1 <i>Multiple Linear Regression Analysis.</i> .....	19
3.3.2 <i>Logistic Regression Analysis.</i> .....	21
3.4 RESULTS OF THE STATISTICAL ANALYSIS .....	22
<b>4 DIAGONAL TENSION .....</b>	<b>32</b>
4.1 VERIFICATION OF SHEAR FORCE AND MOMENT ENVELOPES .....	32
4.1.1 <i>Analysis Method for Continuous Bridges.</i> .....	32
4.1.2 <i>AASHTO Loading.</i> .....	32
4.2 CALCULATION OF SHEAR STRESSES IN UNCRACKED, ELASTIC GIRDER .....	34
4.2.1 <i>Analysis Method.</i> .....	34
4.2.2 <i>Results.</i> .....	35
4.3 COMPARISON OF REQUIRED VERTICAL REINFORCEMENT .....	35
4.3.1 <i>AASHTO Method.</i> .....	35
4.3.2 <i>ACI Method.</i> .....	37
<b>5 EARLY-AGE CRACKING .....</b>	<b>38</b>
5.1 STRESSES DUE TO PRESTRESS TRANSFER.....	38

5.1.1	<i>Gergely - Sozen Model.</i>	38
5.1.2	<i>Modified Gergely - Sozen Model.</i>	38
5.2	RESIDUAL STRESSES FROM FINITE ELEMENT ANALYSIS OF EARLY-AGE BEHAVIOR	41
5.2.1	<i>Model Properties</i>	42
5.2.1.1	Elements.	42
5.2.1.2	Model Geometry and Meshing.	42
5.2.1.3	Boundary Conditions and Loads.	43
5.2.1.4	Loading Procedure	46
5.2.2	<i>Material Properties</i>	47
5.2.3	<i>Stress Profiles</i>	47
5.2.3.1	High Performance Concrete	48
5.2.3.2	Normal Strength Concrete	48
5.2.4	<i>Design Implications</i>	53
<b>6</b>	<b>DIAPHRAGM DETAILING</b>	<b>54</b>
6.1	OVERVIEW OF CURRENT PRACTICE	54
6.2	STRAINS DUE TO SERVICE TEMPERATURES (THERMAL GRADIENTS)	54
6.2.1	<i>Missouri's HPC Bridge and the Influence of Service Temperatures</i>	54
6.2.2	<i>Alabama DOT's Experience with Thermal Gradients</i>	57
6.3	DESIGN DETAILS FROM OTHER DOT'S AND POTENTIAL PERFORMANCE IMPLICATIONS	58
6.3.1	<i>Alabama</i>	58
6.3.2	<i>Nebraska</i>	58
6.3.3	<i>Illinois</i>	60
6.3.4	<i>Florida and Georgia</i>	61
6.3.5	<i>Other Experience</i>	62
<b>7</b>	<b>BRIDGE MEASUREMENTS</b>	<b>64</b>
7.1	BRIDGES A4565 AND A5736	64
7.2	MEASUREMENT METHODS	64
7.3	RESULTS	65
7.4	DISCUSSION OF RESULTS	70

<b>8</b>	<b>THERMAL STRESS CALCULATION</b>	<b>71</b>
8.1	BASIC THEORY OF THERMAL STRESSES	71
8.2	SIMPLIFIED/VERIFICATION ANALYSES	72
8.3	PARAMETRIC STUDY	79
8.3.1	<i>Effective Flange Width</i>	79
8.3.2	<i>Study Parameters</i>	80
8.3.3	<i>Results and Discussion</i>	86
8.3.4	<i>Sensitivity</i>	93
8.4	SIMPLIFIED MATHEMATICAL APPROACH	95
8.5	DISCUSSION OF RESULTS	97
<b>9</b>	<b>CONCLUSIONS</b>	<b>99</b>
9.1	DATABASE ANALYSIS	99
9.2	EARLY-AGE BEHAVIOR OF PRESTRESSED CONCRETE GIRDERS	99
9.3	DIAPHRAGM DETAILING	99
9.4	DIAGONAL SHEAR CRACKING	100
9.5	BRIDGE MEASUREMENTS	100
9.6	THERMAL STRESS ANALYSES	101
<b>10</b>	<b>RECOMMENDATIONS</b>	<b>102</b>
10.1	DESIGN IMPLEMENTATION RECOMMENDATIONS	102
10.1.1	<i>Thermal Stresses in Design</i>	102
10.1.2	<i>Alternate Support Details</i>	102
10.1.3	<i>Early-age Stresses</i>	104
10.1.4	<i>Diagonal Shear Cracking</i>	104
10.1.5	<i>Repair of the Girders</i>	105
10.2	RECOMMENDATIONS FOR FUTURE RESEARCH	106
	<b>REFERENCES</b>	<b>107</b>
	<b>APPENDIX A</b>	<b>111</b>
	<b>APPENDIX B</b>	<b>115</b>
	<b>APPENDIX C</b>	<b>130</b>
	<b>APPENDIX D</b>	<b>134</b>

**APPENDIX E .....139**

**APPENDIX F .....148**

**APPENDIX G .....153**

**APPENDIX H .....158**

**APPENDIX I .....161**

    I.1 BACKGROUND..... 162

    I.2 DESIGN EXAMPLE CALCULATIONS..... 163

    I.3 DISCUSSION OF RESULTS ..... 168

**APPENDIX J .....171**

### list of figures

Figure 1.1 Vertical Crack in the Girder-end at the Diaphragm. ....	3
Figure 1.2 Cracking in the Diaphragm Also Indicates Pull-Out/Push-In Type of Loading of the Girders under Service Conditions. ....	3
Figure 1.3 Shear Cracking Due To Diagonal Tension and Vertical Cracking in a Prestressed Girder.	4
Figure 1.4 Web Cracking in the “Reverse Shear Direction” .....	4
Figure 1.5 Typical Failure of the Continuity Connection.....	7
Figure 1.6 Plan View of the Same Typical Failure .....	7
Figure 1.7 AASHTO Recommended Thermal Gradients (1989).....	11
Figure 1.8 Gergely-Sozen Model .....	12
Figure 3.1 Percentage of Girder Ends Cracked vs. Girder Spacing .....	25
Figure 3.2 Contour Plot for Chert Aggregate and Non-interstate Highways .....	33
Figure 3.3 Contour Plot for Chert Aggregate and Interstate Highways .....	33
Figure 3.4 Contour Plot for Non-chert Aggregate and Non-interstate Highways .....	34
Figure 3.5 Contour Plot for Non-chert Aggregate and Interstate Highways .....	34
Figure 4.1 AASHTO HS-20 Modified Live Loads and Load Configurations. ....	38
Figure 4.2 Comparison of Moment Envelopes from BR200 and CEMU .....	38
Figure 4.3 Comparison of Shear Force Envelopes from BR200 and CEMU.....	39
Figure 4.4 Element at Girder Centroid and Mohr’s Circle Characterization of This Stress State	40
Figure 4.5 Area of Stirrup Reinforcement Required per 12” Length According to ACI, AASHTO and BR200 Guidelines. ....	42
Figure 5.1 Gergely - Sozen Model for Determining Girder-End Vertical Stress Due to Prestress Transfer	44
Figure 5.2 Modified Gergely - Sozen Model.....	45
Figure 5.3 Location of Strain Gages on Stirrups in the HPC Girders. ....	46
Figure 5.4 Assumed Stress Distribution from Unbalanced Moment.....	46
Figure 5.5 Dimensions of MoDOT Girder Types Used in the Finite Element Models.....	49
Figure 5.6 Finite Element Mesh and Boundary Conditions for Girder Models .....	49
Figure 5.7 Maximum Difference in Temperatures at a Cross-section.....	50
Figure 5.8 Heat Development (Top) And Maximum Difference in Temperatures at a Cross-section for Normal Strength Girders .....	51
Figure 5.9 Residual Stress Profile for HPC Type II Girder (psi) .....	55

Figure 5.10 Residual Stress Profile for NSC Type II Girder (psi) .....	55
Figure 5.11 Residual Stress Profile for HPC Type III Girder (psi) .....	56
Figure 5.12 Residual Stress Profile for NSC Type III Girder (psi) .....	56
Figure 5.13 Residual Stress Profile for HPC Type VI Girder (psi) .....	57
Figure 5.14 Residual Stress Profile for NSC Type VI Girder (psi) .....	57
Figure 6.1 Daily Temperature Variations at Various Locations in the Girder and The Diaphragm During a 3-Day Cooling Period in Spring.....	62
Figure 6.2 Variations in Girder Strains During the Period Corresponding to Figure 6.1..	62
Figure 6.3 Strains Due To Service Temperatures during Period of Increasing Temperature in Spring 64	
Figure 6.4 Strains Due To Service Temperatures during Period of Decreased Temperature in Fall	64
Figure 6.5 Diaphragm Detailing Used by Nebraska Department Of Roads.....	67
Figure 6.6 Diaphragm Detailing Used by Illinois Department Of Transportation.....	69
Figure 7.1 Example Layout of Girder Temperature Measurements .....	73
Figure 7.2 Typical Layout of Bridge Survey Points .....	73
Figure 7.3 Maximum and Minimum Temperature Profiles, Bridge A4565 .....	75
Figure 7.4 Maximum and Minimum Temperature Profiles, Bridge A5736 .....	75
Figure 7.5 Comparison of AASHTO Positive and Bridge A4565 Gradients .....	76
Figure 7.6 Comparison of AASHTO Positive and Bridge A5736 Gradients .....	77
Figure 7.7 Thermal Deflections, Bridge A4565 .....	78
Figure 7.8 Thermal Deflections, Bridge A5736 .....	79
Figure 8.1 Cross Section and Side View of Rectangular Member .....	82
Figure 8.2 Thermal Stresses of an Unrestrained Member .....	83
Figure 8.3 Cross Section Dimensions of the Simplified Sections .....	84
Figure 8.4 AASHTO Gradients, as Applied to the Square Cross Section.....	86
Figure 8.5 Element Configuration #1 .....	87
Figure 8.6 Element Configuration #2 .....	87
Figure 8.7 Thermal Stresses Induced by the AASHTO Positive Gradient, on a Simplified Square Cross Section at Midspan.....	88
Figure 8.8 Thermal Stresses Induced by the AASHTO Negative Gradient, on a Simplified Square Cross Section at Midspan.....	89
Figure 8.9 Linear and Non-linear Thermal Gradients .....	90
Figure 8.10 Thermal Stresses for Linear and Non-linear Thermal Gradients, as Applied to an Unrestrained Member .....	91

Figure 8.11 Effective Flange Width Detail.....	92
Figure 8.12 Cross Section of Girder Type II .....	95
Figure 8.13 Cross Section of Girder Type III.....	95
Figure 8.14 Cross Section of Girder Type IV.....	95
Figure 8.15 Cross Section of Girder Type VI.....	96
Figure 8.16 Cross Section of Girder Type VII.....	96
Figure 8.17 Thermal Stresses – Fully Restrained – Positive Gradient .....	100
Figure 8.18 Thermal Stresses – Fully Restrained – Negative Gradient .....	100
Figure 8.19 Thermal Stresses – Positive Gradient –Girder Type II.....	101
Figure 8.20 Thermal Stresses – Negative Gradient –Girder Type II.....	101
Figure 8.21 Thermal Stresses – Unrestrained – Positive Gradient.....	102
Figure 8.22 Thermal Stresses – Unrestrained – Negative Gradient .....	103
Figure 8.23 Thermal Stresses –Girder Type II .....	103
Figure 8.24 Thermal Stresses – Girder Type III.....	104
Figure 8.25 Thermal Stresses – Girder Type IV.....	104
Figure 8.26 Thermal Stresses – Girder Type VI.....	105
Figure 8.27 Thermal Stresses – Girder Type VII.....	105
Figure 8.28 Sensitivity of Thermal Stresses – Positive Gradient .....	107
Figure 8.29 Sensitivity of Thermal Stresses – Negative Gradient.....	108
Figure 8.30 Comparison of Results for the Positive Gradient .....	110
Figure 8.31 Comparison of Results for the Negative Gradient .....	110
Figure 10.1 Simple Span Girders with Continuous Deck.....	119
Figure 10.2 Joint Placement to Isolate Girder Continuity.....	119
Figure 10.3 Anchorage Region.....	121
Figure 10.4 Schematic of the Anchorage System.....	122
Figure B.1 Histogram of Precast Company.....	135
Figure B.2 Histogram of Plant Location.....	135
Figure B.3 Histogram of Bridge Length.....	135
Figure B.4 Histogram of Average Daily Traffic .....	136
Figure B.5 Histogram of Number of Spans .....	136
Figure B.6 Histogram of Width of Diaphragm.....	136
Figure B.7 Histogram of Column Height .....	137

Figure B.8 Histogram of District .....	137
Figure B.9 Histogram of Skew .....	137
Figure B.10 Histogram of Girder Length.....	138
Figure B.11 Histogram of Girder Spacing.....	138
Figure B.12 Histogram of Girder Height.....	138
Figure B.13 Histogram of Bottom Flange Width.....	139
Figure B.14 Histogram of Top Flange Width.....	139
Figure B.15 Histogram of Bottom Flange Height .....	139
Figure B.16 Histogram of Top Flange Height .....	140
Figure B.17 Histogram of Web Height.....	140
Figure B.18 Histogram of Web Width.....	140
Figure B.19 Histogram of Girder Type .....	141
Figure B.20 Histogram of Girder Area.....	141
Figure B.21 Histogram of Number of Tendons .....	141
Figure B.22 Histogram of Number of Straight Tendons .....	142
Figure B.23 Histogram of Number of Draped Tendons .....	142
Figure B.24 Histogram of Shear Reinforcement End Space .....	142
Figure B.25 Histogram of Shear Spacing – 1st Section .....	143
Figure B.26 Histogram of Shear Spacing – 2nd Section.....	143
Figure B.27 Histogram of Shear Spacing – 3rd Section.....	143
Figure B.28 Histogram of Number of Girder Ends Cracked .....	144
Figure B.29 Histogram of Percentage of Girder Ends Cracked .....	144
Figure B.30 Histogram of Distance Traveled.....	144
Figure B.31 Histogram of Field Construction Year .....	145
Figure B.32 Histogram of Field Construction Season.....	145
Figure B.33 Histogram of Cement Source .....	145
Figure B.34 Histogram of Coarse Aggregate Source .....	146
Figure B.35 Histogram of Fine Aggregate Source .....	146
Figure B.36 Histogram of Age at Release .....	146
Figure B.37 Histogram of Strength at Release .....	147
Figure B.38 Histogram of Curing Strength.....	147
Figure B.39 Histogram of Curing Time .....	147

Figure B.40 Histogram of Minimum Curing Temperature .....	148
Figure B.41 Histogram of Maximum Curing Temperature .....	148
Figure B.42 Histogram of Deck Panel Thickness .....	148
Figure E.1 Generic Boxplot.....	162
Figure E.2 Boxplots of Span Length, by Girder Type, for the Cracked Bridges .....	163
Figure E.3 Boxplots of Span Length, by Girder Type, for the Uncracked Bridges .....	163
Figure E.4 Bridges by Girder Type, as a Function of Cracked Status .....	164
Figure E.5 Cracked Bridges by Girder Type, as a Function of Number of Spans .....	165
Figure E.6 Uncracked Bridges by Girder Type, as a Function of Number of Spans .....	166
Figure E.7 Cracked Bridges by Girder Type, as a Function of Route Type.....	166
Figure E.8 Uncracked Bridges by Girder Type, as a Function of Route Type.....	167
Figure E.9 Cracked Bridges by Girder Type, as a Function of Span Length.....	168
Figure E.10 Uncracked Bridges by Girder Type, as a Function of Span Length.....	168
Figure I.1 Type III Girder Cross Section and Strand Arrangement .....	184
Figure I.2 Stresses Due to Dead Load, Live Load and Prestressing.....	186
Figure I.3 Stresses Due to Loading and Positive Thermal Gradient, Fully Restrained ...	189
Figure I.4 Stresses Due to Loading and Positive Thermal Gradient, Unrestrained.....	189
Figure I.5 Stresses Due to Loading and Negative Thermal Gradient, Fully Restrained .	190
Figure I.6 Stresses Due to Loading and Negative Thermal Gradient, Unrestrained .....	190
Figure J.1 Extensometer EFPI Strain Gage .....	195
Figure J.2 Close-up of the Fiber Optic Gage .....	196
Figure J.3 Test Setup .....	197
Figure J.4 Crack Opening Versus Time .....	198

### list of tableS

Table 3.1 Variables Included in the Preliminary Database .....	16
Table 3.2 Summary of F-test Results .....	19
Table 3.3 Variables Included in the Revised Database .....	21
Table 3.4 Results of the Validation Using $P = 0.50$ .....	28
Table 3.5 Properties of the Cracked Girders in the Verification Sample .....	29
Table 3.6 Properties of the Uncracked Bridges in the Verification Sample.....	30
Table 3.7 Results of the Validation Using $P=0.15$ .....	31
Table 3.8 Equations Based on Possible Variable Combinations .....	32
Table 3.9 Summary of Selected Probability Values .....	35
Table 4.1 Diagonal Tension ( $\sigma_1$ ) and Inclination of Principal Direction ( $\theta$ ) for the Interior Girders at Critical Shear Locations.....	41
Table 5.1 Experimental Determination of “Zero-Strain” Location from Stirrup Strain Data	45
Table 5.2 Maximum Tensile Stress and Location Due To Prestress Transfer Using the Gergely - Sozen Model (1967).....	47
Table 5.3 Applied Temperature Drop Used in the Finite Elements Analysis of Early-Age Behavior of Prestressed Concrete I-Girders.....	52
Table 5.4 Material Properties Used in Finite Element Analysis .....	53
Table 5.5 Residual Stress Distribution for Type II Girders .....	54
Table 5.6 Residual Stress Distribution for Type III Girders .....	54
Table 5.7 Residual Stress Distribution for Type VI Girders .....	54
Table 5.8 Suggested Reductions in Allowable Tensile Stress Due To Residual Stresses from Early-Age Thermal Loading.....	58
Table 6.1 Summary of Some Alternate Designs at Bents Used by Other States to Minimize/Prevent Girder-End/Diaphragm Cracking.....	66
Table 8.1 Simplified Model Parameters .....	85
Table 8.2 Summary of FEM Results .....	85
Table 8.3 Parametric Study Parameters and Values .....	94
Table 8.4 Girder Properties.....	95
Table 8.5 Effective Flange Width Values for Type II Girder.....	97
Table 8.6 Effective Flange Width Values for Type III Girder .....	97
Table 8.7 Effective Flange Width Values for Type IV Girder .....	98
Table 8.8 Effective Flange Width Values for Type VI Girder .....	98

Table 8.9 Effective Flange Width Values for Type VII Girder.....	98
Table 8.10 Simplified Equations for P and M .....	109
Table C.1 Form of the ANOVA Table for Simple Linear Regression.....	152
Table I.1 Allowable Stress Values for Design Example .....	191
Table I.2 Girder Stresses Positive Gradient -- Fully Restrained .....	192
Table I.3 Girder Stresses Positive Gradient -- Unrestrained .....	192
Table I.4 Girder Stresses Negative Gradient -- Fully Restrained.....	192
Table I.5 Girder Stresses Negative Gradient -- Unrestrained.....	193

### list of SYMBOLS

A	= gross area of girder cross section
$A_v$	= area of stirrup steel required to provide $V_s$
aggzone	= also aggregate zone, refers to whether the deck concrete contains chert aggregate
b	= the width of the member
$b_0$	= approximation of $\beta_0$ determined by the statistical analyses
$b_1$	= approximation of $\beta_1$ determined by the statistical analyses
$b'$	= web thickness
C	= resultant force from stress distribution on bottom flange bulb
$D_3$	= depth used to determine the AASHTO positive and negative temperature gradients
d	= depth of the bridge superstructure
E	= elastic modulus of a material
$E_{ct}$	= elastic modulus of concrete at time, t
e	= eccentricity of centroid of prestressing, P
$e_i$	= the residuals in the statistical analyses
F	= also known as the F-value, the ratio of $MS_{reg}$ to $MS_{res}$
$f'_c$	= compressive strength of concrete
$(f'_c)_t$	= compressive strength of concrete at time, t
$f_{sy}$	= yield strength of stirrup steel
g(x)	= the link function in the statistical analyses
garea	= the area of a bridge girder
garspl	= the product of the bridge girder area and the span length of the bridge
h	= total height of girder
$h_f$	= height of bottom flange bulb
I	= first moment of inertia about the centroid of section
jd	= internal moment arm (distance between compressive and tensile force)
L	= the overall length of the member
$l_m$	= the location of the median within the ordered data set
$l_q$	= the location of the first and third quartiles in the ordered data set, with respect to the beginning and end of the data set, respectively
M	= internal unbalanced moment
M	= the resultant moment of the thermal stresses
$MS_{reg}$	= the mean squared of the regression model
$MS_{res}$	= the mean squared for the residuals

m	= gradient of stress distribution on girder end segment
n	= the number of observations or data points in the statistical analyses
p	= probability of not cracking, in the statistical analysis
P	= the resultant force of the thermal stresses
P	= total horizontal component of prestressing force
Q	= first moment of inertia about centroid of area above depth under consideration
Q <sub>1</sub>	= the first quartile of the data set
Q <sub>3</sub>	= the third quartile of the data set
$Q(b_0, b_1)$	= the sum of the squared deviations
rt1	= refers to the type of route on which the bridge is located
SS <sub>reg</sub>	= the variability explained by the statistical model
SS <sub>res</sub>	= the variability attributed to error in the statistical analyses
SS <sub>total</sub>	= the overall variability of the data in the statistical analyses
s	= stirrup spacing
sec3	= the reinforcement in the 3 <sup>rd</sup> section of the bridge
spl	= the span length of the bridge
T(y)	= the temperature distribution as a function of y
T <sub>1p</sub>	= temperature at the top of the cross section for the AASHTO positive gradient
T <sub>2p</sub>	= temperature 0.33 ft from the top of the cross section for the AASHTO positive gradient
T <sub>3p</sub>	= temperature 1 ft from the top of the cross section for the AASHTO positive gradient
T <sub>1n</sub>	= temperature at the top of the cross section for the AASHTO negative gradient
T <sub>2n</sub>	= temperature 0.33 ft from the top and bottom of the cross section for the AASHTO negative gradient
T <sub>3n</sub>	= temperature 1 ft from the top and bottom of the cross section for the AASHTO negative gradient
T <sub>4n</sub>	= temperature at the bottom of the cross section for the AASHTO negative gradient
t	= age of concrete in days
t	= thickness of cross section at depth under consideration
t <sub>w</sub>	= web thickness
V	= externally applied shear force
V <sub>C</sub>	= shear resistance provided by concrete
V <sub>D</sub>	= shear force due to dead loads
V <sub>L+I</sub>	= shear force due to live loads with impact factor applied
V <sub>N</sub>	= nominal shear strength

$V_P$	= vertical component of prestressing force
$V_S$	= shear resistance provided by vertical stirrup reinforcement
$V_U$	= factored shear force at ultimate
$X$	= length of girder used in Gergely-Sozen analysis
$x$	= distance between concentrated loads in AASHTO live-loads
$x_i$ or $x$	= the values of the explanatory variables in the statistical analyses
$y$	= depth under consideration (elastic stress computations)
$y$	= location along girder height above bottom flange bulb (Gergely-Sozen analysis)
$y$	= the depth of the member
$y_f$	= height of resultant force from stress distribution on bottom flange bulb
$y_i$ or $y$	= the actual value of the variable to be predicted in the statistical analyses
$\hat{y}_i$ or $\hat{y}$	= the predicted value of the variable in the statistical analyses
$y_{ps}$	= height of centroid of prestressing force, $P$
$\tilde{y}$	= median of the data set
$\alpha$	= thermal coefficient of expansion of a material
$\beta_0$	= the intercept term in the statistical analyses
$\beta_1$	= the slope parameter in the statistical analyses
$\beta_k$	= collective term for the intercept and slope parameters in the statistical analyses
$\gamma$	= unit weight of a material
$\Delta L$	= the change in length of the member
$\Delta T$	= the uniform change in temperature of the entire member
$\varepsilon_i$	= the error terms in the statistical analyses
$\Phi$	= resistance factor in ultimate shear analysis
$\theta$	= angle above horizontal that defines direction of principal stresses, $\sigma_1$ and $\sigma_3$
$\mu$	= coefficient of friction
$\mu_{str}$	= microstrain ( $10^{-6}$ in/in or mm/mm)
$\nu$	= Poisson's ratio of a material
$\nu$	= shear stress
$\sigma_f$	= magnitude of stress distribution at top of bottom flange bulb
$S_{fully\ restrained}$	= the thermal stresses induced in a fully restrained member
$\sigma_h$	= axial compression due to prestressing
$\sigma_p$	= principal stress
$\sigma_t$	= magnitude of stress distribution at location of maximum moment, $y$

$S_{unrestrained}$  = the thermal stresses induced in an unrestrained member

$\sigma_{yy}$  = vertical normal stress

$\sigma_1$  = principal tensile stress

$\sigma_3$  = principal compressive stress

## **Introduction**

### ***Project overview***

This project was a joint investigation effort of the Universities of Missouri at Columbia and Rolla, Missouri (UMC and UMR, respectively) in collaboration with the Research, Development and Technology, Bridge, and Maintenance Divisions of the Missouri Department of Transportation (MoDOT). The objectives of this effort were to identify causes for the types of cracking that have been observed at girder-ends of prestressed I-girder bridges; study if these cracks warrant structural repairs; suggest suitable repair techniques; and recommend potential design revisions to prevent cracking in future girders. Seven specific research tasks were identified to meet these goals. These research tasks were divided between the two participating universities based upon the available research expertise and interests. Sections 3 through 8 detail six tasks of the research, while the design modification recommendation made by UMR (Task VII) is addressed in Section 10. Bylines are included in each independently authored section as appropriate; sections without bylines are authored jointly.

### ***background information***

The State of Missouri's highway bridge system is eighth in the Nation in terms of total number of bridges (FHWA, 1998). Of these approximately 25,000 bridges, 33 percent, or approximately 8100 bridges, are interstate and state highway bridges, which are managed by MoDOT. Prestress concrete (PC) I-girder bridges comprise 11 percent of those approximately 8100 bridges. Continuous multi-girder construction is the most common type of bridge constructed in Missouri (Dunker and Rabbat, 1992). Recently, the Missouri Department of Transportation (MoDOT) had become concerned with the number of bridges constructed using simple span PC I-girders made continuous that were experiencing cracking. MoDOT had detected visible cracks near the girder ends of 110 bridges that utilized simple span PC I-girders made continuous.

In an attempt to determine whether this type of cracking was common in other states, MoDOT sent a survey to all fifty State DOT's asking if they had similar problems with prestressed I-girder construction. Of the twenty State DOT's that responded to the survey, the majority stated they did not have this problem. However, most added they do not design bridges with simple span PC I-girders made continuous. Three states, Alabama, Alaska and California, indicated they have several bridges with girder cracking similar to that experienced by MoDOT. Information regarding the investigations conducted by Alabama and Alaska was provided to the researchers and is discussed in Section 1.4.

The use of precast/prestressed concrete in bridges has increased considerably since its first use in the 1950's due to its superior durability performance and cost effectiveness. The use of PC I-girders with continuous detailing was initiated by the use of precast/prestressed concrete. The intent of continuity detailing is to provide negative moment capacity over the piers with the use of longitudinal reinforcement. In general, continuous construction has several advantages over a simple-span construction. They include:

- the elimination of maintenance costs associated with expansion joints and the subsequent deterioration of substructure components due to leakage/drainage through these joints,

- the decrease of the live load positive moment at midspan, due to negative moment induced at the piers, and
- the decrease in the number of prestressing strands required, due to the decreased positive moment.

However, when the structural integrity of the bridge is diminished due to cracking at the girder ends or in the diaphragm, these advantages may no longer be relevant to the structure.

The cracks observed in the girders were of three main types: vertical cracks (Figures 1.1 through 1.3), diagonal shear cracks (Figure 1.3), and reverse diagonal cracks (in a direction perpendicular to typical shear cracks, Figure 1.4). The vertical cracks are accompanied in some cases with damage to the diaphragm (Figures 1.1 and 1.2), suggesting that the girders are pulling out from the diaphragm (or in some instances pushing into the diaphragm). Reverse diagonal cracking was also observed in girders after casting, but before placement on the bridge, suggesting that they may be due to early-age behavior of the girder. Other types of early-age cracking in the girder included horizontal cracks in the girder web near the junction between the bottom flange and the web (Figure 1.4b). This type of cracking may not be readily visible after construction of the bridge, as the girder-ends are embedded in the diaphragm.

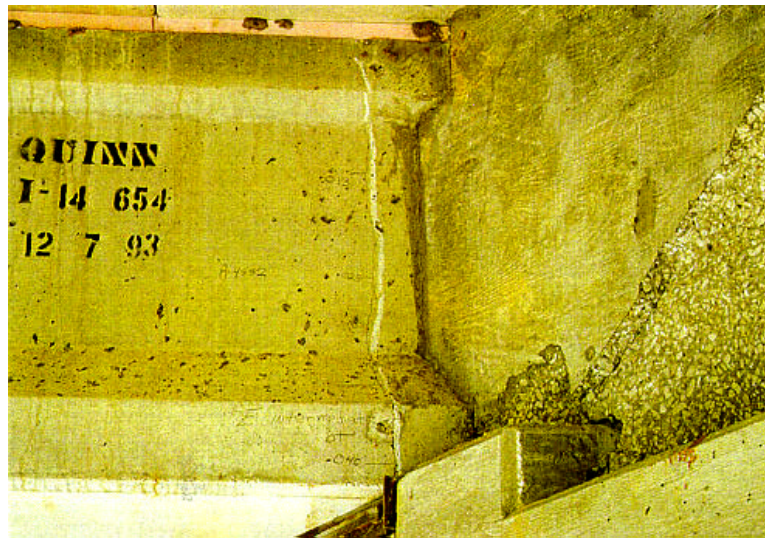


**Figure 0.1 Vertical Crack in the Girder-end at the Diaphragm**

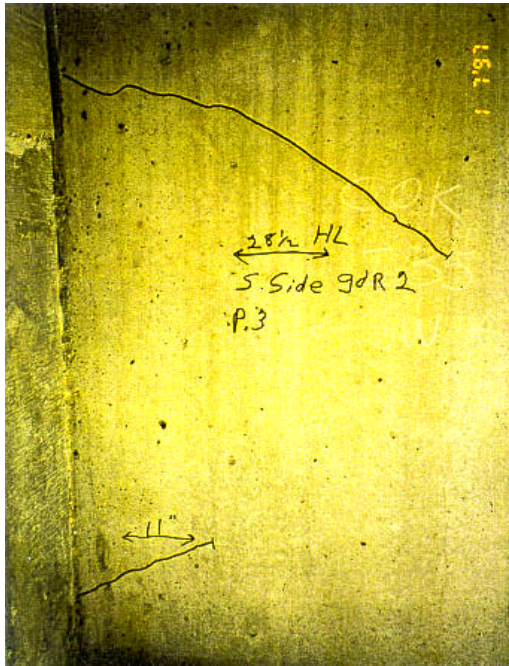


**Figure 0.2 Cracking in the Diaphragm Also Indicates Pull-out/Push-in Type of Loading of the Girders under Service Conditions**



Note: The right girder demonstrates a typical crack due to diagonal tension, and the left girder shows a typical vertical crack

**Figure 0.3 Shear Cracking Due To Diagonal Tension and Vertical Cracking in a Prestressed Girder**



**a:** girder embedded in a diaphragm



**b:** just fabricated girder stored at the precasting yard

### **Figure 0.4 Web Cracking in the “Reverse Shear Direction” objective**

As discussed earlier, the research effort was shared between UMC and UMR. Specific tasks were identified and were divided amongst the two universities.

- Complete the existing database on cracked bridges and draw conclusions of causes (UMR),
- Study shear design procedures in light of diagonal cracks observed (UMC),
- Study the early-age response due to differential thermal effects from heat of hydration and restraint from forms (UMC),
- Investigate the detailing of continuity at supports and resultant impact on performance (UMC),
- Experimentally monitor two typical bridges (cracked and uncracked) (UMR),
- Conduct a parametric study to determine the magnitude of thermal stresses anticipated in Missouri bridges (UMR), and
- Develop a proposed modification to the current design (UMR).

Section 2 will discuss the technical approach taken to accomplish each task.

### ***previous research***

A survey of available literature was performed to determine the extent of research that had been conducted on continuous concrete bridges. Additionally, the literature review would yield information on whether the cracking experienced in Missouri was typical of other states/regions. Much research exists on

the design of continuous bridges, however, there is little research addressing the problems that were experienced in Missouri. An outline of the available literature is included herein.

The first studies on the design of continuous bridges were conducted by the Portland Cement Association (PCA) in the 1960's. This research was summarized by Freyermuth (1969) as a design recommendation. This publication presents a design method for the positive moments that can be created at intermediate bents. These moments are attributed only to time dependant (creep and shrinkage) strains, and the method is largely empirical. It was found that positive moment reinforcement could most easily be provided using mild steel reinforcing bars bent 90° vertically into the diaphragm and embedded in the girder ends. The method is, however, very involved and it is suggested that typical plans be created for each type of girder used.

Research performed by Salmons (1972) provides the rationale for detailing of PC I-girder bridges in continuous construction. The report entitled "End Connections for Continuous Pretensioned Bridge Beams" outlines the research performed to establish the positive moment reinforcement required at the diaphragm using extensions of the girder prestressing strands. This eliminates the problem of fitting additional mild steel bars into the girder-ends. Salmons recognized that the effects of creep, shrinkage, and thermal gradients would cause a positive moment at the location of the diaphragm. However, the magnitude of the positive moment that might be generated due to these effects is never examined or compared to the moment capacity of the connection. The possibility of thermal stress was not examined in this study. Furthermore, Salmons noted that failure of the connection would occur as the girder pulled out from the diaphragm, due to diagonal cracking which propagated from the interior of the diaphragm outward, as illustrated in Figures 1.5 and 1.6.

Salmons' specimens modeled a girder-diaphragm interface; some modeled only the girder-diaphragm interface while others modeled the girder-diaphragm-deck interface. Both types of specimens exhibited the type of cracking illustrated in Figures 1.5 and 1.6 at failure. Figure 1.5 illustrates a cross-sectional view of the I-girder and diaphragm interface, while Figure 1.6 illustrates this same section in plan view. This is precisely the type of cracking that has been exhibited at several of the PC I-girder bridges in this study. Additionally, this type of cracking configuration could pose a long-term durability concern if it were to result in the propagation of a crack parallel to the bent line on the surface of the deck.

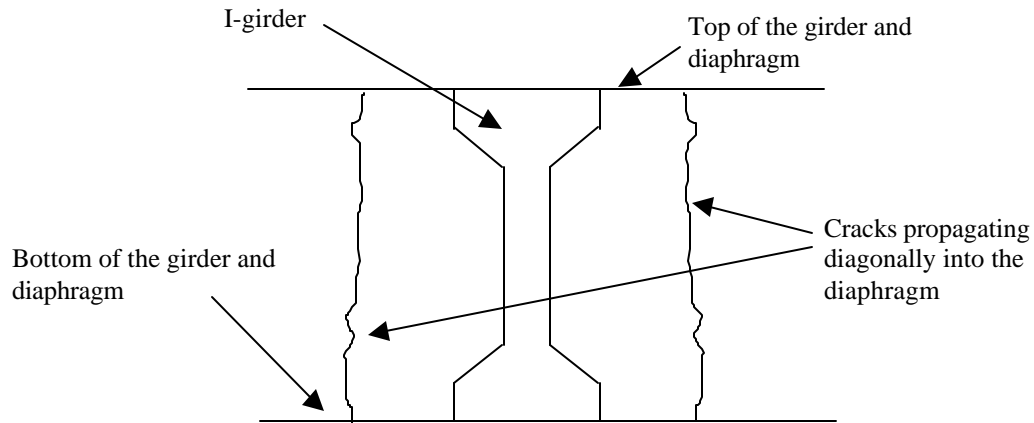


**Figure 0.5 Typical Failure of the Continuity Connection**

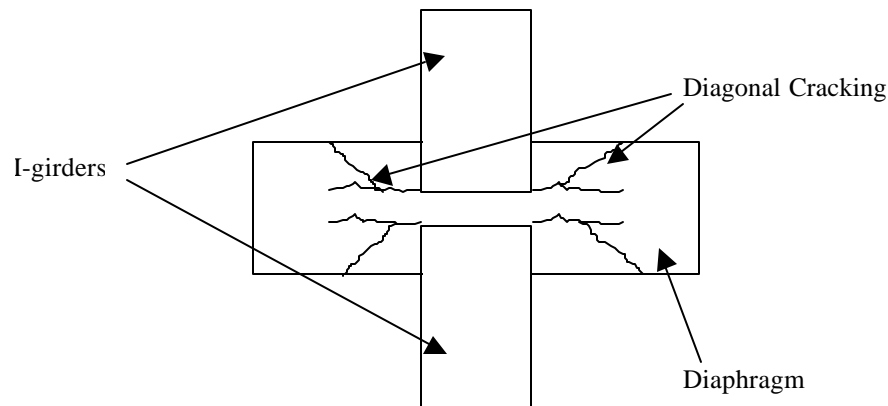


**Figure 0.6 Plan View of the Same Typical Failure**

More recent research on continuity was reported in National Cooperative Highway Research Program (NCHRP) Report 322, entitled “Design of Precast Prestressed Bridge Girders Made Continuous” (Oesterle, et. al, 1989). This study examines the potential for creep and shrinkage to occur and their effects with regard to continuous construction. The study concluded that positive reinforcement at the piers is not recommended, although it recognizes that a crack will form at the bottom of the diaphragm. Though the study does recognize thermal effects as a potential “loading” of a continuous bridge structure, it fails to quantify the thermal stresses; therefore, the positive moment resulting over the pier may be underestimated. Additionally, the report states that the positive restraint moment (due to additional dead load, live load, and creep and shrinkage effects) resulting from the presence of the reinforcement in the support will cause an increase in the positive moment at midspan. This study also acknowledges that the girder age at which continuity is created can influence the negative moment created. When continuity is established at late girder ages, the negative restraint moments (due to additional dead load, live load, and creep and shrinkage

effects) at the support are much larger than when continuity is established at an early age. Moreover, while casting of the diaphragm prior to casting of the deck can decrease slightly the midspan positive moments, it will also increase deck crack occurrence. It should be noted that a follow-up project, NCHRP Project 12-53, is underway at the University of Cincinnati that has the objective of recommending details and specifications for the design of more durable and constructable connections to achieve continuity.

Information about the influence of the construction sequence of the diaphragm and deck on the moment envelope of the structure is also provided by Ma, et al (1998), and can be summarized as follows:

- One possible construction sequence is to cast the diaphragm and the deck at the same time. This will lead to the development of negative moment over the pier when the superimposed dead load is applied. The later the concrete is cast, the larger this negative moment will be.
- The second case is when the diaphragm is cast and, after some time, the deck is cast. This will cause a negative moment larger than that developed when the diaphragm and deck are cast simultaneously. After the time effects of creep and shrinkage, and possibly thermal effects, this negative moment may be negated causing the member to act as a simply supported member. Therefore, the negative moment could be helpful in the sense that a larger negative moment would be harder to overcome. If the negative moment is overcome and positive moment results over the pier, a crack at the diaphragm/girder interface is probable. (Wollman, 1999)

Abdella, et al (1994) conducted a study comparing experimentally measured values for the positive moment created at the bents to those calculated using both the PCA method and the method in NCHRP 322. The tests considered only superimposed loading and time-dependant deformations. The PCA method was found to only give good results in cases where the diaphragm and slab were cast while the girders are relatively young. The method proposed by NCHRP 322 showed good results at all ages. In this study, like Salmons (1972), flexural cracking in the diaphragm was found to relieve much of the positive moment. The authors suggest, thus, that the level of positive moment designed for could be reduced.

One of the most pertinent research studies discovered was from the Alabama Department of Transportation (1994). Alabama had experienced similar cracking of their PC continuous bridges and wanted to determine the causes. It was established that there were several possible causes of the cracking. These causes include temperature differentials through the depth of the bridge, settlement of supports, creep, and shrinkage, which could all cause a positive moment to develop over the interior piers of the bridge. It was concluded that the potential tensile stress developed for a thermal differential of 30°F (16.67°C) could be on the order of 896 psi (6.17 MPa), which is enough to crack a conventional strength concrete that has a tensile strength around 600 psi (4.13 MPa). No information was presented to describe the temperature variation through the bridge depth and it is not clear whether the stress of 896 psi (6.17 MPa) is due to thermal stresses alone or a combination of all applied loads. Additionally, it was suggested that cracking at the girder ends could cause the prestress transfer length to increase. This increase in transfer length could move the critical positive moment section from within the diaphragm to the location

of positive steel termination. The positive moments developed over the piers in combination with the discontinuity of positive steel could cause tensile cracking in this region. This is a possible explanation for the cracking that has occurred at a distance of 2 to 4 ft. (0.61 to 1.22 m) from the face of the diaphragm. The Alabama DOT also concluded that an upward deflection, or cambering, of the girders due to thermal effects was occurring and that this deflection could be greater than the downward deflection due to traffic loads.

Another internal Department of Transportation report, from the Alaska Department of Transportation and Public Facilities (AKDOT&PF), outlines the suspected causes of girder end cracking that were observed. The conclusions of the AKDOT&PF are: (1) the cracking was not caused by a flexural failure, a diagonal tension failure, or a compression failure, (2) the observed cracks were initiated during fabrication, possibly due to elastic shortening induced by prestress transfer, and (3) thermal induced stresses originating from longitudinal restraint at the abutments have played a role in crack propagation.

Potgieter and Gamble (1989) also suggested that thermal gradient could be responsible for this sort of cracking. The authors collected temperature data from locations around the U.S. and developed a computer model to determine the thermal gradients that a bridge in that region would experience. One location modeled was Columbia, MO. The calculated temperature differential, between the maximum deck temperature and the minimum temperature of the bridge at the same time, was 45°F (25°C). Potgieter and Gamble compared the measured gradients, used to check their program, to the thermal gradient proposed by the New Zealand Code with good agreement. The New Zealand Code thermal gradient is outlined by Cooke, et al. (1984) as a fifth order function of the depth of the member with a maximum gradient differential of 57.6°F (32°C), for a bridge with no blacktop.

Other thermal gradients are defined by AASHTO (1989) and Shushkewich (1998). First, the *AASHTO Guide Specifications for Thermal Effects in Concrete Bridge Superstructures* outlines a number of thermal gradients for 4 geographical zones throughout the U.S. and for bridges with and without blacktop. These thermal gradients are recommended by AASHTO for use in considering thermal stresses and their effects on reinforced concrete (RC) or PC bridges. Figure 1.7 illustrates the general outline of the negative and positive thermal gradients recommended by AASHTO.

The geographical region in which the bridge is located and the surfacing type of the bridge determine the temperatures “ $T_{1p}$ ”, “ $T_{2p}$ ”, “ $T_{3p}$ ”, etc. Additionally, the depth of the superstructure, “ $d$ ”, is a function of the bridge of interest. Shushkewich reports the AASHTO gradient (1989) for segmental bridges and the modification to this gradient that have been proposed in other AASHTO specifications in 1994 and 1998.

It should be noted that the AASHTO (1989) thermal gradient is the “benchmark” gradient for this study to which the measured gradient will be compared. These gradients were used due to the fact that this gradient is a published and recommended thermal gradient for design of bridges in the U.S. Additionally, as will be discussed Section 7, these gradients have been validated for the climatic conditions in the State of Missouri.

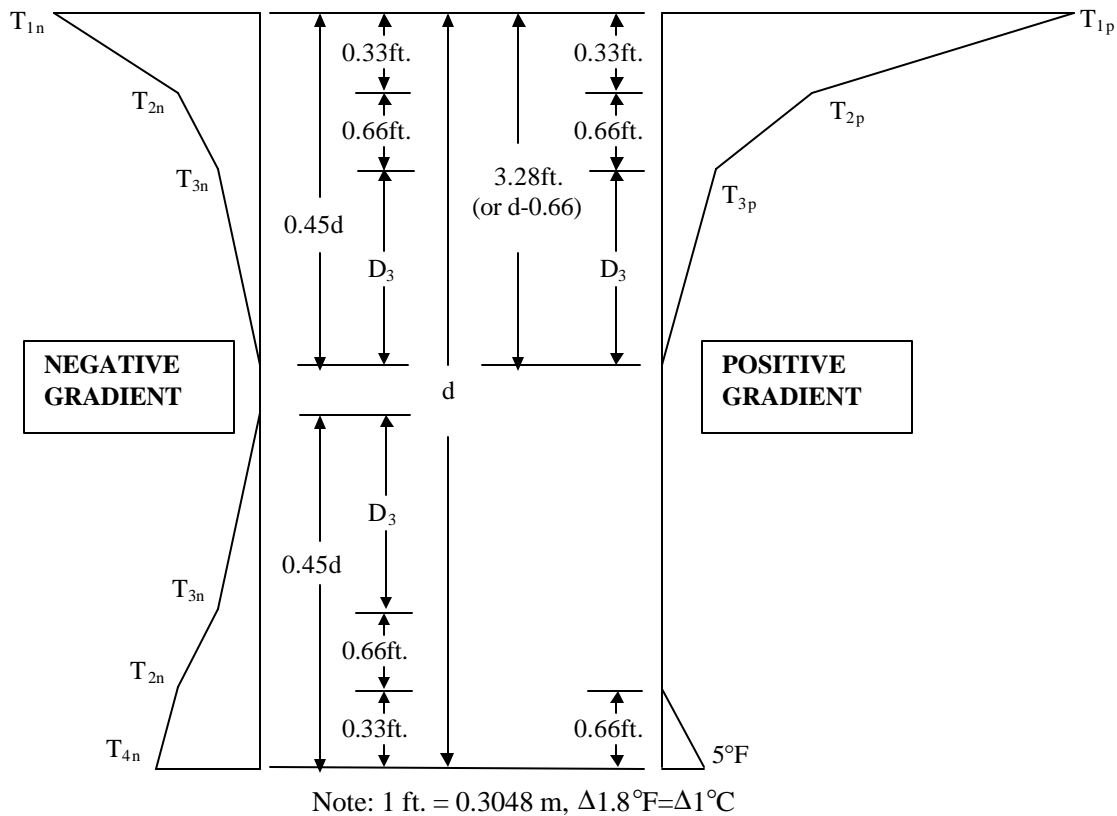


**Figure 0.7 AASHTO Recommended Thermal Gradients (1989)**

A study performed by Emanuel, et al (1972) was conducted with the intent of using the results for composite steel-concrete bridges, however the conclusions regarding continuity are valid for concrete bridges as well. They concluded that the major factor affecting longitudinal and vertical movements of bridges were thermal effects, shrinkage, creep, wind, braking forces, and movements of the abutment fill. Emanuel, et al (1972), proposed an instrumentation setup for potential monitoring of a full scale bridge to determine the necessary information about bridge movements, as related to the aforementioned factors. A further study was performed by Emanuel and Wisch (1977), in which a laboratory study of thermal stresses was conducted. While, again, the magnitudes of the stresses measured are not applicable to concrete bridges, they did establish that thermal stresses could occur to an appreciable degree. They recommended a future study of the effects of the diaphragm on the development of thermal stresses. A considerable amount of background material on the prediction of the temperature gradients and thermal stresses is presented in the Ph.D. dissertation of Hulsey (1976).

Stresses developed due to stressing operations were first investigated in the early 1960's by Marshall and Mattock (1962). It was determined that an adequate amount of stirrup reinforcement should be provided to prevent the spread of horizontal cracks that develop when the prestress force is transferred. A design method is presented for

determining the required amount of stirrup reinforcement. These studies were empirical, but did provide some insight for future studies. The authors suggested that girder-end cracking might be initiated by restrained shrinkage and thermal contraction provided by the form during curing, but no analysis of this was performed.

An analytical model to predict the vertical tensile stresses in the girder end region of PC I-Beams was proposed by Gergely and Sozen (1967). The model, shown in Figure 1.8, assumes that when a section is taken at the bottom of girder-end, the resultant portion of the internal stress distribution is not sufficient to resist the large prestressing force, and a reaction moment is created internally. This moment thus creates tensile stresses at the girder end. Gamble (1997) and Kannel, et al (1997) noted cracking in girders used in Illinois and Minnesota bridges, respectively, that is similar to cracks found in Missouri bridges. Gamble observed that the model proposed by Gergely and Sozen could be used to accurately predict the location of these cracks. However, no mention was made of prediction of the stress levels in the girder-end.

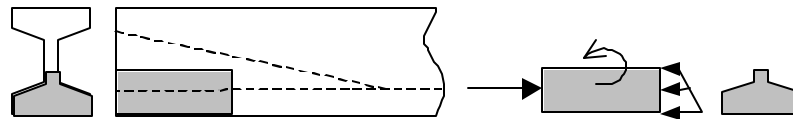


**Figure 0.8 Gergely-Sozen Model**

Thermal strains created in girders due to in-service temperature variations were studied by Saetta, et al (1995), and the development of heat during curing in HPC girders was studied by Khan, et al (1998) and Steeg, et al (1996). However, to the best of the authors' knowledge, no literature exists on a method for calculating residual stresses created due to restraint provided by the formwork.

### Technical approach

Following is a brief summary of the technical approach taken to investigate each research task. The analysis and results of each task are presented in Sections 3 through 8. The authoring school of each section is also indicated.

*Task I (UMR):* A database containing information on 150 PC I-girder bridges in the state of Missouri was developed and statistically analyzed to determine potential causes of the observed cracking.

*Task II (UMC):* Diagonal tension was investigated using an elastic stress analysis to determine the potential for cracking. An ultimate analysis was performed using current design codes to determine the structural integrity of the girders in light of the cracking observed.

*Task III (UMC):* The investigation of early-age cracking was expanded to include an analysis of vertical stresses due to the transfer of the prestressing force. This was done due to the observation of cracks in girders before their placement on the bridge and after prestress transfer (Figure 1.4b). Stresses due to thermal loads and restraint provided by the form were investigated using a finite element model of the girder and the form. ANSYS Version 5.4 (1999) was used for this. End stresses due to prestress transfer were analyzed using a model developed by Gergely and Sozen (1967). Some modifications were made to the original model based upon observations of crack patterns and data provided by another research study (Eatherton, 1999, Gopalaratnam and Eatherton, 2001).

*Task IV (UMC):* A literature review and limited survey of diaphragm detailing from other states was studied to investigate potential alternate design detailing. Service temperature and strain data from another ongoing project (Eatherton, 1999, Gopalaratnam and Eatherton, 2001) was analyzed to demonstrate that service temperatures could play an important role in stresses created at the diaphragm.

*Task V (UMR):* Monitoring of one cracked bridge and one uncracked bridge was conducted. Measurements of deflection and temperature were taken at the bridges to ascertain a representative thermal gradient and if thermal-induced deflection was appreciable.

*Task VI (UMR):* A parametric study was conducted to determine the magnitude of thermal stresses induced due to the AASHTO (1989) positive and negative thermal gradients. A design example was also conducted to illustrate incorporation of thermal stresses into the MoDOT design procedure.

*Task VII (UMR):* A modification to the current MoDOT bridge design procedure was proposed in an attempt to prevent cracking in prestressed concrete I-girder bridges which are made continuous.

Additionally, the overall project objectives, which were to identify causes for the observed cracking, study if these cracks warrant structural repairs, suggest suitable repair techniques, and recommend potential design revisions to prevent cracking in future girders, are addressed in the conclusions and recommendations outlined in Sections 9 and 10, respectively.

## **Completion of the database**

J. Myers, A. Nanni, and D. Stone

### ***Preliminary database***

In the summer of 1998, MoDOT gathered information on 110 PC I-girder bridges that had exhibited cracking at or near the girder ends. The information contained in the database included variables related to geographical location, fabricator, age, bridge geometry, girder geometry, materials used, reinforcement details, curing conditions, transportation and handling details, and traffic level. This database is referred to as the preliminary database. This first phase of the research was conducted to establish whether further research would be necessary to determine the causes of the aforementioned cracking.

Table 0.1 includes a list of the variables included in the preliminary database provided by MoDOT and those added during analysis. Several of the variables that were included in the database exhibited only three or fewer values/conditions (e.g., all the prestressing tendons were 7-wire steel strands). These variables are denoted in Table 3.1 and Appendix A with an asterisk and were ignored in the analysis because of their relative consistency. Additionally, a description of these variables is included in Appendix A. There were many qualitative, or non-numeric, variables included in the database. These variables were assigned numerical “identifiers,” which facilitated statistical analysis and are defined in the variable descriptions. An extensive database of numerous variables was considered in an attempt to include every possible factor and increase the confidence in the modeling.

**Table 0.1 Variables Included in the Preliminary Database**

Fabricator Information	Pre-Cast Company
	Plant Location
Bridge Geometry	Deck Type*
	Support Pad*
	Number of Spans
	Bridge Length
	Skew
	Girder Length
	Girder Spacing
	Number of Girders per Span
Girder Geometry	Girder Height
	Bottom Flange Width
	Top Flange Width
	Bottom Flange Height
	Top Flange Height
	Web Height
	Web Width
	Girder Type
	Girder Area
Prestressing Details	Number of Tendons
	Number of Straight Tendons
	Number of Draped Tendons
	Tendon Diameter*
	Tendon Type*
	Tendon Strength*
	Initial Stress as a Percent of Ultimate*
	Tendon Release Sequence*
Shear Reinforcement	Mild Steel Size*
	Mild Steel Strength*
	Shear Reinforcement End Space
	Shear Reinforcement First Section
	Additional Bars Within the End Area
	Shear Reinforcement Second Section
	Shear Reinforcement Third Section
	Shear Spacing Section 1
	Shear Spacing Section 2
	Shear Spacing Section 3

**Table 0.1 Variables Included in the Preliminary Database (continued)**

Girder Cracking	Number of Girder Ends Cracked
	Percentage of Girder Ends Cracked
Transportation and Construction	Casting Date
	Transportation Date
	Transportation Method*
	Distance Traveled
	Field Construction Date
	Erection Method
Concrete Mixture	Cement Source
	Coarse Aggregate Source
	Fine Aggregate Source
	Water Source*
	Class of Concrete*
	Cement*
	Coarse Aggregate*
	Fine Aggregate*
	Water*
Admixtures*	
Curing Details	Age at Release
	Strength at Release
	Curing Strength
	Curing Type*
	Curing Time
	Curing Temperature
Miscellaneous	Width of Diaphragm
	Column Height
	District
	Average Daily Traffic

A preliminary inspection of the data was performed using histograms of each variable to assess their distributions. While many of the variables exhibited no significant trends within the investigation, there are a few important trends to note.

The results of the histograms (see Appendix B) indicate that most of the bridges have a total length of 350 feet (106.7 m) or less, were designed for an average daily traffic (ADT) of 10,000 or less, and have three or four spans. The histograms also indicate that typically five percent of girder ends are cracked

in a bridge. In reference to the histograms, it should be noted that not all of the information being collected was available for each bridge in the preliminary database. Therefore, some of the histograms will contain fewer than 110 data points.

The manufacturer of the girders was a variable that was examined. While the pre-cast company CSR Quinn manufactured the girders in 67 percent of the bridges, it should be noted that they are also the largest precast concrete company in Missouri. The number of CSR Quinn manufactured girders in the database is approximately proportional to the percentage of the market for which CSR Quinn is responsible (Mayo, 1998).

Year of construction and season of construction seem not to affect the cracking of the girders in the way expected. Common sense would dictate that an older bridge would have more cracking than a new bridge, due potentially to the increased use, traffic flow, and/or deterioration. Additionally, a bridge constructed in the summer might experience a larger differential thermal gradient at an earlier age, which could cause cracking. However, the data in the histograms of the database information illustrate that there is a gradual increase in the number of cracked girder bridges until 1992 then a sharp decrease until the final year of data, 1995. Additionally, the bridges were equally distributed amongst the four seasons. It is important to note that little information is available as to the time or stage of construction during which the cracks first appeared in the bridges.

One other variable included in the database is district. Additional information regarding the number of cracked bridges in each district was obtained during the study to determine the percentage of cracked bridges with respect to the total number of PC I-girder bridges in each district. Of the ten districts, Districts 5, 8, and 9, were found to have the highest percentage of cracked bridges, exhibiting 23 percent, 31 percent, and 35 percent of PC I-girder bridges that are cracked, respectively. A geologic map of Missouri indicates that these districts are in the region of the State that has the thinnest surface soils (Missouri Geologic Survey, 1979). Typically, in an area of thin surface soils a spread footing type foundation will be used, as opposed to a pile footing. The issue of foundation type and foundation stiffness was not investigated within the scope of this project, but may be an issue that warrants further investigation.

After the preliminary analysis was performed, the data was analyzed using a commercially available statistical analysis package. The analysis of variance procedure was used to perform an F-test on the variables. See Appendix C for a detailed outline of the F-test procedure. This analysis was based on a linear regression fit of the data. Linear regression uses the least squares method to optimize the model solution. An outline of the statistical analyses performed on the preliminary database can be found in Vining (1998). The results of many of the F-tests are illustrated in Table 3.2. The variables included are those variables that are numerical variables rather than categorical variables. These variables can be considered to be continuous random variables, that is,

they can theoretically take any value within a specified interval. Unlike the discrete random variables (categorical variables) that can only take on predefined values, the continuous response variables can be analyzed using this procedure.

**Table 0.2 Summary of F-test Results**

Variable	t-value*
ADT	0.2687
Bridge Length	0.309
Number of Spans	0.9253
Diaphragm Width	0.5029
Skew	0.5066
Girder Length	0.912
Girder Spacing	0.3515
Girder Height	0.5289
Girder Area	0.6723
Number of Tendons	0.4243
Number of Straight Tendons	0.4472
Number of Draped Tendons	0.6406
Shear Reinforcement Sec. 1	0.5105
Shear Reinforcement Sec. 2	0.7674
Shear Reinforcement Sec. 3	0.1136

\* A t-value less than the selected significance level indicates statistical significance.

It is generally accepted that if the t-value is less than 0.05, or 5 percent, then the variable is considered statistically significant. This is the significance level that was initially used in the statistical analysis of the preliminary database. At this significance level, the results of the F-test analyses show that there are no individual variables that exhibit a statistical significance with respect to the number of girder ends cracked. Even when the significance level is raised to 0.10, or 10 percent, there continues to be no statistical significance exhibited by the variables individually.

Due to inconclusive results, it was determined that it would be necessary to obtain information about bridges that were uncracked as well. In order to ascertain a variable, or set of variables, which could be contributing to the cracking of the bridges, it would be necessary to compare them to bridges that had not cracked.

Based on the decision to include uncracked bridges in a new database, a sample size of 150 bridges was selected. The sample would include 75 cracked bridges and 75 uncracked bridges, giving a large enough population of each from which to draw conclusions. The 75 cracked bridges were randomly selected from the 110 bridges in the preliminary database and the 75 uncracked bridge were randomly selected from the remaining PC I-girder bridges, which were assumed to be uncracked.

Using the knowledge gained from the analysis of the preliminary database, the variables included in the database and the analysis procedure were modified. Also, the analyses were not performed on the variables individually, as in the previously outlined analysis, because this could be a potential reason that no statistical significance was exhibited.

### *Development of the revised database*

The revised database did not include all the variables that were included in the preliminary database. Based on the results of the preliminary analysis and on engineering judgment, several variables were eliminated from the database. Additionally, based on discussions with MoDOT personnel, a number of variables, which were determined to be potentially important, were added to the database. Ultimately, the revised database included the variables outlined in Table 0.3. See Appendix D for a detailed description of each variable; also included in Appendix D is the revised database.

**Table 0.3 Variables Included in the Revised Database**

Bridge Geometry	Number of Spans
	Bridge Length
	Skew
	Girder Spacing
Girder Geometry	Girder Type
	Girder Area
Shear Reinforcement	Shear Reinforcement End Space
	Shear Reinforcement First Section
	Additional Bars Within the End Area
	Shear Reinforcement Second Section
	Shear Reinforcement Third Section
	Shear Spacing Section 1
	Shear Spacing Section 2
Shear Spacing Section 3	
Girder Cracking	Cracked Condition
	Percentage of Girder Ends Cracked
Miscellaneous	Route Type
	County

	District
	Average Daily Traffic (ADT)

In the statistical analyses, each of these variables was considered, as were combinations of several variables. For example, based on the assumption that the bridge spans are all of equal length, the length of each span was calculated by dividing the bridge length by the number of spans; this variable was also included in the analyses and is one example of two variables used in combination.

Additional variables that were included in the analysis include “thermal zone,” and “aggregate zone.” The variable for “thermal zone” took into account the assumption that there may be a larger temperature differential in the southern part of the state. “Thermal zone” was a dummy variable that took a value of “0” for Districts 1 through 6 and a value of “1” for Districts 7 through 10. The variable for “aggregate zone” considered that aggregate composed of chert is used in the cast-in-place decks in Districts 7, 8, and 9. This consideration was important because chert aggregate has been documented to have a coefficient of thermal expansion (CTE) that is twice that of dolomitic limestone, which is composed largely of magnesium carbonate. This difference in CTE is suspected to influence the cracking that is under investigation. “Aggregate zone” was another dummy variable that took a value of “1” for Districts 1 through 6 and 10 and a value of “0” for Districts 7 through 9.

Several assumptions about the database were made during the analyses. One of these assumptions was that of the 876 total PC I-girder bridges in the state of Missouri, only the 110 bridges from the preliminary database were considered to be cracked. Although it was suspected that there were bridges with undetected cracks, this matter was not considered in the statistical analysis. While the statistical analysis could not take this assumption into consideration, efforts were made to verify this suspicion.

MoDOT performed snooper truck inspections of a number of bridges throughout the course of the project. The snooper truck inspection is a close-up visual inspection of the bridges. Of the 10 bridges that were inspected with the snooper truck, 100 percent exhibited more cracking than originally reported in the database. It is possible that additional cracking occurred in the bridge between the first inspection, which would be the data included in the preliminary database, and the second snooper truck inspection. However, it is also possible that the closer inspection with the snooper truck detected cracks that were undetected during the inspection from ground level. Whichever is the cause of the increased number of cracks, this investigation indicates that there are indeed more bridges cracked than the 110 of the preliminary database.

Again, a preliminary investigation of the database was performed prior to any statistical analysis. This investigation, which included the production of box plots and bar charts of certain variables that were of interest, is outlined in Appendix E. In general, the cracked bridges have shorter span lengths than the uncracked bridges. More Type III girders crack than remain uncracked. Type VI girders tend to remain uncracked. Type II and Type IV girders seem to be somewhere in between, with approximately equal proportions of cracked and uncracked bridges. Interstate bridges crack less than the other route types and

U.S. highway bridges tend to crack more often. Three span bridges are the most common of the bridges in Missouri utilizing simple span PC I-girder made continuous.

### ***Statistical Analysis of the Revised Database***

Whereas the goal of the preliminary database analysis was to determine if the variables, individually, could predict the percentage of girder ends cracked, a different approach was taken for the revised database. Two types of statistical analyses were performed on the revised database, with each analysis focusing on an area of interest with respect to bridge maintenance issues. The first, which would attempt to predict the percentage of girder ends cracked, is multiple linear regression analysis. The second, which would model the cracked status of a bridge, is logistic regression analysis.

A multiple linear regression is based on the least squares method, while a logistic regression is based on the method of maximum likelihood. The solution of a multi-variable linear regression using the least squares method follows the same principles outlined for the simple linear regression. Both multi-variable linear regression and the method of maximum likelihood are considerably more complicated as a number of explanatory variables must be considered. This was one reason that a statistical software package was used for the analysis.

The models considered during the statistical analysis followed the hierarchical principle. This simply means that if a variable is considered in the model as a product with another variable then both of those variables must be considered separately in the model as well. For example, if the product of bridge length and skew, “ $x_1x_2$ ”, is included in the model then the variables themselves must also be considered individually (i.e., “ $x_1$ ” and “ $x_2$ ”).

**Multiple Linear Regression Analysis.** For the multiple linear regression analysis, the model would be of the form expressed below:

$$y_i = b_0 + b_1x_{1i} + b_2x_{2i} + \cdots + b_px_{pi} + e_i \quad (0.1)$$

where:

“ $y_i$ ” is the actual value of the variable to be predicted,

“ $\beta_0$ ” is the intercept term,

“ $\beta_i$ ” are the slope parameters,

“ $x_i$ ” are the explanatory variables under consideration, and

“ $\epsilon_i$ ” are the error terms.

Collectively, “ $\beta_0$ ” and “ $\beta_i$ ” are called “ $\beta_k$ ”. In this case, “ $y_i$ ” is the percentage of girder ends cracked, “ $x_i$ ” are the explanatory variables in the database, and “ $\beta_k$ ” are to be determined by the statistical analysis. As previously mentioned, the multiple linear regression performed by the commercially available statistical analysis package uses the least squares method.

During the course of the analysis, a number of models were considered which included various combinations of the variables in the database. Based on the R-squared values of the models, these trials did not yield a high level of accuracy. It should be noted that a model that fits the data perfectly will have an R-squared value of 1.0 and a model that does not fit the data at all will have an R-squared value of 0.0. The R-squared values for the models considered ranged between 0.1 and 0.3.

Due to the poor fit of all models considered, this analysis was abandoned. One suspected cause for the poor fit was that there seems to be two populations of data. One population, those bridges with a low percentage of girders cracked, may have been those bridges that had been inspected for cracks from ground level. With the other population being those bridges exhibiting a higher percentage of girder ends cracked, possibly having been inspected using a snooper truck.

Figure 0.1 seems to illustrate the two populations the most clearly, with the data split approximately between the 20 and 25 percent lines. The researchers were not able to prove or disprove this assumption due to the fact that the means of crack inspection was not reported in the preliminary database provided by MoDOT.

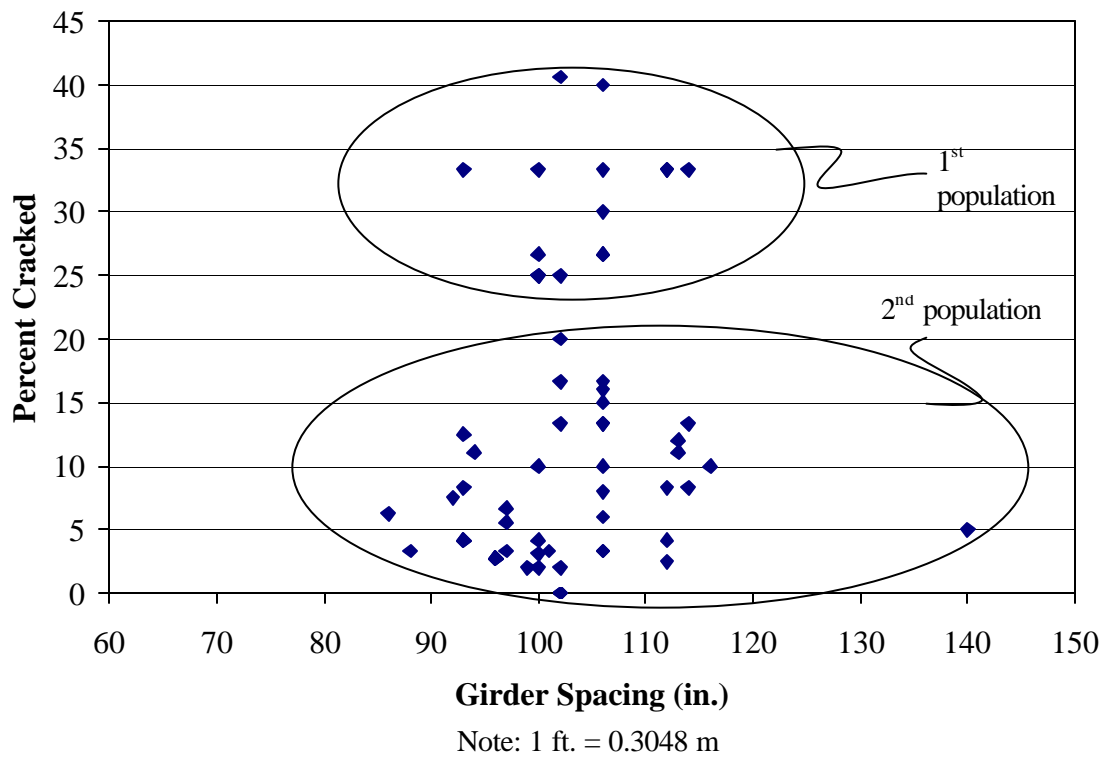


**Figure 0.1 Percentage of Girder Ends Cracked vs. Girder Spacing**

Bridges inspected from their base would have fewer cracks observed, due to a number of factors, including lack of lighting under the deck of the bridge, the height of the bridge deck, or bridge accessibility (e.g., due to water crossing).

**Logistic Regression Analysis.** A logistic regression can be used to predict the response of a binary variable. In this case, the cracked status of a bridge was the variable; a bridge can either be cracked or uncracked. In the database the cracked status of the uncracked bridges was denoted by a “0” and the cracked bridges were denoted by a “1.” Since a value other than “0” or “1” does not indicate anything, according to the variable definition, the probability of the bridge being cracked or uncracked is what is actually modeled.

For the logistic regression analysis, the model would be of the form,

$$p = \frac{e^{g(x)}}{1 + e^{g(x)}} \quad (0.2)$$

where:

“p” is the probability of not cracking,

$$g(x) = \mathbf{b}_0 + \mathbf{b}_1 x_{1i} + \mathbf{b}_2 x_{2i} + \cdots + \mathbf{b}_n x_{ni}, \quad (0.3)$$

“ $\beta_0$ ” is the intercept term,

“ $\beta_i$ ” are the slope parameters, and

“ $x_i$ ” are the variables under consideration.

Again, collectively, “ $\beta_0$ ” and “ $\beta_i$ ” are called “ $\beta_k$ ”. The function “g(x)” is called the link function.

The model uses the explanatory variables that are input and the response variable “ $y_j$ ” to produce the best estimates for “ $\beta_k$ ”. As previously mentioned, analysis performed by the commercially available statistical analysis package uses the maximum likelihood method. Using these parameter estimates and the specific characteristics of the bridge (i.e., the values of “ $x_i$ ”), a value for the link function, “g(x)”, can be determined and a probability value calculated by Equation 3.2.

In this case, because the cracked bridges were denoted by a one and the uncracked bridges denoted by a zero, the probability calculated in this way will be the probability of not cracking. This is a quirk of the software package used. To calculate the probability of cracking, which seems to be a more logical indicator of performance, simply subtract the probability of not cracking from one (if expressed as a decimal), or from 100 percent (if expressed as a percentage).

The next step was to determine the “goodness of fit” of each model. In this way, the best model can be selected and accurate predictions can be made about whether a bridge with certain characteristics will crack.

For this project, the best model was defined as that model which exhibited the highest accuracy in predicting the cracked status of a bridge. The output of a logistic analysis can be seen in Appendix F. Based on the model output, a cut-off probability value can be selected that will maximize the accuracy of

the model prediction. The selected cut-off probability value is used to establish the predicted cracked status of a bridge. The accuracy of the statistical model can be found under the heading “Classification Table.” For this model, the highest accuracy can be achieved if a cut-off probability value of 0.50 is selected; this gives an accuracy of approximately 77 percent. This means that if the parameters of a given bridge were used in the model (e.g. span length, girder area, etc.) and a probability value of 0.55 were calculated, then the bridge would classify as uncracked because the calculated probability value of 0.55 is larger than the selected cut-off probability value of 0.50. As mentioned previously, this choice of cut-off probability resulted in a prediction accuracy of 77 percent. It may be noted, however, that this accuracy is computed using the prediction performance of the data used to build the model. Thus, validation of this accuracy using an independent data set was warranted.

### ***Results of the statistical analysis***

The foremost result of the logistic regression is the building of a model to predict the cracked status of a bridge. The model chosen, on the aforementioned basis of maximum accuracy of crack prediction, included the variables of shear reinforcement spacing in the center of the beam, span length, cross sectional area of one bridge girder, route type (i.e. interstate highway or other), and aggregate zone (i.e. chert or non-chert). The example logistic regression output in Appendix F, examined previously, is the output of the selected model. It should be noted that the researchers are not indicating these variables as the causes of cracking; these variables were indicated by this modeling technique as significant variables. There is a possibility that variables not identified by this study could be the primary causes of cracking.

A validation of the model was performed using 25 bridges, 10 of which were known to be cracked and 15 of which were known to be uncracked. As mentioned previously, the accuracy of the model attained on the original data set is 77 percent. Usually, the accuracy of an independent test data set would be lower than this value. Initially, the validation was performed using a selected cut-off probability value,  $P$ , of 0.5. See Table 0.4 for results.

For the cracked bridges, the model has exhibited 70 percent accuracy. However, for the uncracked bridges, the accuracy decreases to 40 percent. The combined accuracy, with a selected cut-off probability value of 0.5 is 52 percent. Several limitations in the analysis lead to this decrease in accuracy.

**Table 0.4 Results of the Validation Using P = 0.50**

Cracked Bridges		Uncracked Bridges	
Calculated Probability	Cracked Status Predicted	Calculated Probability	Cracked Status Predicted
	P=0.5		P=0.5
0.935	No	0.651	No
0.029	Yes	0.036	Yes
0.043	Yes	0.464	Yes
0.068	Yes	0.066	Yes
0.033	Yes	0.561	No
0.057	Yes	0.484	Yes
0.715	No	0.101	Yes
0.721	No	0.642	No
0.030	Yes	0.390	Yes
0.032	Yes	0.516	No
<b>Accuracy =</b>	<b>0.7</b>	0.959	No
		0.179	Yes
		0.947	No
		0.462	Yes
		0.365	Yes
		<b>Accuracy =</b>	<b>0.4</b>
	<b>Combined accuracy (p=0.5) = 0.52</b>		

First, it was suspected that the lower accuracy is due to the characteristics of the bridges in the verification sample. Although the bridges were randomly sampled from the group of bridges that were not used in the model building stage, they were all non-interstate highway bridges and most were “aggregate zone” 1, signifying non-chert aggregate. Recall, from the preliminary analysis of the revised database, that interstate bridges exhibited a lower proportion of cracked bridges than the non-interstate bridges, as did the “aggregate zone” 1 bridges as compared to the “aggregate zone” 0 bridges. Overall, this would tend to decrease the accuracy exhibited for the verification data because the proportions of the parameter values are not the same between the samples and the whole population (i.e., between the verification sample, the database, and all Missouri bridges of this type). See Tables 3.5 and 3.6 for an outline of the bridge parameters for the verification sample bridges. It may be noted that the variable “Rt1” will take a value of “1” for interstate bridges and a value of “0” for non-interstate bridge.

**Table 0.5 Properties of the Cracked Girders in the Verification Sample**

Bridge Number	Bridge Length (ft)	Number of Spans	Route Type	District	Span length (ft)	Rt1	Aggregate zone	Girder Area (in <sup>2</sup> )
A4823	337	4	2	1	84.25	0	1	643.6
A5053	352	7	4	7	50.29	0	0	381.9

A4358	179	3	4	8	59.67	0	0	428.9
A4478	197	3	3	8	65.67	0	0	428.9
A3822	157	3	3	8	52.33	0	0	381.9
A4565	306	5	4	9	61.20	0	0	381.9
A4908	378	5	4	5	75.60	0	1	336.5
A4929S	367	4	2	7	91.75	0	0	643.6
A5052	356	7	4	7	50.86	0	0	381.9
A3412	365	7	4	9	52.14	0	0	381.9

Note: 1 ft. = 0.3048 m, 1 in<sup>2</sup> = 645.2 mm<sup>2</sup>

Second, the proportion of cracked to uncracked bridges in the database does not match the proportion in the state of Missouri. The sample of 150 bridges in the revised database was 50 percent cracked and 50 percent uncracked. Recall, one assumption for this analysis was that of the entire population of PC I-girder bridges in the state only the 110 bridges from the preliminary database were cracked. This assumption would mean that approximately 11 percent of the PC bridges are cracked. This difference in proportion of cracked bridges may partially account for the lower accuracy exhibited by the verification sample.

One means of remedying the difference in parameter proportions is to lower the selected cut-off probability value. At the previous selected cut-off probability value of 0.5, any bridge prior to analysis has a five in ten chance of being cracked. That is to say that half of the possible outcomes of the analysis could conclude that the bridge is cracked and half could conclude that the bridge is uncracked. By lowering the cut-off probability value, the number of possible outcomes indicating a cracked bridge will decrease.

**Table 0.6 Properties of the Uncracked Bridges in the Verification Sample**

Bridge Number	Bridge Length (ft)	Number of Spans	Route Type	District	Span length (ft)	Rt1	Aggregate zone	Girder Area(in <sup>2</sup> )
A4598	211	3	2	1	70.33	0	1	428.9
A2628	129	3	2	7	43.00	0	0	310.9
A4781	304	5	2	5	60.80	0	1	428.9
A4475	261	4	3	9	65.25	0	0	428.9
A3976	333	5	3	4	66.60	0	1	473.9
A4755	266	4	3	4	66.50	0	1	643.6
A5362	158	3	2	5	52.67	0	1	643.6
A3500	211	3	2	3	70.33	0	1	518.9
A5512	160	3	2	2	53.33	0	1	381.9
A4057	184	3	3	3	61.33	0	1	381.9
A4319	262	3	4	4	87.33	0	1	643.6
A3077	171	3	3	4	57.00	0	1	643.6
A4589	257	3	3	3	85.67	0	1	643.6
A4896	182	3	3	6	60.67	0	1	428.9
A4622	155	3	3	10	51.67	0	1	381.9

Note: 1 ft. = 0.3048 m, 1 in<sup>2</sup> = 645.2 mm<sup>2</sup>

The verification data was examined again using a lower selected cut-off probability value. This time a selected cut-off probability value of 0.15 was used. The probability value of 0.15 was selected because, as mentioned previously, there are assumed to be approximately 11 percent of bridges that are actually cracked in the State. The value of 0.15 is conservative, compared to a value of 0.11, because, as mentioned throughout the duration of the project, it is suspected that more bridges are cracked than the known 11 percent. See Table 0.7 for the results of this analysis.

The results indicate that the combined accuracy of the model, using a selected cut-off probability value of 0.15, is 76 percent. This is very close to the accuracy of the model obtained for the model-building data.

**Table 0.7 Results of the Validation Using P=0.15**

Cracked Bridges		Uncracked Bridges	
Calculated Probability	Cracked Status Predicted	Calculated Probability	Cracked Status Predicted
	P=0.15		P=0.15
0.935	No	0.651	No
0.029	Yes	0.036	Yes
0.043	Yes	0.464	No
0.068	Yes	0.066	Yes
0.033	Yes	0.561	No
0.057	Yes	0.484	No
0.715	No	0.101	Yes
0.721	No	0.642	No
0.030	Yes	0.390	No
0.032	Yes	0.516	No
<b>Accuracy =</b>	<b>0.7</b>	0.959	No
		0.179	No
		0.947	No
		0.462	No
		0.365	No
		<b>Accuracy =</b>	<b>0.80</b>
	<b>Combined accuracy (p=0.15) = 0.76</b>		

While the prediction of cracking is the primary objective of this procedure, another method of utilizing the probability values is to produce contour plots of the probability of cracking. The link function, “g(x)”, for the selected model is expressed as,

$$g(x) = -0.4793 + 0.1804 \cdot sec3 - 0.0664 \cdot spl - 0.0245 \cdot garea + 0.000342 \cdot garspl + 1.8788 \cdot rt1 + 2.8704 \cdot aggzone \quad (0.4)$$

where the variable abbreviations are defined as follows:

“sec3” is the shear reinforcement spacing near the center of the beam,

“spl” is the span length,

“garea” is the girder area,

“garspl” is the product of the girder area and the span length,

“rt1” is a dummy variable to indicate the route type, and

“aggzone” is the dummy variable used to denote the presence of chert type aggregate.

Of the variables included in the model, girder area and span length would be of most interest to a bridge designer. The contour plots created will be a function of these two variables. However, the values of all of the other variables in the model must be substituted into the link function to get the probability as a function of girder area and span length. For the shear reinforcement spacing in the center of the beam,

“sec3”, an average value of 17.14 in. will be used. Note that all units used in these equations should be English units, as these are the units for which the equations were derived. Substituting the average shear reinforcement spacing into Equation 3.4, the expression becomes

$$g(x) = 2.6134 - 0.0664 \cdot spl - 0.0245 \cdot garea + 0.000342 \cdot garspl + 1.8788 \cdot rt1 + 2.8704 \cdot aggzone \tag{0.5}$$

For the other two variables, there are four possible combinations. (See Table 0.8.)

**Table 0.8 Equations Based on Possible Variable Combinations**

	aggzone	rt1	g(x)
<b>Plot 1</b>	0	0	$2.6134 - 0.0664 \cdot spl - 0.0245 \cdot garea + 0.000342 \cdot garspl$
<b>Plot 2</b>	0	1	$4.4922 - 0.0664 \cdot spl - 0.0245 \cdot garea + 0.000342 \cdot garspl$
<b>Plot 3</b>	1	0	$5.4838 - 0.0664 \cdot spl - 0.0245 \cdot garea + 0.000342 \cdot garspl$
<b>Plot 4</b>	1	1	$7.3626 - 0.0664 \cdot spl - 0.0245 \cdot garea + 0.000342 \cdot garspl$

Recall that ‘aggzone’ equal to zero represents the presence of chert aggregate and ‘aggzone’ equal to one represents the presence of non-chert aggregate. Additionally, ‘rt1’ equal to zero represents a non-interstate highway and ‘rt1’ equal to one represents an interstate highway. The contour plots provided in Figures 3.2 through 3.5 were created for these four possible combinations of variables, respectively, and illustrate the probability of cracking as a function of girder area and span length.

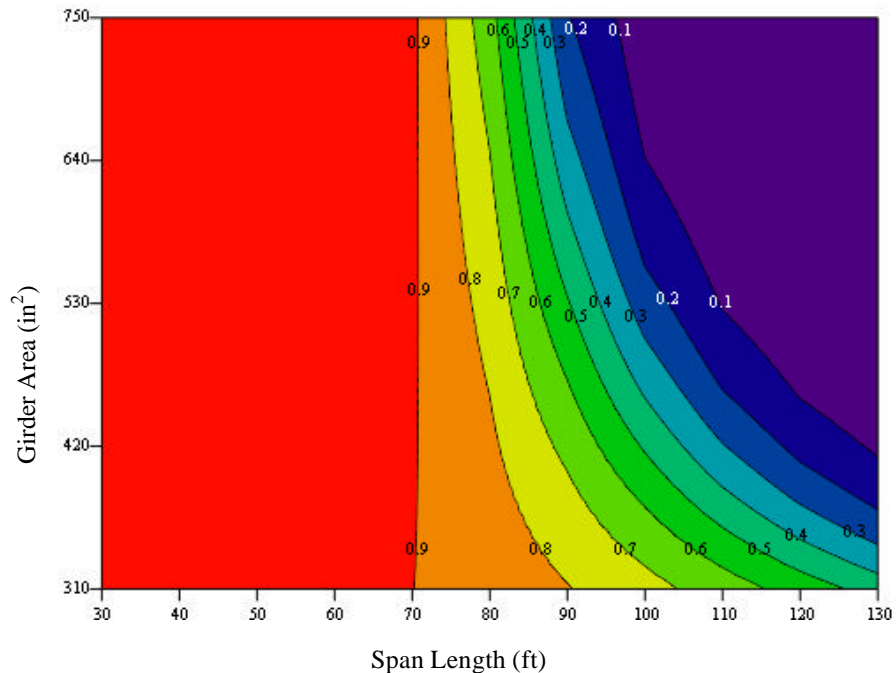


**Figure 3.2 Contour Plot for Chert Aggregate and Non-interstate Highways**

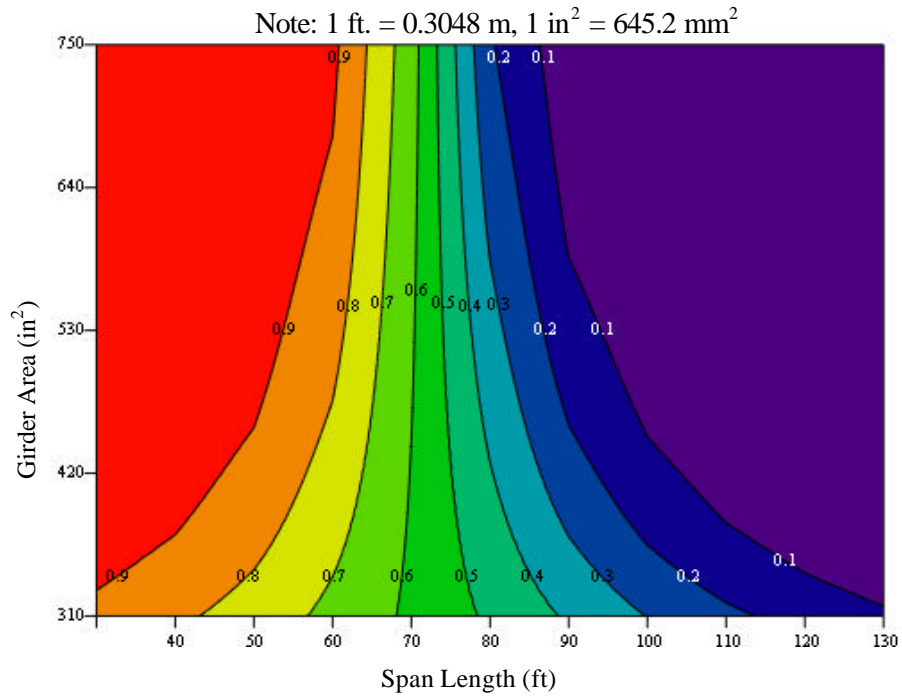


**Figure 0.3 Contour Plot for Chert Aggregate and Interstate Highways**

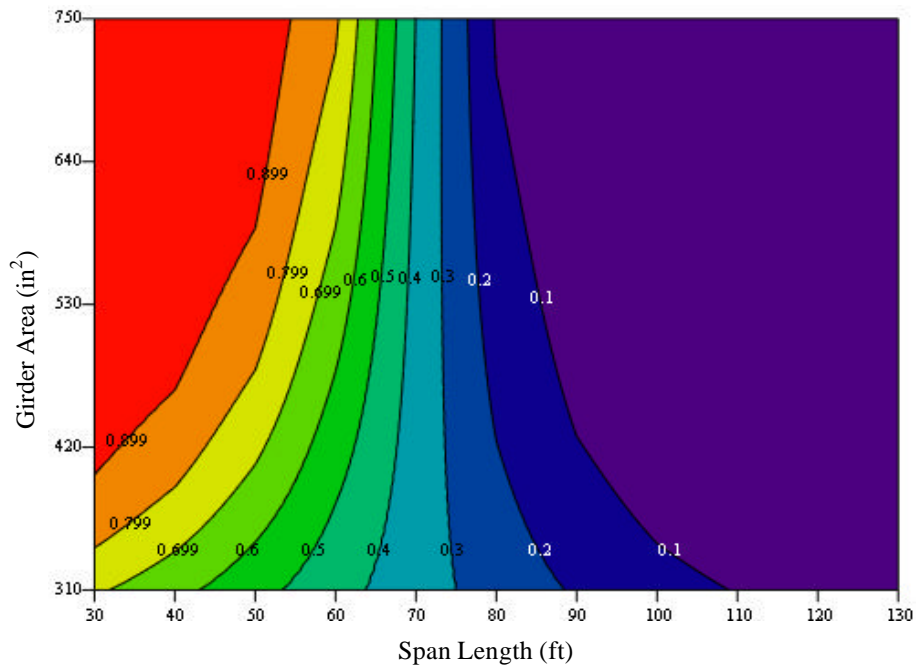


**Figure 0.4 Contour Plot for Non-chert Aggregate and Non-interstate Highways**

Note: 1 ft. = 0.3048 m, 1 in<sup>2</sup> = 645.2 mm<sup>2</sup>

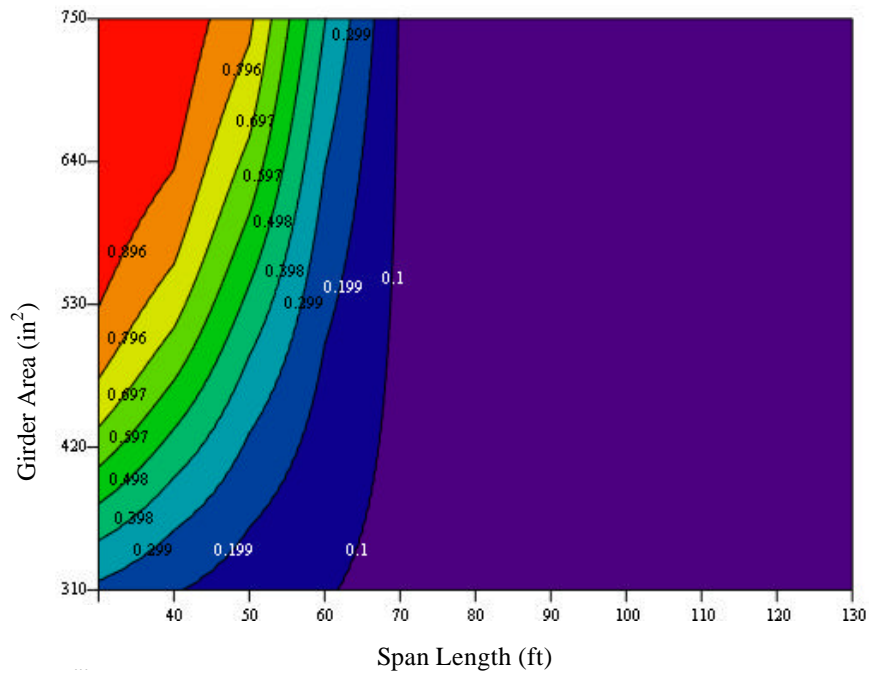


**Figure 0.5 Contour Plot for Non-chert Aggregate and Interstate Highways**

It would be appropriate at this point to note the typical ranges of girder area and span length for this type of bridge in Missouri. The typical range for girder area is from 310.9 to 751.6 in<sup>2</sup> (0.20 to 0.49 m<sup>2</sup>); this corresponds to Type 2 through Type 6 girders. Also, the typical range for the span length is from 36 to 90 feet (10.97 to 27.43 meters) (Missouri Department of Transportation, 1988, Bridge Manual, Section 3.55 1.1.8).

Depending on the span length considered, the probability of cracking would either increase or decrease as the girder area increases according to the statistical model considered.

The contour plots indicate that there is a lower probability of cracking for the interstate highway bridges. This is evident in the comparison between Figure 0.2 and Figure 0.3 (chert aggregate), and between Figure 0.4 and Figure 0.5 (non-chert aggregate). For example, for a span length of 80 feet (24.38 meters) and a girder area of 600 square inches (0.39 square meters), the probability of cracking can be compared between the two sets of plots in Table 0.9.

**Table 0.9 Summary of Selected Probability Values**

	Chert Aggregate	Non-chert Aggregate
<b>Interstate Highways</b>	29%	2%
<b>Non-interstate Highways</b>	72%	13%

For non-interstate bridges with chert aggregate (Figure 0.2) the probability of cracking is approximately 72 percent, while for interstate bridge with chert aggregate (Figure 0.3) the probability

decreases to 29 percent. This also evident by a comparison of non-interstate bridges without chert aggregate (Figure 0.4) and interstate bridge without chert aggregate (Figure 0.5), which exhibit probability values of 13 percent and 2 percent, respectively. There is a consistent decrease in probability of cracking for the interstate highway bridges, as compared to the non-interstate highway bridges.

Also evident is an increased probability of cracking for those bridges that contain chert aggregate in the cast-in-place deck. For the same conditions outlined in the previous example (see Table 0.9), the comparisons of Figure 0.2 to Figure 0.4, and of Figure 0.3 to Figure 0.5 exhibit this trend. First for the non-interstate bridges without chert aggregate (Figure 0.4) exhibits a probability of cracking of 13 percent, compared to a percentage of 72 percent from non-interstate bridges with chert aggregate (Figure 0.2). Additionally, interstate bridge without chert aggregate (Figure 0.5) exhibits a probability of 2 percent while interstate bridge with chert aggregate (Figure 0.3) exhibits a probability of 29 percent. There is a consistent increase in probability of cracking for the chert aggregate bridges, as compared to the non-chert aggregate bridges.

Caution should be exhibited when attempting to draw conclusions about the effects of the explanatory variables on the response variable. While the prediction ability of the model may be good, to claim that the explanatory variables used in that model actually determine the magnitude of the response variable, those variables must not only predict, but must also control, the response variable. (Gunst and Mason, 1980, pg. 17) In other words, to claim that the variables identified in this study actually cause girder cracking, there must be proof that these variables can also control the occurrence of girder cracking.

The results of the statistical analysis can be summarized as follows:

- There seems to be two populations of data, those inspected by the snooper truck and those inspected from ground level.
- There are more PC I-girder bridges in Missouri that are cracked than previously expected or reported.
- The cracked status of a bridge can be predicted with approximately 77 percent accuracy using the proposed model, which is a function of the shear reinforcement spacing near the center of the girder, girder area, span length, aggregate type, and route type.
- Chert aggregate use increases the probability of cracking, as calculated by the proposed model. The chert aggregate is used in the deck concrete of some bridges in southern Missouri.
- Interstate highway bridges have a lower probability of cracking, compared to non-interstate highway bridges, as calculated by the proposed model.
- For a given girder area, longer span lengths decrease the probability of cracking given by the proposed model.

Additionally, for the logistic regression, the explanatory variables used in the models were not standardized; that is, made to vary between  $-1$  and  $+1$  regardless of their actual range. Therefore, the

conclusion cannot be drawn that a variable with a larger coefficient influences the response variable more than a variable that has a lower coefficient.

## Diagonal Tension

V. S. Gopalaratnam and T. P. Earney

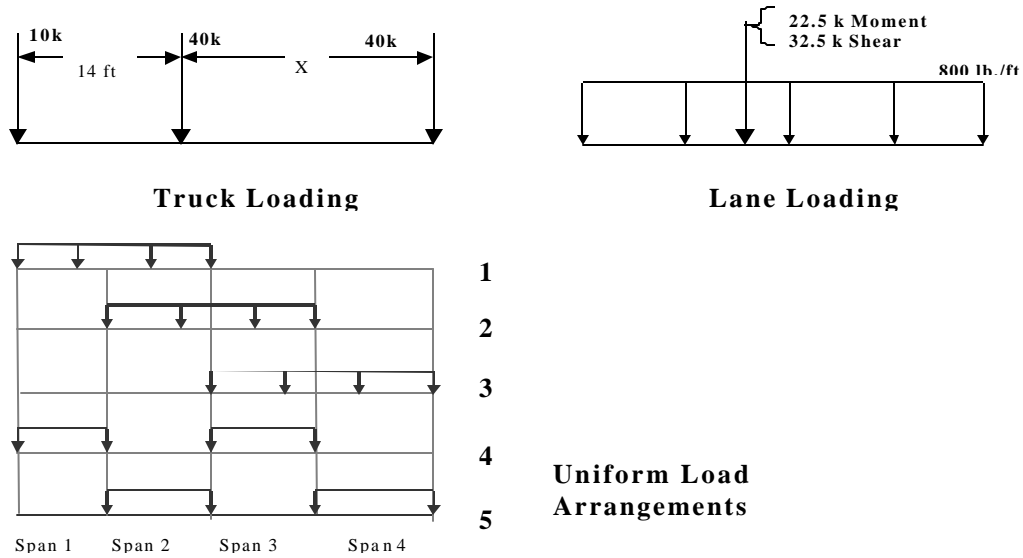
### *verification of shear force and moment envelopes*

MoDOT uses an in-house software, BR200 (MoDOT, 1998), for the analysis of bridge loading. Results from this software were independently verified using another similar software developed at UMC by Hiley (1994). Data from the HPC bridge (Eatherton, 1999, Gopalaratnam and Eatherton, 2001) was used for this verification since detailed information was readily available. The procedures used and the results from the analyses are presented and discussed in this section.

**Analysis Method for Continuous Bridges.** The HPC bridge is composed of four spans (51', 82', 82', and 66' (15.6, 25.0, 25.0, 20.1 m)) designated Span 12, Span 23, Span 34 and Span 45, respectively. The design principle for multi-span bridges that are made continuous for live load is based on a two step approach: (1) The girders are analyzed as simple spans for self weight and weight of the slab, and (2) The girders are analyzed as fully continuous using design live loads, and dead loads due to barrier curb and future wearing surface.

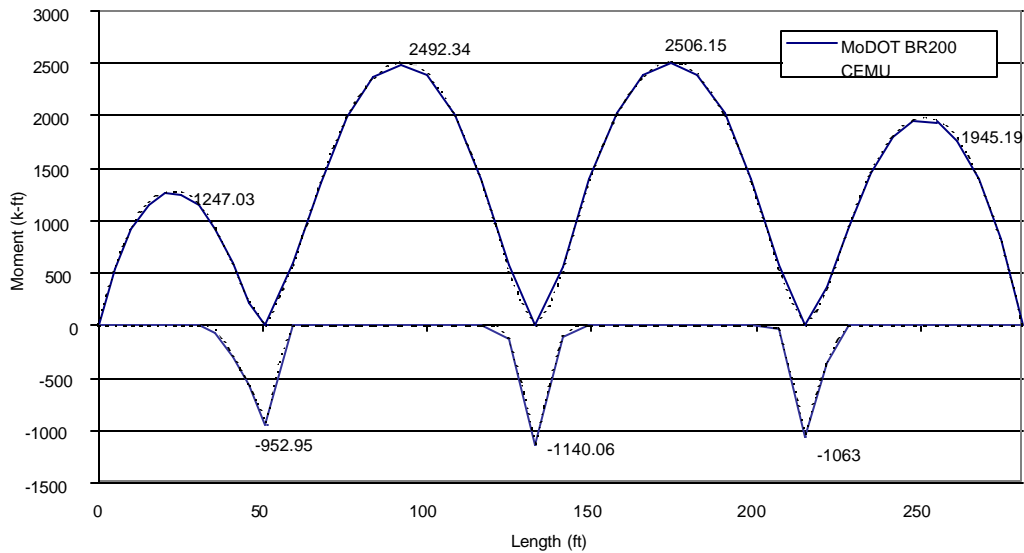
**AASHTO Loading.** In order to be sure that the design loads were applied according to AASHTO (1996) specifications, the bridge was analyzed using another program that allows the user to input all of the load combinations specified in AASHTO individually. The program used was CEMU, developed by Hiley (1994). This program uses the stiffness method to generate shear and moment envelopes. The specified loading, HS-20 Modified (HS-25), was used and is summarized in Figure 4.1. The distance "x" used in the truck loading was found by incrementally decreasing it from the maximum allowable (30 ft, 9.2 m) until a maximum moment was reached. It was determined that the minimum value (14 ft, 4.3 m) produced the greatest moments. When using equivalent lane loads, AASHTO (1996) specifies (Section 3.11.3) that two concentrated loads be applied such that the maximum negative moment is created. The required location of these loads was found by analyzing the bridge with adjacent spans loaded only with the uniform load. The location of the maximum positive moments is where the concentrated loads should be placed. This method is easily verified using simple structural analysis.

Finally, the maximum value from all of the load combinations was taken and the impact factor was applied. As illustrated in Figure 4.2. and Figure 4.3., it can be seen that BR200's output for moment and shear force envelopes, respectively, nearly identically matches those obtained using CEMU.



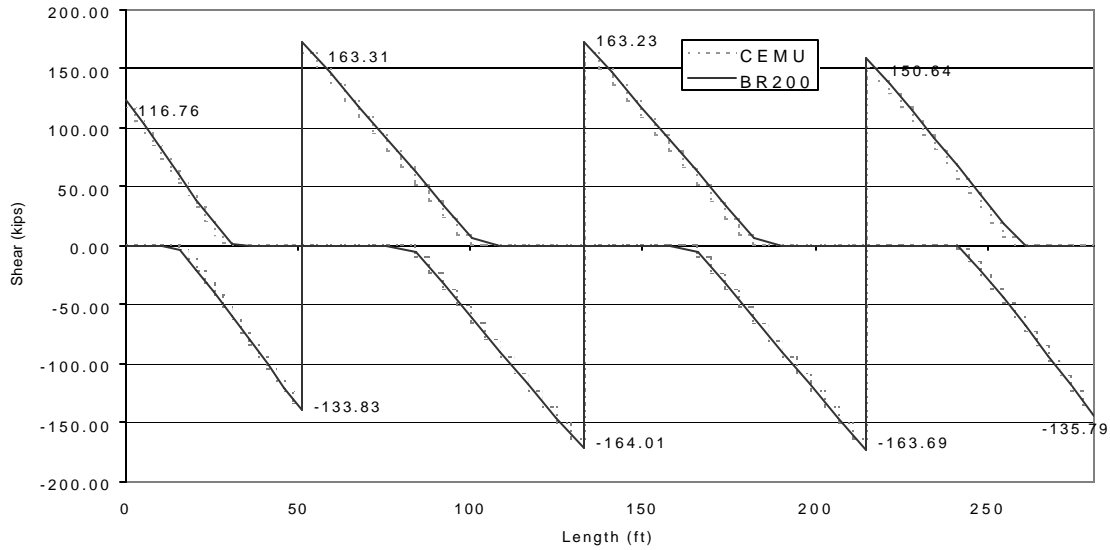
Note: 1 kip = 4.4 kN, 1 lb/ft = 1.3 kN/m

**Figure 0.1 AASHTO HS-20 Modified Live Loads and Load Configurations**



Note: 1 k-ft = 1.4 kN-m, 1 ft = 0.3048 m

**Figure 0.2 Comparison of Moment Envelopes from BR200 and CEMU**



Note: 1 k = 4.4 kN, 1 ft = 0.3048 m

**Figure 0.3 Comparison of Shear Force Envelopes from BR200 and CEMU**

*calculation of shear stresses in uncracked, elastic girder*

**Analysis Method.** In order to evaluate the potential for diagonal tension forces causing cracking, an uncracked elastic analysis was performed. This analysis is based upon a simple two-dimensional application of Mohr's Circle. An element was taken at the centroid of each girder at a distance "d/2" and "d" away from the end, which are the critical sections for shear stress induced cracking. The shear stress at any depth, computed using elastic analysis is given by:

$$v = \frac{V \cdot Q}{I \cdot t} \quad (4.1)$$

The axial compression due to prestressing can be determined at any depth "y" from centric and eccentric contributions to the normal stress:

$$s_h = \frac{P}{A} + \frac{Pe \cdot y}{I} \quad (4.2)$$

Figure 4.4 shows the stress state of the element and its Mohr's circle representation.

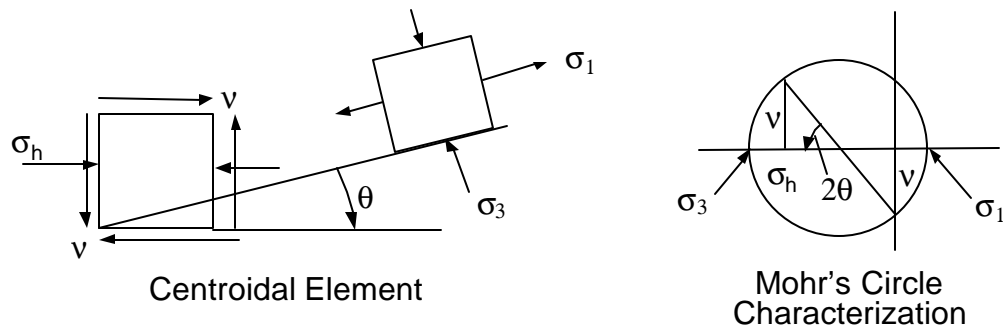


**Figure 0.4 Element at Girder Centroid and Mohr's Circle Characterization of This Stress State**

**Results.** Using the analysis method described above and using unfactored service loads, the principal stresses and their orientation were found for each critical section of the interior girders of the HPC bridge. Interior girders were chosen since they have greater shear loading than the exterior girders. Results are presented in Table 4.1. It can be observed that the maximum tensile stress is around 230 psi (1.7 MPa). The modulus of rupture is assumed to be  $7.5\sqrt{f'_c}$ . Depending upon the concrete compressive strength, the modulus of rupture for concrete can typically vary in the range of 500-750 psi (3.5 – 5.3 Mpa). So the diagonal tension stress under service loads by itself may not be adequate to cause cracking. There is however, potential that the diagonal tension may act in combination with other forces to produce shear-type cracking (for example, stress from service temperature variations, time dependent loads from creep and shrinkage, and residual stress from early-age loading).

#### ***Comparison of required vertical reinforcement***

In order to determine whether enough vertical shear reinforcement was used to ensure ultimate strength, the required vertical shear reinforcement output from BR200 was compared to the reinforcement required based upon the AASHTO design code (1996), and the ACI Building Code (1995). It was found that the output from BR200 is conservative compared with both methods (Figure 4.5).

**AASHTO Method.** The 1979 AASHTO method was used for determining shear reinforcement requirements. The procedures described in this edition are used in the BR200 Code and hence comparisons of the two designs are appropriate.

**Table 0.1 Diagonal Tension ( $S_1$ ) and Inclination of Principal Direction ( $q$ ) for the Interior Girders at Critical Shear Locations**

Location*	Shear stress $v$ (psi)	Axial compression at the centroid $\sigma_h$ (psi)	Principal Tension $\sigma_1$ (psi)	Principal Compression $\sigma_3$ (psi)	Principal Direction, $\theta$ (degrees)
Span 12 (1h/2)	417	-770	183	-953	23.7
Span 12 (1h)	383	-770	158	-928	22.4
Span 12 (2h)	449	-770	206	-976	24.7
Span 12 (2h/2)	479	-770	229	-999	25.6
Span 23 (2h/2)	501	-1345	166	-1511	18.3
Span 23 (2h)	475	-1345	151	-1496	17.6
Span 23 (3h)	475	-1345	151	-1496	17.6
Span 23 (3h/2)	502	-1345	166	-1512	18.4
Span 34 (3h/2)	505	-1345	168	-1514	18.4
Span 34 (3h)	479	-1345	153	-1498	17.7
Span 34 (4h)	478	-1345	152	-1498	17.7
Span 34 (4h/2)	504	-1345	168	-1513	18.4
Span 45 (4h/2)	460	-960	185	-1144	21.9
Span 45 (4h)	433	-960	167	-1126	21.0
Span 45 (5h)	370	-960	126	-1086	18.8
Span 45 (5h/2)	402	-960	146	-1106	19.9

\* Span 12 (51'), Span 23 (82'), Span 34 (82'), Span 45 (66'). The first number within brackets in the table refers to the proximity to the numbered end. h/2 and h refer to distance from the end for the cross-section under consideration, where h is the depth of the girder Note: 1 psi = 6.89 kPa

This method is listed in the current AASHTO (1996) as an alternative (Section 9.20).

This method is simpler than the current AASHTO code in that the shear contribution of the concrete does not account for shear and moment interaction or the contribution of vertical prestressing. The concrete shear capacity in the 1979 AASHTO code is a function of the area in shear,  $b'jd$ . The newer version, however, is less conservative than the 1979 version. The 1979 procedure is to first find the factored applied shear force,  $V_u$ :

$$\phi V_N = V_u \text{ where } : V_u = 1.3(V_D + 1.67V_{L+I}), \Phi = 0.9. \quad (4.3)$$

Now the area of steel required can be computed using:

$$A_v = \frac{(V_N - V_C) \cdot s}{2f_{sy}jd}. \quad (4.4)$$

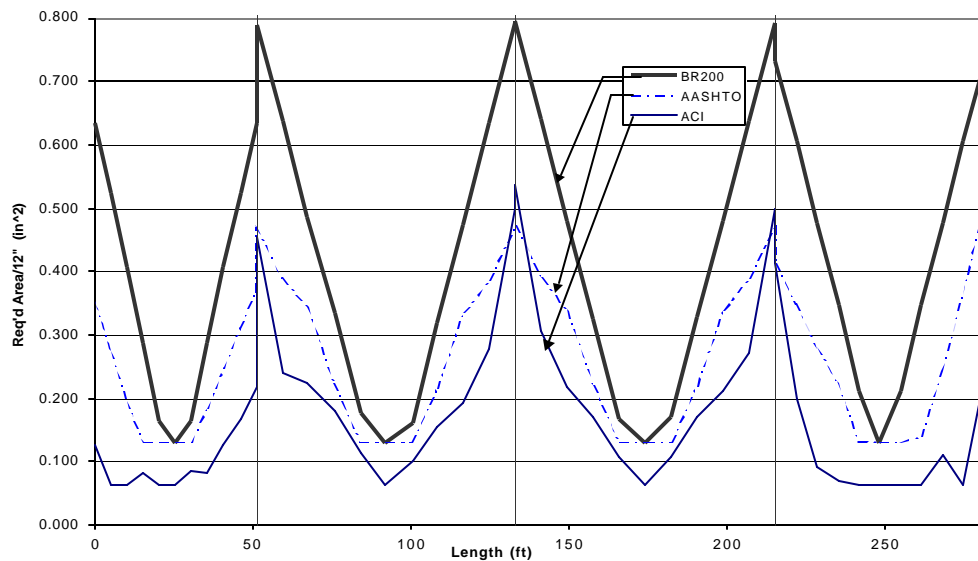
$V_C$  is the portion of the of the shear resistance provided by the concrete and is found as:

$$V_C = 180b'jd \text{ for } f'c \geq 3,000 \text{ psi.} \quad (4.5)$$

The results of this analysis are shown in Figure 4.5. It can be seen, in general, that the BR200 solution for stirrup design is conservative compared to the AASHTO design procedure. Some discrepancies do

exist between the two methods. BR200 makes assumptions about the moment arm, “jd”, that are somewhat different from an exact analysis. Finally, in the negative moment regions, BR200 doubles the required area of reinforcement.

**ACI Method.** The ACI Building Code (1995) was used to calculate the area of shear for comparison purposes. This method is significantly less conservative than the 1979 AASHTO Code. It addresses the influence of shear and moment interaction on the shear resistance provided by concrete. It also includes the two types of shear cracking, web and flexural shear cracking. This procedure resulted in stirrup reinforcement areas that are smaller than 1979 AASHTO requirements. It should however be noted that ACI shear design procedures are not specifically intended for bridge girder design, but are nearly identical to the current AASHTO procedure. Figure 4.5 also includes results from the ACI design procedure for stirrup design.



Note: 1 ft = 0.3048 m, 1 in<sup>2</sup> = 645.2 mm<sup>2</sup>

**Figure 0.5 Area of Stirrup Reinforcement required per 12” Length According to ACI, AASHTO and BR200 Guidelines**

## EARLY-AGE CRACKING

V. S. Gopalaratnam and T. P. Earney

### *STRESSES DUE TO PRESTRESS TRANSFER*

It was decided early in the project that the stresses due to the transfer of the prestressing force should be included in the investigation of early-age cracking since they contribute to the vertical tensile stresses in the ends of the girders. Gergely and Sozen (1967) developed a model to determine the end stresses in post-tensioned girders, which is, with modifications, applicable to the case of pre-tensioned girders. The original model will be presented, followed by the modifications that were made based upon observations during this project and available experimental data. Finally, the results from this analysis and their implications on design are presented.

**Gergely - Sozen Model.** A model to evaluate the vertical stresses created in the end of a girder due the transfer of the prestressing force was developed by Gergely and Sozen (1967). The model, shown in Figure 5.1, is used to demonstrate that the release of the prestressing strands produces tensile stresses at the girder-ends due to an unbalanced moment in a free body of the bottom of the girder-ends. Concrete at this location is therefore subjected to tensile stress. Consider the free body of the bottom of the girder-end, Figure 5.1. The concentrated force from the prestressing strands cannot be resisted solely by the normal stresses at the other end of the free body. The resultant unbalanced moment required for equilibrium on the top face of the free body generates tensile stress in the concrete at the girder-end near the junction between the web and the bottom flange. The model assumes that the maximum vertical stress will occur at the top of the bottom flange bulb when the length of the section is equal to the height of the girder.

**Modified Gergely - Sozen Model.** As was alluded to above, the Gergely and Sozen model includes assumptions that may not be valid based on the experimental data gathered from a companion investigation (Eatherton, 1999, Gopalaratnam and Eatherton, 2001). It was assumed that the stress would be a maximum at the top of the bottom flange bulb. It was observed, however, in the girders that exhibited horizontal cracking, that the cracks were higher in the web than this (Figure 1.4b). By solving for the unbalanced moment as a function of the amount of web included in the section, it can be

shown that the maximum moment occurs higher in the web. This model is shown in Figure 5.2 with the unknown depth above the bottom flange bulb labeled “y”. The unbalanced moment is solved in terms of “y”.

$$M = P(y + h_f - y_{ps}) - C(y + h_f - y_f) - \left( s_f - \frac{y}{3m} \right) y^2 \frac{t_w}{2} \quad (5.1)$$

Computing the first derivative of Equation 5.1 and setting it equal to zero allows one to establish the depth at which the moment reaches a maximum value. This depth is given by:

$$y = \frac{s_f \cdot t_w \pm \sqrt{(s_f \cdot t_w)^2 - 2 \frac{t_w}{m} (P - C)}}{\frac{t_w}{m}} \quad (5.2)$$

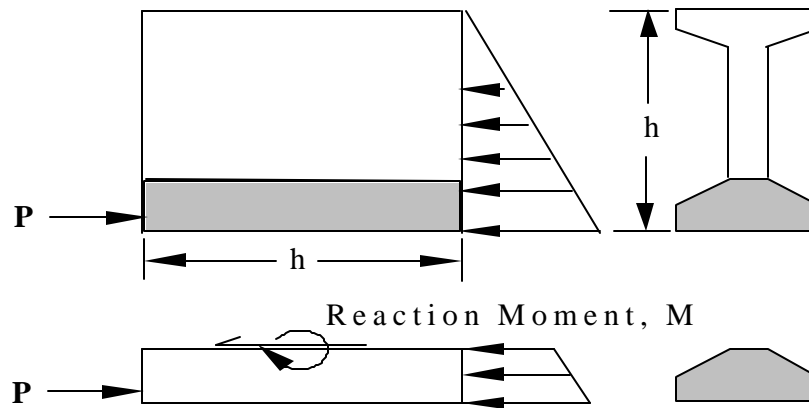


**Figure 0.1 Gergely - Sozen Model for Determining Girder-End Vertical Stress Due to Prestress Transfer**

In order to find the stress in the girder-end due to this moment, a length of girder must be used (labeled “x” in Figure 5.2). Gergely and Sozen had suggested that “x” be assumed equal to the total height of the girder. For a pretensioned girder, it is expected that this length should at least be equal to the transfer length. Since data from stirrup strains during prestress transfer operations for the High Performance Concrete (HPC) Bridge project (Eatherton, 1999, Gopalaratnam and Eatherton, 2001) was readily available, it was possible to evaluate the Gergely - Sozen recommendation for girder length to be considered.

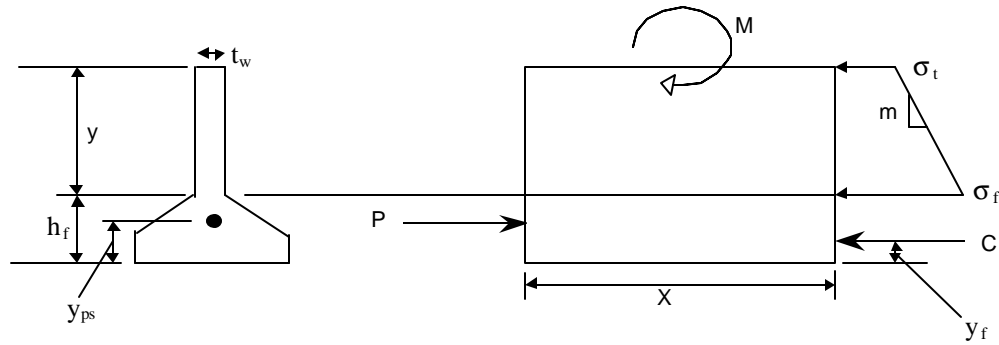


**Figure 0.2 Modified Gergely - Sozen Model**

Two stirrups were instrumented in the ends of each of the four girders, Figure 5.3. One stirrup is located a distance “h/2” from the end of the girder, and the second is located “h” from the end. Additionally, these stirrups are each instrumented at two locations along the height of the stirrup. The strains at “h/2”- and “h” -away were opposite in sign suggesting that the point of “zero-strain” occurs somewhere between these two locations. As illustrated in Figure 5.4, this point of “zero-strain” is located “x/2” from the end for the Gergely - Sozen model. Due to the limited number of experimental data points, the influence of girder geometry, prestressing force used, prestressing profile, and transfer length on the location of “x” cannot be ascertained for a general case. However, for Type VI MoDOT girders used in the HPC project, this location can be established experimentally from the data available.

**Table 0.1 Experimental Determination of “Zero-Strain” Location from Stirrup Strain Data**

Gage Location	Strain at h/2 (μstr)	Strain at h (μstr)	Location of “zero-strain”, x/2, from girder-end (in)
Top of Short Girder	10.0	-6.0	43.9
Middle of Short Girder	28.0	-25.0	41.3
Top of Long Girder	--	-18.0	--
Middle of Long Girder	15.0	-36.0	34.9

Note: 1 in = 25.4 mm, short girder ≅ 51’ span, long girder ≅ 82’ span

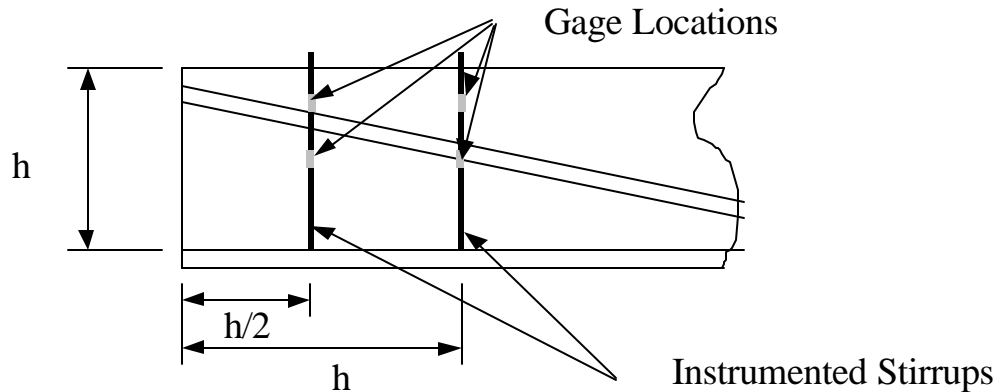


**Figure 0.3 Location of Strain Gages on Stirrups in the HPC Girders**

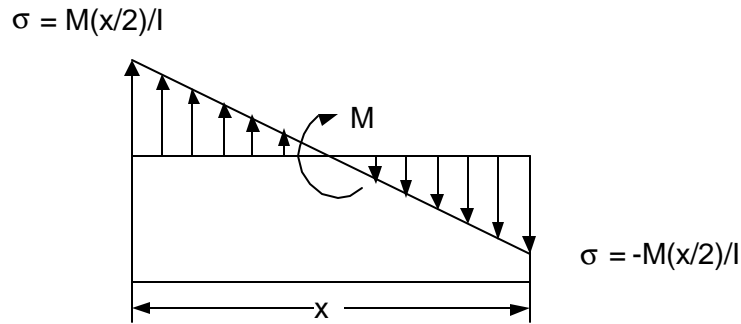


**Figure 0.4 Assumed Stress Distribution from Unbalanced Moment**

The strain data, as well as the calculated distance (based on linear interpolation), “x”, are shown in Table 5.1. If the Gergely - Sozen assumption is used, this distance would be  $h/2 = 27$  inches for both girders. This length is shorter than that computed from experimental measurements of stirrup strain and results in stresses that are significantly higher. Table 5.2 lists the computed values for maximum unbalanced moment for each of these girders, the corresponding location, and the maximum vertical tensile stress produced using the Gergely - Sozen assumption for “x”, as well as the experimentally computed length, “x”.

The maximum tensile stresses in the girder-ends due to prestress transfer (~350 psi, 2.4 MPa) are approximately 40% to 50% of the tensile strength of concrete (~550-750 psi, 3.8 – 5.2 MPa). While these stresses by themselves may not be sufficient to cause cracking, when they are considered in conjunction with the residual tensile stresses due to hydration/curing gradients, discussed in Section 5.2, horizontal girder-end cracking is possible.

**Table 0.2 Maximum Tensile Stress and Location Due To Prestress Transfer Using the Gergely - Sozen Model (1967)**

Girder	Location of Max. Moment, (in.) From Bottom of Girder	Max. Unbalanced Moment (k-in)	Max. Tensile Stress (psi) Experimental Data	Max. Tensile Stress (psi) Gergely - Sozen Model
Long	23.0	2360	349	747
Short	20.4	1749	315	554

Note: 1 in = 25.4 mm, 1 k-in = 16.8 kN-m, 1 psi = 6.89 kPa

***RESIDUAL STRESSES FROM FINITE ELEMENT ANALYSIS OF EARLY-AGE BEHAVIOR***

In order to determine the effects that thermal expansion and hardening have on producing residual stresses in the concrete during curing, a finite element model was created and solved using ANSYS Version 5.4 (1999). The restrained movement of the girder inside the steel form is modeled using typical temperature gradients to produce residual stress profiles. The model properties and boundary conditions are discussed, followed by a discussion of the thermal gradients used. Next, the analysis procedure is presented. Finally, the residual stress profiles are presented and discussed.

### **Model Properties**

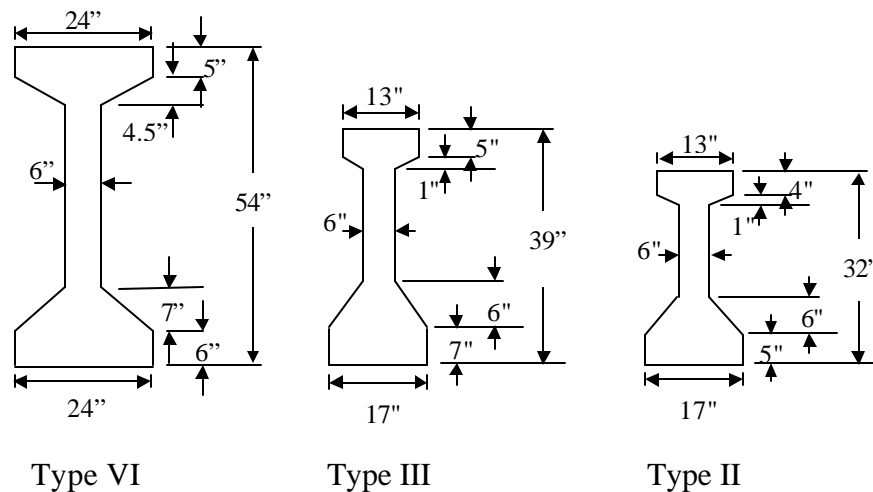
**Elements.** Two types of elements are used in this numerical model. Four-node, two-dimensional plane, structural solid elements were used to model both the concrete and the steel mold. Two-node, two-dimensional, point-to-point contact elements were used to model the interface between the concrete and the steel mold.

For the plane elements, a plane strain option is chosen, which allows for stress in the z-direction (perpendicular to the cross section) while the strain in the z-direction is assumed to be zero. These elements have two degrees of freedom at each node: x- and y-direction displacements. Small displacement theory is used in conjunction with linear elastic material behavior. The contact elements are incorporated such that they model two surfaces that allow for compressive normal forces as well as frictional sliding forces, but do not transfer tensile forces. This allows the concrete to separate from the steel mold preventing any normal tensile force from developing at the steel-concrete interface. The frictional force is calculated as the compressive normal force times the coefficient of friction, " $\mu$ ". The coefficient of friction was assumed as  $\mu = 0.5$ . The normal stiffness must be specified explicitly and is varied in order to achieve convergence. It was found that for these models, a normal stiffness value around one tenth of the modulus of elasticity of the concrete was required (which is in the range recommended by ANSYS (1999)).

**Model Geometry and Meshing.** Late in the project, it was decided that it would be desirable to create stress profiles for three types of girders, a Type VI (as originally proposed) and, additionally Type II and Type III girders. Two types of concrete, HPC and Normal Strength Concrete (NSC) were studied. HPC has design strength of 10,000 psi (70 MPa), while NSC's is 6,000 psi (42 MPa). This would give a representative range of residual stresses in the different types of girders used in Missouri and facilitate design computations of Type III girders in the companion UMR study. The mesh was

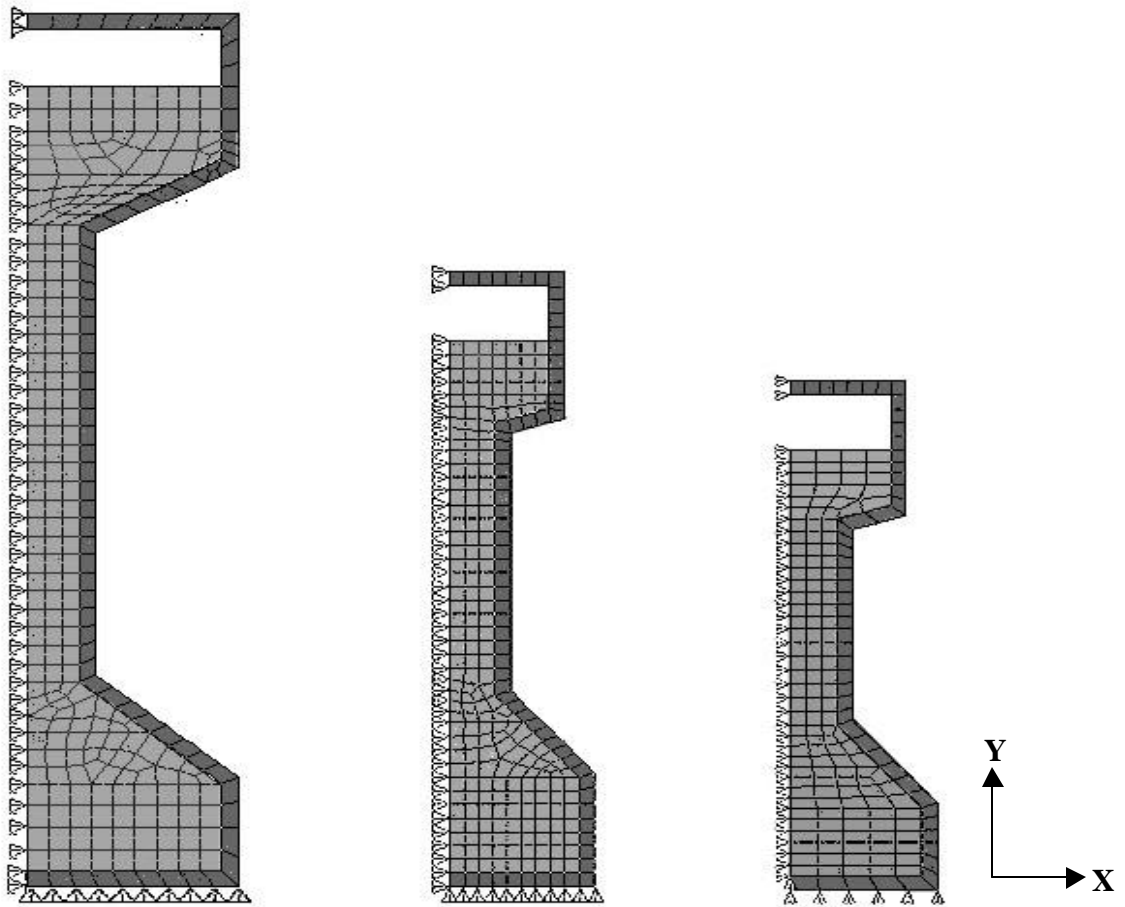
created to preserve as nearly as possible an aspect ratio of 1:1 for the plane elements. In all cases, mesh refinement studies were conducted to establish that mesh size had little influence on the stress solutions. Figure 5.5 shows the girder dimensions for the all three types of girders, and Figure 5.6 shows the element mesh for the girders. The steel mold is one inch (25.4 mm) thick, which, with modifications to the web steel properties accounts for the additional stiffness provided by the stiffeners on the sides of the mold. The top brace on the model is to simulate the bracing used to prevent the form from splaying open. This bracing is located 4 inches (101.6 mm) above the top of the concrete (Figure 5.6).

**Boundary Conditions and Loads.** The boundary conditions were chosen to model the girder sitting on a rigid platform, and to reflect the symmetry of the cross-section. This was done by restraining vertical movement of nodes along the bottom edge of the form and by restraining horizontal movement of nodes along the centerline of the girder cross-section (Figure 5.6).



NOTE: 1 in = 25.4 mm

**Figure 0.5 Dimensions of MoDOT Girder Types Used in the Finite Element Models**

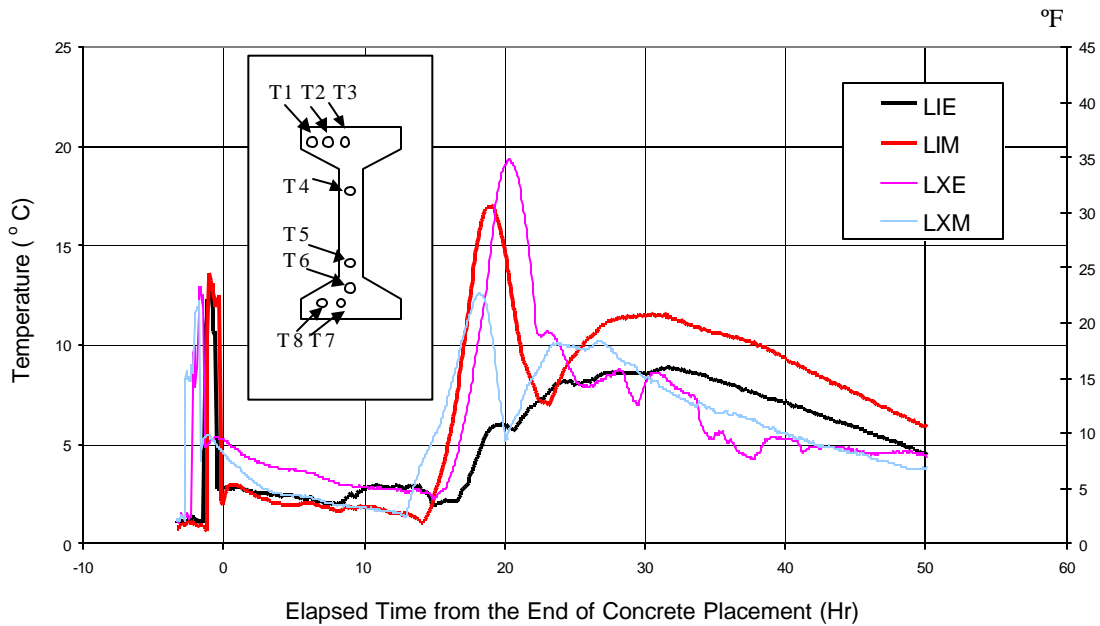


NOTE: Steel mold is shown in a darker shade

### Figure 0.6 Finite Element Mesh and Boundary Conditions for Girder Models

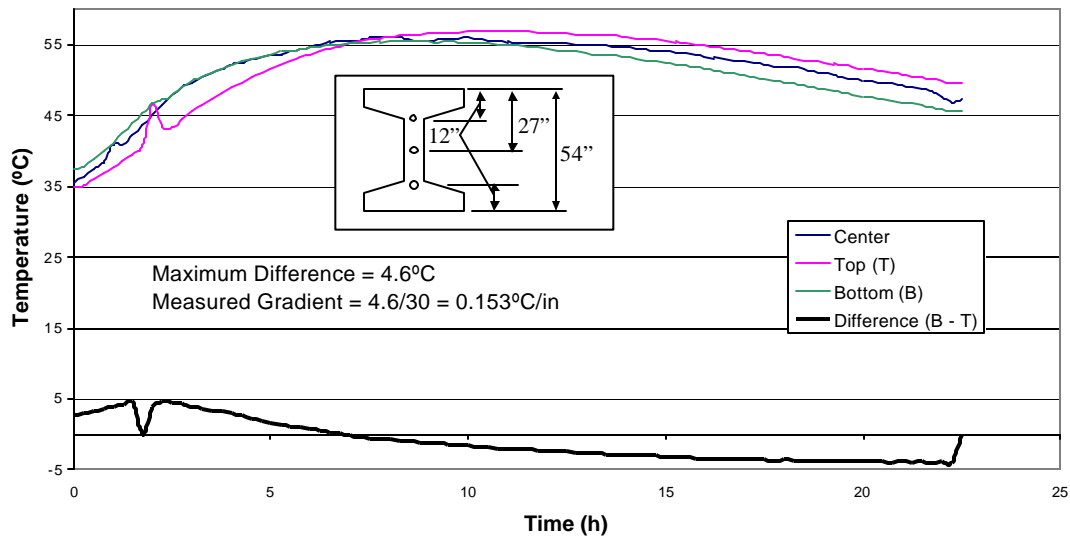
The model is subjected to thermal loading and loading due to self-weight. Unit weights of  $150 \text{ lb/ft}^3$  ( $23.6 \text{ kN/m}^3$ ) for the concrete and  $490 \text{ lb/ft}^3$  ( $76.9 \text{ kN/m}^3$ ) for the steel were used. The temperature values were based on experimental data recorded during curing of the girders for the HPC bridge (Eatherton, 1999, Gopalaratnam and Eatherton, 2001) and its companion bridge's girders, made of NSC (Chojnacki, 1999).

Figure 5.7 shows the experimentally measured temperature difference for four HPC girder cross-sections. The values plotted are the absolute maximum difference in temperature among eight thermocouples (locations shown in the inset to the figure) at each of two cross sections in the two (of the four) instrumented girders: one cross-section at midspan, and one at the end. Figure 5.8 shows the temperature development and the maximum difference observed between the top and bottom thermocouples of the NSC girders using data collected by MoDOT (Chojnacki, 1999). Thermal gradients measured experimentally from the NSC girders were extrapolated linearly to the total depth of the girder. This was necessary because of differences in the location of temperature measurements between the HPC and NSC girders (see insets in Figures 5.7 and 5.8).



NOTE: (Data from UMC for HPC Girders (Eatherton, 1999, and Gopalaratnam and Eatherton 2001)). Inset legend: L: Long girder, I: Interior girder, X: Exterior girder, E: Cross-section near end, M: Cross-section at midspan.  $\Delta 1\text{ }^{\circ}\text{F} = \Delta 1.8\text{ }^{\circ}\text{C}$

**Figure 0.7 Maximum Difference in Temperatures at a Cross-section**



NOTE: Data from Chojnacki (1999),  $\Delta 1\text{ }^{\circ}\text{F} = \Delta 1.8\text{ }^{\circ}\text{C}$ ,  $1\text{ }^{\circ}\text{F} = 1.8\text{ }^{\circ}\text{C} + 32$

**Figure 0.8 Heat Development (Top) And Maximum Difference in Temperatures at a Cross-section for Normal Strength Girders**

Based upon the data in Figures 5.7 and 5.8 it was decided to use a maximum temperature differential of 20°C (68°F) for the Type VI HPC girder and 8°C (46°F) for the Type VI NSC girder, linearly distributed along girder depth. The thermal gradients used for Type II and Type III girders were identical to the gradient used for Type VI girders (temperature difference between top and bottom of the girder proportional to girder depth).

**Loading Procedure.** In order to keep the finite element model as simple as possible, assumptions were made about the behavior of the curing concrete under temperature loading. It was decided that a single load step would be used. When concrete cures, its stiffness increases with time. During the time when the steam curing is started (about 12 hours after casting), the concrete has a relatively low stiffness. Using the equations (Equation 5.3-5.4) proposed by Branson (1977), shown below, the 12-hour modulus of elasticity is about 60% of the 28-day modulus of elasticity. The 12-hour modulus is  $2.6 \times 10^6$  psi (18.2 GPa), and the 28-day modulus is  $4.4 \times 10^6$  psi (30.8 GPa) for normal strength concrete. For HPC, these modulus values are  $3.3 \times 10^6$  psi (23.1 GPa), and  $5.7 \times 10^6$  psi (39.9 GPa), respectively.

$$(f'_c)_t = \frac{t}{1.00 + .95t} (f'_c)_{28d} \quad (5.3)$$

$$E_{c_t} = 57000 \sqrt{(f'_c)_t} \quad (5.4)$$

When examining the temperature history shown in Figures 5.7 and 5.8, it can be seen that the temperature increase occurs very early in the life of the girder. The temperature does not return to “near ambient” conditions until approximately 42-72 hours. Thus, the thermal expansion occurs when the concrete is not very stiff. Also since the steel mold has a higher coefficient of thermal expansion (Table 5.4), it produces no significant restraint during this time. Both of these influences, it is assumed, result in little accumulation of residual stress in concrete during this time. When cooling takes place, the hardened concrete behaves in a relatively stiff manner.

Based on these observations and assumptions, residual stress profiles were generated for the cooling portion of the early-age response. This was accomplished by applying a drop in nodal temperatures to replicate the experimentally measured change in temperatures from the maximum temperatures back to ambient temperature. For NSC and HPC, the maximum top flange temperature was found to be 10°C (50°F) above the ambient temperature. Thus, the nodal temperature drop applied to the Type VI NSC model ranged from 10°C (50°F) at the top of the girder to 15°C at the bottom. For the Type VI HPC, the range was from 10°C to 30°C (50°F to 86°F). Table 5.3 summarizes the temperature loading applied to all of the girders. For the smaller girders (Types II and III), the gradient was kept the same and the bottom flange value was proportionately scaled to reflect the shorter height of the girder.

**Table 0.3 Applied Temperature Drop Used in the Finite Elements Analysis of Early-Age Behavior of Prestressed Concrete I-Girders**

Girder Type	Type II		Type III		Type VI	
	HPC	NSC	HPC	NSC	HPC	NSC
Top Fiber, °C	10	10	10	10	10	10
Bottom Fiber, °C	22	15	24	16	30	18

NOTE: 1 °F = 1.8°C +32

**Material Properties.** The material properties needed to perform the analysis are listed in Table 5.4. These properties were all taken from Bever, (1986) except as noted in the footnote to the table. The elastic modulus value for concrete is based on a 3-day age. The curing process for the HPC girders for which the analysis has been completed typically takes between 2-3 days. Use of a 3-day elastic modulus would thus represent a conservative value of stiffness (higher magnitudes of residual stress). Web steel properties have been adjusted to include the effect of stiffeners provided in the web along the sides of the mold.

**Table 0.4 Material Properties Used in Finite Element Analysis**

Material	Poisson's Ratio, $\nu$	Unit Weight, $\gamma$ , (pcf)	Thermal coefficient of expansion, $\alpha$ , (in/in/°C)	Young's Modulus, E, (psi)
HPC	.15	150	$9.9 \times 10^{-6}$	$5.0 \times 10^6$ *
NSC	.15	150	$9.9 \times 10^{-6}$	$3.9 \times 10^6$ *
Steel	.30	490	$11.7 \times 10^{-6}$	$30 \times 10^6$
Steel in web	.30	490	$11.7 \times 10^{-6}$	$90 \times 10^6$

\*Values found using Branson (1977) method. 1 lb/ft<sup>3</sup> = 157 N/m<sup>3</sup>,  
1 in/in/°C = 1.8 in/in/°F, 1 psi = 6.89 kPa

**Stress Profiles.** For each model a principal stress contour plot (tension assumed positive) showing the entire cross section and a close-up of the region of maximum stress is included (Figs 5.9 through 5.14). Generally, the location of maximum tensile stress was observed to be at the reentrant corner at the junction of the web and the top or bottom flange bulbs. These figures and the accompanying tables of results (Tables 5.5 through 5.7) show stresses in the y-direction of the girder. This is the direction from top flange to bottom flange. Due to the nature of the analysis, it is not possible to predict the stresses in other directions.

The orientation of the principal stresses is not shown in Figures 5.9 through 5.14. However, for every case it was found that the principal tensile stresses in the concrete act in a direction parallel to the

contour of the mold. This observation is consistent with early-age cracks observed after the HPC girders were cured and the prestressing force transferred. Tables 5.5 through 5.7 provide a statistical summary of the nodal stresses for each girder type.

**High Performance Concrete.** Expectedly, the stress levels for the high performance concrete were higher in all cases than the stresses on the same cross section with normal strength concrete. This is a combined effect of higher temperatures and a higher modulus of elasticity. For the Type VI girder, the maximum stress is 437 psi (3.0 MPa) and is located near the bottom flange. For the Type III girder, a maximum stress of 360 psi (2.5 MPa) was achieved near the bottom flange, and in the Type II the maximum stress was 162 psi (1.1 MPa), located near the top flange.

**Normal Strength Concrete.** Principal stress values are 40%- 50% lower for all of the NSC models compared to the HPC. For the Type VI girder, the maximum stress is 237 psi (1.6 MPa), located near the bottom flange. For Type III the maximum stress is 143 psi (1.0 MPa) and is located near the top flange. In Type II girder, the maximum stress in the region of the bottom flange is about 63 psi (0.4 MPa).

**Table 0.5 Residual Stress Distribution for Type II Girders**

Parameter	High Performance Concrete		Normal Strength Concrete	
	$\sigma_p$ (psi)	$\sigma_{yy}$ (psi)	$\sigma_p$ (psi)	$\sigma_{yy}$ (psi)
Max. Stress	162	121	63	51
Min Stress	-51	-119	-27	-82
Avg. Stress	39	30	13	7
Median Stress	38	32	12	8
Std. Dev.	34	39	12	14

NOTE: 1 psi = 6.89 kPa

**Table 0.6 Residual Stress Distribution for Type III Girders**

Parameter	High Performance Concrete		Normal Strength Concrete	
	$\sigma_p$ (psi)	$\sigma_{yy}$ (psi)	$\sigma_p$ (psi)	$\sigma_{yy}$ (psi)
Max. Stress	360	234	143	138
Min Stress	-62	-233	-30	-86
Avg. Stress	65	35	24	10
Median Stress	69	34	31	8
Std. Dev.	52	58	37	19

NOTE: 1 psi = 6.89 kPa

**Table 0.7 Residual Stress Distribution for Type VI Girders**

Parameter	High Performance Concrete		Normal Strength Concrete	
	$\sigma_p$ (psi)	$\sigma_{yy}$ (psi)	$\sigma_p$ (psi)	$\sigma_{yy}$ (psi)
Max. Stress	437	359	237	189
Min Stress	-48	-312	-36	-262
Avg. Stress	108	80	68	47
Median Stress	111	66	79	42
Std. Dev.	80	95	47	57

NOTE: 1 psi = 6.89

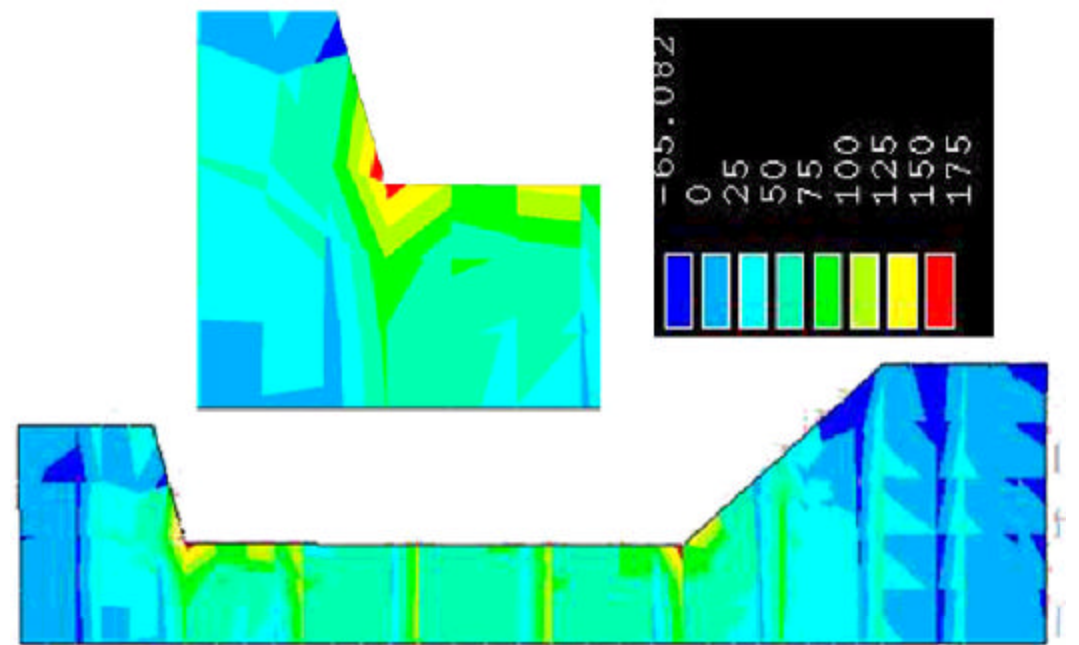
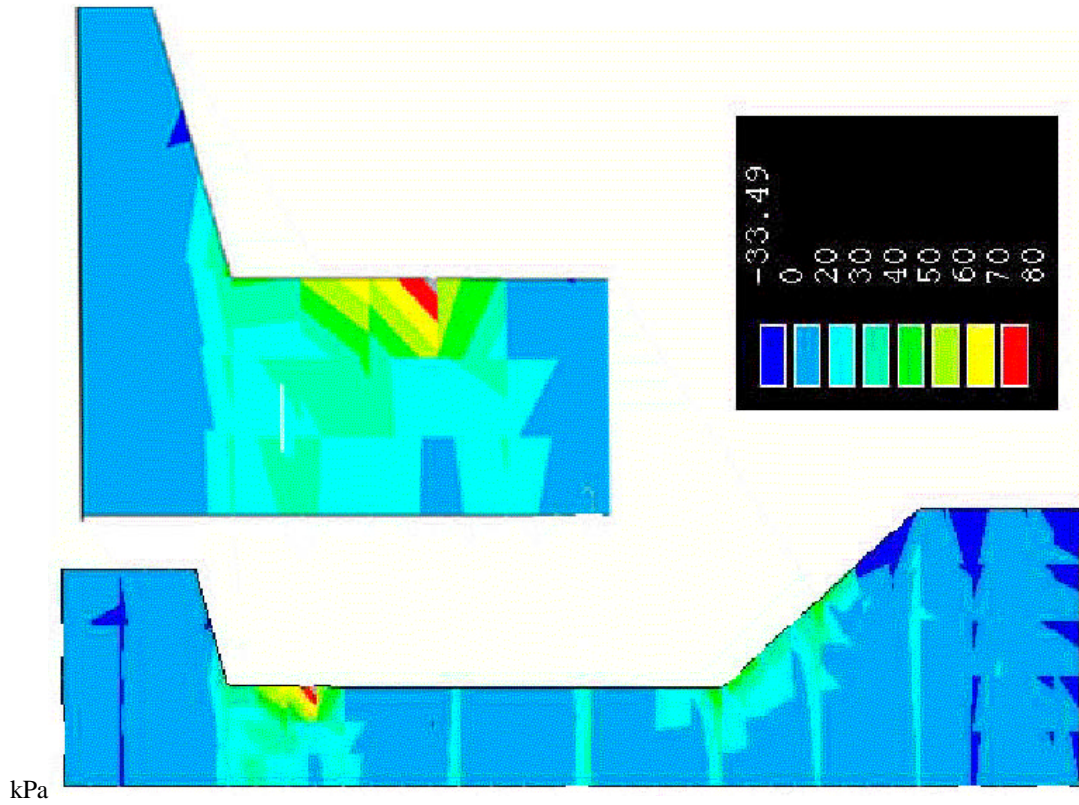
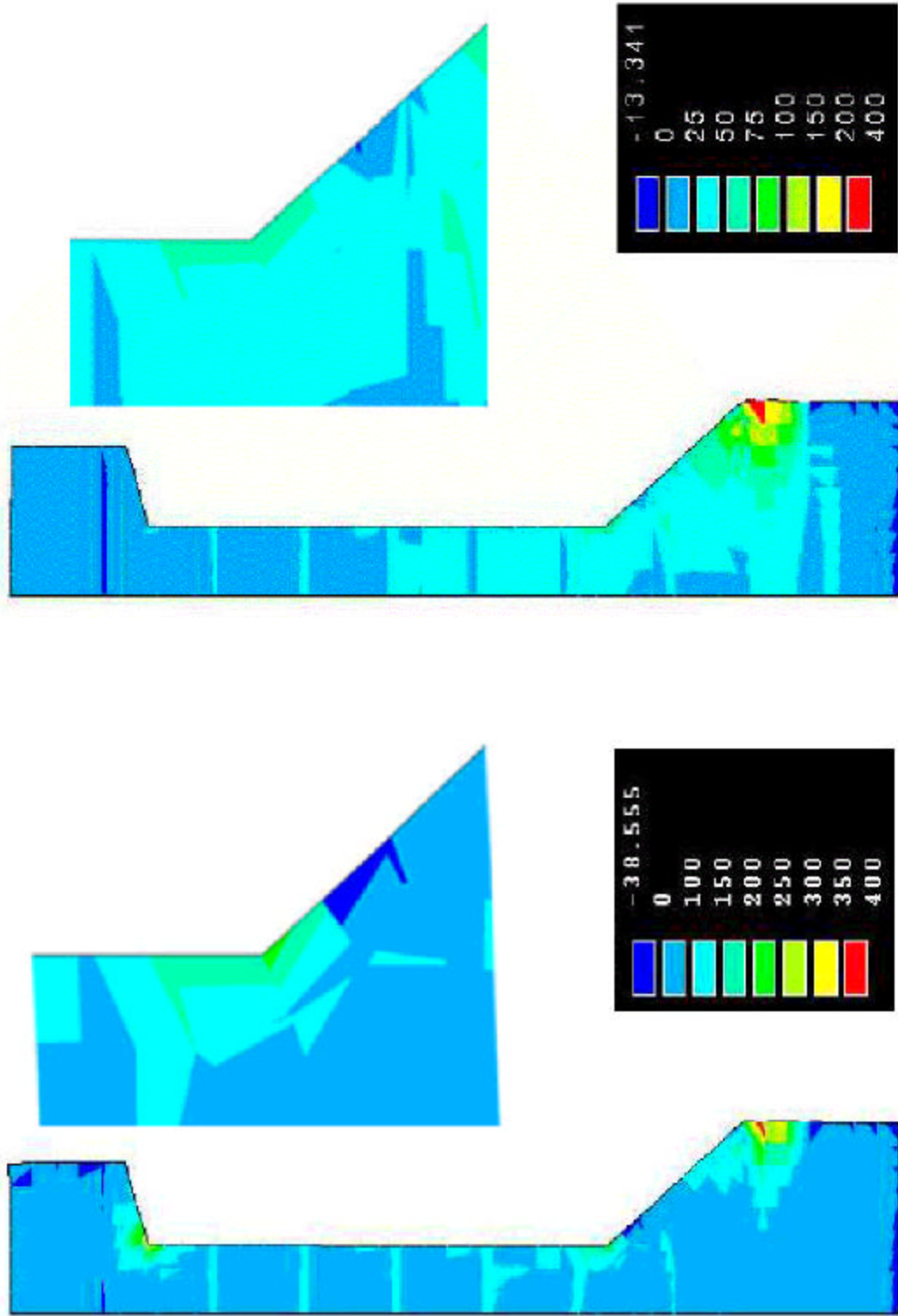


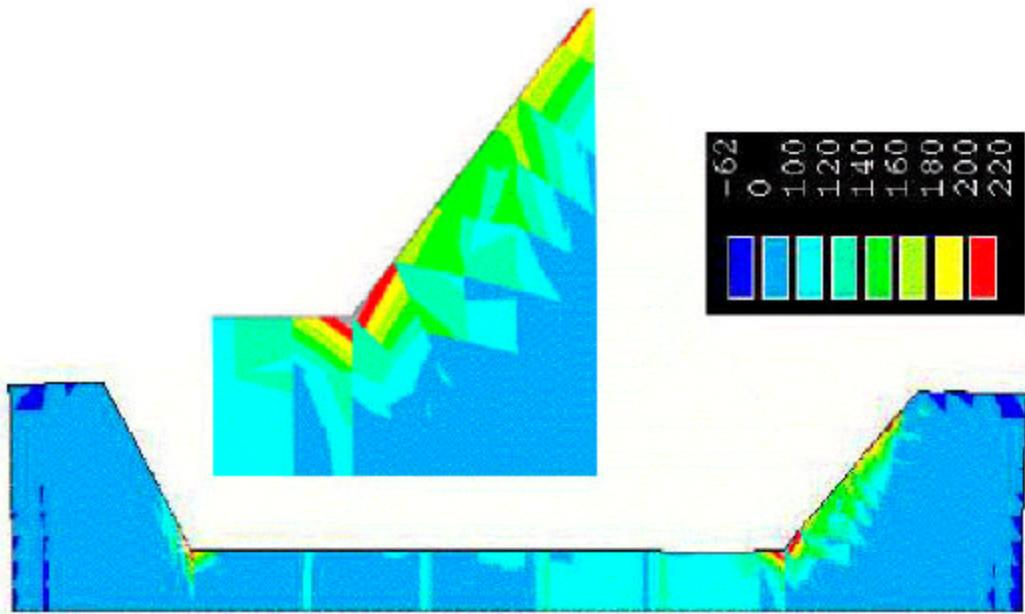
Figure 5.9 Residual Stress Profile for HPC Type II Girder (psi) Figure 5.10 Residual Stress Profile for NSC Type II Girder (psi)



NOTE: 1 psi = 6.89 kPa

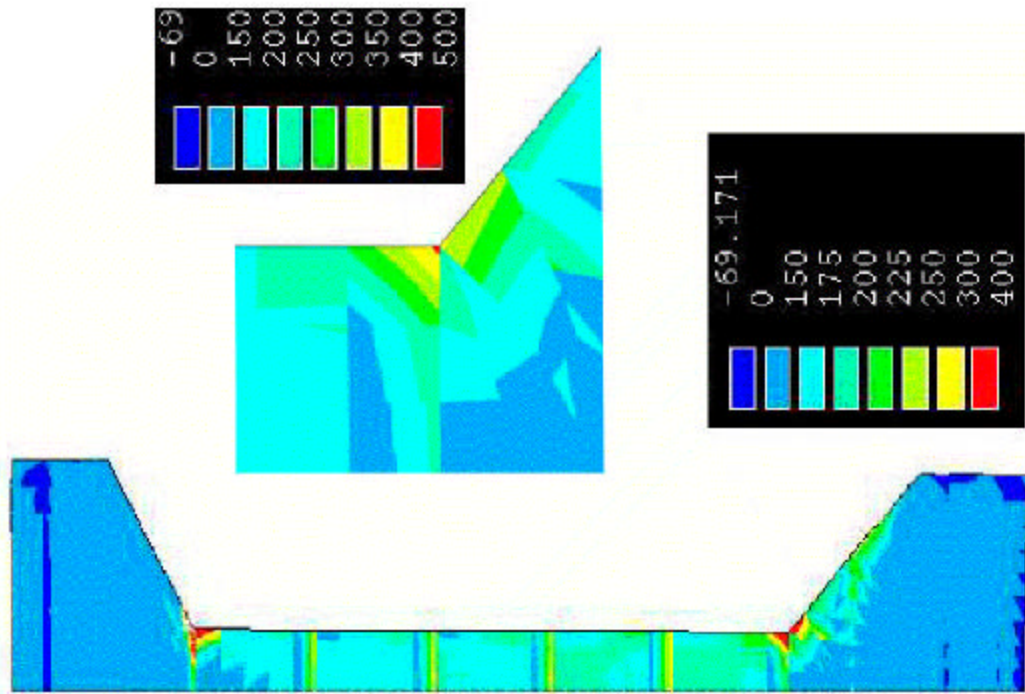
NOTE: 1 psi = 6.89 kPa

**Figure 5.11 Residual Stress Profile for HPC Type III Girder (psi)** **Figure 5.12 Residual Stress Profile for NSC Type III Girder (psi)**



NOTE: 1 psi = 6.89 kPa

Figure 5.14 Residual Stress Profile for HPC Type VI Girder (psi)



NOTE: 1 psi = 6.89 kPa

Figure 5.13 Residual Stress Profile for NSC Type VI Girder (psi)

**Table 5.8 Suggested Reductions in Allowable Tensile Stress Due To Residual Stresses from Early-Age Thermal Loading**

Concrete Type	MOR ( $7.5\sqrt{f_c}$ ), psi	Recommended Reduction, psi		
		Type II	Type III	Type VI
HPC	750	73	117	188
NSC	580	25	61	115

NOTE: 1 psi = 6.89 kPa

**Design Implications.** It can be seen in the results that a uniform residual tensile stress is locked into the web of these girders due to early-age thermal loading. The principal stresses in the web are on the order of the average nodal stress plus one standard deviation. Since cracking is most likely to occur in this region, it is necessary that the allowable vertical tensile stress capacity be reduced to account for residual tensile stresses due to early-age thermal loading.

Based upon the numbers and figures presented in this section it is recommended that, for design, the allowable vertical tensile stress be reduced by a value equal to the average principal nodal stress plus one standard deviation. Table 5.8 shows this reduction, as well as typical values for the modulus of rupture (MOR) of concrete (flexural tensile strength). It should be noted that the direct tensile strength (which governs cracking) is typically smaller than the MOR. It can be seen that the recommended reduction in allowable tensile stress is between 10% and 25% of MOR for the HPC girders, and between 5% and 20% of MOR for the NSC girders. These values are not critical by themselves, however when combined with the tensile stresses at girder-ends due to prestress transfer, (Table 5.2) the potential for cracking is greatly increased.

The numerical model was developed to analyze only the in-plane stresses of the cross section during the curing of the girders (while they are still in the forms). The analysis method does not allow for the determination of the horizontal (out of plane) stresses created during this time. It is intended that the vertical tensile stresses found using this model be used solely to evaluate the potential for horizontal cracks to develop during the prestress transfer process as discussed in Section 5.1. The residual vertical tensile stresses act to reduce the effective tensile capacity of the girder concrete to resist the vertical stress at the end cross sections due to the transfer of the prestressing force.

## 6 DIAPHRAM DETAILING

V. S. Gopalaratnam and T. P. Earney

### **6.1 OVERVIEW OF CURRENT PRACTICE**

Many states make precast concrete girder bridges continuous for live load by pouring a continuous deck with monolithic diaphragms at the bents that encase the ends of the girders (Oesterle, et al., 1989). This eliminates the necessity of expansion joints in the slab on top of the bents. Expansion joints pose considerable maintenance issues for both the slab and the bent cap. These diaphragms are not typically designed for each bridge, but rather a standard detail is used for all bridges.

Problems have been encountered with this design where girders are made continuous by using diaphragms (Miller, 2000). The primary cause for this cracking was believed previously to be due to moments created due to time-dependant deformations of the girders (Oesterle, et al., 1989). These deformations create positive moments over the bents that cause the diaphragm to crack. Providing reinforcement to resist positive moments will reduce the crack widths, but were found to provide no structural advantage (Oesterle, et al., 1989). When positive moment reinforcement is provided, the positive moments near the bents are increased, and when no reinforcement is provided, a small crack will develop in the bottom of the diaphragm. Positive mid-span moments under all loads (including dead load and live load) are nearly the same in both cases. With reinforcement, there is a greater moment to overcome at the support, and, without reinforcement, the crack must first be closed. This does not account for the vertical cracking that has been observed in the girder-ends in Missouri (Figure 1.1), or the spalling of large portions of the diaphragm (Figure 1.1 and 1.2), however. Data collected from Missouri's HPC Bridge and published by Eatherton (1999), Gopalaratnam and Eatherton (2001), and Barrett (2000) has shown that large strains can be created due to thermal gradients and seasonal temperature changes. The influence of temperature-induced strains on continuous bridges has also been observed by Russell and Gerken (1994).

### **6.2 STRAINS DUE TO SERVICE TEMPERATURES (THERMAL GRADIENTS)**

Thermal gradients cause cambering of bridge spans due to daily temperature variations. During the day, the top of the bridge deck is subjected to much heat from the sun, which causes it to expand. In contrast, the girders are subjected to lower temperatures and do not expand as much. This causes the girders to deflect upwards in the middle of the spans, and creates negative moments in the center of the spans and positive moments over the bents. Data has shown that these moments can be of the same order as live load moments and moments due to creep and shrinkage (Conway, 1999). Data available on the influence of service temperatures on strains in prestressed I-girder bridges too suggests that strains from such loading may be more significant than design loads (Eatherton, 1999, Gopalaratnam and Eatherton, 2001). In addition, Alabama DOT (Conway, 1999, Alabama Department of Transportation, 1994) experiences with regard to this problem are detailed in Section 6.2.2. Data collected from Missouri's HPC Bridge (Barrett, 2000), additionally shows that seasonal temperature variations cause axial lengthening and shortening of the girders, which could account for the vertical cracking that has been observed.

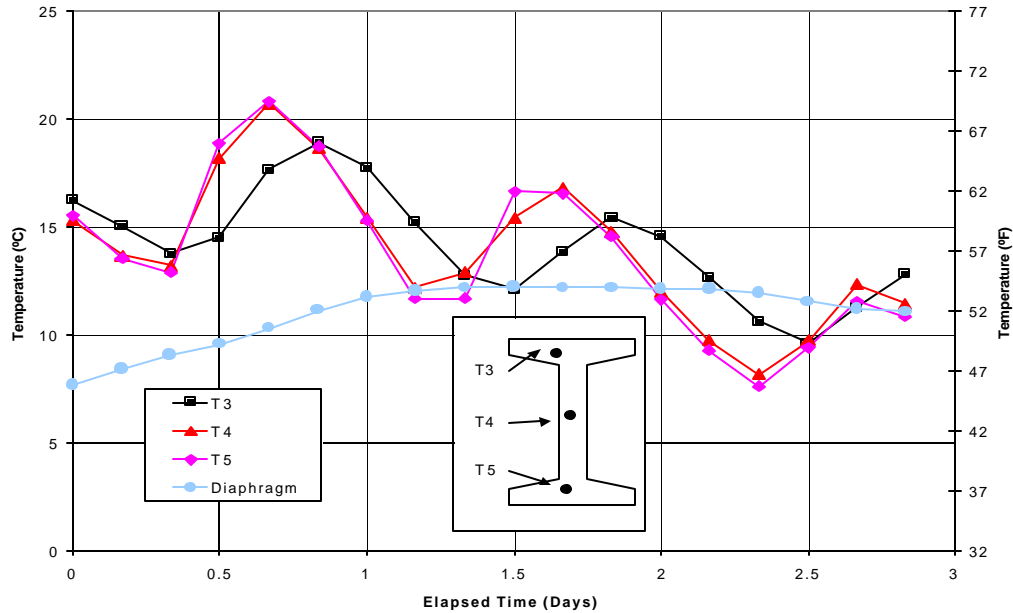
**6.2.1 Missouri's HPC Bridge and the Influence of Service Temperatures.** Bridge A5529, Missouri's first HPC bridge was instrumented with thermocouples and strain gages with the intent of monitoring four of the twenty prestressed I-girders right from when concrete was poured to when the bridge completed one year in

service. Several interesting observations have become known not only on the performance of prestressed HPC bridge girders but on prestressed concrete bridges that are made continuous for live loads. These observations are detailed in other reports (Barrett, 2000, Eatherton, 1999, Gopalaratnam and Eatherton, 2001).

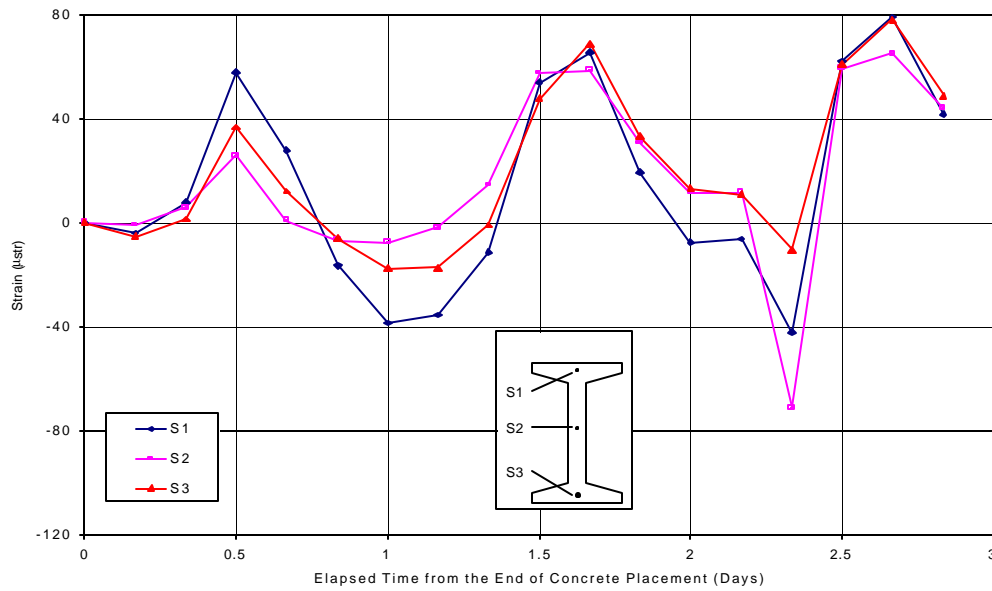
One point of interest to this investigation is the observation that strains causing positive moments at the supports from nominal variations in service temperatures are significant in magnitude and may be in excess of strains due to design loads. Figure 6.1 shows a three-day window of temperature variations during springtime when average temperatures dropped each day (Eatherton, 1999). Daily variations of approximately 10°C (50°F) and a 3-day variation of approximately 15°C (59°F) can be observed. During this cooling period, the top flange typically peaked later than the web and the bottom flange and exhibited less magnitude of excursions in temperature during the day. This is perhaps because the top flange, which is connected to the deck slab, acts like mass concrete delaying and attenuating daily temperature variations during the cooling period. Exactly the opposite effect happens during a warming period, when the top flange leads the web and bottom flange in peaking and attaining higher magnitudes of temperatures. Figure 6.1 also shows the very gradual change in diaphragm temperatures (masking variations during the day exhibited by thermocouples in the girder).

Figure 6.2 shows variations in girder strain during the same period. Maximum strain excursions of approximately 150  $\mu\text{str}$  are observed (Eatherton, 1999). A strain of 150  $\mu\text{str}$  would create stresses of 750 psi (5.2 MPa) in HPC and 585 psi (4.0 MPa) in NSC. It should be noted that strains measured from a quasi-static load test using a loaded truck (simulating moments similar to a MoDOT modified H-20 truck with 10,400 lb. (4700 kg) on the front axle, 15,480 lb. (7020 kg) for the first rear axle and 15,900 lb (7210 kg) for the second rear axle, for a total truck load of 41,780 lb (19,000 kg)) produced maximum strain excursions of approximately 23  $\mu\text{str}$  (for the same short girder 52' (15.8 m) span) as the truck moved across the four-span bridge directly over the instrumented girders (Eatherton, 1999). A strain of 23  $\mu\text{str}$  would create stresses of 115 psi (793 kPa) and 90 psi (620 kPa) for HPC and NSC, respectively. Strains from mechanical loading were observed to be typically smaller than that due to daily temperature variations. When recent data of seasonal temperatures over a 3-month period is considered the influence of service temperature offers better insight into strains developed in the girder during long-term heating and cooling events (Gopalaratnam and Eatherton 2001, Barrett, 2000).

Figure 6.3 shows a window where the average daily temperature (location T<sub>4</sub>) increases during a 3-month period. V1 through V3 represent girder-end strains measured using a vibrating wire strain gage at the cross sectional locations indicated in the inset. During this period, compressive strains were observed to develop (increases in compressive stress magnitudes) in the girders. Figure 6.4 shows the same girder during period of long-term cooling. Tensile stresses develop in the girder (decreases in compressive stress magnitudes) due to the restraint provided by the diaphragm to shortening of the girder. In bridges that are constructed during the summer, when temperatures are near their highest, the girders are likely to have their longest lengths. If, during this time, the girder-ends are built into the diaphragm, they will be restrained from shortening during cooling. This will cause tensile stresses to develop in the end regions.



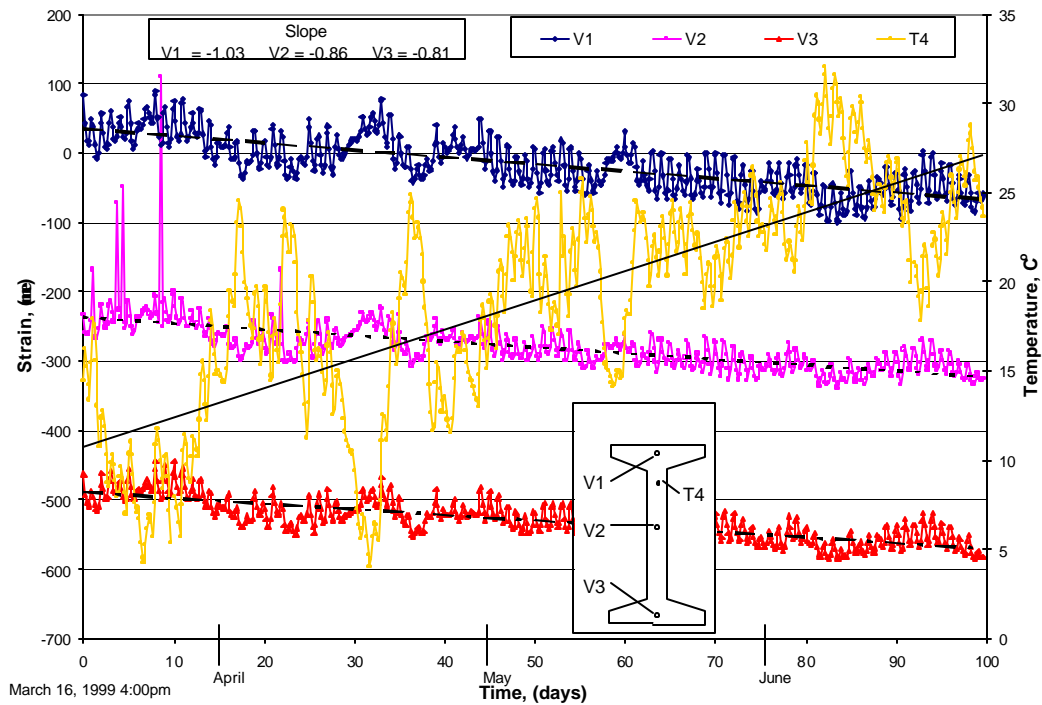
**Figure 6.1 Daily Temperature Variations at Various Locations in the Girder and The Diaphragm During a 3-Day Cooling Period in Spring**



**Figure 6.2 Variations in Girder Strains During the Period Corresponding to Figure 6.1**

It should be noted that the strains shown in Figures 6.1 through 6.4 are not solely due to temperature variation, but also include the effects of creep and shrinkage. The correlation between the change in temperature and the change in strain, however, is very apparent. When examining a short period of data (several days) the effects of creep and shrinkage are not going to be significant since the strain rate of creep and shrinkage is several orders of magnitude smaller than that due temperature variation. When examining the long term data, a portion of the strain measured can be attributed to creep and shrinkage. However, these time-dependant strains are typically monotonic (particularly creep strain, which always increases with time). Clearly, the trends observed show decreasing strains (increasing compression) during Spring, and increasing strains (decreasing compression) during Fall (Figures 6.3, 6.4) which appear to be temperature dominated.

**Alabama DOT's Experience with Thermal Gradients.** Alabama DOT had experience with stresses due to thermal gradients causing either cracking in the diaphragm or vertical cracking in the bulb-tee girders according to Conway (1999), a bridge designer for Alabama DOT. They conducted tests and observed that positive upward deflections were greater than actual downward deflections under design live loads (Alabama Department of Transportation, 1994). In load testing that was done to determine if the vertical cracks in the girder affected the strength or stiffness of the bridge, it was found that they do not reduce either the strength or stiffness. No differential movements were detected between the two faces of the cracks in their tests. Live load deflections were reported to be nearly identical for cracked and uncracked bridges (Alabama Department of Transportation, 1994) suggesting that vertical girder-end cracks at diaphragms may not pose problems with regard to structural performance of such bridges. Information on long-term characteristics of such cracks is unavailable in published literature to make any significant observations on durability issues related to such cracking.



Note: °F = °C \* 1.8 + 32

**Figure 0.1 Strains Due To Service Temperatures during Period of Increasing Temperature in Spring**

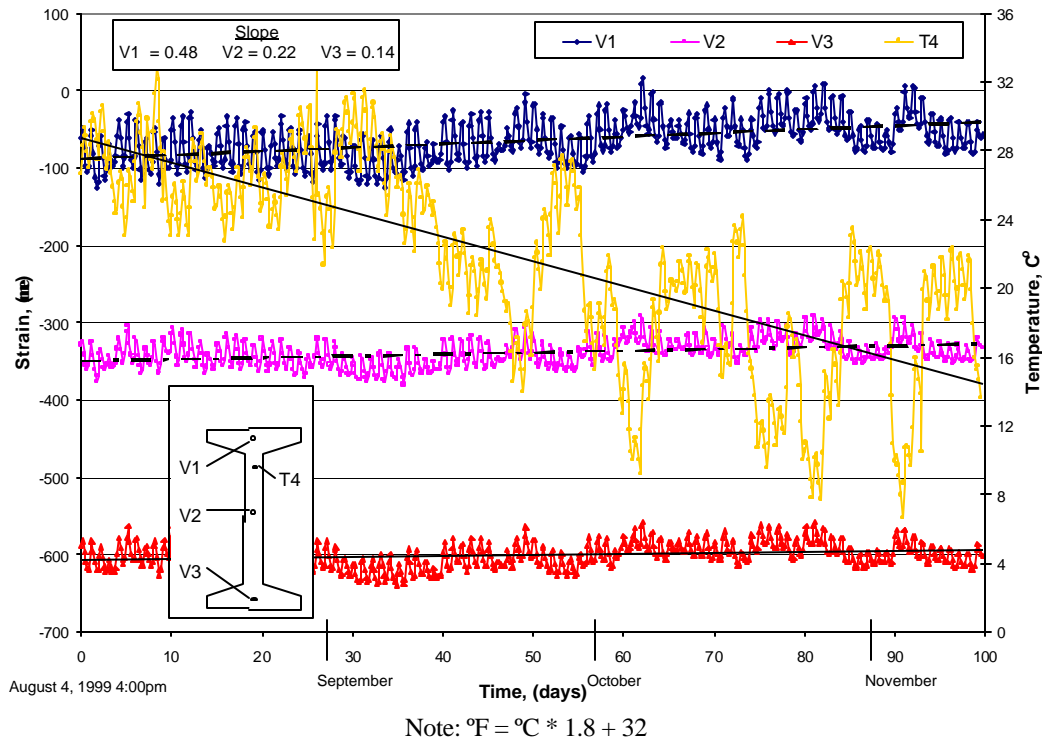


**Figure 0.2 Strains Due To Service Temperatures during Period of Decreased Temperature in Fall**  
*design details from other dot'S and potential performance implications*

A brief summary of some alternative designs at bents used in the other states to minimize/prevent girder-end cracking at the diaphragms is listed in Table 6.1. These options are described in detail in this section.

**Alabama.** Due to the mild climate in Alabama, deicing salts are seldom used on the roadways, nor are snowplows used. Alabama's solution to the problem of girder and diaphragm cracking was thus to return to a simple span design with open expansion joints on top of the bents (Conway, 1999). The ends of the slab are armored to prevent impact loads from damaging the ends of the slabs.

**Nebraska.** According to Barnhill of the Nebraska Department of Roads (NeDOR) (Barnhill, 1999), Nebraska experiences no problems with bridges made continuous for live load using diaphragms. In reviewing the diaphragm detail provided, some important differences were observed between Nebraska's diaphragm design and that used in Missouri. Details of the diaphragm design used in Nebraska are shown in Figure 6.5. The important differences include:

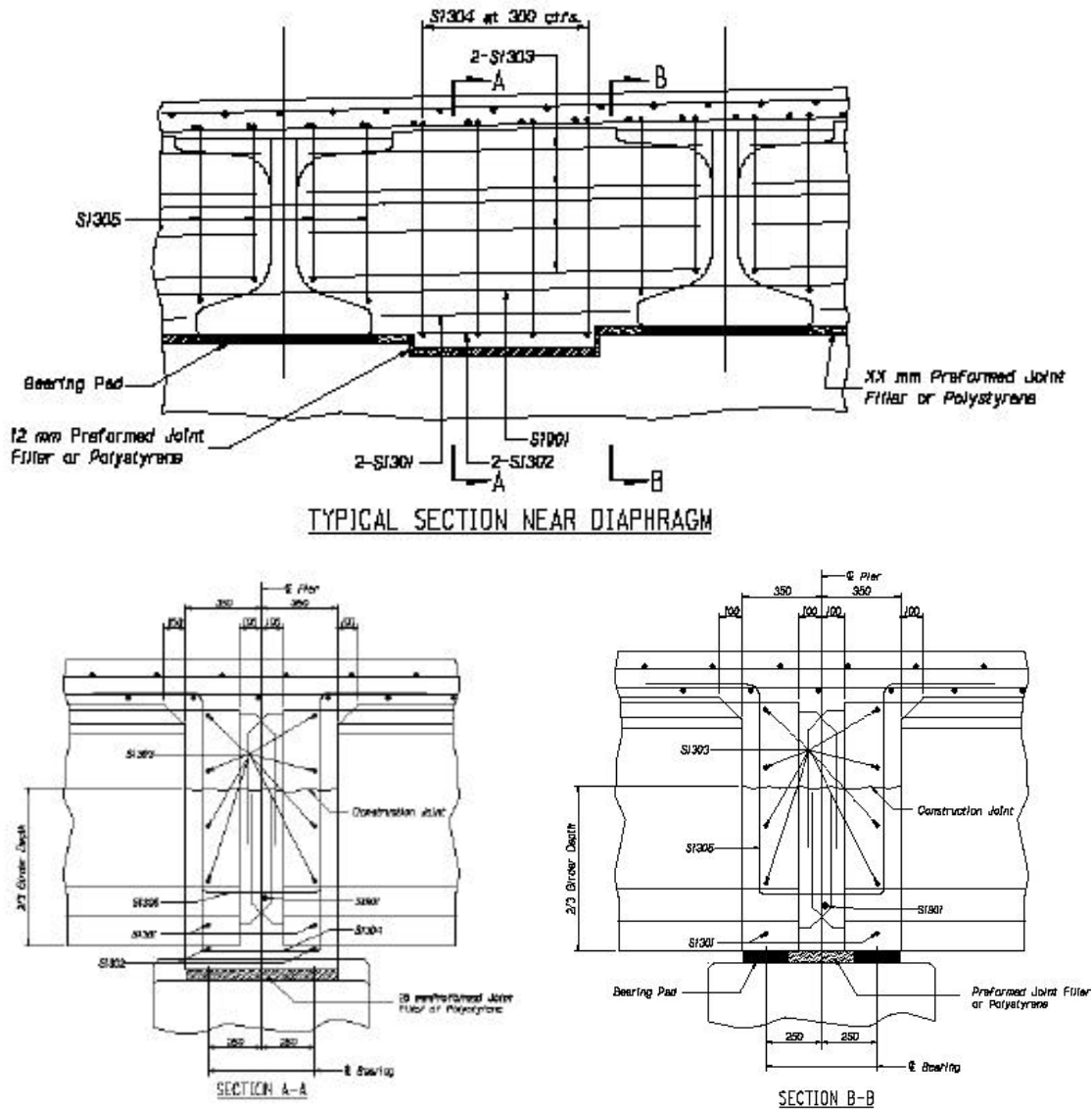
- (1) An expansion material is placed along the entire interface between the diaphragm and the bent cap. This expansion material is as thick as the bearing pad, and thus provides considerable movement capabilities to the diaphragm. This capability may reduce or eliminate restraining forces in the diaphragm, which are responsible for the observed cracking. Tadros et al. (1993) and Ma et al. (1998) conducted a study on continuity and the Nebraska NU Type girders and observed that if the diaphragm

and deck are cast simultaneously, an unbonded joint between the diaphragm and the bent cap is necessary to allow the diaphragm to rotate and prevent cracking.

- (2) A construction joint is allowed to be included at two-thirds of the height of the diaphragm. This joint is often included because contractors in Nebraska prefer to pre-pour the diaphragm. However pre-pouring the entire diaphragm may sacrifice live load continuity at the slab-diaphragm interface and can lead to cracking of the deck slab. NeDOR, consequently, allows the diaphragm to be pre-poured only two-thirds of the way. Barnhill (1999) reports that this type of joint detail in the diaphragm poses no known maintenance issues. It should be noted that Nebraska, like Missouri, uses deicing salts on its highways and bridges during wintertime.
- (3) A third difference is that NeDOR recommends sawing off the portion of the top flanges of the girders that extend into the diaphragm. This is done to primarily facilitate the diaphragm pour since NeDOR uses bulb-tee sections with wide top flanges. However, this may have an additional effect on the continuity of the bridge at the diaphragm. When the top flanges are removed within the diaphragm, the bending rigidity of the girders in the positive bending direction is greatly reduced. This would reduce the positive moments produced at the bents, and help to minimize/prevent the cracking of the diaphragm and girders.

**Table 0.1 Summary of Some Alternate Designs at Bents Used by Other States to Minimize/Prevent Girder-End/Diaphragm Cracking**

State	Design detail comments
Alabama	<ul style="list-style-type: none"> <li>• Discontinued use of diaphragms</li> <li>• Uses open expansion joints over bents</li> <li>• Does not use deicing salts</li> </ul>
Florida	<ul style="list-style-type: none"> <li>• Discontinued use of diaphragms</li> <li>• Pour slab continuous with preformed crack over bents</li> <li>• Does not use deicing salts</li> </ul>
Georgia	<ul style="list-style-type: none"> <li>• Discontinued use of diaphragms</li> <li>• Pour slab continuous with preformed crack over bents</li> <li>• Does not use deicing salts</li> </ul>
Illinois	<ul style="list-style-type: none"> <li>• Place bond breaker between sides of girder and diaphragm</li> <li>• Leave gap between diaphragm and bent cap</li> </ul>
Nebraska	<ul style="list-style-type: none"> <li>• Uses expansion material to isolate diaphragm from bent cap</li> <li>• Places construction joint in diaphragm at 2/3 height</li> <li>• Top flanges of girders sawed-off within diaphragm</li> </ul>



Note (1) polystyrene pad separating diaphragm from bent beam, (2) construction joint at 2/3 of the diaphragm height, and (3) sawed-off top flange at girder-ends.

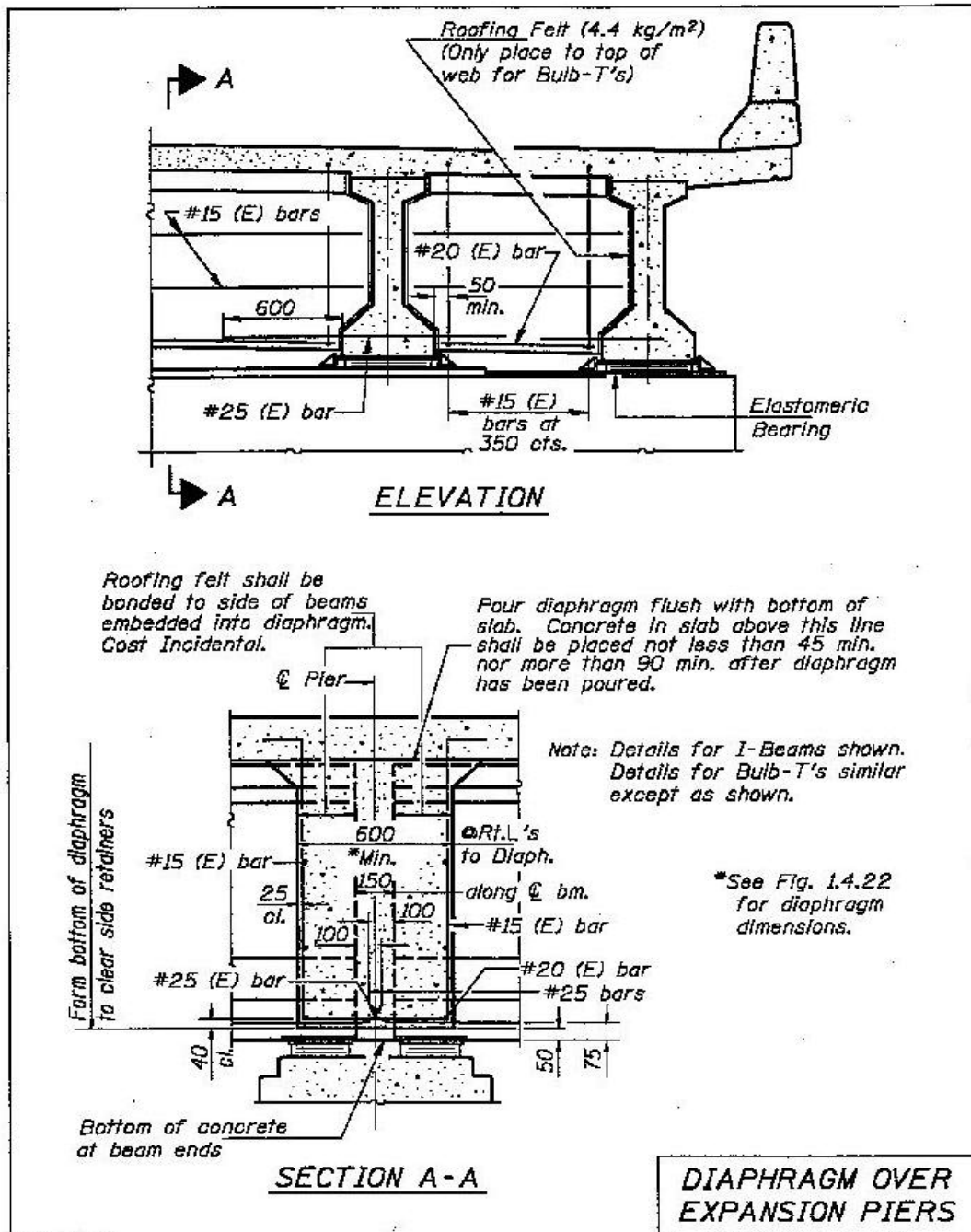
**Figure 0.3 Diaphragm Detailing Used by Nebraska Department Of Roads**

**Illinois.** Figure 6.4 shows the diaphragm detail used by the Illinois Department of Transportation at expansion bents. A second detail is used for bents to which the girders are fixed. Differences between the diaphragm detailing at fixed and expansion bents are discussed later. The design illustrates several significant aspects that may help to alleviate stresses created due to girder movement. First is the use of a bond breaker on the sides of the girders. This bond breaker is achieved by bonding roofing felt to the sides of the girders where they are embedded in the diaphragm. This detail is identical at fixed bents and expansion bents. There is no allowance made for the lengthening of the girders, but the bond breaker would serve to reduce tensile stresses created due to the shortening of the girders. If the girders were cast during the heat of the summer, this would be sufficient,

as they are not likely to lengthen further. If, however, the girders were placed during cold weather, where future lengthening is likely, an expansion material should be placed on the back of the girder to allow for this lengthening.

A second significant feature of the Illinois detail is that a space is provided between the diaphragm and the bent cap. This space is equal in height to the height of the elastomeric bearing pads. By separating the diaphragm from the bent cap, significant rotational capability is provided. This serves to relieve stresses due to live load and differential thermal heating of the bridge spans. The fixed bents are handled slightly differently. Rather than providing an open space between the diaphragm and the bent cap, an expansion material (preformed joint filler) is used in fixed bents. This would provide for less rotational movement than at the expansion bents, but more than if the diaphragm is poured directly on the bent cap. Additionally, at fixed bents the diaphragm and girders are connected to the bent cap with dowels.

**Florida and Georgia.** Florida and Georgia Departments of Transportation too have encountered cracking due to thermal gradients, creep and shrinkage in prestressed I- girder bridges made continuous at the bents (Conway, 1999). The solution implemented was to eliminate the diaphragm, but continue to pour the slab continuously over the whole bridge. In order to allow for the movement that occurs in the slab with such a design, a crack is preformed in the deck over the bents by placing a thin layer of expansion material through the thickness of the slab. This design may not be adequate in Missouri, however, due to use of deicing salts and snowplows unlike in these southern states.



NOTE: 1) Open space between diaphragm and bent beam, and 2) Use of roofing felt as bond breaker on sides of girders

**Figure 6.6 Diaphragm Detailing Used by Illinois Department Of Transportation**

**Other Experience.** Miller (2000) at the University of Cincinnati conducted a survey as part of a not-yet-published NCHRP report of current practice regarding the design and construction of continuous, precast concrete girder bridges. In this survey, respondents were asked to describe problems that have been encountered by using diaphragms to provide continuity. Of thirty-six responses, sixteen reported experiencing diaphragm cracking, six reported girder cracking, and seven observe girder pullout. Illinois was the only

respondent to report a remedy in the survey. They report that if a bond breaker is provided between the diaphragm and the girder sides, diaphragm/girder cracking is eliminated. The diaphragm detail used by Illinois was discussed in detail in the previous section.

## **Bridge measurements**

J. Myers, A. Nanni, and D. Stone

This section will outline the measurements taken at two typical bridges that utilized simple span PC I-girders made continuous. Measurements of the thermal gradient of the bridge through the cross section of the deck and girders were taken, as well as surveys of the elevation of the bridge deck. The objective was to determine the actual thermal gradient experienced at the bridges and to determine if a measurable deflection occurred due to this gradient.

First, the characteristics of the two bridges are discussed, followed by a description of the measurements that were taken. Then, the results of the measurements are presented and conclusions are drawn from these results.

### ***Bridges A4565 and A5736***

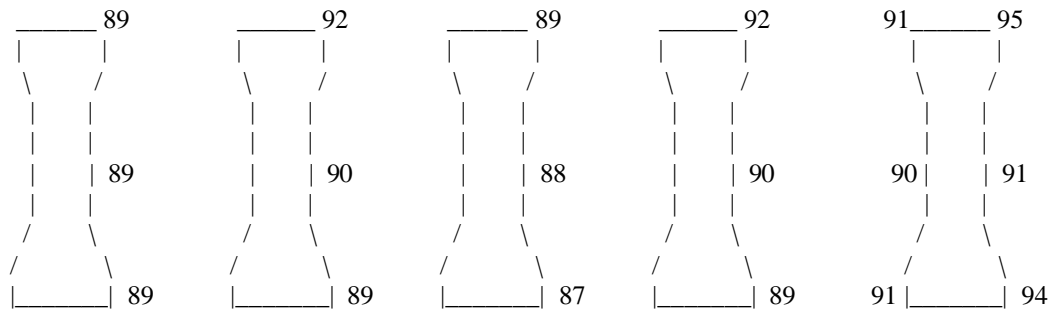
The first bridge, Bridge A4565, is located in MoDOT District 9, Shannon County, Missouri on County Route A. Bridge A4565, which was constructed in the fall of 1991, has already exhibited girder end cracking. The 306-foot (93.27-m) long bridge has five spans and four Type III girders per span. The bridge is not skewed and has an average daily traffic count of 3000 vehicles. The concrete mix design was composed of Type III Ash Grove cement, Burlington Limestone coarse aggregate and Missouri River Sand fine aggregate.

The second bridge, Bridge A5736, is located in MoDOT District 9, Phelps County, Missouri on State Highway 72. Bridge A5736 was constructed in the fall of 1997 and has not exhibited any girder cracking to date. The 130-foot (39.62-m) long bridge has three spans and five Type II girders per span. The bridge is skewed 30 degrees and has an average daily traffic of 5000 vehicles. The concrete mix design was composed of Type I River cement, Little Piney River gravel coarse aggregate and Little Piney River sand fine aggregate.

### ***measurement methods***

The bridge measurements were conducted to determine the thermal gradients of the bridges and the upward deflection, or bowing, of the bridge decks. During the project, measurements were taken a total of four times at each bridge. The days and times of the measurements were selected in order to obtain several different thermal gradients; readings were taken on sunny days and cloudy days, during the morning hours when the gradient was minimal and in the afternoon when the gradient would be the largest (Hulsey, 1976, pg. 69).

The thermal gradient through the depth of the bridge was established by measuring the temperature on the top of the bridge deck, the bottom of the bridge deck, and at various points throughout the depth of the girders themselves. For the top of the bridge deck, a total of ten readings were taken at random points throughout the area of the bridge deck. The average of these ten values was taken to be the temperature at the top of the bridge deck. The same procedure was used for the bottom of the bridge deck, with the average of the ten readings taken as the temperature at the bottom of the bridge deck. For the girders, several readings were taken along the cross section of the bridge. Figure 0.1 is an example of the readings and where they were taken. Because the points were not marked on the girders, the temperature was not taken at exactly the same point each time the measurements were taken. However, the position of the measurement was not considered critical. The goal was to establish the thermal gradient and compare it to the thermal gradient recommended by AASHTO (1989). Additionally, it may be noted that the measurements that were taken captured the positive thermal gradient. Measurements were not taken when the top of the deck was at a lower temperature than the girders, as would be exhibited for the negative gradient. A negative gradient most often occurs late at night or near daybreak when measurements were not practical for researchers, due to safety issues and the proximity of the bridges to UMR.



Note: °F=1.8\*°C+32

**Figure 0.1** Girder Temperature Measurements

To determine the amount of upward movement in the deck due to thermal effects, a level and Philadelphia rod were used to survey the bridges. While there are more precise means of measurement, as previously stated, the purpose was to see if measurable deflections of the bridge decks were taking place under only thermal and dead loads. The surveys were conducted along the length of the bridge on the left side, the right side, and the centerline of the bridge deck; measurements were taken across the bridge at these three points at each pier line and at each mid-span section. See Figure 7.2 for a typical layout of survey points.

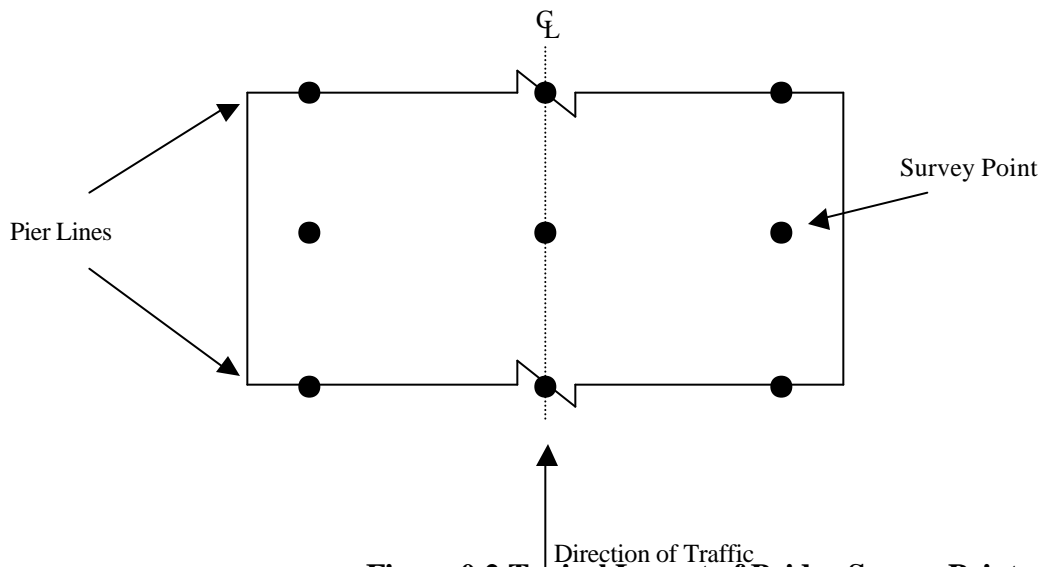


**Figure 0.2** Typical Layout of Bridge Survey Points

It was assumed that the bridge decks were fixed at the piers, i.e., there was no vertical movement. The elevation of the bridge deck was calculated from the survey measurements under the assumption that the height of the instrument was 100 feet (30.48 meters); the absolute elevations of the points were not necessary, only the relative movements.

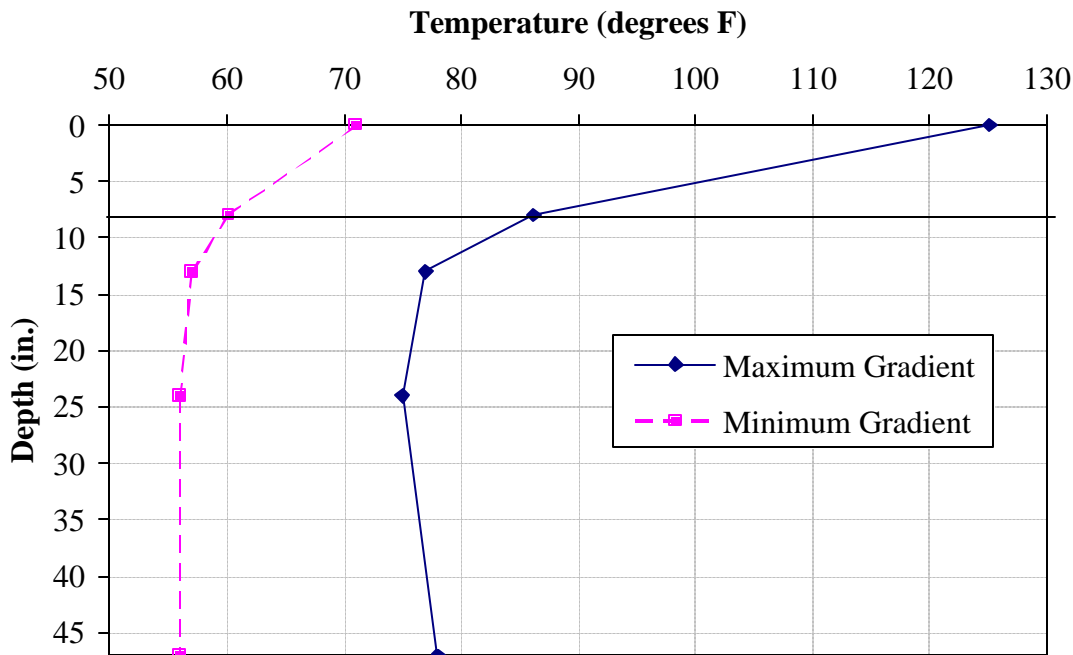
**results**

The results of the bridge measurements are presented in Appendix G. Temperature measurements indicate that a thermal gradient does exist at these two bridges. The differential is generally greatest through the deck, with a much smaller differential occurring along the depth of the girders. Referring back to Figure 0.1, for this set of readings the average temperature at the top of the deck was

119.1°F (48.4°C) and the average temperature at the bottom of the deck was 95.4°F (35.2°C). The temperature differential through the deck is approximately 24°F (13.3°C). The maximum differential between the average temperature at the bottom of the deck and the minimum girder temperature is roughly 8°F (4.4°C).

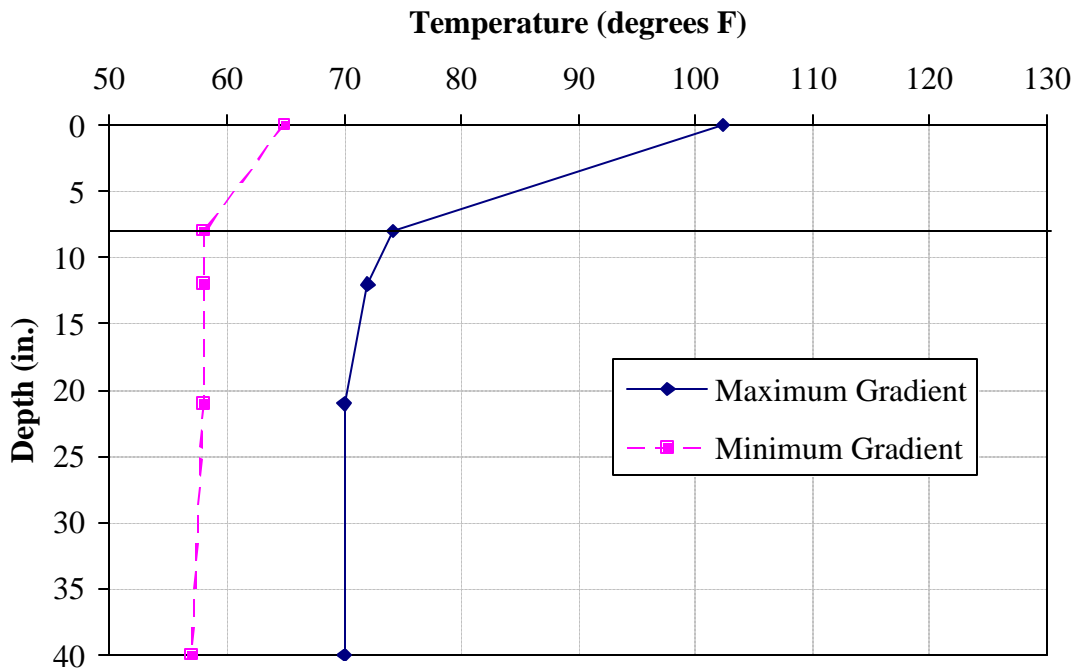
Figures 7.3 and 7.4 exhibit the maximum and minimum temperature profiles as measured at the two bridges. The solid horizontal line across the graph represents the position of the bottom of the deck. The solid curve illustrates the maximum observed gradient; the dashed line illustrates the minimum observed gradient.

In Figure 0.3, the maximum and minimum profiles, corresponding to a difference between the temperatures at the top and bottom of the deck, are 39°F (21.7°C) and 11°F (6.1°C), respectively. For Figure 0.4, these values are 28°F (15.6°C) and 7°F (3.9°C). Again, these two figures illustrate the trend of a relatively large gradient through the deck, with a smaller gradient occurring through the depth of the girders.



Note: °F=1.8\*°C+32, 1 in. = 25.4 mm

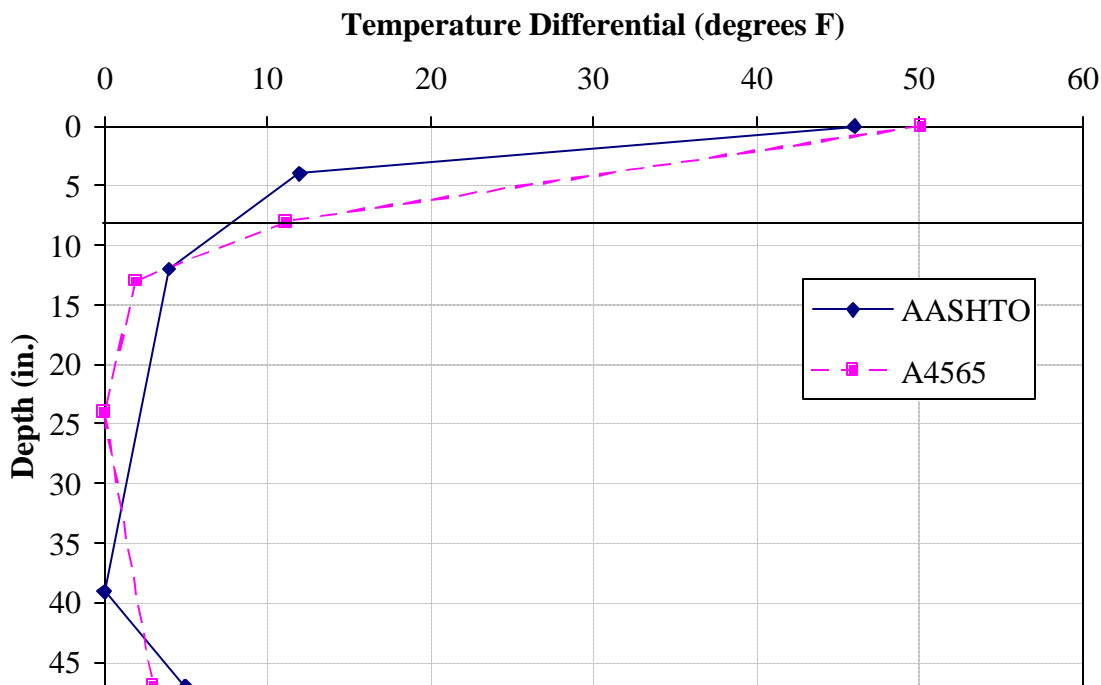
**Figure 0.3** Maximum and Minimum Temperature Profiles, Bridge A4565



Note: °F=1.8\*°C+32, 1 in. = 25.4 mm

**Figure 0.4 Maximum and Minimum Temperature Profiles, Bridge A5736**

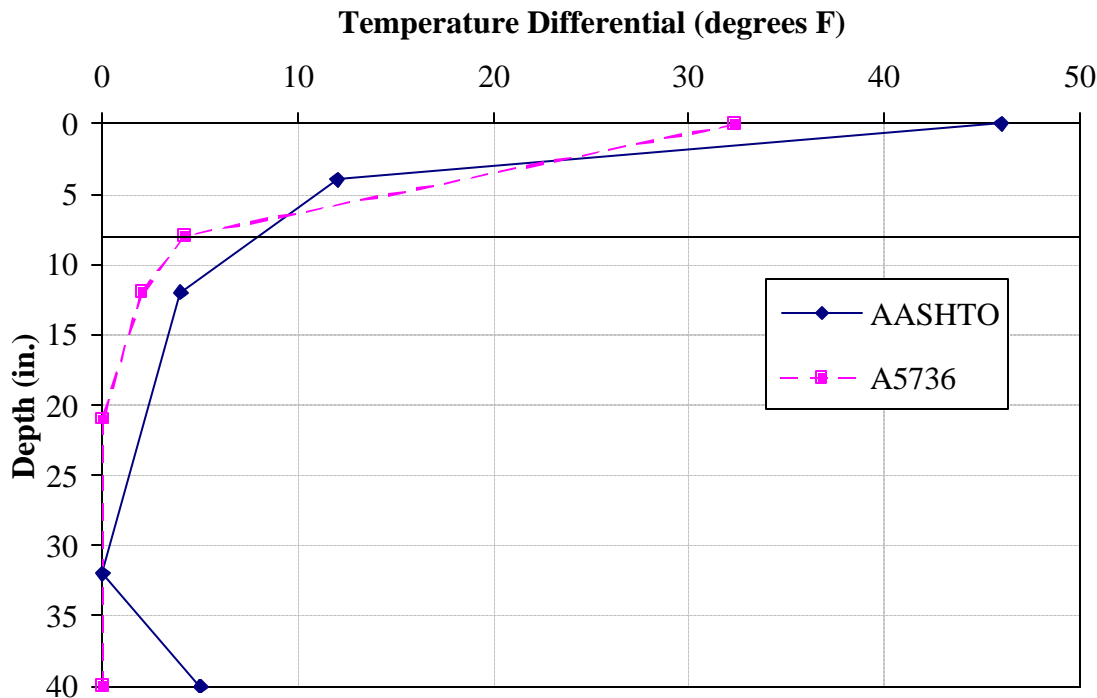
In order to validate the measured gradient, a comparison of the maximum measured gradient at each bridge was made to the positive gradient recommended by AASHTO (1989, pg. 4). The AASHTO recommendation for Zone 2, which includes Missouri, and a plain concrete surface were used. Figures 7.5 and 7.6 compare the maximum thermal gradient measured to the thermal gradient recommended by AASHTO for Bridges A4565 and A5736, respectively.



Note: Δ1.8°F=Δ1°C, 1 in. = 25.4 mm

**Figure 0.5 Comparison of AASHTO Positive and Bridge A4565 Gradients**

It may be noted that the AASHTO recommended positive gradient is a function of the depth of the bridge. (Recall Figure 1.7.) For both bridges, there is good correlation between the measured and recommended gradients, although it may be noted in Figure 0.5 that the AASHTO gradient is slightly unconservative compared to the temperatures measured in the field.

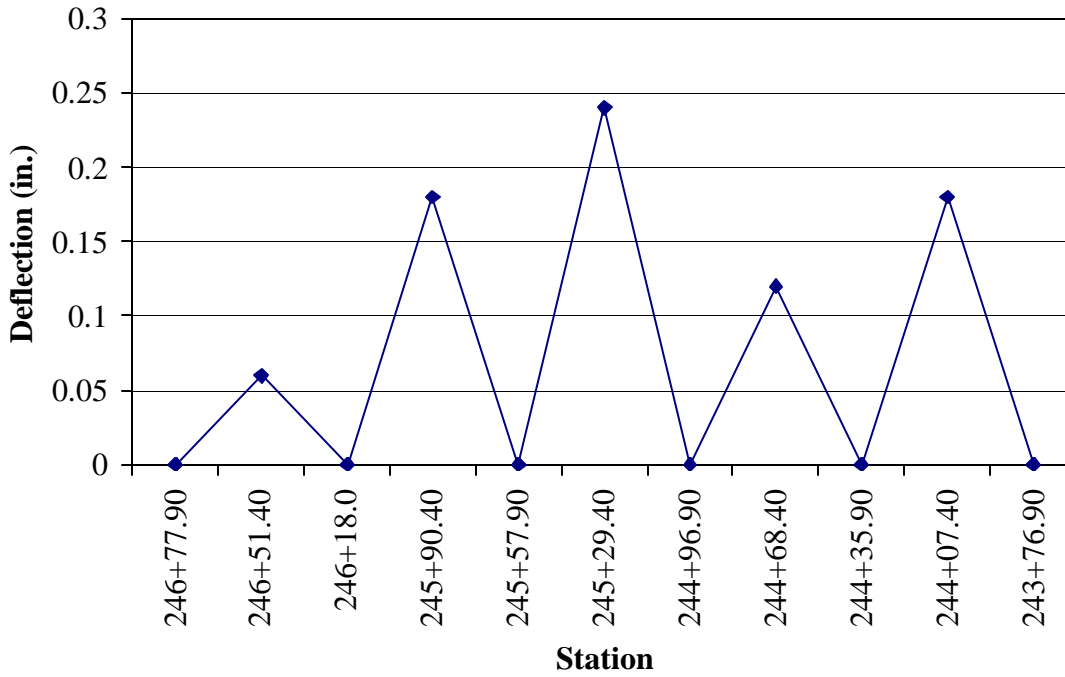


Note:  $\Delta 1.8^{\circ}\text{F} = \Delta 1^{\circ}\text{C}$ , 1 in. = 25.4 mm

**Figure 0.6 Comparison of AASHTO Positive and Bridge A5736 Gradients**

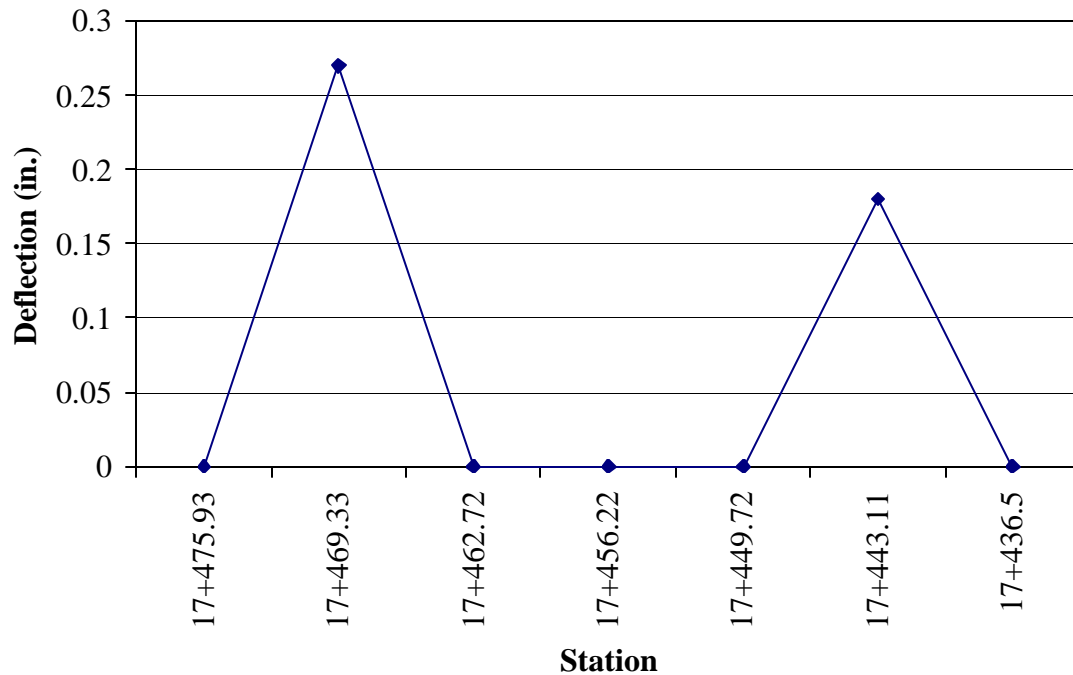
At the outset of the project it was unclear whether measurable deflections were taking place at the two monitored bridges. As mentioned previously, the main goal was to determine whether measurable deflections were occurring and, if so, the magnitude of these deflections. Typical plots of the deflections of the bridge decks are illustrated in Figures 7.7 and 7.8.

Figure 0.7 illustrates the deflections along the centerline of Bridge A4565. The elevations of the bridge deck for the minimum thermal gradient were subtracted from the elevations for the maximum thermal gradient. The difference between the maximum and the minimum temperature differentials at Bridge A4565 is 28°F (15.6°C). Figure 7.7 illustrates the fact that there is an upward deflection for an increase in temperature differential. All deflections are on the order of 0.25 in (6.35 mm) or less.



Note: 1 in. = 25.4 mm  
**Figure 0.7 Thermal Deflections, Bridge A4565**

Figure 0.8 illustrates the deflections along the centerline of Bridge A5736. Again, the elevations of the bridge deck for the minimum thermal gradient were subtracted from the elevations for the maximum thermal gradient. The difference between the maximum and the minimum temperature differentials at Bridge A5736 is 21°F (11.6°C). Figure 7.8 also illustrates that there is an upward deflection for an increase in temperature differential. All deflections are on the order of 0.30 in (7.62 mm) or less.



Note: 1 in. = 25.4 mm

**Figure 0.8 Thermal Deflections, Bridge A5736**

### *discussion of results*

Based on the measurements taken during the project, only general conclusions can be made. These conclusions are as follows:

- There exists a positive thermal gradient at the two monitored bridges.
- The temperature differential is largest through the deck, with a smaller differential occurring between the top and bottom of the girders.
- The maximum measured temperature differential through the depth of the bridge deck was 39°F (21.7°C).
- The measured thermal gradients are in good agreement with the recommended positive thermal gradients proposed by AASHTO for the purposes of design.
- The bridges are experiencing measurable changes in deflection in the absence of traffic loads.
- For an increase in temperature differential, there is an upward movement, or bowing, of the bridge decks.
- These deflections are assumed to have been caused by the measured thermal gradients, due to the absence of traffic or other external forces.

Based on these conclusions, additional monitoring of these structures is suggested. A long-term monitoring project would allow for monitoring of the growth/movement of existing cracks, the development of additional cracks, and ultimately, substantiate whether the gradients will result in a long-term durability problem or structural performance issue.

### Thermal stress calculation

J. Myers, A. Nanni, and D. Stone

In the previous section, it was established that the AASHTO recommended gradient was representative of the thermal gradient experienced by Missouri bridges. In order to establish whether or not this gradient could cause the type of cracking being investigated, the stresses associated with these gradients must be considered. Due to the complexity and the three-dimensional nature of the bridges, a finite element analysis (FEA) was undertaken to establish the magnitude of these stresses; a commercially available software package was used for the FEA. This section will outline some basic theories of thermal stresses, the simplified analyses performed to validate the modeling of the boundary conditions, and the parametric study that was performed to determine the thermal stress distributions to be used for design purposes.

#### basic Theory of thermal stresses

The theory of thermal stresses in elastic materials was studied as early as 1835 by Duhamel, who considered the stresses caused by temperature changes in the recently devised formulations of elasticity (Boley, 1960, pg. v). More recently, and beginning with Timoshenko and Goodier’s *Theory of Elasticity* in 1951, reference can be made to a number of texts that outline the calculations of thermal stresses (Gatewood, 1957; Boley, 1960; Ghali and Favre, 1994).

To begin with the simplest case, the change in length of a beam due to a uniform change in temperature can be easily calculated as follows:

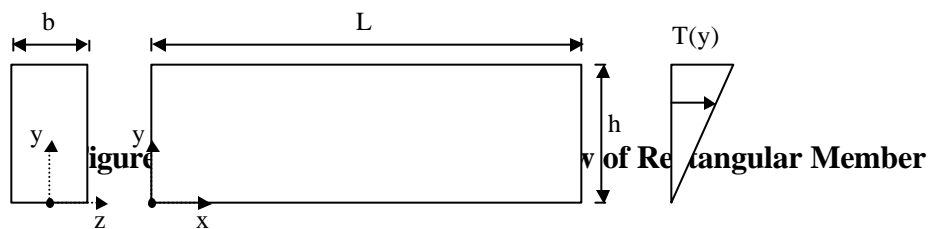
$$\Delta L = \alpha L \Delta T \tag{0.1}$$

where:

- “ $\Delta L$ ” is the change in length of the member,
- “ $\alpha$ ” is the coefficient of thermal expansion,
- “ $L$ ” is the overall length of the member, and
- “ $\Delta T$ ” is the uniform change in temperature of the entire member.

If the member is assumed to be homogeneous and isotropic, then the longitudinal thermal stresses induced in both unrestrained and fully restrained beams are easily calculated.

The following conditions assume a cross section and side view of the member as outlined in Figure 0.1. Additionally, the temperature distribution is one-dimensional, that is, it varied only with depth, “ $y$ ”. It may also be noted that a positive stress denotes tension, while a negative stress denotes compression.



First, for the fully restrained condition, the thermal stresses are calculated as follows:

$$s_{fully\ restrained} = -\alpha E T(y) \tag{0.2}$$

where:

“ $\alpha$ ” is the coefficient of thermal expansion,  
 “E” is Young’s modulus of the material of the member, and  
 “T(y)” is the temperature distribution as a function of depth, “y”.

Equation 8.2 is Equation 8.1 expressed in terms of stress instead of change in length. It may also be noted that Equation 8.2 holds true for any thermal gradient, be it linear or non-linear. For a fully restrained member, it is assumed that no rotation or movement is allowed at the ends of the member. When loaded with a uniform, linear or non-linear temperature differential, a fully restrained member should experience stress without experiencing any strain (Gatewood, 1957, pg. 1).

For the unrestrained condition, the thermal stresses can be calculated as follows in Equation 8.3.

$$s_{unrestrained} = -\alpha E T(y) + \frac{P}{bh} + \frac{M y}{I} \tag{0.3}$$

where:

“P” is the resultant force of the thermal stresses and can be calculated by the expression,  $P = \int_0^h \alpha E T(y) b dy$ ,

“M” is the resultant moment of the thermal stresses and can be calculated by the expression,  $M = \int_0^h \alpha E T(y) b y dy$ , and

“I” is the moment of inertia of the member.

If a linear temperature differential and a rectangular cross section were to be considered, such as in Figure 0.1, the stressed can be illustrated as follows:

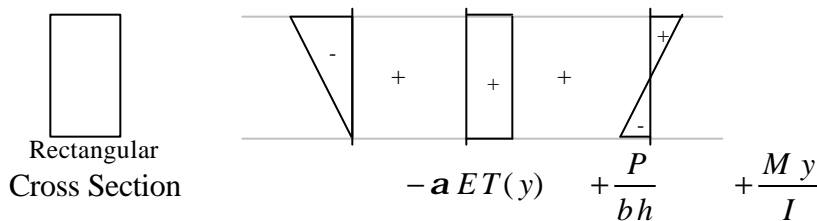


**Figure 0.2 Thermal Stresses of an Unrestrained Member**

For the unrestrained member, it is assumed that there is absolutely no restraint to the expansion that should occur due to the increased temperature. An unrestrained member subjected to a uniform temperature differential should experience axial deformation without experiencing any stresses. Additionally, if an unrestrained member were subjected to a temperature differential that varies linearly through the depth, the member would also experience axial deformation and curvature without experiencing any induced stresses due to the temperature differential. That is, for these temperature differentials, an unrestrained member would experience strain without experiencing any stress. It may also be noted that an unrestrained member subjected to a non-linear temperature differential through the depth would experience both stress and strain (Gatewood, 1957, pg. 9). Ghali and Favre (1994) explain the origin of these stresses by the fact that “any fibre, being attached to other fibres, cannot exhibit free temperature expansion” (pg. 299).

***simplified/verification analyses***

Initially, a series of simplified analyses were performed in order to determine the appropriate FEA procedures to model the most common boundary conditions of an unrestrained member or a fully restrained member. These simplified cases were also used to

verify the results calculated by the FEA software. The exact solution was compared to the results of the FEA to insure that the analyses were being performed properly.

Two simplified cross sections were selected for these analyses. The square and double-t cross sections were chosen for simplicity and are shown in Figure 8.3. It may be noted that the cross-sectional area of these two sections is the same.

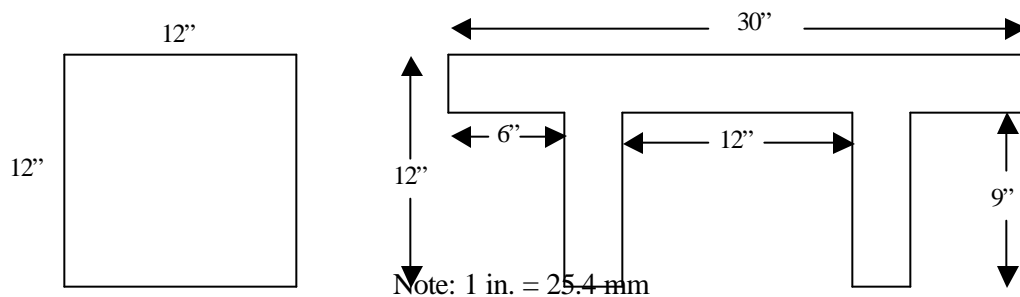


**Figure 0.3 Cross Section Dimensions of the Simplified Sections**

For the first set of verification analyses, the temperature differentials were arbitrarily selected. It should be noted that neither of the arbitrary temperature differentials represents conditions that exist in this project. Table 0.1 contains the conditions tested for the first set of verification analyses.

Both uniform and linear temperature differentials were applied to unrestrained and fully restrained square members in an attempt to obtain the theoretical results described previously. Various parameters of the analyses were modified until there was good agreement between the results from the FEA and the theories of thermal stresses. Again, this would assure that the boundary conditions were modeled properly.

**Table 0.1 Simplified Model Parameters**

Boundary Conditions	Cross Sections	Temperature Differentials
Unrestrained	Square	Uniform (+20°F)
Fully Restrained	Double-T	Linear (+10°F to -10°F)

Note:  $\Delta 1.8^{\circ}\text{F} = \Delta 1^{\circ}\text{C}$

A summary of the analysis results is illustrated in Table 0.2. It may be noted that not all combinations of the parameters in Table 0.1 were modeled. It may also be noted that the stresses reported for cases D and F are those at 1.5 inches (38.1 mm) from the bottom of the cross section; they will be less than the maximum stress occurring at the bottom of the cross section. Additionally, the stresses in cases C and E are constant throughout the cross section, as are the strains in case A.

**Table 0.2 Summary of FEM Results**

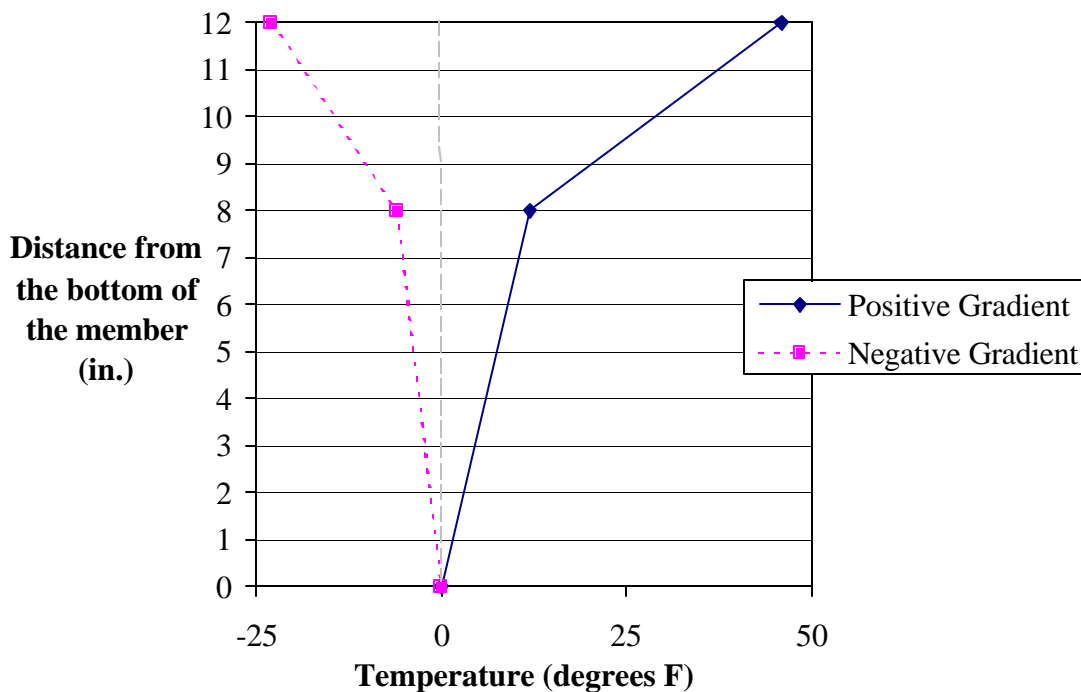
Case	Cross Section	Boundary Conditions	Thermal Gradient	Stress (psi)	Strain
------	---------------	---------------------	------------------	--------------	--------

A	Square	Unrestrained	Uniform	0	1.20E-04
B			Linear	0	1.20E-04
C		Fully Restrained	Uniform	-600	0
D			Linear	304.7	0
E	Double-T	Fully Restrained	Uniform	-600	0
F			Linear	311.7	0

Note: 1 psi = 6.89 kPa

A comparison of the results presented in Table 0.2 yields a verification of the magnitudes of the stresses and/or strains developed in the members. Again, it may be noted that a positive stress value denotes tension, while a negative stress value denotes compression. Cases A and B, the unrestrained cases, exhibit strain without stresses, while the other cases, C through F, exhibit the opposite condition of stress without strain. These results are consistent with the elastic theory presented previously. Additionally, the magnitude of the stresses developed in cases C and E are the same, as are the magnitudes of the stresses developed in cases D and F. This is due to the fact that the boundary conditions and thermal gradients are the same and that the areas of the cross sections are equal. The thermal stresses developed are equal to those calculated by elastic theory, as well. This first set of verification data leads to the conclusion that the boundary conditions are modeled correctly because the stresses and strains calculated are consistent with those calculated using elastic theory.

For the second set of analyses, the AASHTO recommended positive and negative gradients were applied to the square cross section. Although AASHTO suggests that the gradients only be applied to structures having a depth of two feet or greater (1989, pg. 4), they were used in this case only for the purposes of verification. Again, the AASHTO recommended gradients for Zone 2 and a plain concrete surface were selected. The AASHTO temperature differentials applied to the square cross section are illustrated in Figure 8.4.



Note:  $\Delta 1.8^{\circ}\text{F} = \Delta 1^{\circ}\text{C}$ , 1 in. = 25.4 mm

### Figure 0.4 AASHTO Gradients, as Applied to the Square Cross Section

Again, the exact solution was compared to the solution provided by the FEA; the analysis performed was for an unrestrained member. The exact solutions were provided by elastic theory and are outlined in Appendix H. The FEA was performed using three-dimensional twenty-node quadratic elements. Both the positive gradient and the negative gradient were analyzed separately; each was modeled using two different element configurations. The two element configurations are illustrated in Figures 8.5 and 8.6.

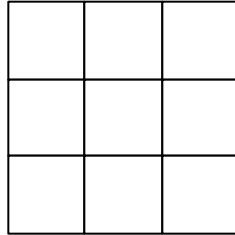


**Figure 0.5 Element Configuration #1**

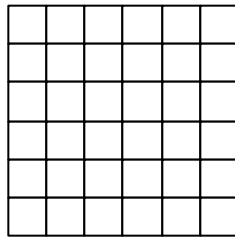
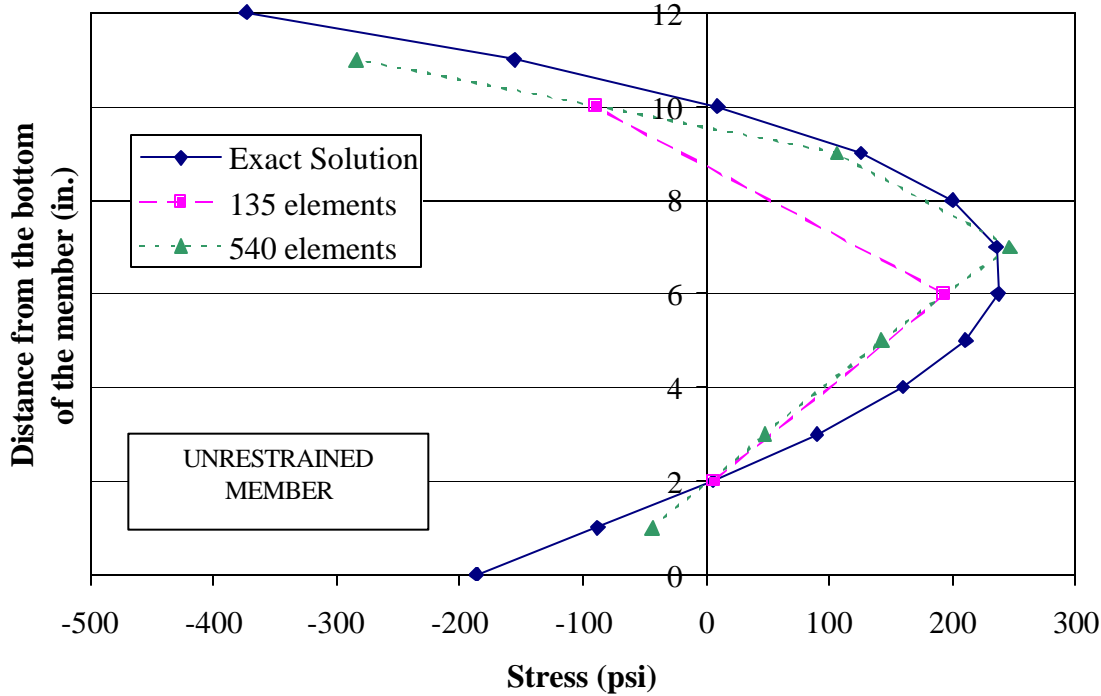


**Figure 0.6 Element Configuration #2**

The first element configuration, Figure 8.5, used 4-in. x 4-in. x 4-in. (101.6-mm x 101.6-mm x 101.6-mm) elements throughout the 12-in. x 12-in. x 60-in. (304.8-mm x 304.8-mm x 1524-mm) member. This yields a total number of elements of 135. The second element configuration, Figure 8.6, used 2-in. x 2-in. x 4-in. (50.8-mm x 50.8-mm x 101.6-mm) elements, yielding a total number of elements of 540. Two different element configurations were modeled in this simple cross section in order to establish the relative number of elements that would be required to assure a reasonable level of accuracy in the final FEM model, which approximated a portion of the cross section of the bridges.

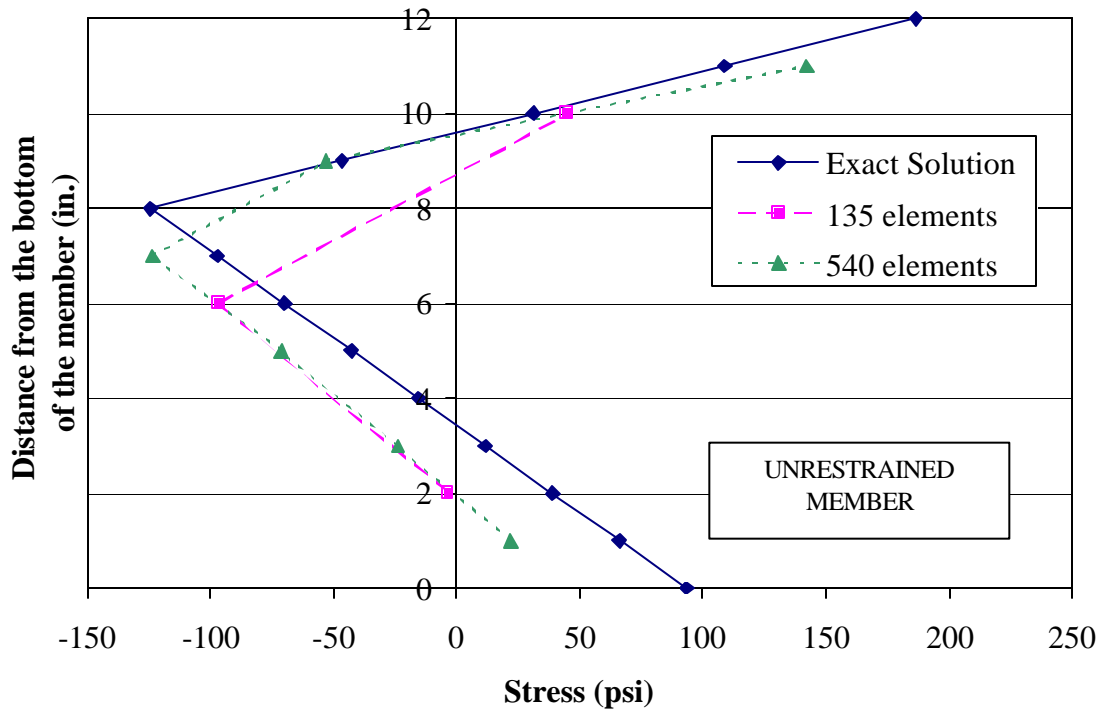
Plots of the results are exhibited in Figures 8.7 and 8.8, where they are compared to the results given by the FEA. Figure 8.7 illustrates the results of the positive AASHTO gradient; Figure 8.8 illustrates the results of the AASHTO negative gradient. Again note that a negative stress denotes compression, while a positive stress denotes tension.



Note: 1 psi = 6.89 kPa, 1 in. = 25.4 mm

**Figure 0.7 Thermal Stresses Induced by the AASHTO Positive Gradient, on a Simplified Square Cross Section at Midspan**

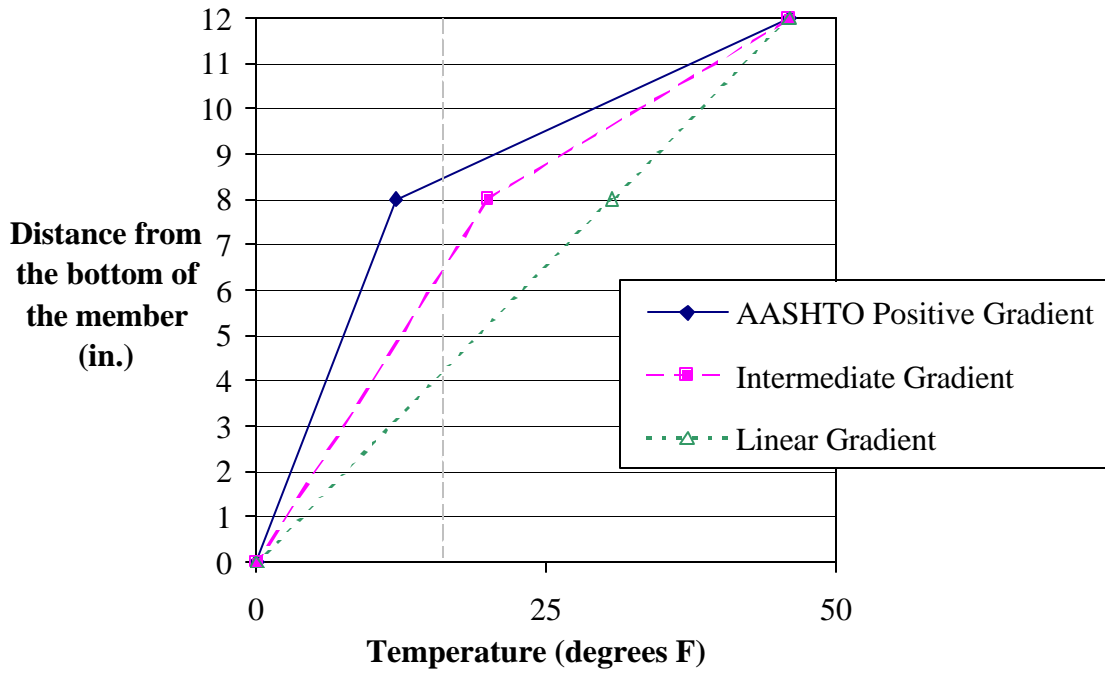
In general, the more elements that are used to approximate a member, the better the approximation will be; that is, the more closely the approximate solution provided by the FEA will match with the exact solution. Theoretically, if an infinite number of elements were used to approximate the member, the FEA solution would be identical to the exact solution. The increased accuracy of the 540-element model over the 135-element model is illustrated in Figures 8.7 and 8.8. The results of the FEM model yield confidence that the model is correct and could give the exact solution if enough elements were used. The second set of verification analyses again validate the magnitude of the stresses calculated, via comparison with elastic analysis, and illustrate the tendency of the FEM solution toward the numerical solution with an increased number of elements.



Note: 1 psi = 6.89 kPa, 1 in. = 25.4 mm

**Figure 0.8 Thermal Stresses Induced by the AASHTO Negative Gradient, on a Simplified Square Cross Section at Midspan**

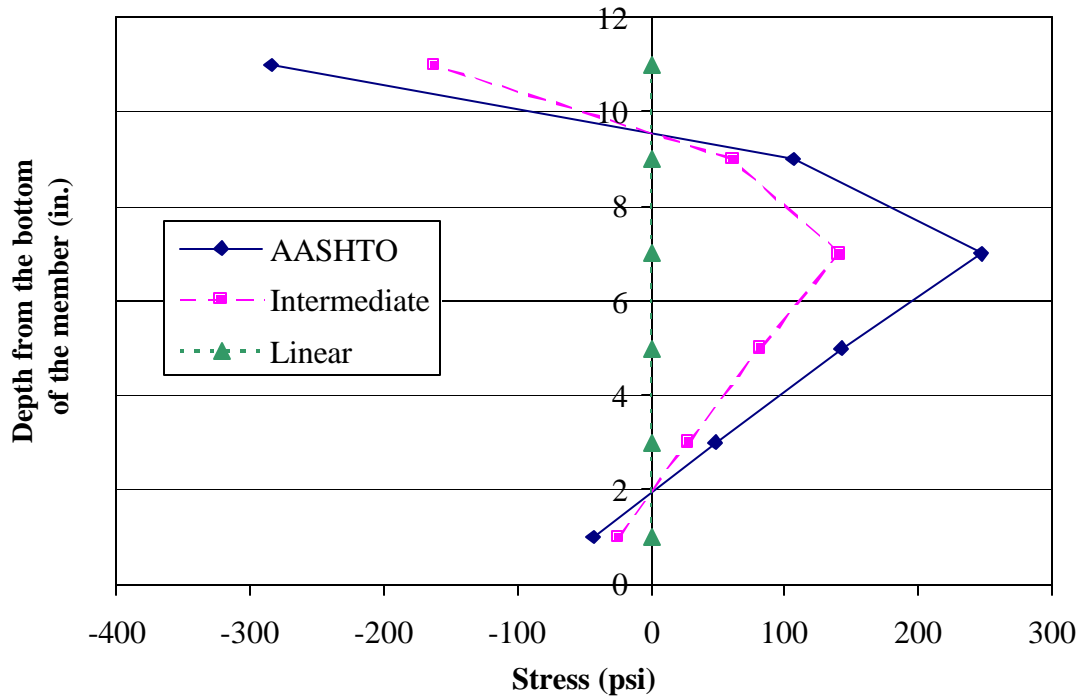
For the third set of verification analyses, it was desired to illustrate that a linear thermal gradient applied to an unrestrained member will yield no stress while a non-linear gradient, such as those outlined in Figures 8.7 and 8.8, will induce stresses. The positive AASHTO gradient was used, varying the temperature at the 8-in. (203-mm) location from the current value to a value that would give a linear thermal gradient. See Figure 8.9.



Note: 1 in. = 25.4 mm,  $\Delta 1.8^{\circ}\text{F} = \Delta 1^{\circ}\text{C}$

**Figure 0.9 Linear and Non-linear Thermal Gradients**

For each of these three thermal gradients, the thermal stresses were calculated using the 540-element FEA of the unrestrained square member. The values are illustrated in Figure 0.10 and illustrate that as the thermal gradient progressed from the AASHTO gradient toward a linear thermal gradient the stresses decreased in magnitude; the stresses in the case of the linear thermal gradient are zero throughout the depth of the member.



Note: 1 psi = 6.89 kPa, 1 in. = 25.4 mm

**Figure 0.10 Thermal Stresses for Linear and Non-linear Thermal Gradients, as Applied to an Unrestrained Member**

***Parametric study***

After successful development and validation of the FEA, a parametric study was undertaken. The parametric study was performed to examine the effects of span length, girder type/area, and girder spacing on the thermal stresses of fully restrained and unrestrained members. The parametric study examined the stresses induced by the AASHTO positive and negative gradients and the subsequent forces/stresses developed. The concept of the effective flange width was used as based on AASHTO (1996). Based on the simplification of the cross-section via use of the effective flange width, the analyses were performed using the exact solution.

**Effective Flange Width.** The effective flange width for a girder depends upon whether the girder is an interior girder or an exterior girder. The interior effective flange width considered is a function of four variables, span length, web thickness, slab thickness, and girder spacing. The exterior effective flange width considered is a function of the cantilever length at the exterior of the bridge and the interior effective flange width. See Figure 0.11 for a representative detail of the respective effective flange widths.

Equations 8.4 through 8.6 outline the calculation of the interior effective flange width.

$$\frac{1}{4} \cdot \text{Span length} \tag{0.4}$$

$$\text{Web thickness} + 2 \cdot (6 \cdot \text{Slab thickness}) \tag{0.5}$$

*Girder spacing***(0.6)**

where:

Span length is the distance from one pier line to the next,

Web thickness is the width of the web of the girder,

Slab thickness is the total thickness of the deck slab<sup>1</sup>, and

Girder Spacing is the center to center distance between girders.

The interior effective flange width is the smallest of three values calculated.

The exterior effective flange width can be calculated by Equation 8.7, but can not be larger than the interior effective flange width.

$$\text{Cantilever length} + \frac{1}{2} \cdot \text{Interior effective deck width} \quad (0.7)$$

The exterior effective flange width shall be the smaller of the value calculated from Equation 8.7 and the interior effective flange width.

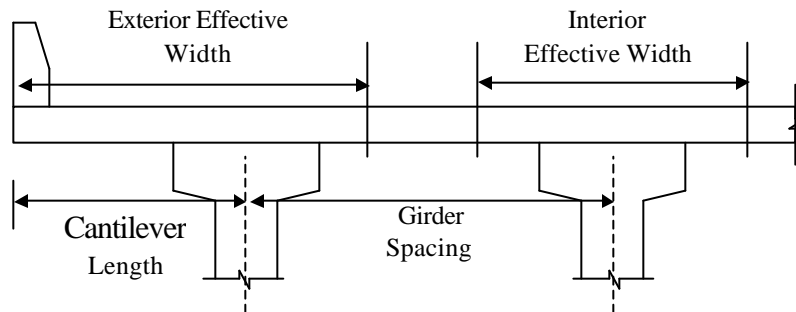


**Figure 0.11 Effective Flange Width Detail**

It may be noted that the interior effective width was used for the purposes of this study, due to the following reasons:

- The effective width of the interior girder is equal to or greater than that of the exterior girder in all cases. The use of the larger width is conservative.
- This is also consistent with current MoDOT design procedure where the exterior girders are typically designed the same as the interior girders to accommodate future bridge widening.

All references to effective flange width henceforth will refer to the interior effective flange width.

**Study Parameters.** Table 0.3 outlines the parameters that were modeled in the parametric study and the values that they assumed. For each of the five girder types, three different span lengths and three different girder

<sup>1</sup> MoDOT uses an effective deck thickness instead of the total slab thickness, which is calculated as the total slab thickness minus a 1-in. (25.4-mm) wearing surface.

spacing values were considered. These conditions were selected with the intention that a majority of MoDOT I-girder bridges would be covered with the parametric study. Both the AASHTO positive and negative gradients were applied in each case. Additionally, the boundary conditions of the models were considered as both unrestrained or fully restrained.

The actual boundary conditions at the pier cap/diaphragm interface for the typical continuous bridge will be somewhere in between fully restrained and unrestrained. Two approaches were considered for the determination of a design stress distribution due to thermal effects. First, a degree of fixity for the modeling could have been selected based on a recommendation for fixity of bridges within the State. However, this would have been impractical due to the significant variation in bridge geometries throughout the State. Or, secondly, and more practical, a more conservative approach could have been taken where both the restrained and unrestrained models were examined. The second option was used for the parametric study, whereby both fully restrained and unrestrained models would be examined, due to the conservative nature of the thermal stress distribution yielded.

**Table 0.3 Parametric Study Parameters and Values**

Girder Type	Span Length								
	30'	40'	50'	60'	70'	80'	90'	100'	110'
Type II	7'-9"	7'-9"	7'-9"						
	8'-4"	8'-4"	8'-4"						
	9'-6"	9'-6"	9'-6"						
Type III		7'-9"	7'-9"	7'-9"					
		8'-4"	8'-4"	8'-4"					
		9'-6"	9'-6"	9'-6"					
Type IV			7'-9"	7'-9"	7'-9"				
			8'-4"	8'-4"	8'-4"				
			9'-6"	9'-6"	9'-6"				
Type VI				7'-9"	7'-9"	7'-9"			
				8'-4"	8'-4"	8'-4"			
				9'-6"	9'-6"	9'-6"			
Type VII							7'-9"	7'-9"	7'-9"
							8'-4"	8'-4"	8'-4"
							9'-6"	9'-6"	9'-6"

Note: 12 in. = 1 ft., 1 ft. = 0.3048 m

The five girder types vary in size, and therefore, have varying areas, centers of gravity, and moments of inertia, as outlined in Table 0.4. Additionally, each of the five girder types is illustrated in Figures 8.12 through 8.16.

Additional parameters necessary for the thermal stress calculations were the coefficient of thermal expansion and strength of the concrete. According to Mindess and Young (1981), the coefficient of thermal expansion for concrete can range from approximately  $4.5 \times 10^{-6} / ^\circ\text{F}$  ( $8.1 \times 10^{-6} / ^\circ\text{C}$ ) to  $11.0 \times 10^{-6} / ^\circ\text{F}$  ( $19.8 \times 10^{-6} / ^\circ\text{C}$ ). For the purposes of this study, the coefficient of thermal expansion was assumed to be  $6.0 \times 10^{-6} / ^\circ\text{F}$  ( $10.8 \times 10^{-6} / ^\circ\text{C}$ ), which is the coefficient of thermal expansion recommended by AASHTO (1998). The concrete strength of the deck was assumed to be 4000 psi (27.56 MPa), while the concrete strength of the girder was assumed to be 5000 psi (34.45 MPa). These values for concrete strength were chosen based on current MoDOT design procedures.

**Table 0.4 Girder Properties**

Girder Type	Area (in <sup>2</sup> )	Y <sub>b</sub> (in)	I (in <sup>4</sup> )
II	310.9	14.08	33,974
III	381.9	17.08	61,841
IV	428.9	19.54	92,450
VI	643.6	25.92	235,735
VII	787.4	37.58	571,047

Note: 12 in. = 1 ft., 1 ft. = 0.3048 m

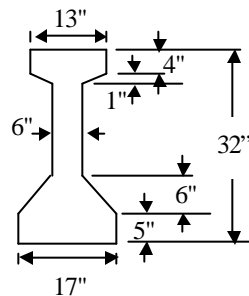


**Figure 0.12 Cross Section of Girder Type II**

Note: 12 in. = 1 ft., 1 ft. = 0.3048 m

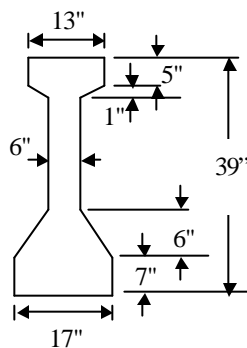


**Figure 0.13 Cross Section of Girder Type III**

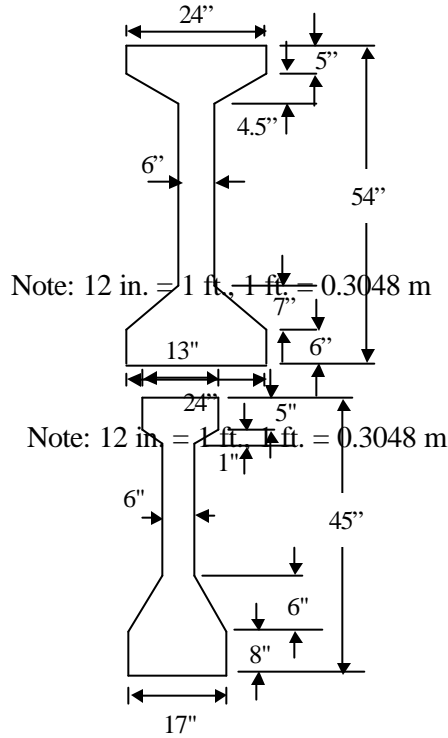


**Figure 0.14 Cross Section of Girder Type IV**

**Figure 0.15 Cross Section of Girder Type VI**  
 Note: 12 in. = 1 ft., 1 ft. = 0.3048 m

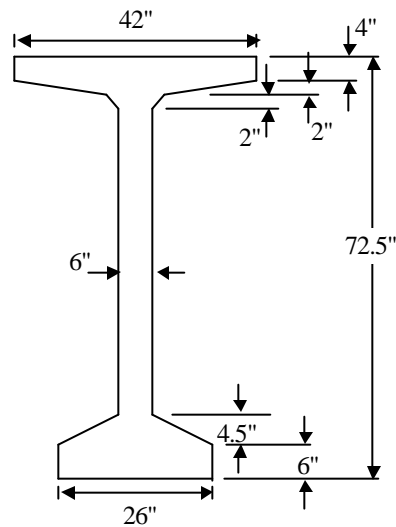


**Figure 0.16 Cross Section of Girder Type VII**  
 Note: 12 in. = 1 ft., 1 ft. = 0.3048 m

Additionally, it is important to note that the thermal stresses developed will not be a function of span length. Recall, from Equations 8.2 and 8.3 that the length of the member does not enter into the calculation of the thermal stresses for either the fully restrained or the unrestrained conditions. This fact decreases the parameters of the study to girder type and girder spacing. Although span length could potentially influence the interior effective flange width, see Equation 8.4, this value will only determine the actual effective flange width when the span length is relatively short.

The first step of the parametric study was to determine the effective flange width for each of the span length-girder spacing combinations. The effective flange width values are illustrated in Tables 8.5 through 8.9, with each table outlining the values for one of the girder types.

**Table 0.5 Effective Flange Width Values for Type II Girder**

Span Length	Girder Spacing	Effective Flange Width
30'	7'-9"	90"
	8'-4"	
	9'-6"	
40'	7'-9"	93"
	8'-4"	100"
	9'-6"	108"
50'	7'-9"	93"
	8'-4"	100"
	9'-6"	108"

Note: 12 in. = 1 ft., 1 ft. = 0.3048 m

**Table 0.6 Effective Flange Width Values for Type III Girder**

Span Length	Girder Spacing	Effective Flange Width
40'	7'-9"	93"
	8'-4"	100"
	9'-6"	108"
50'	7'-9"	93"
	8'-4"	100"
	9'-6"	108"
60'	7'-9"	93"
	8'-4"	100"
	9'-6"	108"

Note: 12 in. = 1 ft., 1 ft. = 0.3048 m

**Table 0.7 Effective Flange Width Values for Type IV Girder**

Span Length	Girder Spacing	Effective Flange Width
50'	7'-9"	93"
	8'-4"	100"
	9'-6"	108"
60'	7'-9"	93"
	8'-4"	100"
	9'-6"	108"
70'	7'-9"	93"
	8'-4"	100"
	9'-6"	108"

Note: 12 in. = 1 ft., 1 ft. = 0.3048 m

**Table 0.8 Effective Flange Width Values for Type VI Girder**

Span Length	Girder Spacing	Effective Flange Width
60'	7'-9"	93"
	8'-4"	100"
	9'-6"	108.5"
70'	7'-9"	93"
	8'-4"	100"
	9'-6"	108.5"
80'	7'-9"	93"
	8'-4"	100"
	9'-6"	108.5"

Note: 12 in. = 1 ft., 1 ft. = 0.3048 m

**Table 0.9 Effective Flange Width Values for Type VII Girder**

Span Length	Girder Spacing	Effective Flange Width
90'	7'-9"	93"
	8'-4"	100"
	9'-6"	108"
100'	7'-9"	93"
	8'-4"	100"
	9'-6"	108"
110'	7'-9"	93"
	8'-4"	100"
	9'-6"	108"

Note: 12 in. = 1 ft., 1 ft. = 0.3048 m

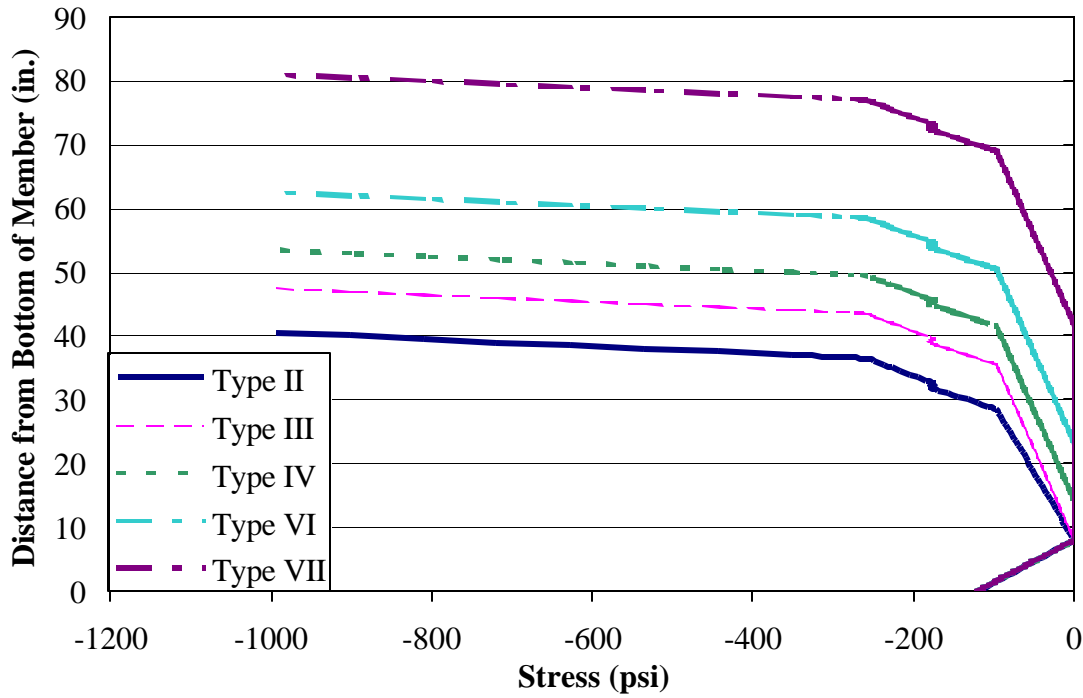
Once the effective flange width values were determined, the thermal gradients for each girder type were calculated. As mentioned previously, the thermal gradients are a function of the depth of the member.

Therefore, the gradient considered is different for each girder type.

Having determined the geometry of the girders, including the effective flange width, and the thermal gradients to be applied, the thermal stresses for each condition were calculated. Recall that, for each girder, four thermal stress distributions were calculated based on the possible combinations of the two boundary conditions with the two thermal gradients.

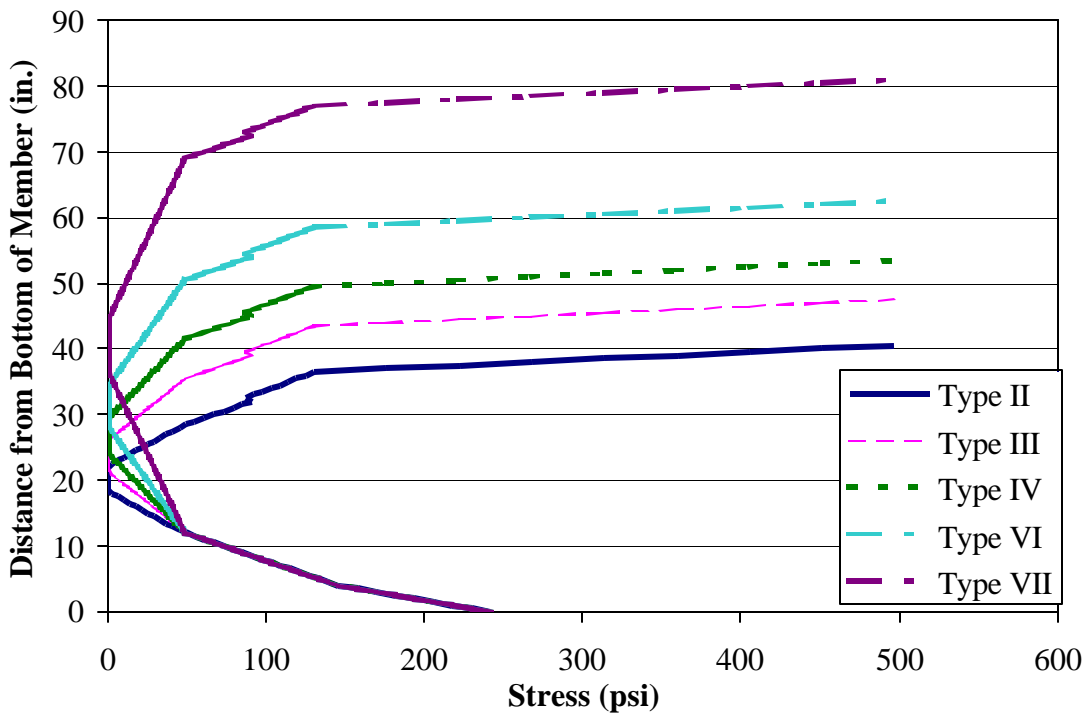
**Results and Discussion.** The results of the thermal stress calculations for the fixed boundary conditions are identical for all effective flange widths considered. This is due to the fact that the geometric parameters of the girders are not considered in the calculations. (See Equation 8.2.) Figures 8.17 and 8.18 illustrate the thermal stresses for each of the five girder types in a fully restrained condition for the positive and negative thermal gradients, respectively.

Conversely, the results for the unrestrained condition are not identical for the various effective flange width values. However, due to the relatively small range of effective flange width values, the results are, for all practical purposes, the same. Figures 8.19 and 8.20 illustrate the thermal stresses for an Type II girder in an unrestrained condition and 90 in. (2.29 m.) and 93 in. (2.36 m.) effective flange width values. Figure 8.19 illustrates the results for the positive thermal gradient; Figure 8.20 illustrates the results for the negative thermal gradient.



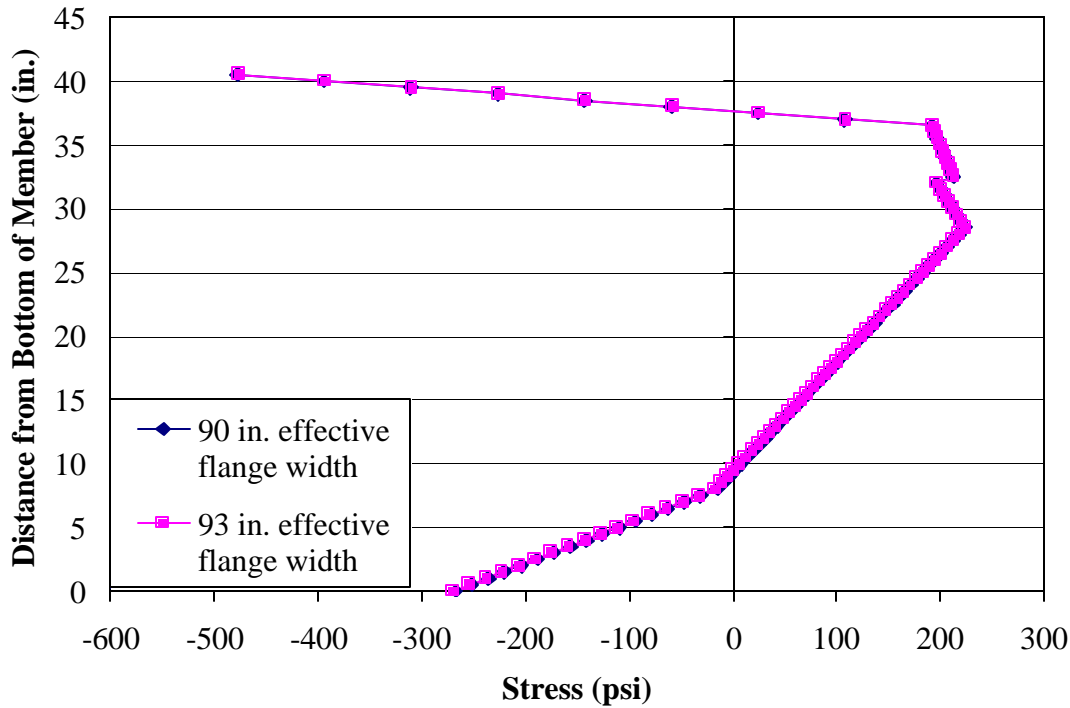
Note: 1 psi = 6.89 kPa, 1 in. = 25.4 mm

Figure 0.17 Thermal Stresses – Fully Restrained – Positive Gradient



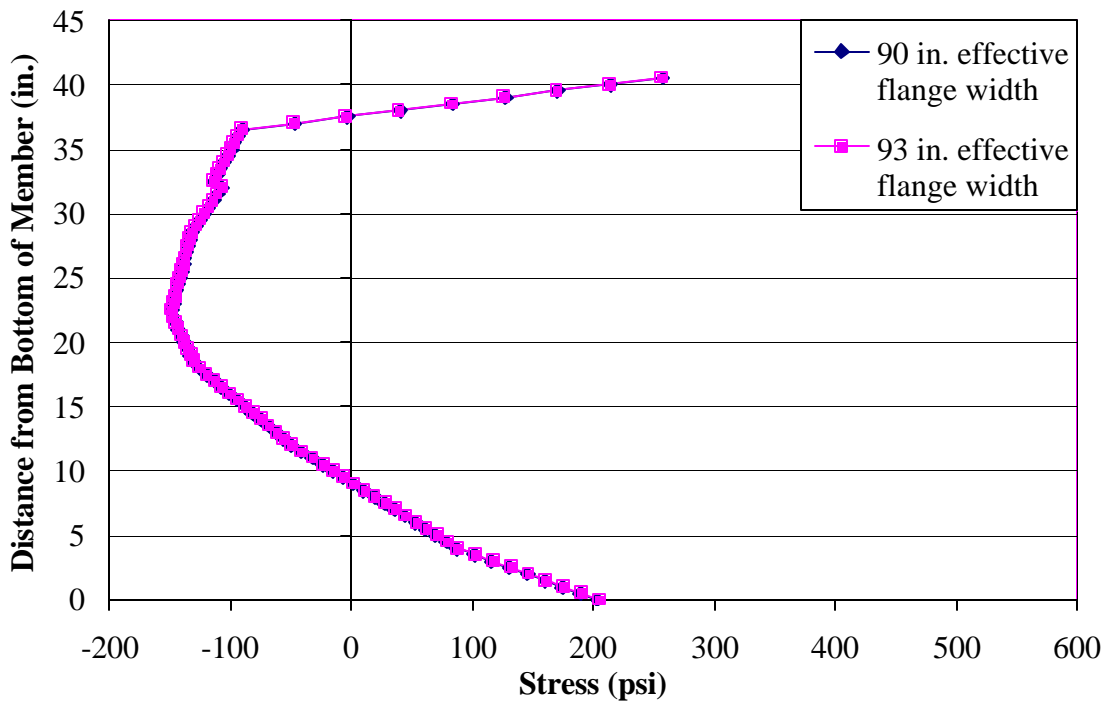
Note: 1 psi = 6.89 kPa, 1 in. = 25.4 mm

Figure 0.18 Thermal Stresses – Fully Restrained – Negative Gradient



Note: 1 psi = 6.89 kPa, 1 in. = 25.4 mm

**Figure 0.19 Thermal Stresses – Positive Gradient –Girder Type II**

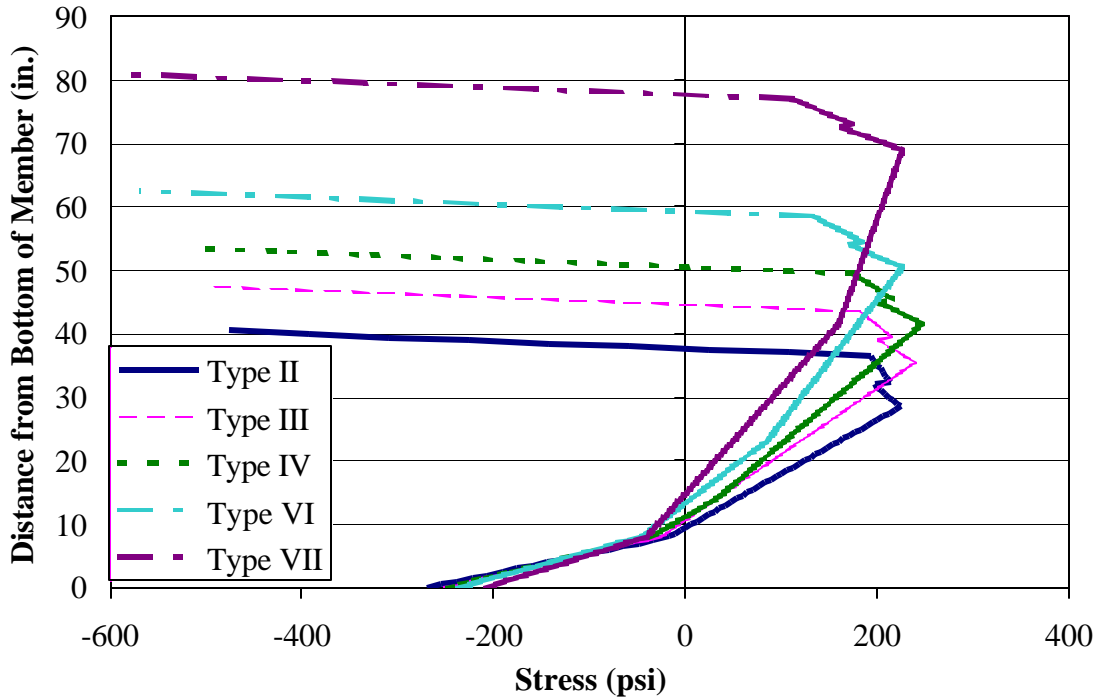


Note: 1 psi = 6.89 kPa, 1 in. = 25.4 mm

**Figure 0.20 Thermal Stresses – Negative Gradient –Girder Type II**

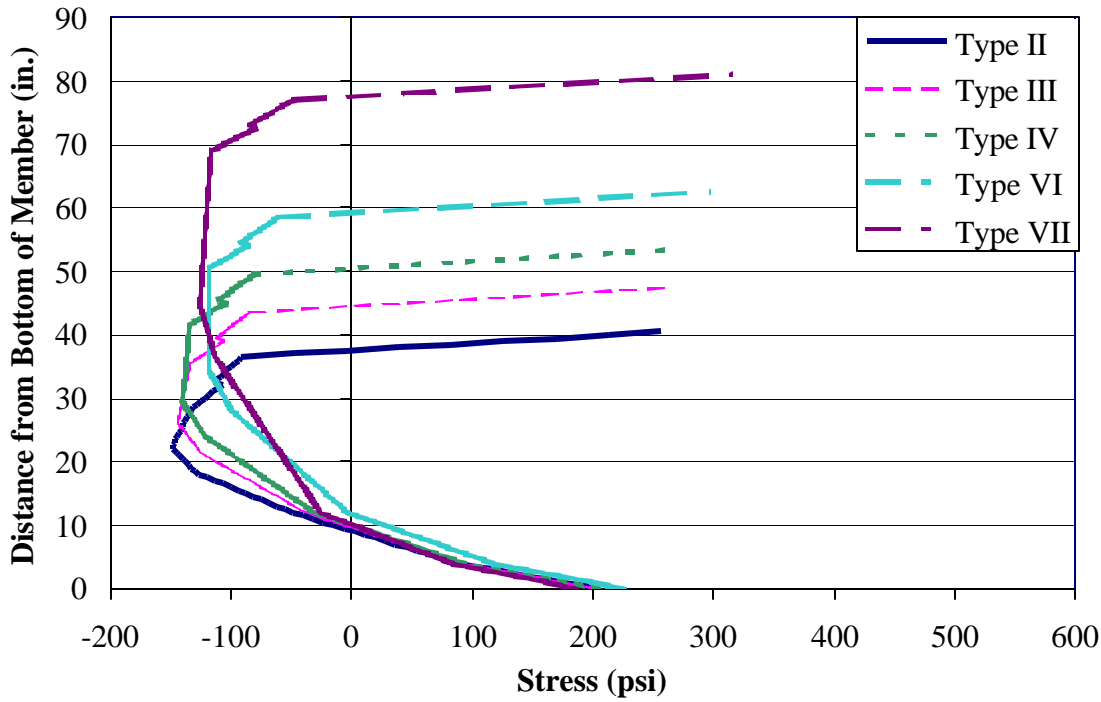
Based on the fact that the results for the three effective flange width values are virtually identical, the results reported henceforth will be for a 93-in. (2.36-m.) effective flange width. It may also be noted that each

girder type was analyzed using an effective flange width of 93 inches (2.36 meters). Figures 8.21 and 8.22 illustrate the thermal stresses for each of the five girder types for the unrestrained condition for the positive and negative thermal gradients, respectively. Additionally, Figures 8.23 through 8.27 illustrate the results for both the positive and negative gradients, and both boundary conditions, by girder type.



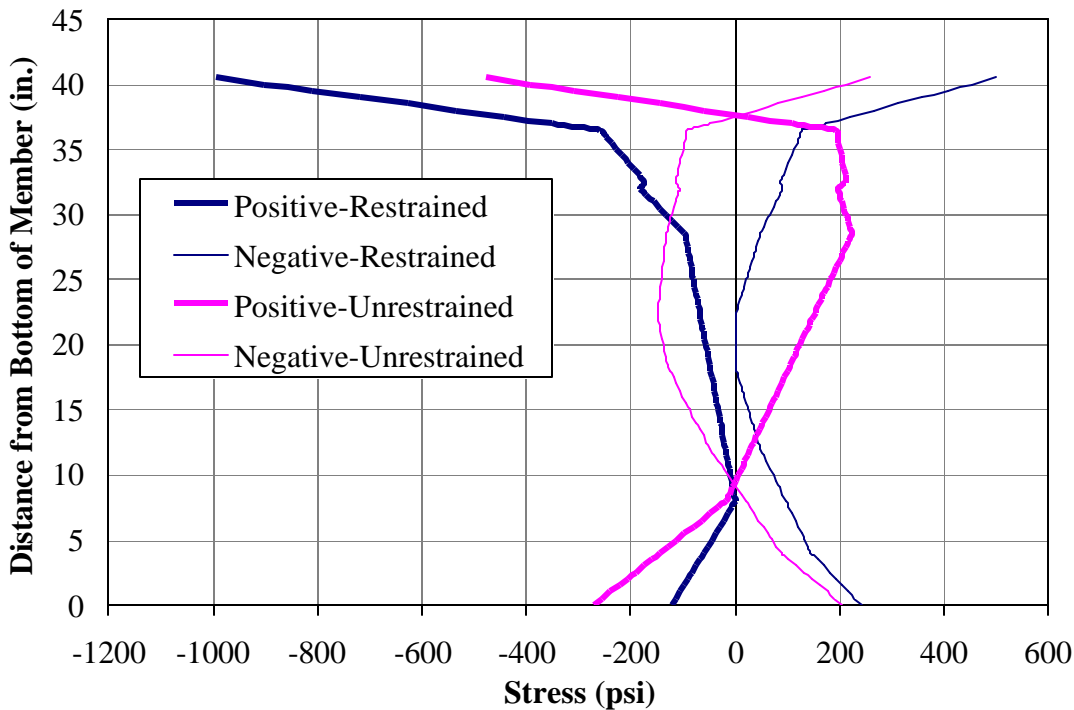
Note: 1 psi = 6.89 kPa, 1 in. = 25.4 mm

**Figure 0.21 Thermal Stresses – Unrestrained – Positive Gradient**



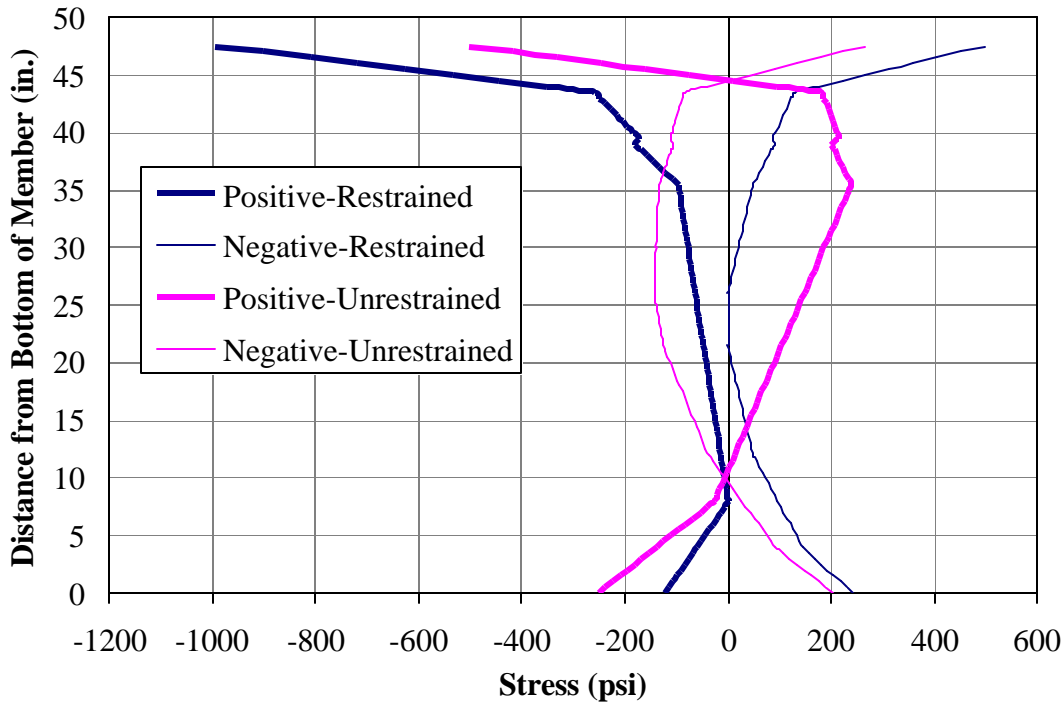
Note: 1 psi = 6.89 kPa, 1 in. = 25.4 mm

**Figure 0.22 Thermal Stresses – Unrestrained – Negative Gradient**



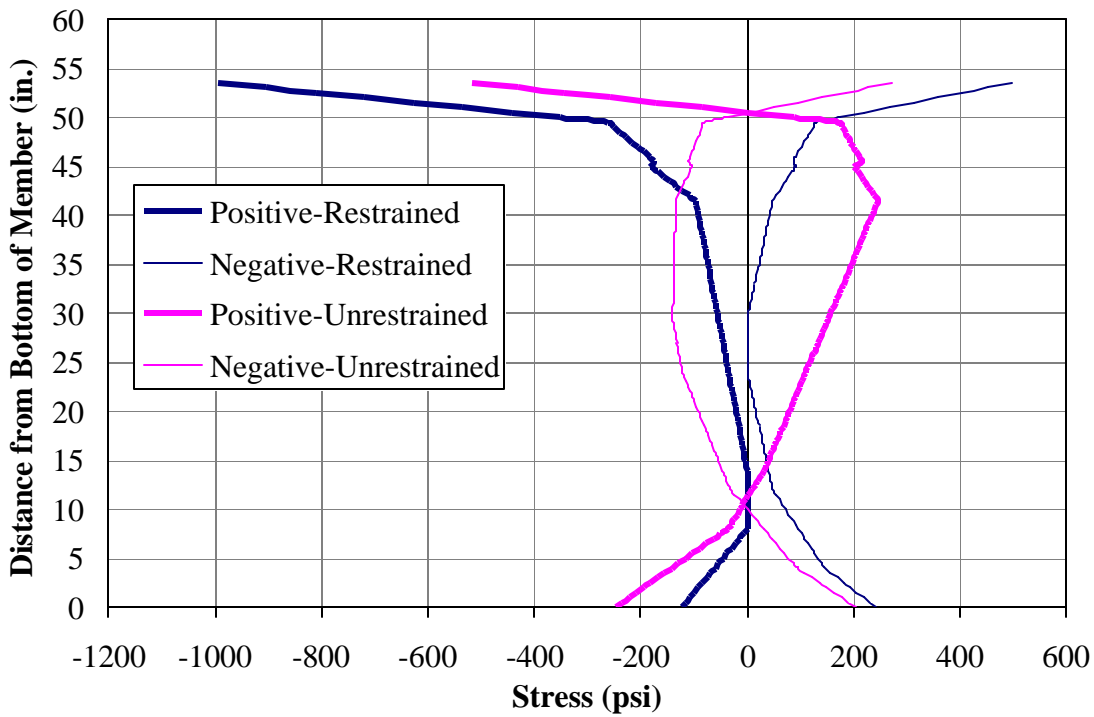
Note: 1 psi = 6.89 kPa, 1 in. = 25.4 mm

**Figure 0.23 Thermal Stresses –Girder Type II**



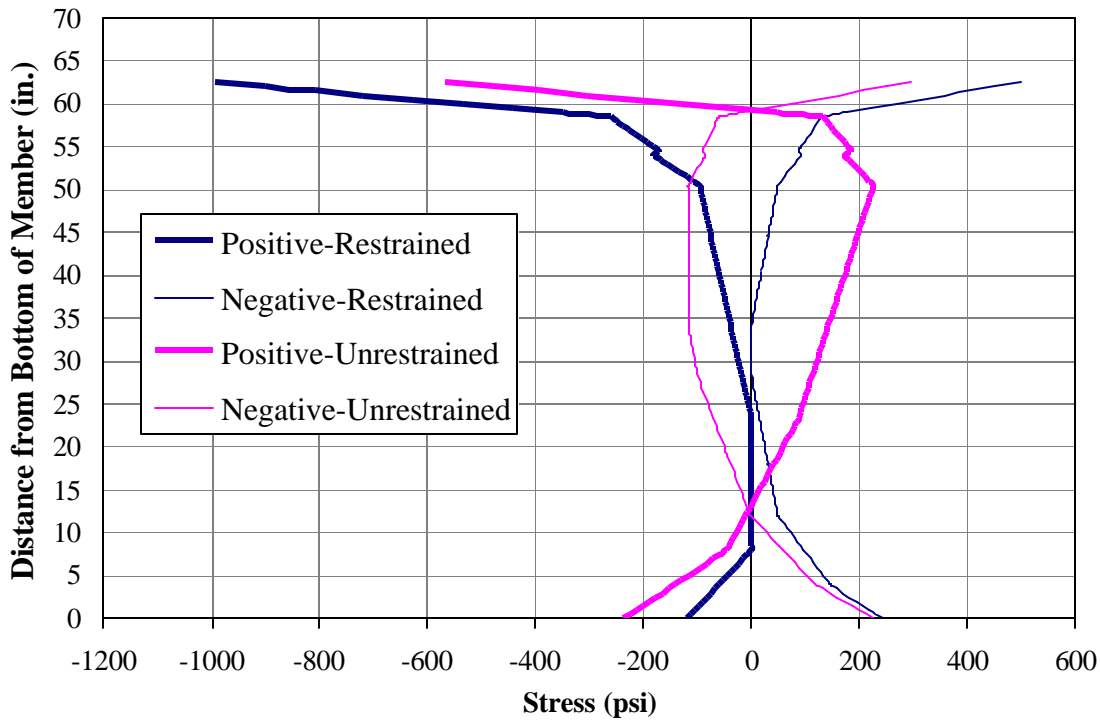
Note: 1 psi = 6.89 kPa, 1 in. = 25.4 mm

**Figure 0.24 Thermal Stresses – Girder Type III**



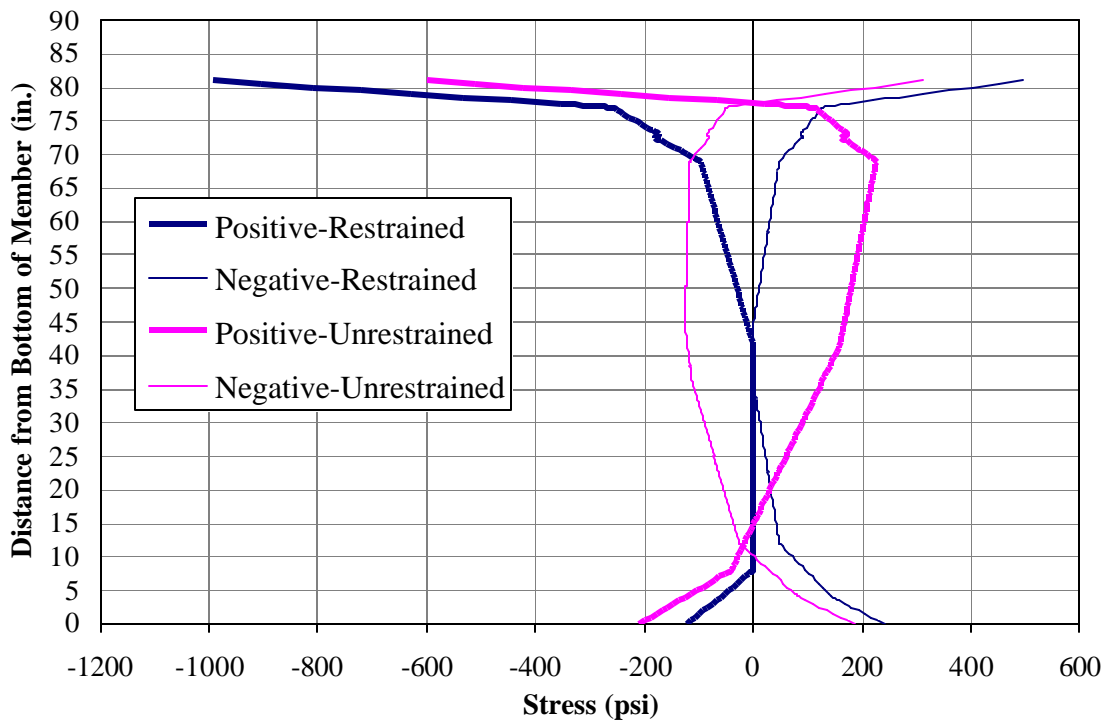
Note: 1 psi = 6.89 kPa, 1 in. = 25.4 mm

**Figure 0.25 Thermal Stresses – Girder Type IV**



Note: 1 psi = 6.89 kPa, 1 in. = 25.4 mm

**Figure 0.26 Thermal Stresses – Girder Type VI**



Note: 1 psi = 6.89 kPa, 1 in. = 25.4 mm

**Figure 0.27 Thermal Stresses – Girder Type VII**

Examination of the results indicates that for the conditions modeled the following was true:

- With respect to the maximum tensile stresses developed,
  - the thermal stresses for the positive gradient were greater for the unrestrained condition than for the fully restrained condition, and
  - the thermal stresses for the negative gradient were greater for the fully restrained condition than for the unrestrained condition.
- With respect to the maximum compressive stresses developed,
  - the thermal stresses for the positive gradient were greater for the fully restrained condition than for the unrestrained condition, and
  - the thermal stresses developed for the negative gradient were greater for the unrestrained condition than for the fully restrained condition.

Additionally, it is important to note the relatively large magnitude of the stresses developed due exclusively to thermal effects, with stresses ranging from approximately 1000 psi (6.89 MPa) in compression to approximately 500 psi (3.45 MPa) in tension.

**Sensitivity.** The overall sensitivity of the results of the parametric study was examined with respect to the concrete strength and effective flange width. The sensitivity with respect to the effective flange width was examined in Section 8.3.3. It is widely accepted that the actual strength of concrete will exceed the design strength. This is due to a number of reasons, including additional strength gain over time due to hydration of cementitious materials and the overdesign strength of the mix design by the concrete producer to ensure design strengths are met. To assure that the accuracy of the results would not be compromised due to a potential difference in concrete strength, the sensitivity of the parametric study results to concrete strength was examined.

The parametric study was conducted using the MoDOT concrete design strength requirements of 4000 psi (27.56 MPa) for the deck and 5000 psi (34.45 MPa) for the girders. A second analysis was performed using a 5000-psi (34.45-MPa) concrete strength for the deck and a 7000-psi (48.23-MPa) concrete strength for the girders. This analysis was performed on the Type II girder with fixed boundary conditions for both the positive and negative gradients. The sensitivity of the results was assessed by comparing these two sets of results. Figure 8.28 compares the thermal stresses for the positive gradient and the restrained condition. Figure 8.29 compares the thermal stresses for the negative gradient and the restrained condition.

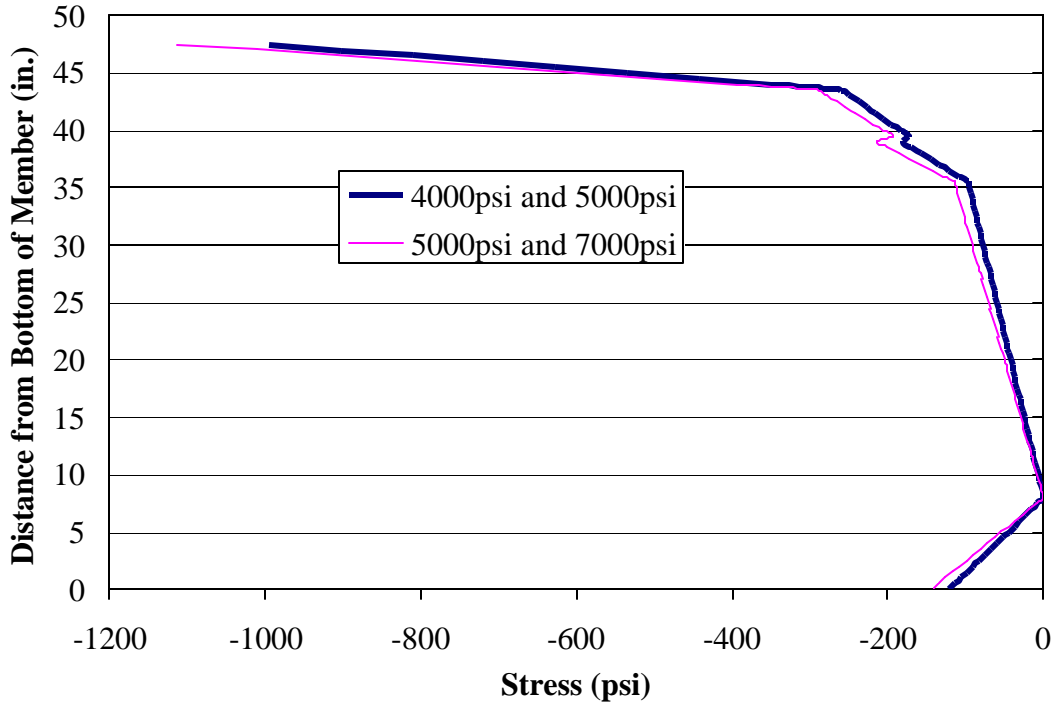
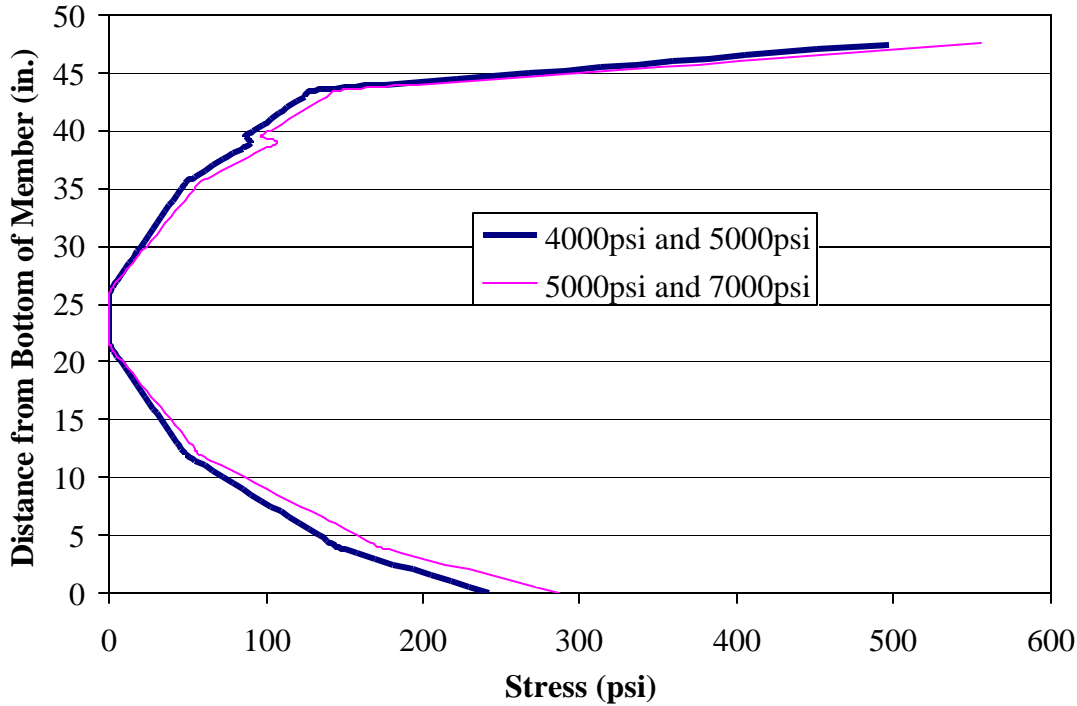


**Figure 0.28 Sensitivity of Thermal Stresses – Positive Gradient**

The difference in thermal stresses for the two cases is as much as ten percent and, therefore, too large to assume that the results are equal. However, the main issue that is being investigated in this study is the development of cracks in the girders. Since the modulus of rupture of the concrete is empirically proportional to the concrete strength, it is higher in the case of a higher strength concrete and lower in the case of a lower strength concrete. The modulus of rupture of the concrete was calculated as approximately 474 psi (3.27 MPa), 530 psi (3.65 MPa), and 627 psi (4.32 MPa) for the 4000-psi (27.56 MPa), 5000-psi (34.45 MPa) and 7000-psi (48.23 MPa) concrete strengths, respectively.



Note: 1 psi = 6.89 kPa, 1 in. = 25.4 mm

**Figure 0.29 Sensitivity of Thermal Stresses – Negative Gradient**

*Simplified mathematical approach*

While the calculation of the thermal stresses for the restrained condition are simple in nature, the calculations for the unrestrained condition are more complex. In order to develop a simplified mathematical approach to the calculation of thermal stress for the unrestrained condition, a relationship was establish whereby the resultant force and the resultant moment could be more easily calculated, without compromising the accuracy of the analysis. This approach was taken in order for the thermal stresses to be easily determined by the practicing engineer.

By examining the values for “P” and “M” calculated by the exact solution, a series of simplified equations could be developed. These equations are a function of girder type and effective flange width (EFW). Table 8.10 summarizes these relationships. It may be noted that the average error of the force and moment approximations was on the order of 0.2% and 0.9%, respectively.

**Table 0.10 Simplified Equations for P and M**

Beam Type	Positive Gradient		Negative Gradient	
	P	M	P	M
II	3680*EFW	-25570*EFW	-2030*EFW	7825*EFW
III	3710*EFW	-33080*EFW	-2055*EFW	10240*EFW
IV	3710*EFW	-40115*EFW	-2075*EFW	12425*EFW

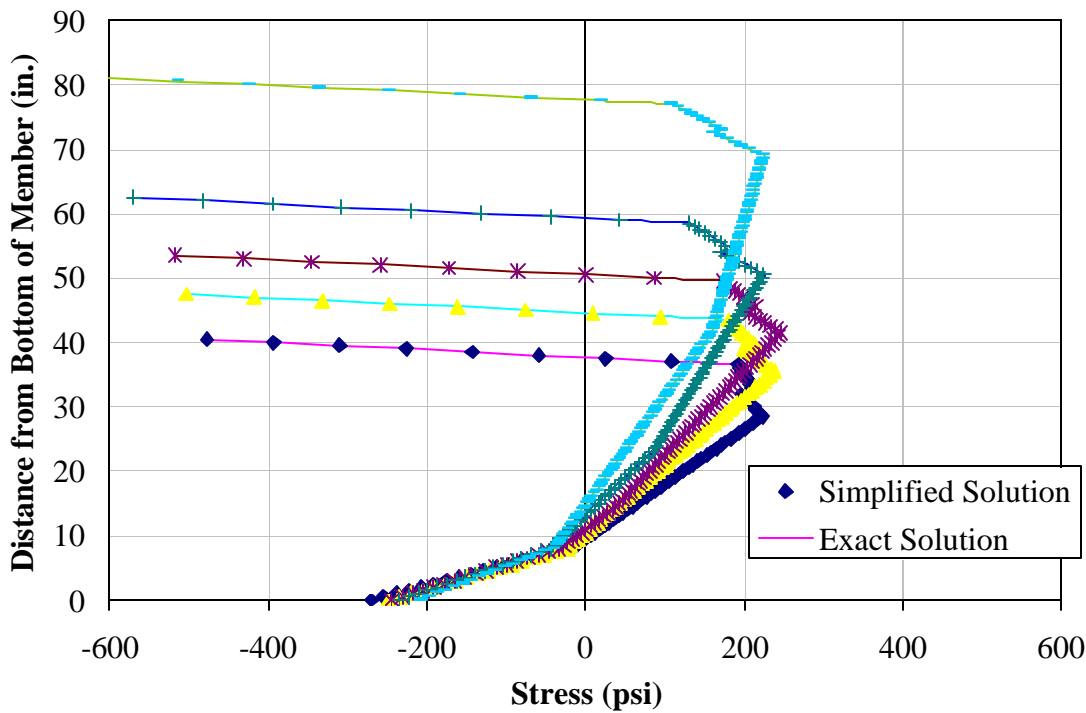
<b>VI</b>	3710*EFW	-54830*EFW	-2075*EFW	18980*EFW
<b>VII</b>	3950*EFW	-72925*EFW	-2305*EFW	19580*EFW

Note: 1 psi = 6.89 kPa, 1 in. = 25.4 mm

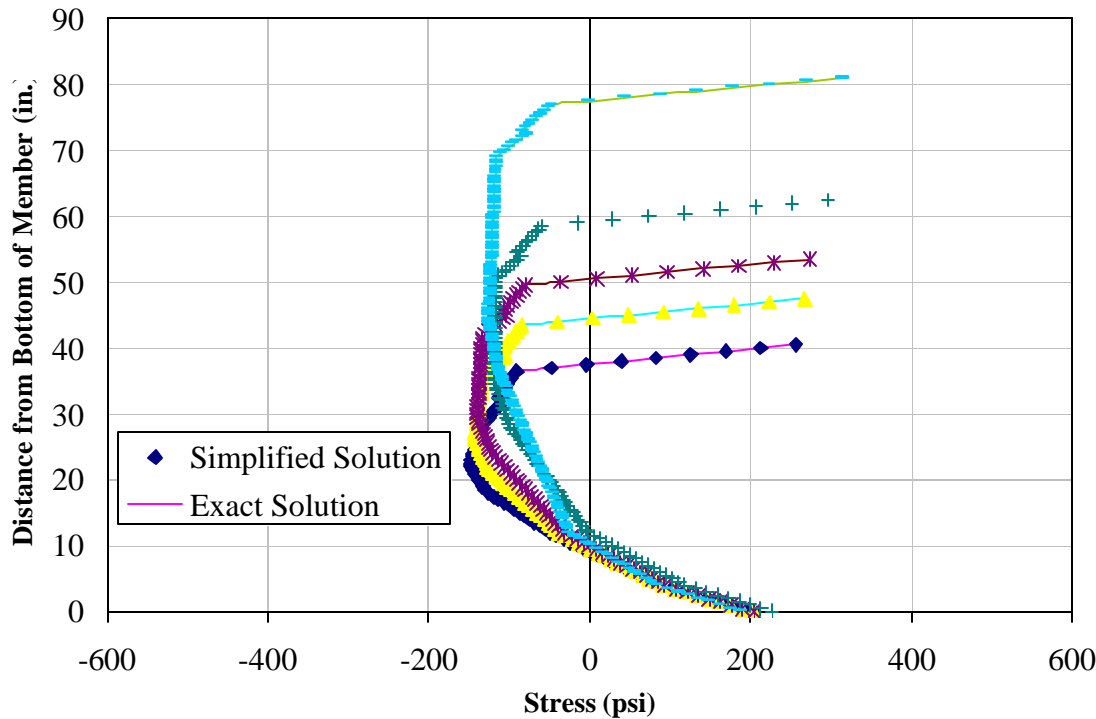
Using the values outlined in Table 8.10, Figures 8.30 and 8.31 were generated. Recall Equation 8.3 in which the resultant force and resultant moment are used to calculate the thermal stresses induced in an unrestrained member.

$$s_{unrestrained} = -aET(y) + \frac{P}{bh} + \frac{My}{I}$$

Figures 8.30 and 8.31 compare the results obtained using the simplified method to the results obtained by the exact solution, for each girder type, for the positive and negative thermal gradients, respectively. In these two figures, the solid lines represent the exact solution and the data points represent the simplified solution.



Note: 1 psi = 6.89 kPa, 1 in. = 25.4 mm  
**Figure 0.30 Comparison of Results for the Positive Gradient**



Note: 1 psi = 6.89 kPa, 1 in. = 25.4 mm

**Figure 0.31 Comparison of Results for the Negative Gradient**

The simplified solution results match the exact solution within approximately one percent. The high degree of accuracy exhibited by the simplified solution indicates that this method would be suitable for use in calculation of thermal stresses for the conditions modeled.

### *discussion of results*

The authors recommend that thermal stresses should be considered in the design of concrete bridges in the State of Missouri. In support of this recommendation is AASHTO (1989, pg. 1), which states, “All concrete bridges should be designed for temperature effects resulting from time-dependent fluctuations in the effective bridge temperature. Both longitudinal and transverse stresses and movements resulting from the positive and negative vertical temperature gradients...shall be considered for service stability crack control.”

Based on the analyses outlined herein, there are three possible recommendations that could be made to MoDOT in order to facilitate the calculation of such thermal stresses.

- First, the exact solution could be used to calculate the thermal stresses. This could be accomplished with the use of a commercially available mathematical program. This method would provide the highest level of accuracy, but it would also be the most time consuming for the practicing engineer. However, since the analysis has already been performed by UMR, it could be possible to furnish the necessary files to MoDOT for their use.
- Second, the simplified solution results could be used. The high degree of accuracy of this solution and the more “user-friendly” format for calculating the P and M are quite desirable.
- Third, the figures provided could be used to obtain the thermal stress at a particular depth of the member. This method would be the least accurate, due to the possibility of human error in the reading of the figures.

Based on the high degree of accuracy and ease of use of the simplified solution the authors recommend that MoDOT use this methodology for calculating the thermal stress distribution to be incorporated in to the design of its concrete bridges.

Having recommended that MoDOT incorporate these thermal stresses into their current design procedure, a design example was performed to illustrate the incorporation of the thermal stresses. The design example analysis took into account all dead and live loads, in addition to prestress losses, as is current MoDOT design procedure. The thermal stress distribution calculated by the simplified solution was also considered in the analysis procedure. The bridge used in the design example was Bridge A4565, which is the cracked bridge that was selected for monitoring purposes in Section 7. In this way, the design example would determine whether the additional consideration of the thermal stresses would indicate that the bridge would crack. It may be noted that, for the design example considered, the thermal stresses are approximately 0.3 to 1.3 times the stresses due to dead load, live load and prestressing. See Appendix I for the design example calculations and discussion.

### **conclusions**

Conclusions drawn based on each research task undertaken are outlined in this section. Possible causes for cracking in the ends of the girders and of the diaphragm in continuous, composite, prestressed I-girder bridges were studied. Each cause was specific to the type of cracking observed: cracks in a direction perpendicular to shear cracks, vertical cracks, and cracks typical of shear stress induced cracking. Each type of crack was analyzed to determine the underlying causes and, wherever relevant, the associated stress levels and directions of principal stresses.

### ***database analysis***

The results of the statistical analysis can be summarized as follows:

- There seems to be two populations of data within the database, those inspected by the snoop truck and those inspected from ground level.
- There are more PC I-girder bridges in Missouri that are cracked than previously expected or reported.
- The cracked status of a bridge can be predicted with approximately 77 percent accuracy using the proposed model, which is a function of the shear reinforcement spacing near the center of the girder, girder area, span length, aggregate type, and route type.
- Chert aggregate use increases the probability of cracking for those bridges, as calculated by the proposed model. The chert aggregate is used in the deck concrete of some bridges in southern Missouri.
- Interstate highway bridges have a lower probability of cracking, compared to non-interstate highway bridges, as calculated by the proposed model.
- For a given girder area, longer span lengths will decrease the probability of cracking given by the proposed model.

### ***early-age behavior of prestressed concrete girders***

Early-age cracking due to heat of hydration and steam curing was studied using a finite element procedure and a modified version of the Gergely - Sozen model (1967) was used to compute principal tensile stress at the girder-ends. The results of these analyses were as follows:

- Residual principal tensile stresses in the web region during curing were found to be 5% to 25% of typical modulus of rupture values.
- It was found that maximum vertical end stresses due to stress transfer could be in excess of 50% of the modulus of rupture.
- It is possible that a combination of these two things could result in girder-end cracking.
- Such cracks are essentially in the web and along the axis of the girder (horizontal cracks). Horizontal cracks are typically located near the junction of the bottom flange and the web. Diagonal cracks originating from the top flange and progressing down into the web (direction perpendicular to typical shear cracks) can also result from early-age loading on the girders.

### ***diaphragm detailing***

The effects of continuity on cracking in girders and diaphragms were studied. Based on analysis of in service temperature data and a limited survey of other states' diaphragm details the conclusions were made:

- Vertical cracks in girders near the end, spalling of diaphragms and girders pulling out of diaphragms were attributed to service temperature loading and continuity detailing used. Similar cracking in the

past has also been attributed to creep and shrinkage of concrete (effect similar to service temperature loading when girders are restrained at the diaphragm).

- A survey of diaphragm detailing from several other states' Departments of Transportation was studied and potential solutions used by them were reviewed. One is to eliminate the diaphragm altogether, providing either no continuity, or continuity only with the slab. These options would not work for Missouri, where deicing salts are routinely used in the winter. This would lead to many new maintenance problems associated with chloride penetration and corrosion. Other options involve providing restraint-free movement of the girders or diaphragm so that cracking does not occur.
- Several options similar to those used by Nebraska may be considered, including:
  - (1) provide an unbonded joint between the diaphragm and the bent beam so that the diaphragm may move more freely,
  - (2) allow for a construction joint in mid-height in the diaphragm, and
  - (3) provide a bond breaker on the sides of the girders so that they may slide freely in and out of the diaphragm.

### ***diagonal shear cracking***

Elastic shear stresses were studied to predict cracking, and an ultimate strength analysis was conducted to evaluate the structural integrity of girders with shear cracks in light of the diagonal cracks observed. The following conclusions were made:

- It was found using an elastic stress analysis that principal tensile stresses are only slightly smaller than the direct tensile strength of concrete. When the reduced tensile capacity resulting from residual stresses is considered, shear cracking can be expected to occur.
- It was found that the amount of shear reinforcement provided per MoDOT procedures is conservative compared to both AASHTO (1996) and ACI (1995) recommendations, and hence diagonal shear cracking is of no significant structural concern. However, this does not address the durability issues that arise when girders are cracked.

### ***bridge measurements***

Based on the bridge measurements taken during the project, only general conclusions can be made. These conclusions are as follows:

- There exists a positive thermal gradient at the two monitored bridges.
- The temperature differential is largest through the deck, with a smaller differential occurring between the top and bottom of the girders.
- The maximum measured temperature differential through the depth of the bridge deck was 39°F (21.7°C).
- The measured thermal gradients are in good agreement with the recommended positive thermal gradients proposed by AASHTO for the purposes of design.
- The bridges are experiencing measurable changes in deflection in the absence of traffic loads.
- For an increase in temperature differential, there is an upward movement, or bowing, of the bridge decks.

- These deflections are assumed to have been caused by the measured thermal gradients, due to the absence of traffic or other external forces.

### *thermal stress analyses*

With respect to the thermal stress calculations, the following conclusions can be drawn:

- Thermal stresses of relatively large magnitude are developed due exclusively to thermal effects, with stresses ranging from approximately 1000 psi (6.89 MPa) in compression to approximately 500 psi (3.45 MPa) in tension. The thermal stresses are on the order of 0.3 to 1.3 times the stress due to dead and live load (as illustrated in the design example).
- A simplified approach for calculation of thermal stresses was developed and proven to be an accurate alternative to the exact solution for the cases examined.

## recommendations

### *Design implementation recommendations*

Potential means of addressing the issue of girder end cracking are threefold. First, the cracking of the girder end could be potentially eliminated in future construction via inclusion of thermal stresses in the concrete bridge design procedure. Secondly, a modification to the support detail could be implemented in future construction. Third, the structural performance of the existing members could be enhanced through the use of external strengthening if long-term monitoring indicates deterioration that could impact structural safety and/or reliability.

**Thermal Stresses in Design.** The authors recommend that thermal stresses should be considered in the design of concrete bridges in the State of Missouri. In support of this recommendation is AASHTO (1989, pg. 1), which states, “All concrete bridges should be designed for temperature effects resulting from time-dependent fluctuations in the effective bridge temperature. Both longitudinal and transverse stresses and movements resulting from the positive and negative vertical temperature gradients...shall be considered for service stability crack control.”

Based on the analyses outlined herein, there are three possible recommendations that could be made to MoDOT in order to facilitate the calculation of such thermal stresses.

- First, the exact solution could be used to calculate the thermal stresses. This could be accomplished with the use of a commercially available mathematical program. This method would provide the highest level of accuracy, but it would also be the most time consuming for the practicing engineer. However, since the analysis has already been performed by UMR, it could be possible to furnish the necessary files to MoDOT for their use.
- Second, the simplified solution results could be used. The high degree of accuracy of this solution and the more “user-friendly” format for calculating the P and M are quite desirable.
- Third, the figures provided could be used to obtain the thermal stress at a particular depth of the member. This method would be the least accurate, due to the possibility of human error in the reading of the figures.

Based on the high degree of accuracy and ease of use of the simplified solution the authors recommend that MoDOT use this methodology for calculating the thermal stress distribution to be incorporated in to the design of its concrete bridges.

**Alternate Support Details.** In the first case, the detail at the girder supports could be modified to eliminate the thermal stresses that are induced due to the current continuity detail. Three potential detail modifications are outlined herein.

One method would be to eliminate the cast-in-place diaphragm. An alternative to the cast-in-place diaphragm is simple span girders constructed with a continuous deck. (See Figure 10.1) In this way, a certain degree of continuity would still exist for negative moment over the piers. Additionally, the girders would be allowed a small degree of displacement/rotation at the end, due to the presence of the bearing pad, which would accommodate the development of the thermal stresses and relative movements in the bridge.

It may be noted that the deck can be cast-in-place reinforced concrete or cast-in-place reinforced concrete with precast/prestressed panels. This detail, with the use of precast/prestressed panels, is used widely in the State of Texas, and has performed well with respect to the elimination of girder cracking. The possible drawback to this detail would be the development of shrinkage-related cracks at the top of the deck. There is a tendency for these shrinkage-related cracks to occur near the bent, due to a significant change

in stiffness at the transition from the girder to the bent cap. (Myers, 1999) It should be commented that these potential cracks would be no more severe or common than the level of deck cracking already typically observed by the authors in Missouri bridge decks. This detail would also avoid cracking in the primary load-resisting components, i.e. the girders.

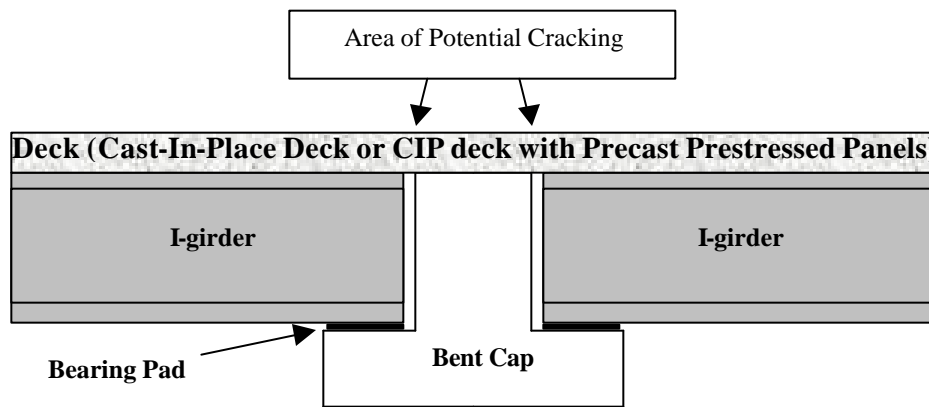


**Figure 0.1 Simple Span Girders with Continuous Deck**

Another design that conceptually addresses the potential of girder-end cracking is to isolate the continuity of the girder from the diaphragm. A construction joint or bond breaker could be placed on either side of the girder to allow displacement/rotation due to thermal stresses. The joint could be provided by either conducting a two-stage concrete pour or by providing a bond breaker to isolate the continuity of the girder from the diaphragm. An experimental research program would need to validate this detail and investigate the potential for deck cracking.

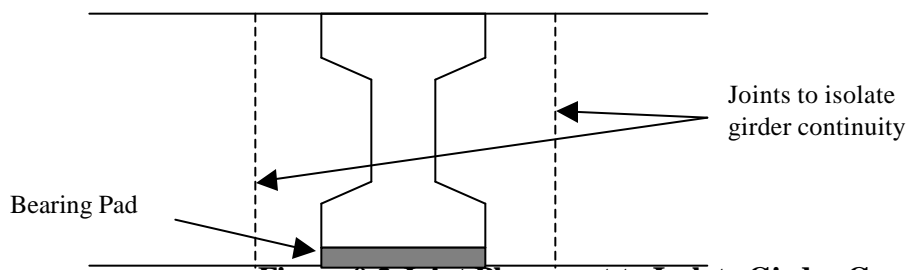


**Figure 0.2 Joint Placement to Isolate Girder Continuity**

A third method to modify the existing detail to avoid girder-end cracking would be the use of end blocks on the I-girders. While the use of end blocks are generally reserved for post-tensioning application where the stresses in the tendon anchorage zone are very high, they could be a potential solution to the cracking that is occurring at the girder ends. By increasing the area of the girder cross section at the end of the girder, the stress in this region could be effectively decreased. The limitation of this detail would be the fact that it would require the precast industry currently fabricating members for Missouri bridges to retool their forms to accommodate the end block.

The use of a bond breaker on the sides of the girders where embedded in the diaphragm would help to reduce the stresses created due to axial lengthening and shortening of the girders caused by seasonal temperature variations. This detail is used by Illinois and is shown in Figure 6.6.

Another possible method to isolate the girder movements caused by daily temperature variations using either an open space or an expansion material to isolate the diaphragm from the bent cap. This detail is used by both Illinois (open space or expansion material, Figure 6.6) and Nebraska (expansion material only, Figure 6.5). By isolating the diaphragm from the bent cap, rotational strains caused by daily temperature variations will not produce significant stresses since the diaphragm can rotate freely.

**Early-age Stresses.** Based upon our analyses of the early-age stresses in prestressed concrete I-Girders, the authors believe that the following recommendations could be followed to help alleviate or reduce early-age stresses

- Residual stresses could be reduced by controlling the thermal gradients that are generated during curing by reducing the heat of hydration and better distribution of heat due to steam curing.
- Additionally, the shape of the girder cross section was found to affect the magnitude and location of maximum residual stresses (based on differences in the location of maximum stress and distribution of stresses for the three girder types analyzed). Increasing the slope of the flange as it transitions to the web could help to reduce residual tensile stresses.
- Increasing the thickness of the web would help to reduce the stresses due to prestress transfer as well as early-age differential thermal loading.
- The tensile response of concrete at the girder-ends could be improved using discrete steel or polypropylene fiber reinforcement. This would also help reduce reinforcement congestion at the girder-ends.
- Use of end-blocks for the prestressed girders may also alleviate the problem of early-age girder-end cracking.

**Diagonal Shear Cracking.** Possible solutions to help eliminate/minimize shear-related cracking would be to:

- Increase the shear capacity of the concrete section by providing end blocks or using a thicker web.
- Use fiber reinforced concrete in the end regions, which would not only increase the tensile capacity of the concrete, but would also allow for a reduction in the amount of stirrup steel provided.

**Repair of the Girders.** If the structural safety or performance of the girders were in question, repair of the girders could be achieved through the use of epoxy injection of the cracks and application of externally bonded FRP reinforcement. Extensive research has been conducted at UMR to validate the use of FRP technology as an effective strengthening technique (Khalifa, 1999; Gose and Nanni, 1999; Huang, 2000).

The special consideration for the use of FRP laminates to the surface of an I-girder beam is the presence of the corners created by the transition for the web to the flange. In this region (see Figure 10.3), the laminate would need to be anchored to the member to assure proper bond, and thus proper load transfer.

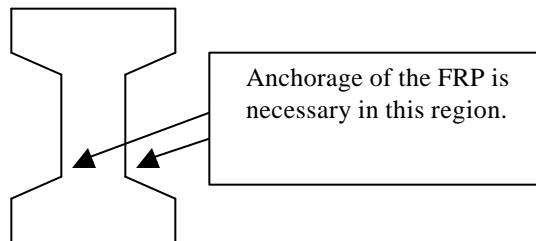


**Figure 0.3 Anchorage Region**

In particular, the work performed by Huang involved the use of such an anchorage system. Huang's research involved the testing of double-t beams with dapped-ends, which are often used in parking structures. The beams were constructed without the required steel reinforcement in the dapped-end area in order to facilitate strengthening of this area with FRP composites. Different configurations of the FRP application were tested and compared to attain a better understanding of the dapped-end behavior, the use of the FRP anchorage system, and the externally bonded FRP composites. The anchorage system involved cutting a groove into concrete, applying the FRP sheet to the concrete, and then anchoring the sheet in the groove with an FRP rod. See Figure 10.4 for a schematic of the anchorage system.

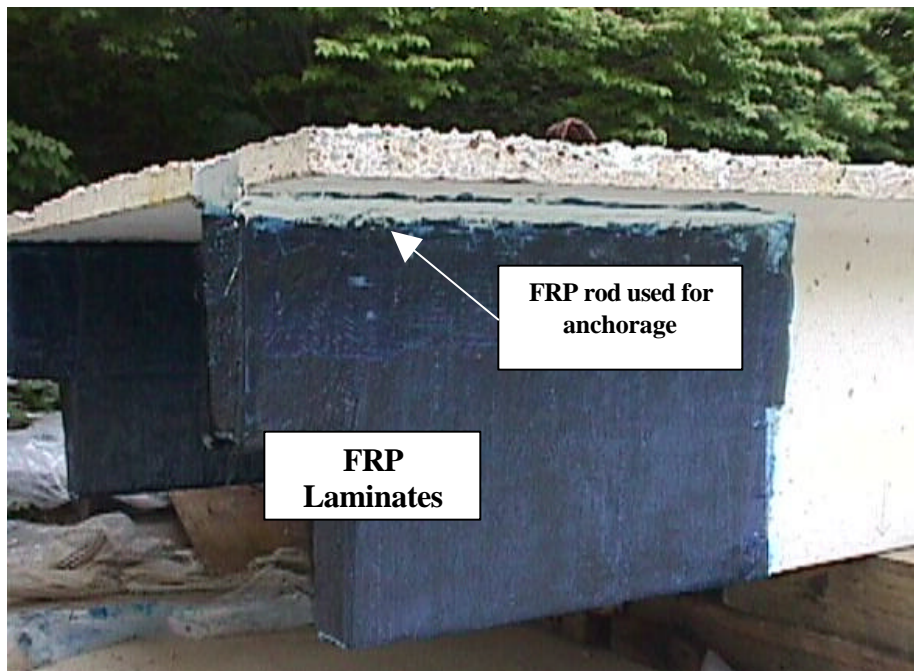


### Figure 0.4 Schematic of the Anchorage System

Judging from the effectiveness of both the strengthening technique and the anchorage system, this method is a viable solution as a potential method of repair and rehabilitation of the cracking experienced in the I-girder bridges. In spite of this, it may be noted that before full acceptance of FRP materials will be granted, the durability of these systems still needs to be validated.

The alternate details and repair method proposed in this section are merely suggestions. Further analysis would be necessary to determine the optimum solution for each bridge depending on its characteristics.

#### *recommendations for future research*

There are several issues that still need to be clarified with respect to thermal stresses induced in PC I-girder bridges in Missouri. Areas for potential future research are outlined as follows:

- As suggested in Section 7, long-term monitoring of the bridges should be conducted (see Appendix J for details), in order to:
  - isolate deflections caused by thermal gradients,
  - examine the negative gradients experienced by the bridges,
  - validate the tensile stresses calculated in the parametric study, and
  - determine the period during which the thermal stresses/deflections are the maximum.
- Laboratory experimentation to determine a potential modification to the continuity detail.
- The impact of the differences in the deck and girder concrete on the thermal stresses. In particular, the differences in the coefficient of thermal expansion have been mentioned as one possible factor.
- Construction sequence of the bridges and its impact on the thermal stresses.

## references

- Abdella, O., Ramirez, J. A., and Lee, R. H. *Continuity in Precast Prestressed Concrete Girder Bridges*. Structures Congress. ASCE. Atlanta Georgia, 1994.
- Alabama Department of Transportation. *Report: Cracks in Precast Prestressed Bulb Tee Girders on Structure No.'s I-565-45-11 A and B. in I-565 in Huntsville, Alabama*. September 22, 1994.
- American Association of State Highway and Transportation Officials. *AASHTO Guide Specifications: Thermal Effects in Concrete Bridge Superstructures*. AASHTO, Washington D.C., 1989.
- American Association of State Highway and Transportation Officials. *AASHTO LRFD Bridge Design Specifications*. AASHTO, Washington D.C., 1998.
- American Association of State Highway and Transportation Officials. *Standard Specifications for Highway Bridges*. AASHTO, Washington D.C., 1996.
- American Concrete Institute. *Cracking in Prestressed Concrete Structures*. Eds. Grant T. Halvorsen and Ned H. Burns. American Concrete Institute, Detroit, MI, 1989.
- American Concrete Institute, *Building Code Requirements for Structural Concrete and Commentary*, American Concrete Institute, Detroit, MI, 1995.
- ANSYS Users Manual, Version 5.4, 1999.
- Barnhill, G., *Experiences of Nebraska Department of Transportation*, Personal Communication, October 1999.
- Barrett, D. G. *Long Term Temperature Effects on High Performance Concrete Bridge Girders*, Honors Research Report, Advisor: Prof. V. S. Gopalaratnam University of Missouri – Columbia, August 2000.
- Bever, Michael B., ed., *Encyclopedia of Materials Science and Engineering*, v2 Permagon Press, Ltd., Oxford, England, 1986.
- Boley, Bruno A. *Theory of Thermal Stresses*. John Wiley & Sons, 1960, USA.
- Branson, D. E., *Deformation of Concrete Structures*, McGraw Hill, 1977.
- Chojnacki, T., *Determination of High Performance Concrete (HPC) Characteristics*, Missouri Department of Transportation, Report RDT 99-008, September 1999.
- Conway, F., *Alabama Department of Transportation Experiences with Continuous Concrete Girder Bridges*, Personal Communication, October 1999.
- Cooke, N., M.J.N. Priestley, and S.J. Thurston. *Analysis and Design of Partially Prestressed Concrete Bridges Under Thermal Loading*. PCI Journal. Vol. 29, no. 3, May/June 1984, pp. 94-115.
- Critchell, Peter L. *Joints and Cracks in Concrete*. CR Books, London, 1968.
- Dunker, Kenneth F. and Basile G. Rabbat. *Performance of Prestressed Concrete Highway Bridges in the United States – The First 40 Years*. PCI Journal. Vol. 37, no. 3, May/June 1992, pp. 48-64.
- Eatherton, M, *Instrumentation and Monitoring of High Performance Concrete Prestressed Bridge Girders*, Master's Thesis, Advisor: Prof. V. S. Gopalaratnam, University of Missouri – Columbia, August 1999.

- Earney, T.P., *Cracking in Prestressed I-Girder Bridges*, Master's Thesis, Advisor: Prof. V. S. Gopalaratnam, University of Missouri – Columbia, August, 2000.
- Elbadry, Mamdouh M. and Amin Ghali. *Temperature Variations in Concrete Bridges*. Journal of Structural Engineering. Vol. 109, no. 10, October 1983, pp. 2355-2374.
- Emanuel, Jack H., John L. Best, J. Leroy Hulsey, Joseph H. Senne, and LeRoy E. Thompson. *An Investigation of Design Criteria for Stresses Induced by Semi-integral end bents: Phase I—Feasibility Study*. Missouri Cooperative Highway Research Program Final Report 72-9.
- Emanuel, Jack H. and J. Leroy Hulsey. *Thermal Stresses and Deformations in Nonprismatic Indeterminate Composite Bridges*. Transportation Research Record 607. Transportation Research Board, Washington D.C., 1976, pp. 4-6.
- Emanuel, Jack H. and David J. Wisch. *Thermal Stresses Induced in a Composite Model Bridge Structure*. Missouri Cooperative Highway Research Program Final Report 75-2, August 1977.
- Federal Highway Administration (FHWA), *National Bridge Inventory Data*, U.S. Department of Transportation, December 1998.
- Freyermuth, Clifford L., *Design of Continuous Highway Bridges with Precast, Prestressed Concrete Girders*, PCI Journal, v14, n2, April 1969, pp. 14-39.
- Gamble, W. M. *Reader's Comments: Release Methodology of Strands to Reduce End Cracking in Pretensioned Concrete Girders* PCI Journal, v42, n4, April, 1997, pp. 102-108.
- Gatewood, B.E. *Thermal Stresses*. McGraw-Hill Book Company, Inc., New York, 1957.
- Gergely, P., and Sozen, M. A., *Design of Anchorage-Zone Reinforcement in Prestressed Concrete Beams*, PCI Journal, v12, n2, April 1967, pp. 63-75.
- Gerwick, Ben C. Jr. *Construction of Prestressed Concrete Structures*. 2<sup>nd</sup> Edition. John Wiley & Sons, Inc., New York, 1993.
- Ghali, A. and R. Favre. *Concrete Structures: Stresses and Deformations* 2<sup>nd</sup> Ed. E&FN SPON, New York, 1994.
- Gopalaratnam, V.S., and Eatherton, M., *Instrumentation and Monitoring of High Performance Concrete Bridge Girders*, Report to Missouri Department of Transportation, University of Missouri – Columbia, May 2001.
- Gose, Stephen and Antonio Nanni. *Anchorage System for Externally Bonded FRP Laminates Using Near Surface Mounted FRP Rods*. Report Number CIES-99/07, University of Missouri-Rolla, 1999.
- Gunst, Richard F. and Robert L. Mason. *Regression Analysis and its Application : A Data-Oriented Approach*. Marcel Dekker, Inc., New York, 1980.
- Hiley, Darren T., *Computer Aided Load Capacity Ratings of Slab-On-Steel and Concrete Girder Bridges*, Master's Thesis, University of Missouri – Columbia, 1994.
- Huang, Pei-Chang. *Dapped-End Strengthening in Precast Prestressed Concrete Double Tee Beams with FRP Composites*. M.S. Thesis (in progress), University of Missouri – Rolla, 2000.
- Hulsey, Johnny Leroy. *Environmental Effects on Composite-girder Bridge Structures*. Ph.D. Thesis, University of Missouri – Rolla, 1976.
- Kannel, J., French, C. and Stolarski, H. *Release Methodology of Strands to Reduce End Cracking in Pretensioned Concrete Girders*. PCI Journal. v42, n1, Jan 1997, pp. 42-54.
- Khalifa, Ahmed. *Shear Performance of Reinforced Concrete Beams Strengthened with Advanced Composites*. Alexandria University, Egypt, Ph.D. Thesis, 1999.

- Khan, A. A., Cook, W. D., and Mitchell, D. *Thermal Properties and Transient Thermal Analysis of Structural Members during Hydration*. ACI Materials Journal, v95, n3 May-June 1998 pp. 293-303.
- Ma, Zhongguo, Xiaoming Huo, Maher K. Tadros, and Mantu Baishya. *Restraint Moments in Precast/Prestressed Concrete Continuous Bridges*. PCI Journal. Vol. 43, no. 6, November/December 1998, pp. 40-57.
- Marshall, W. T. and Mattock, A. H. *Control of Horizontal Cracking in the Ends of Pretensioned Concrete Girders*, PCI Journal, v7, n5, 1962 pp. 56-74.
- Mayo, Randy. *Personal Interview*. August 1998.
- Miller, Richard, *Personal correspondence regarding a survey of the current practice of design of continuous concrete girder bridges*, University of Cincinnati, February 2000.
- Mindess, Sidney and J. Francis Young. *Concrete*. Prentice-Hall, Inc., Englewood Cliffs, New Jersey, 1981.
- Missouri Department of Transportation, *BR 200 – A Computer Program for Analysis and Design of Prestressed Concrete Girders*, PC Version, 1998.
- Missouri Department of Transportation, *Bridge Manual*, Volumes 1 through 4, 1988.
- Missouri Geological Survey. *Geologic Map of Missouri*. 1979.
- Myers, John. *Personal Interview*. October 14, 1999.
- Oesterle, R.G., J.D. Glikin, and S.C. Larson. *Design of Precast Prestressed Bridge Girders Made Continuous*. NCHRP Report 322, November 1989.
- PCI Committee on Quality Control Performance Criteria. *Fabrication and Shipment Cracks in Precast or Prestressed Beams and Columns*. PCI Journal. Vol. 30, no. 3, May/June 1985, pp. 24-49.
- Potgieter, Izak and William Gamble. *Nonlinear Temperature Distributions in Bridges at Different Locations in the United States*. PCI Journal. July-August 1989, pp. 80-103.
- Radolli, M. and R. Green. *Thermal Stress Analysis on Concrete Bridge Superstructures*. Transportation Research Record 607. Transportation Research Board, Washington D.C., 1976, pp. 7-13.
- Russell, H. G., and Gerken, L. J., *Jointless Bridges – the Knowns and the Unknowns*, Concrete International, v16, n4, April 1994, pp. 44-48.
- SAS/STAT User's Guide, Version 6, Fourth Edition*. Volumes 1 and 2. SAS Institute, Inc., 1990.
- Saetta, Anna, Roberto Scotta, and Renato Vitaliani. *Stress Analysis of Concrete Structures Subjected to Variable Thermal Loads*. Journal of Structural Engineering – ASCE. Vol. 121, no. 3, March 1995, pp. 446-457.
- Salmons, John R. *End Connections of Pretensioned I-beam Bridges*. Study Number 72-2 for the Missouri State Highway Department.
- Samaranayake, V.A. *Personal Interview*. June 1999.
- Shushkewich, Kenneth W. *Design of Segmental Bridges for Thermal Gradient*. PCI Journal. Vol. 43, no. 4, July/August 1998, pp. 120-137.
- Stegg, R., Rots, J., and van den Boogaart, T. *Computational Modeling of Early-Age HPC*, Worldwide Advances in Structural Concrete and Masonry Structures – Proceedings, ASCE, New York, NY., 1996, pp. 542-553.
- Tadros, M.K., Ficenec, J. A., Einea, A. and Holdsworth, S., *A New Technique to Create Continuity in Prestressed Concrete Member*, PCI Journal, v38, n5. Sept./Oct., 1993, pp. 30-37.

Timoshenko, S. and J.N. Goodier. *Theory of Elasticity*. McGraw-Hill Book Company, Inc., 1951, New York.

Vining, G. Geoffrey. *Statistical Methods for Engineers*. Duxbury Press, Detroit, Michigan, 1998.

Wollmann, Gregor, Eliezer Shamir, and Authors. *Reader Comments on Restraint Moments in Precast/Prestressed Concrete Continuous Bridges*. PCI Journal. Vol. 96, no. 3, May/June 1999, pp.94-98.

**APPENDIX A**

**J. MYERS, A. NANNI, AND D. STONE**

**VARIABLES INCLUDED IN THE PRELIMINARY DATABASE**

Descriptions of the variables included in the preliminary database provided by MoDOT and those added during analysis are as follows (the asterisk denotes those variables that were ignored in the analysis because of their relative consistency):

- Precast company – There are four precast companies utilized by MoDOT. They are Wilson Concrete Co., CSR Quinn Concrete Co., Egyptian Concrete Co., and Raider Precast Concrete; they are denoted by the numbers 1, 2, 3, and 4, respectively for the purposes of analysis.
- Plant Location – The five locations of the plants are Omaha, NE; Marshall, MO; Kansas City, KS; Bonne Terre, MO; and Burlington, IA. They are designated with the numbers 1 through 5, respectively, for the purposes of analysis.
- District – MoDOT has divided the state of Missouri into 10 districts. This is the district in which the bridge is located.
- Bridge Length – The overall length of a bridge in feet.
- Average Daily Traffic – The average daily traffic over a bridge.
- Number of Spans – The number of spans of the bridge.
- Deck Panel Thickness\* – The thickness of the deck's prestressed panels.
- Support Pad\* – The type of support pad used under the girders at the location of the diaphragm.
- Skew – The degrees to the left or right that the bridge is oblique to the bank.
- Girder Length – The length of an average girder in feet.
- Girder Spacing – The centerline to centerline spacing of the girders in inches.
- Number of Girders per Span – The number of girders spaced across the width of the bridge.
- Girder Height – The height of the bridge girders in inches.
- Bottom Flange Width – The width of the bottom flange of the bridge girders in inches.
- Top Flange Width – The width of the top flange of the bridge girders in inches.
- Bottom Flange Height – The height of the bottom flange of the bridge girders in inches.
- Top Flange Height – The height of the top flange of the bridge girders in inches.
- Web Height – The height of the web of the bridge girders in inches.
- Web Width – The width of the web of the bridge girders in inches.
- Girder Type – Based on the dimensions of the girders, the girder type according to MoDOT was determined.
- Girder Area – The cross sectional area of the girder in square inches.
- Number of Tendons – The total number of tendons used to prestress the bridge girder.
- Number of Straight Tendons – The number of prestressing tendons that were placed straight near the bottom of the bridge girders.
- Number of Draped Tendons – The number of prestressing tendons that were draped in the bridge girders.
- Tendon Diameter\* – The diameter of the prestressing tendons in inches.
- Tendon Type\* – The type of prestressing tendon used (e.g., 7-wire strand).
- Tendon Strength\* – The tensile strength of the prestressing tendons in ksi.
- Initial Stress as a Percent of Ultimate\* – The initial prestressing stress as a percentage of the ultimate strength of the tendons.
- Tendon Release Sequence\* – A description of the pattern in which the prestressing tendons were released after pouring.
- Mild Steel Size\* – The sizes of mild steel bars used to reinforce the bridge girders in ACI standard designations.
- Mild Steel Strength\* – The strength of the mild steel used to reinforce the bridge girders in ksi.
- Shear Reinforcement End Space – The space at the end of the girder where no shear reinforcement is placed in inches.

- Shear Reinforcement First Section – Details the spacing and number of spaces of the shear reinforcement placed in the end section of the bridge girder.
- Additional Bars within the End Area – Details the placement and size of any additional shear reinforcement that was placed near the end of the beam.
- Shear Reinforcement Second Section – Details the spacing and number of spaces of the shear reinforcement placed in the next section (toward the center) of the bridge girder.
- Shear Reinforcement Third Section – Details the spacing and number of spaces of the shear reinforcement placed in the next section (toward the center) of the bridge girder.
- Shear Spacing Section 1 – The shear spacing in the first section.
- Shear Spacing Section 2 – The shear spacing in the second section.
- Shear Spacing Section 3 – The shear spacing in the third section.
- Number of Girder Ends Cracked – The number of girder ends in the bridge that exhibit cracking.
- Percentage of Girder Ends Cracked – The percentage of girder ends that are cracked, as a percentage of the total number of girder ends in the bridge.
- Casting Date – The casting date of the bridge girders.
- Transportation Date – Transportation date of the bridge girder to the bridge site.
- Transportation Method\* – The method of transporting the bridge girders to the bridge site.
- Distance Traveled – The distance traveled by the bridge girders to the bridge site in miles.
- Field Construction Date – The date of construction of the bridge, often just the year of construction. This variable is split into the field construction year and the field construction season. Winter, denoted by a 1, is defined as December, January, and February. Spring, denoted by a 2, is defined as March, April, and May. Summer, denoted by a 3, is defined as June, July, and August. Fall, denoted by a 4, is defined as September, October, and November.
- Erection method\* – The method of placing the bridge girders at the bridge site.
- Cement Source – There are six sources of cement used in the bridges considered. They are Type III Ash Grove, Type III MO Portland, Type III Lafarge, Type III River Cement, Type I River Cement, and Type I Lonestar. A number, 1 through 6, represents each type, respectively.
- Coarse Aggregate Source – The five sources of coarse aggregate are Burlington Limestone (Grade E), Bethany Falls Limestone, Bonne Terre Limestone (Grade E), Plattin Limestone (Grade E), Derby-Doe Run Limestone (Grade E); they are denoted by 1, 2, 3, 4, and 5, respectively.
- Fine Aggregate Source – The four sources of fine aggregate are Missouri River Sand (Grade A), Kansas River Sand (Grade A), Mississippi River Sand (Grade A), and Meramac River Sand (Grade A); they are denoted by 1, 2, 3, and 4, respectively.
- Water Source\* – The source of water used in the concrete mixture.
- Class of Concrete\* – The class of the concrete designation of the bridge girders. This is a Missouri State standard specification for highway construction.
- Cement\* – The amount of cement in the concrete mixture in pounds.
- Coarse Aggregate\* – The amount of coarse aggregate in the concrete mixture in pounds.
- Fine Aggregate\* – The amount of fine aggregate in the concrete mixture in pounds.
- Water\* – The amount of water in the concrete mixture in gallons.

- Admixtures – The type of admixtures added to the concrete mixture.
- Age at Release – The age of the concrete in days at the time of release of the prestressing tendons. If a range of values was given for this variable, then the mean of that range was used for the purposes of analysis.
- Strength at Release – The strength of the concrete, in psi, at the time of release of the prestressing tendons.
- Curing Strength – The design final strength of the concrete, in psi, after 28 days.
- Curing Type – The method used to cure the concrete, either steam or water, denoted by a 1 or 2, respectively.
- Curing Time – The amount of time, in days, that the concrete was cured by the method defined in “curing type.” If a range of values was given for this variable, then the mean of that range was used for the purposes of analysis.
- Curing Temperature – The range of temperatures, in degrees Fahrenheit, at which the concrete was cured. This variable was split so that the minimum curing temperature and the maximum curing temperature could be analyzed separately.
- Width of Diaphragm – The width of the diaphragm of the bridge in inches.
- Column Height – The average height of the columns of the bridge in feet.

## **APPENDIX B**

J. Myers, A. Nanni, and D. Stone

### **HISTOGRAMS OF THE PRELIMINARY DATABASE VARIABLES**

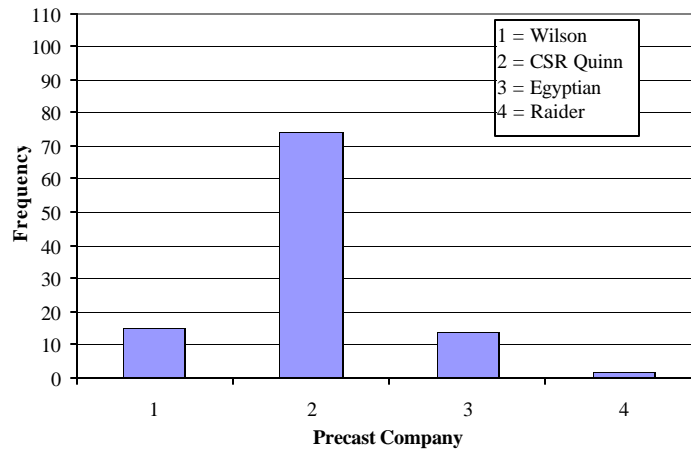


**Figure B.1 Histogram of Precast Company**

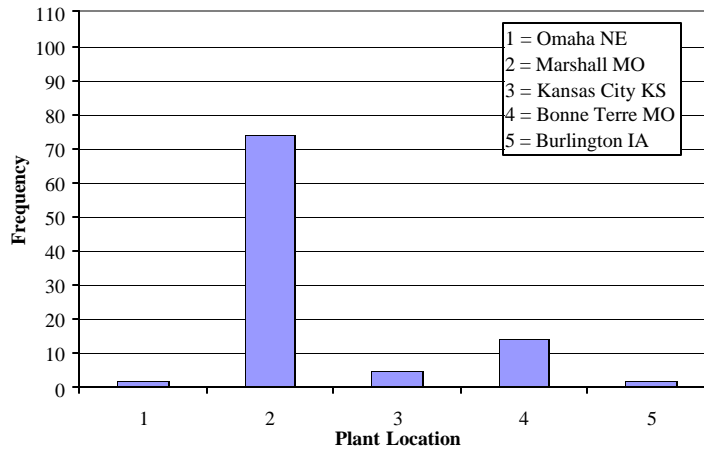


**Figure B.2 Histogram of Plant Location**

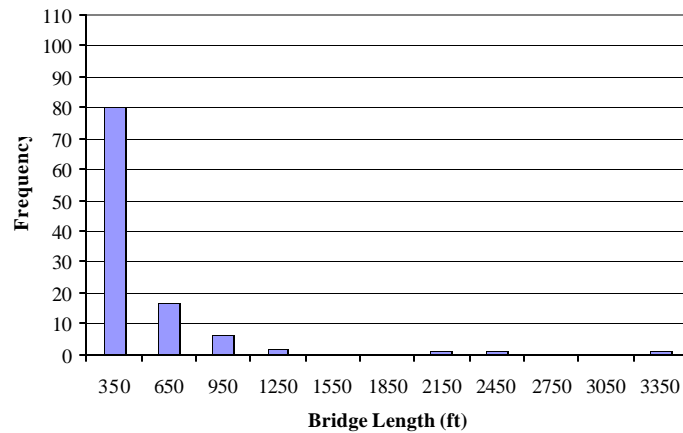


**Figure B.3 Histogram of Bridge Length**

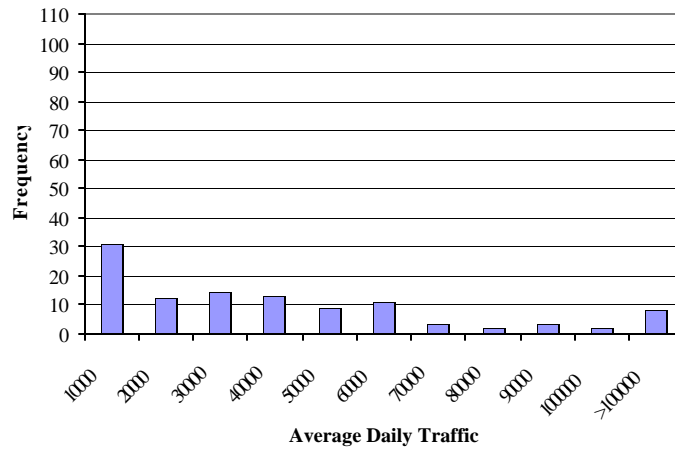


**Figure B.4 Histogram of Average Daily Traffic**

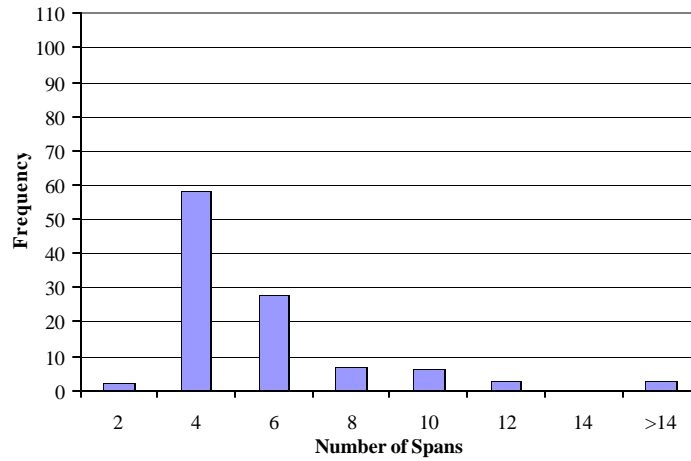


**Figure B.5 Histogram of Number of Spans**

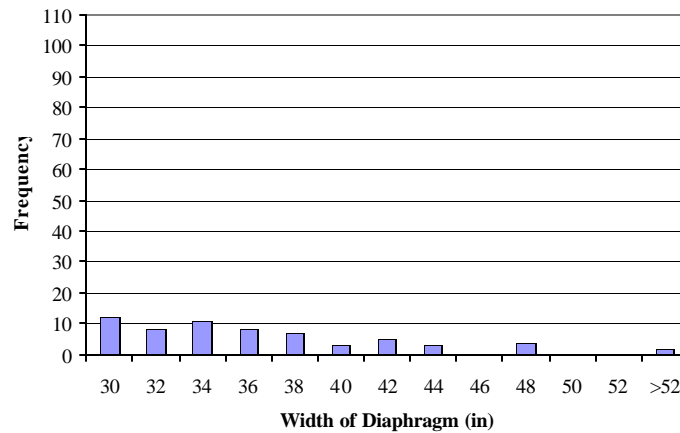


**Figure B.6 Histogram of Width of Diaphragm**

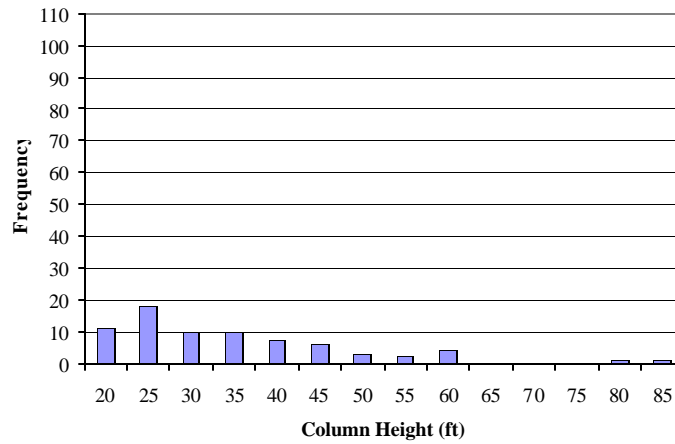


**Figure B.7 Histogram of Column Height**

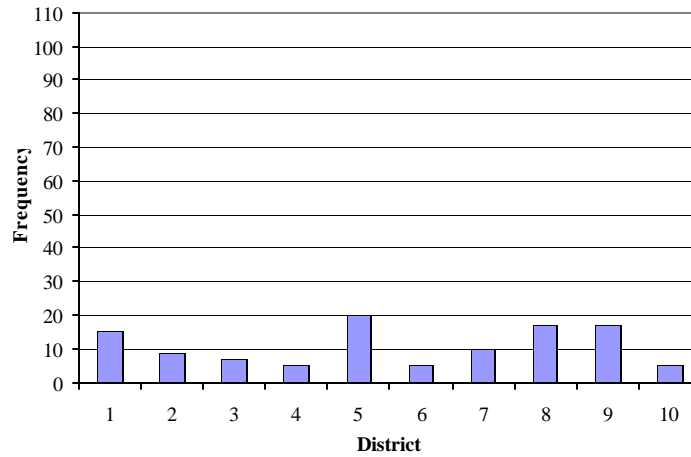


**Figure B.8 Histogram of District**

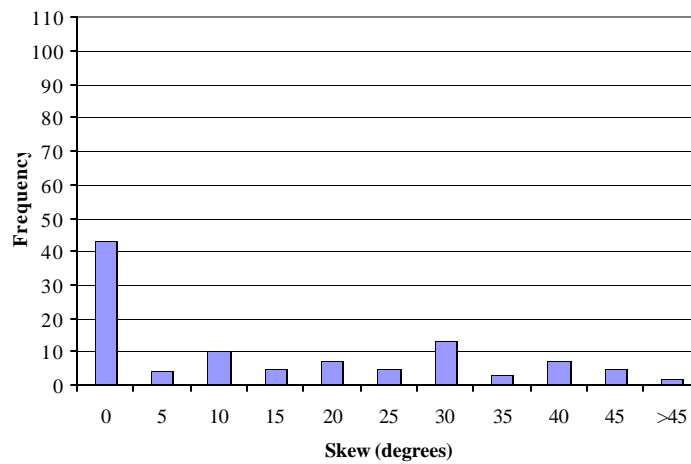


**Figure B.9 Histogram of Skew**

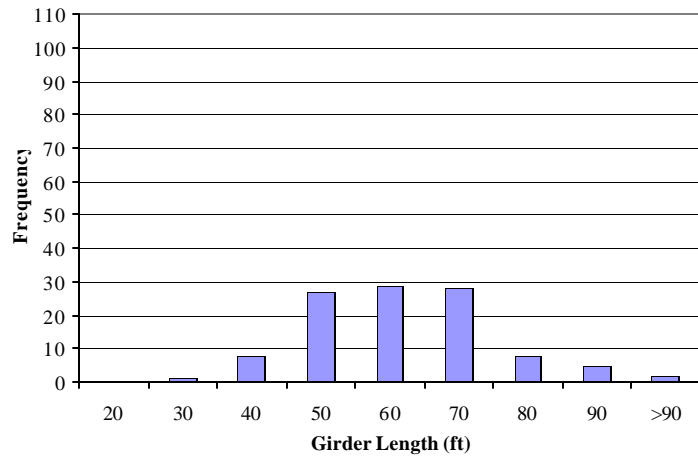


**Figure B.10 Histogram of Girder Length**

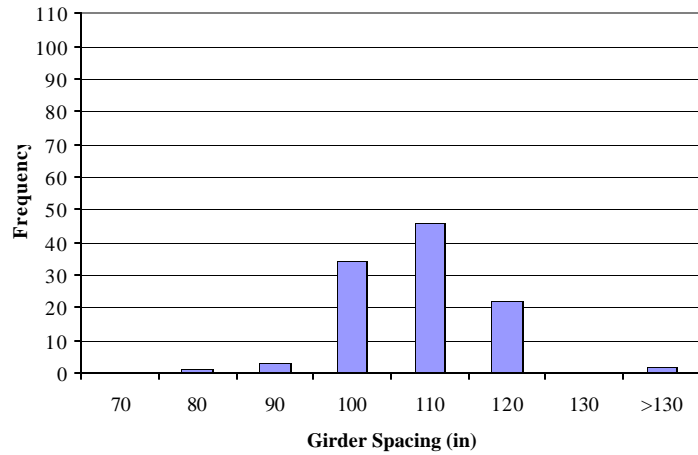


**Figure B.11 Histogram of Girder Spacing**

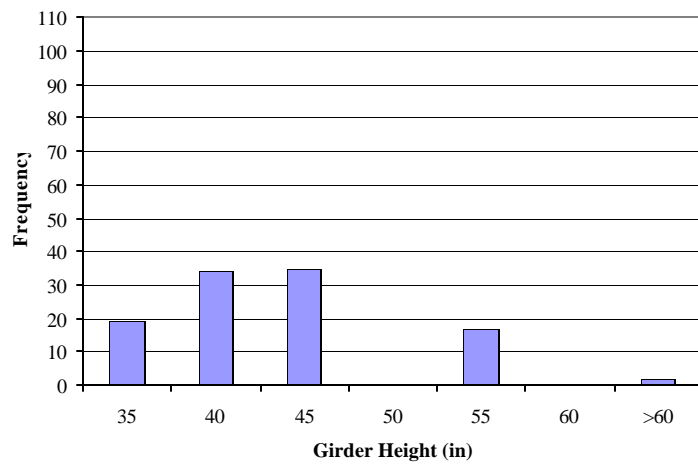


**Figure B.12 Histogram of Girder Height**

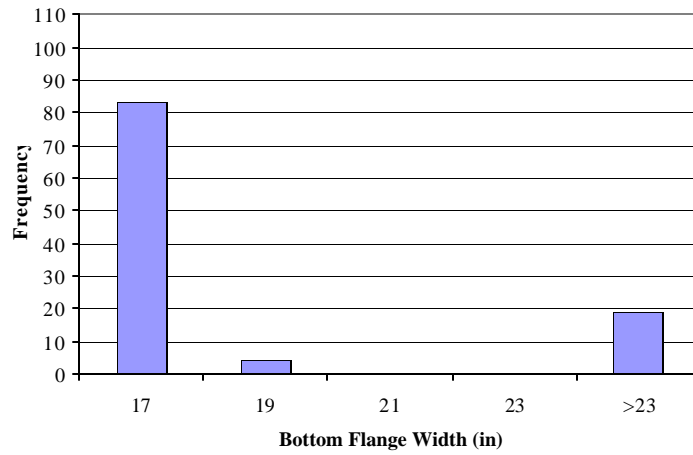


**Figure B.13 Histogram of Bottom Flange Width**

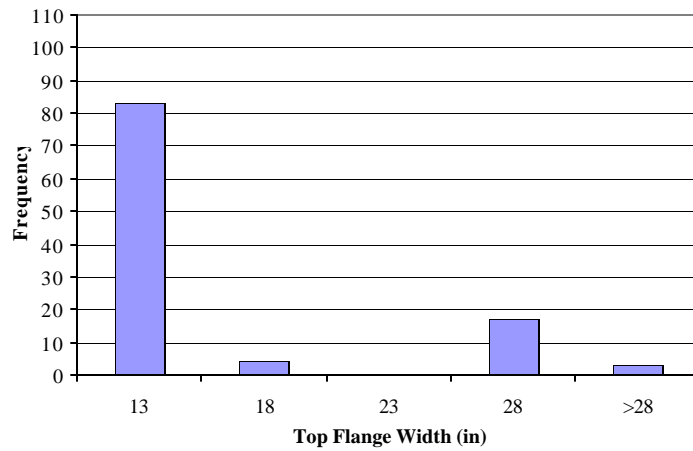


**Figure B.14 Histogram of Top Flange Width**

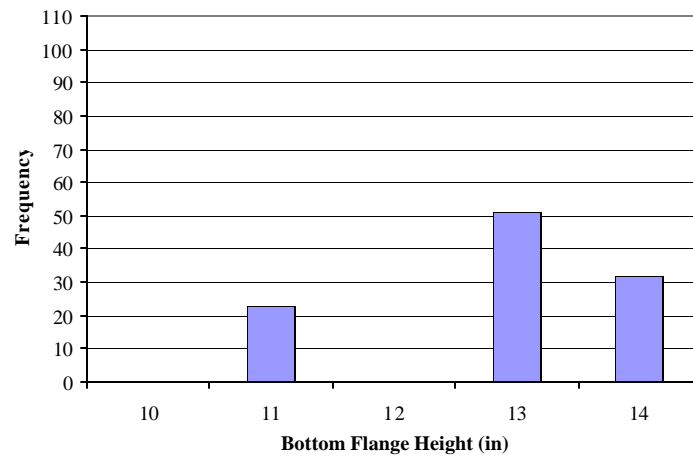


**Figure B.15 Histogram of Bottom Flange Height**

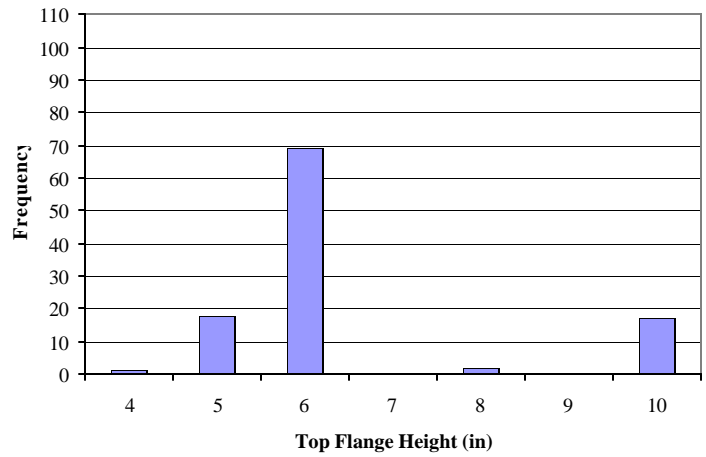


**Figure B.16 Histogram of Top Flange Height**

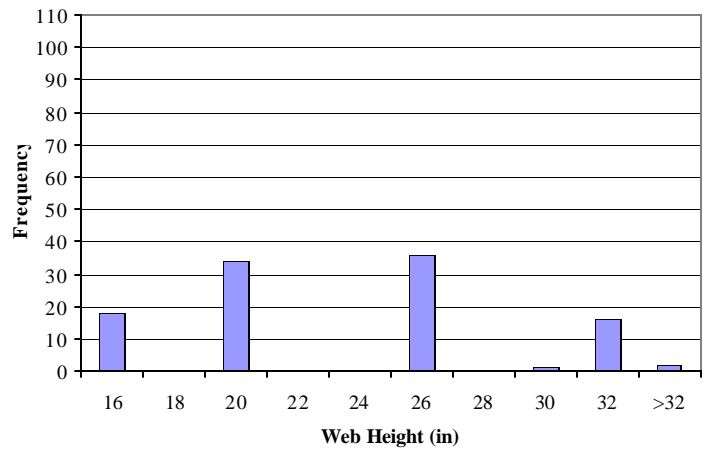


**Figure B.17 Histogram of Web Height**

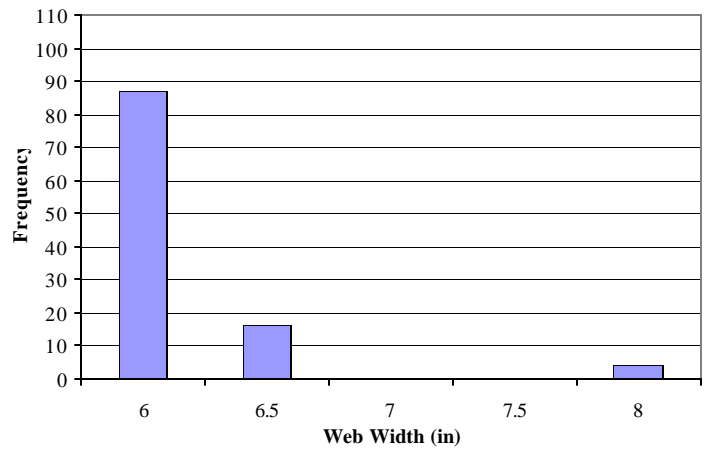


**Figure B.18 Histogram of Web Width**

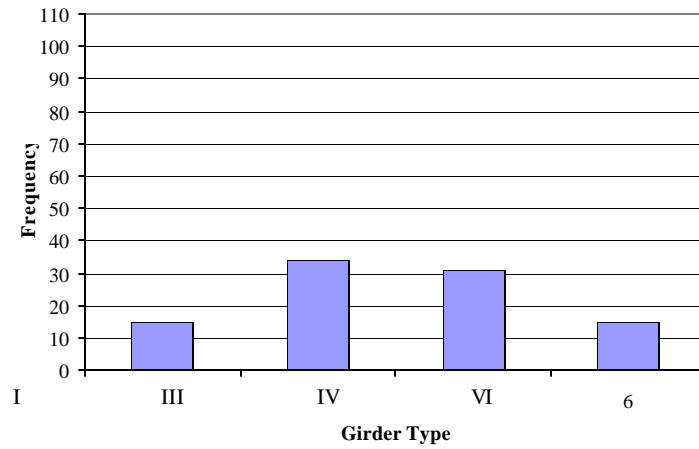


**Figure B.19 Histogram of Girder Type**

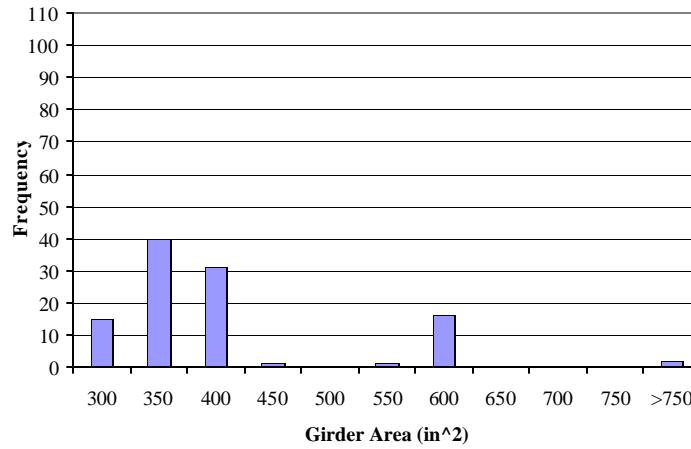


**Figure B.20 Histogram of Girder Area**

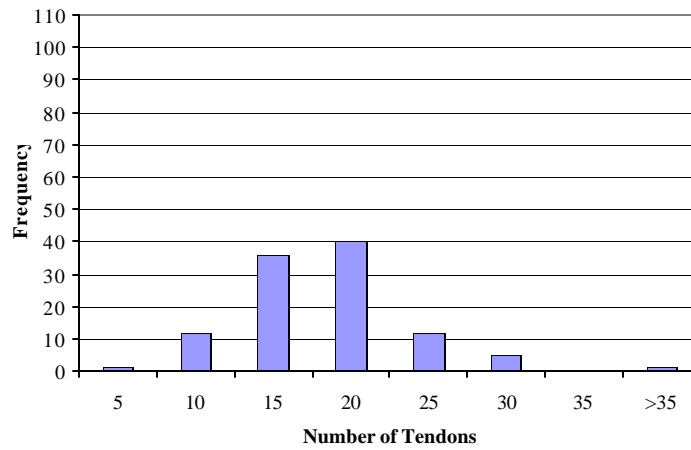


**Figure B.21 Histogram of Number of Tendons**

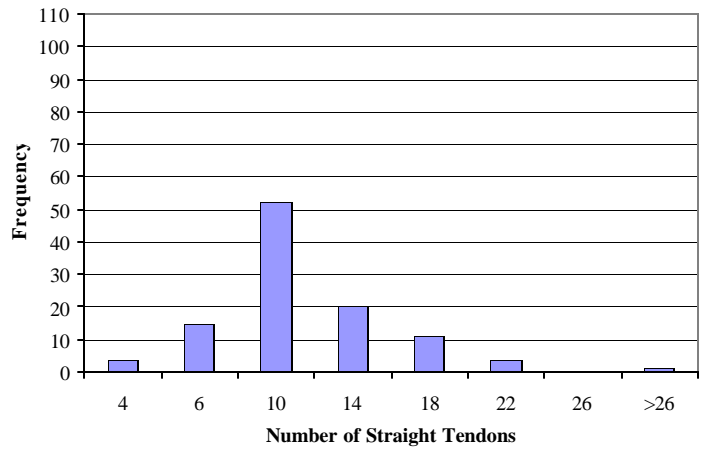


**Figure B.22 Histogram of Number of Straight Tendons**

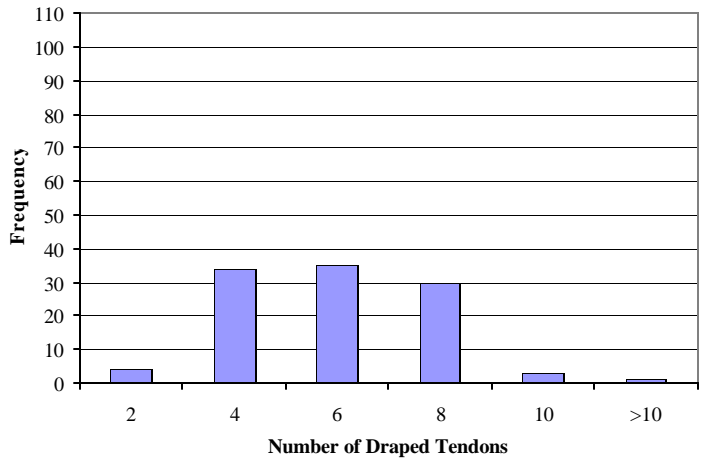


**Figure B.23 Histogram of Number of Draped Tendons**

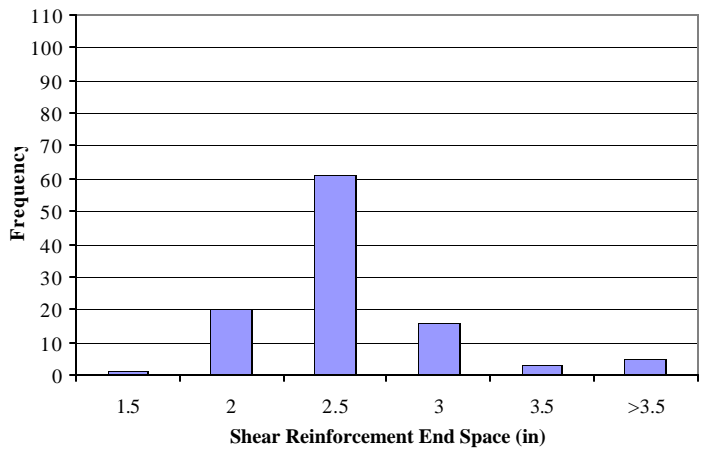


**Figure B.24 Histogram of Shear Reinforcement End Space**

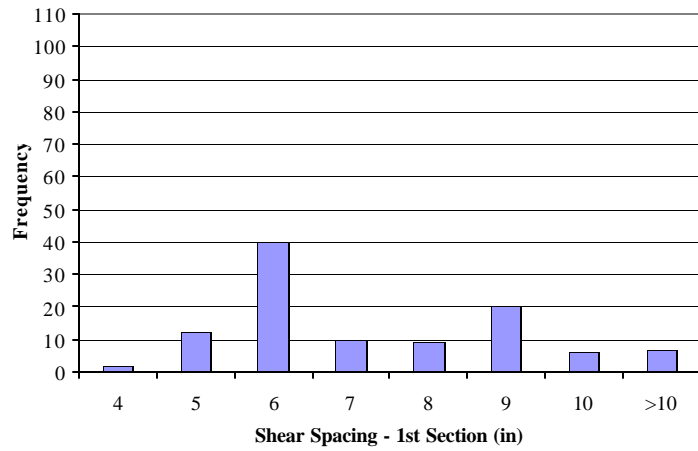


**Figure B.25 Histogram of Shear Spacing – 1<sup>st</sup> Section**

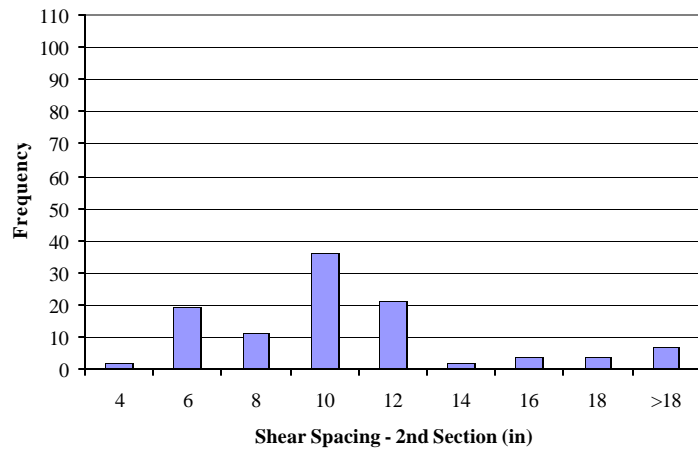


**Figure B.26 Histogram of Shear Spacing – 2<sup>nd</sup> Section**

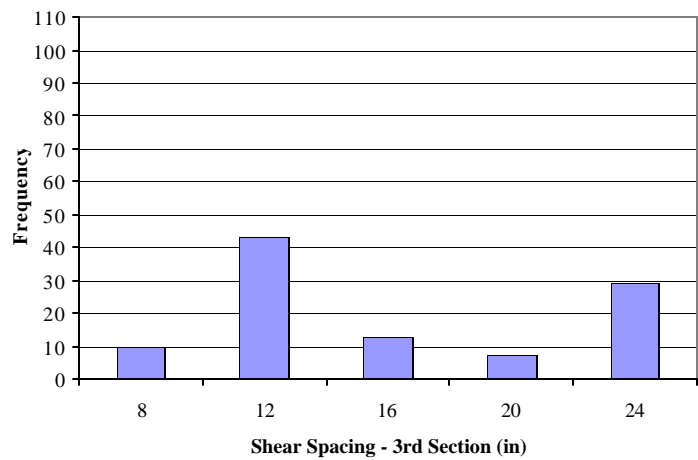


**Figure B.27 Histogram of Shear Spacing – 3<sup>rd</sup> Section**

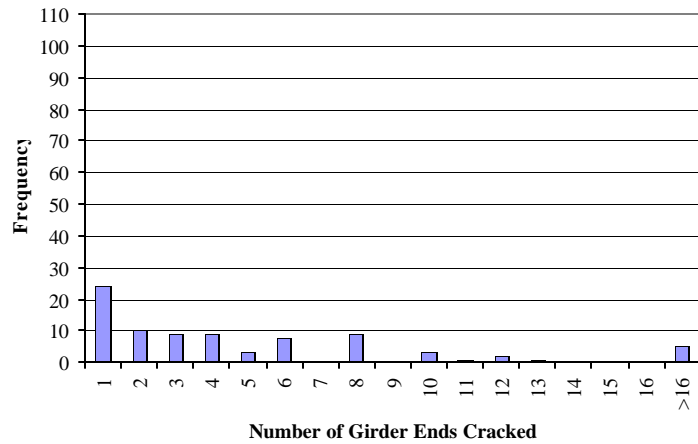


**Figure B.28 Histogram of Number of Girder Ends Cracked**

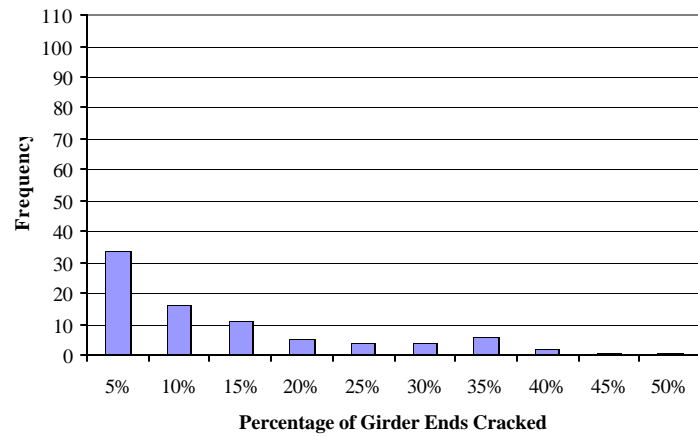


**Figure B.29 Histogram of Percentage of Girder Ends Cracked**

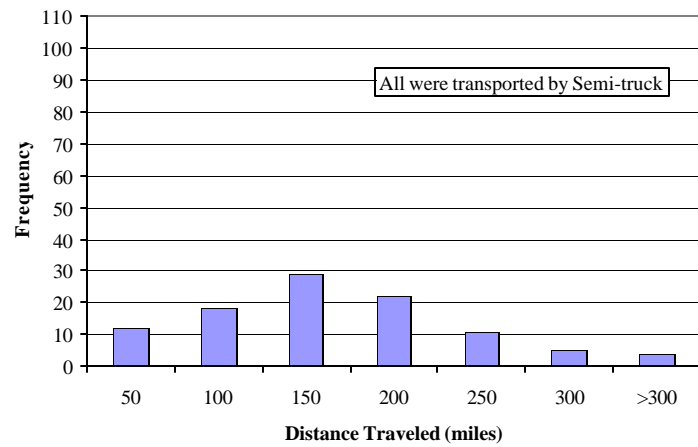


**Figure B.30 Histogram of Distance Traveled**

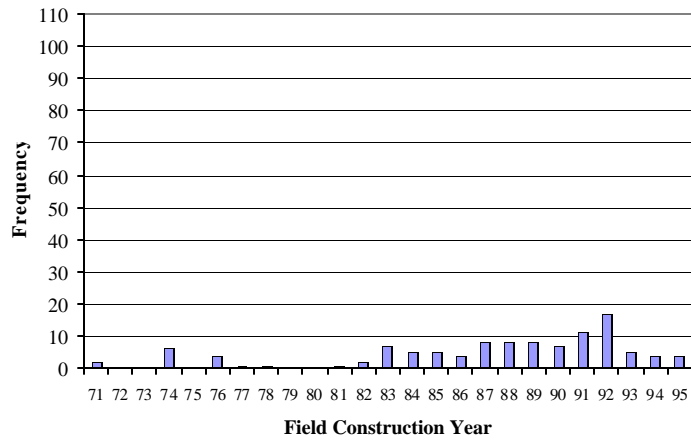


**Figure B.31 Histogram of Field Construction Year**

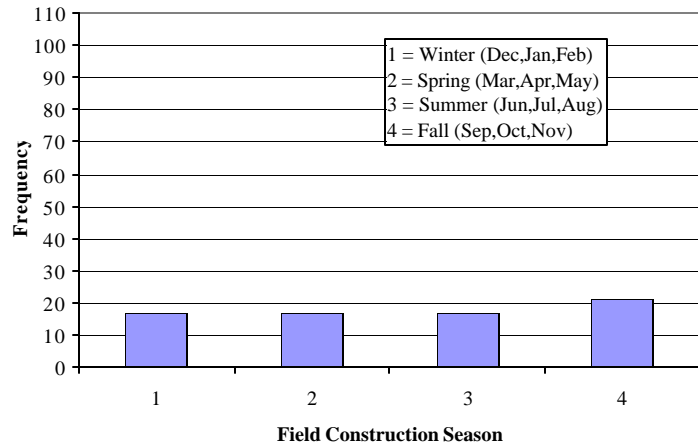


**Figure B.32 Histogram of Field Construction Season**

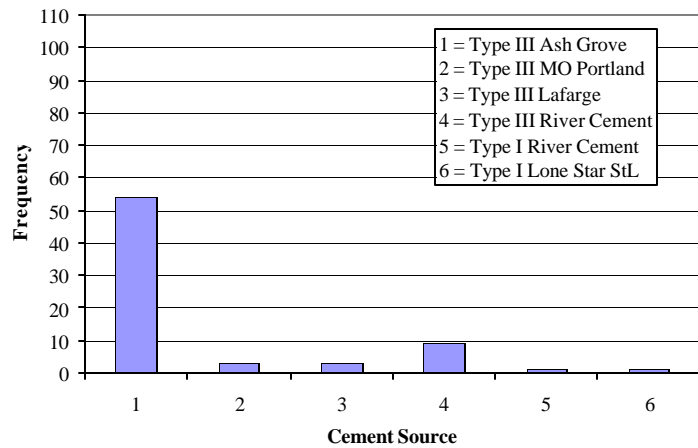


**Figure B.33 Histogram of Cement Source**

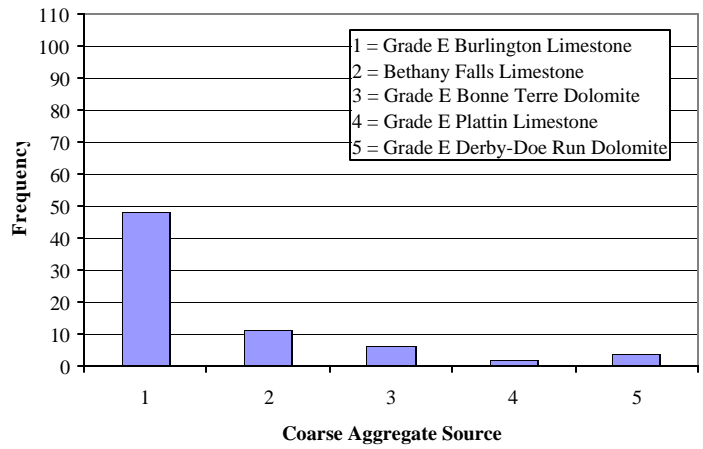


**Figure B.34 Histogram of Coarse Aggregate Source**

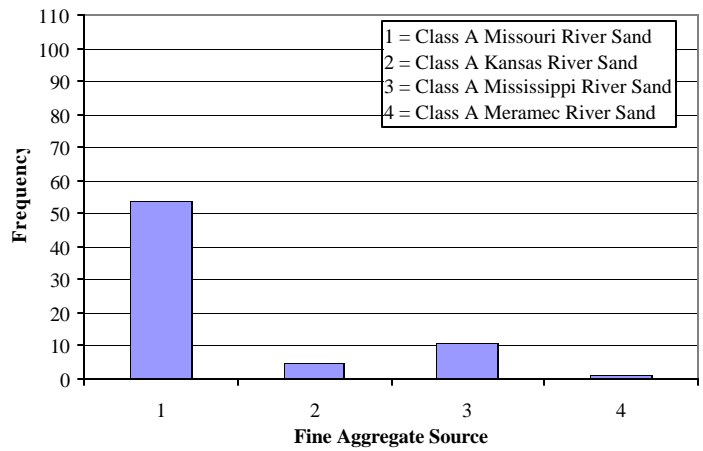


**Figure B.35 Histogram of Fine Aggregate Source**

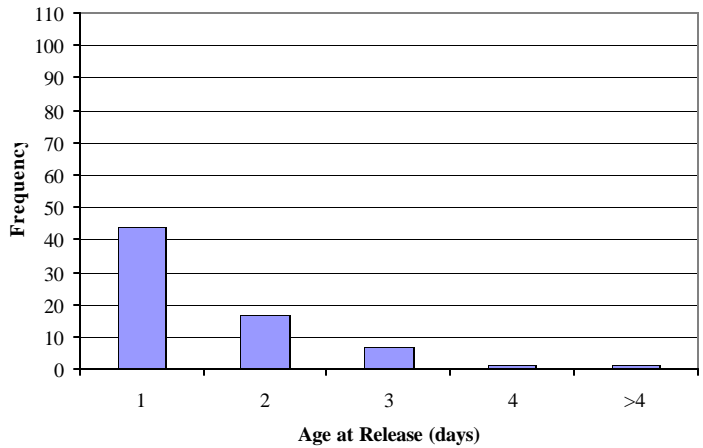


**Figure B.36 Histogram of Age at Release**

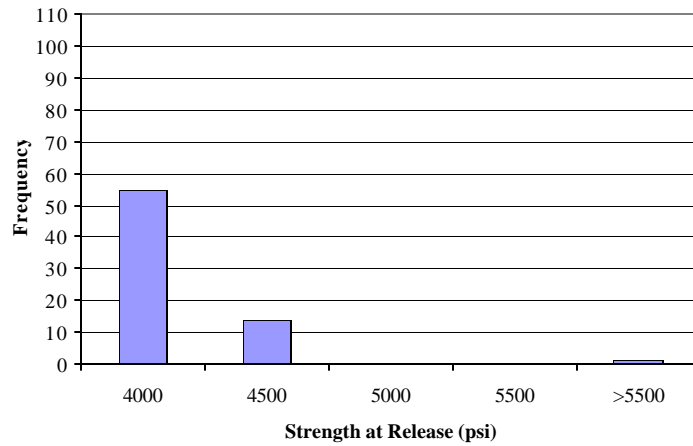


**Figure B.37 Histogram of Strength at Release**

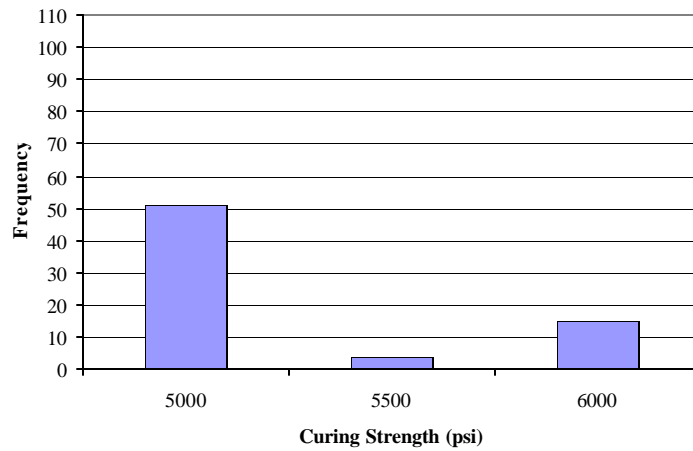


**Figure B.38 Histogram of Curing Strength**

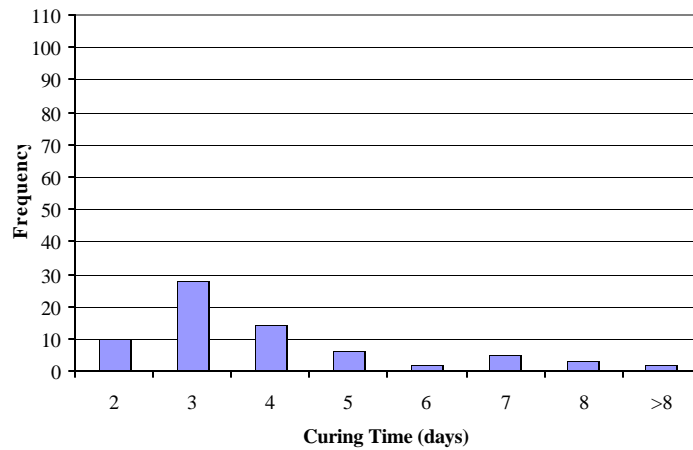


**Figure B.39 Histogram of Curing Time**

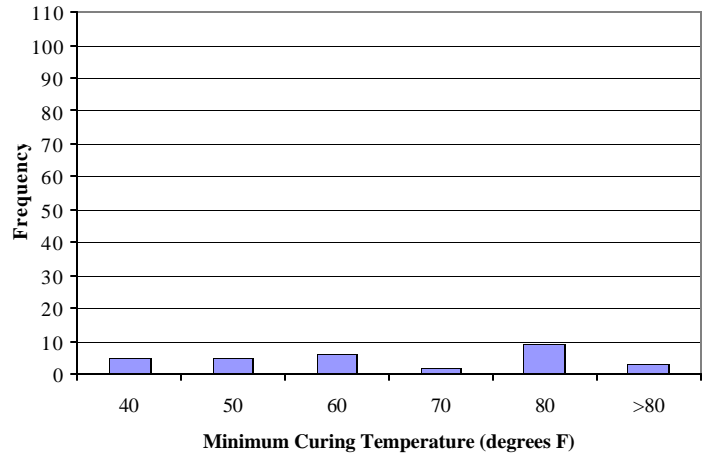


**Figure B.40 Histogram of Minimum Curing Temperature**

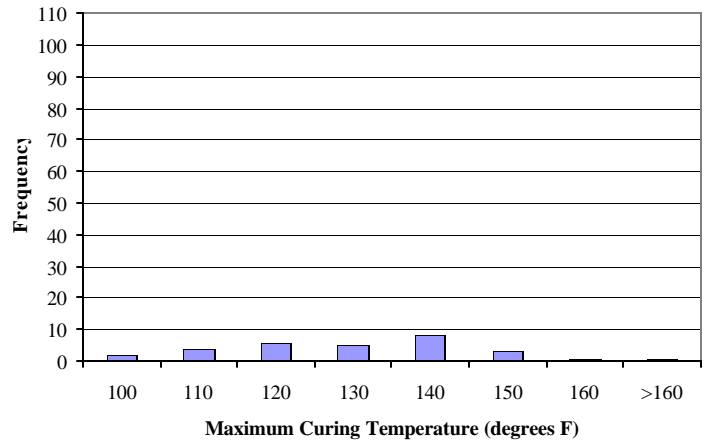


**Figure B.41 Histogram of Maximum Curing Temperature**

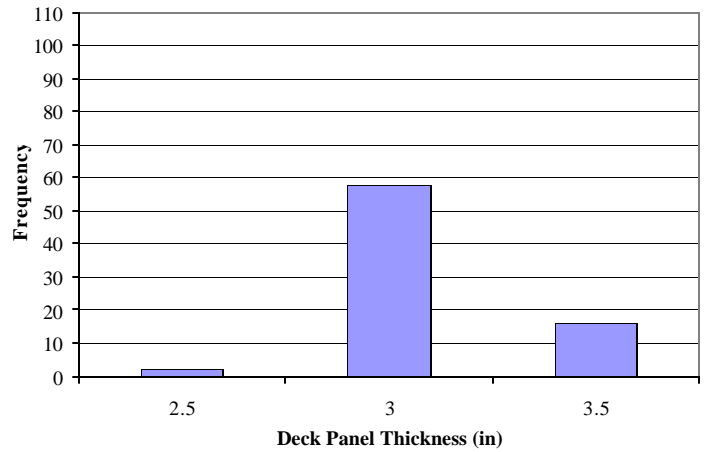


**Figure B.42 Histogram of Deck Panel Thickness**

**APPENDIX C**

J. MYERS, A. NANNI, AND D. STONE

**F-TEST ANALYSIS PROCEDURE**

The least squares method attempts to minimize the sum of the squares of the residuals, “ $e_i$ ”, which are the difference between the actual values, “ $y_i$ ”, and the predicted values, “ $\hat{y}_i$ ”. The least squares method can most clearly be defined using the example of a simple linear regression. In the case of a simple linear regression, the model is of the form,

$$y_i = \mathbf{b}_0 + \mathbf{b}_1 x_i + e_i \quad (\text{C.1})$$

where:

“ $y_i$ ” is the actual value of the variable to be predicted,

“ $\beta_0$ ” is the intercept term,

“ $\beta_1$ ” is the slope parameter,

“ $x_i$ ” are the values of the single explanatory variables under consideration, and

“ $\epsilon_i$ ” are the error terms.

The error terms are included to indicate the variability in the observed values, which cannot be calculated exactly as a linear function of “ $x$ ”. Note that, in the case of a simple linear regression, there is only one explanatory variable, “ $x$ ”.

An approximation to the model (Equation C.1) is determined as follows. Let,

$$\hat{y} = b_0 + b_1 x \quad (\text{C.2})$$

where the coefficients, “ $b_0$ ” and “ $b_1$ ”, are chosen by the least squares method, such that the sum of the squared deviations of the model from the observed is minimized. The sum of the squared deviations can be expressed as a function of “ $\beta_0$ ” and “ $\beta_1$ ” as follows in Equation C.3.

$$Q(\mathbf{b}_0, \mathbf{b}_1) = \sum (e_i)^2 = \sum_{i=1}^n (y_i - \hat{y}_i)^2 = \sum_{i=1}^n (y_i - (\mathbf{b}_0 + \mathbf{b}_1 x_i))^2 \quad (\text{C.3})$$

By differentiating Equation C.3, with respect to both “ $\beta_0$ ” and “ $\beta_1$ ”, we obtain expressions (Equation C.4 and Equation C.5) that can be set to zero in order to minimize  $Q(\beta_0, \beta_1)$ .

$$\frac{\partial f}{\partial \mathbf{b}_0} = \sum_{i=1}^n -2(y_i - (\mathbf{b}_0 + \mathbf{b}_1 x_i)) = 0 \quad (\text{C.4})$$

$$\frac{\partial f}{\partial \mathbf{b}_1} = \sum_{i=1}^n 2(-x_i)(y_i - (\mathbf{b}_0 + \mathbf{b}_1 x_i)) = 0 \quad (\text{C.5})$$

Manipulating Equation C.4 and Equation C.5 into expressions that can be solved for “ $b_0$ ” and “ $b_1$ ”, we obtain Equation C.6 and Equation C.7.

$$nb_0 + (\sum x_i)b_1 = \sum y_i \quad (\text{C.6})$$

$$(\sum x_i)b_0 + \left(\sum x_i^2\right)b_1 = \sum x_i y_i \quad (\text{C.7})$$

Solving these equations for “ $b_1$ ”, we obtain

$$b_1 = \frac{\begin{vmatrix} n & \sum y_i \\ \sum x_i & \sum x_i y_i \end{vmatrix}}{\begin{vmatrix} n & \sum x_i \\ \sum x_i & \sum x_i^2 \end{vmatrix}} = \frac{n \sum x_i y_i - \sum x_i \sum y_i}{n \sum x_i^2 - (\sum x_i)^2} \quad (\text{C.8})$$

Simplifying Equation C.6 through C.8, we obtain solvable expressions for “ $b_0$ ” and “ $b_1$ .”

$$b_1 = \frac{\sum x_i y_i - \frac{\sum x_i \sum y_i}{n}}{\sum x_i^2 - \frac{(\sum x_i)^2}{n}} \quad (\text{C.9})$$

$$b_0 = \bar{y} - b_1 \bar{x} \quad (\text{C.10})$$

The minimum value of the sum of the squared deviations, based on the values of “ $b_0$ ” and “ $b_1$ ”, is referred to as the sum of the squared residuals, “ $SS_{res}$ ”, and is defined as follows:

$$SS_{res} = Q(b_0, b_1) = Q \min = \sum_{i=1}^n (y_i - \hat{y}_i)^2 \quad (\text{C.11})$$

Following the simple linear regression analysis, the ability of each variable to predict the number of girders cracked was evaluated. To do so, an analysis of variance (ANOVA) procedure was performed.

Any data set will contain a certain amount of variability, “ $SS_{total}$ ”, which can only partially be explained by the model to which the data is fit. The ability of the model to predict the response variable, “ $y$ ”, can be measured by the amount of variability that it can explain. The analysis of variance, or ANOVA, procedure is one way to quantify this ability. The ANOVA procedure is so termed because it is an analysis of the variance explained by the model relative to the variance left unexplained.

An ANOVA table for the case of a simple linear regression takes the form of Table C.1. The number of observations, “ $n$ ”, is used to determine the degrees of freedom of each source. The sums of squares are data-dependent estimates of the variability attributed to various sources.

**Table C.1 Form of the ANOVA Table for Simple Linear Regression\***

Source	Degrees of Freedom	Sum of Squares	Mean Squares	F
Regression	1	$SS_{reg}$	$MS_{reg}$	$F$
Residual	$n-2$	$SS_{res}$	$MS_{res}$	
Total	$n-1$	$SS_{total}$		

\* Adapted from Vining, 1998, page 299.

The variability attributed to the model (i.e. explained by the model), “ $SS_{reg}$ ”, and the variability attributed to error, “ $SS_{res}$ ”, sum to the total variability, “ $SS_{total}$ ”. The variability attributed to error, “ $SS_{res}$ ”, has been previously defined as follows,

$$SS_{res} = \sum_{i=1}^n (y_i - \hat{y}_i)^2 \quad (\text{C.12})$$

If “ $SS_{total}$ ” is defined as,

$$SS_{total} = \sum_{i=1}^n (y_i - \bar{y})^2 \quad (\text{C.13})$$

where “ $\bar{y}$ ” is the average value of “ $y$ ”, then it can be shown that “ $SS_{reg}$ ” would be defined as follows,

$$SS_{reg} = \sum_{i=1}^n (\hat{y}_i - \bar{y})^2 \quad (\text{C.14})$$

The mean square is calculated by dividing the sum of squares by the degrees of freedom. Specifically,

$$MS_{reg} = \frac{SS_{reg}}{1} \quad (\text{C.15})$$

and,

$$MS_{res} = \frac{SS_{res}}{n - 2} \quad (\text{C.16})$$

The F-value is calculated by dividing “ $MS_{reg}$ ” by “ $MS_{res}$ ”.

The F-value can be used to determine if the independent variable has an effect on the response variable. When only one variable is considered, the test is equivalent to a t-test. The t-value is equivalent to the positive or negative value of the square root of the F-value.

For a variable to be considered statistically significant, the probability that a t-random variable is greater than the calculated t-value for the analysis must be less than the selected level of significance. This probability value is called the p-value. Generally, the level of significance is set at 0.01, 0.05, or 0.10, or one, five, or ten percent, respectively (Vining, 1998, pg. 158). The probability associated with the t-value can be calculated by using the cumulative distribution function for the t-distribution (Vining, 1998, pg. 458).

## **APPENDIX D**

J. Myers, A. Nanni, and D. Stone

### **VARIABLES INCLUDED IN THE REVISED DATABASE**

A description of the variables included in the revised database is as follows:

- District – As mentioned previously, MoDOT divides the state into 10 districts. It was suspected that geographic location of the bridges could be a factor, as it pertains to geologic properties, daily temperature variation, and the type of aggregate used in the concrete.
- County – There are 114 counties in the state of Missouri. This variable would be a more refined account of geographic location.
- Route – The possible types of routes that the highway bridges are located on are Interstate highway, U.S. highway, State highway, and County road.
- Skew – A skew bridge is one that is built obliquely from bank to bank. The angle between the pier line and a line perpendicular to the edge of the bridge is referred to as the skew of the bridge.
- Bridge length – The overall length of the bridge is a factor that would affect the amount of load carried by the girders, as well as the magnitude of thermal expansion experienced by the bridge.
- Number of spans – This is another factor that would affect the amount of load carried by the girders.
- Girder type – MoDOT standard girders are specified as II, III, IV, VI, or VII. This variable will take the value of the girder type.
- Girder spacing – This is another factor that would affect the amount of load carried by the girders.
- Shear reinforcement end spacing – At the end of the beam, there will be a 2-in. to 3-in. space where there is no reinforcement. Since the original suspicion was that the cracks were shear related, all shear reinforcement spacing is of interest.
- Shear reinforcement spacing – Again, the original suspicion was that the cracks were shear related, all shear reinforcement spacing were included in the database.
- Average Daily Traffic (ADT) – The average number of vehicles that cross the bridge in one day is referred to as the average daily traffic.
- Cracked status – The analysis of the database was intended to determine the differences between the characteristics of the cracked bridges and the uncracked bridges. This was also one variable that was of interest to try to predict with the statistical model.
- Percentage of girder ends cracked – The extent of the cracking in the cracked bridge was also of interest. The differences between the bridges that had only minimal cracking and those with extensive cracking were to be determined, as well. Additionally, the statistical model would attempt to predict this variable.
- Girder Area – While the MoDOT standard numbers are one means of identifying the size of the girders used in the bridge, a better gauge of their relative size would be the area of the girders. For instance, a MoDOT Type II girder is not half the size of a MoDOT Type IV girder.

The information is arranged in the database in the following order: bridge number, district, county, route, skew, bridge length, number of spans, girder type, girder spacing, reinforcement end spacing, reinforcement spacing in section 1, reinforcement spacing in section 2, reinforcement spacing in section 3, ADT, total foundation stiffness (not discussed in this report), average foundation stiffness (not discussed in this report), cracked status of the bridge, percentage of girders cracked, girder area, number of pile footing foundations (not discussed in this report), number of spread footing foundations (not discussed in this report). It should be noted that a “.” denotes that information for that variable for that bridge was not available.

The database is as follows:

```

23741 1 3 1 10 268 5 4 102 2 5 6 8 47000 . . 1 0 428.9 . .
23742 1 3 1 10 268 5 4 102 2 5 6 8 47000 . . 1 0 428.9 . .
4798 1 3 4 40 200 3 4 100 2.5 6 8 9 2000 10 2.5 1 25 428.9 4 0
84 1 11 1 30 228 5 3 100 2.6 12 15 24 100000 . . 1 . 381.9 . .
4214 1 11 3 30 163 3 . 88 2.5 6 12 24 8000 10 2.5 1 3.33 374.9 4 0
4976 1 11 2 0 142 3 2 106 2 5 5 7.5 50000 . . 1 3.33 310.9 . .
2879 1 13 3 25 144 3 3 100 2.5 6 9 12 23000 10 2.5 1 . 381.9 4 0
4620 1 32 2 0 204 3 6 106 2.5 6 12 21 31000 7 1.75 1 13.33 643.6 2 2
2921 1 41 4 0 183 5 2 102 2.5 5.5 6 7 9000 9 1.5 1 2 310.9 2 4
4724 1 41 2 20 124 3 2 102 2.5 5 7.5 12.5 20000 7 1.75 1 16.67 310.9 2 2
4378 1 113 3 0 321 5 4 112 2.5 5.5 7 9 8000 12 2 1 2.5 428.9 4 2
4341 2 17 4 0 152 3 3 112 2.3 8 12 12 3000 10 2.5 1 8.33 381.9 4 0
4528 2 21 3 0 258 5 4 100 2.5 12 18 18 9000 15 2.5 1 2 428.9 6 0
4636 2 45 3 20 148 3 3 112 2.5 9 13 24 4000 10 2.5 1 33.33 381.9 4 0
3256 2 58 2 0 216 6 2 108 2.5 5 5 24 22000 17.5 2.5 1 . 310.9 7 0
3839 2 58 2 35 284 5 6 108 2.5 7 7 24 37000 15 2.5 1 . 643.6 6 0
4545 2 88 2 15 199 3 4 102 2.5 9 24 24 114000 10 2.5 1 25 428.9 4 0
5037 2 88 2 9 275 4 4 112 2.8 6 9 12 89000 12.5 2.5 1 . 428.9 5 0
4353 3 4 3 10 175 3 4 114 2.5 9 9 14 6000 7 1.75 1 8.33 428.9 2 2
2872 3 64 2 44 221 3 4 94 2.5 5 6 9 54000 10 2.5 1 11.1 428.9 4 0
4547 3 87 2 5 257 2 . 106 . . . . 36000 15 2.5 1 . . 6 0
4713 3 87 2 30 253 5 3 106 2 6 6 8 88000 . . 1 16 381.9 . .
4553 3 109 4 45 206 3 . 93 2.5 7 9 9 5000 7 1.75 1 4.17 531.5 2 2
26411 4 19 2 0 108 3 2 102 3.8 6 9 12 73000 10 2.5 1 13.33 310.9 4 0
26412 4 19 2 0 108 3 2 102 3.8 6 9 12 69000 10 2.5 1 20 310.9 4 0
4931 4 54 3 30 250 3 6 106 2.5 6 12 21 25000 10 2.5 1 . 643.6 4 0
4546 5 10 4 20 267 5 3 106 2.5 9 24 12 38000 12 2 1 8 381.9 4 2
5046 5 10 2 30 247 5 3 106 3 6 7.5 10 67000 7.5 1.25 1 . 381.9 1 5
3126 5 14 2 20 137 3 3 106 3 6 10 15 41000 7 1.75 1 26.67 381.9 2 2
3127 5 14 2 0 332 6 4 106 2.5 6 9 12 41000 11.5 1.64 1 33.33 428.9 3 4
3450 5 14 2 36 196 3 6 106 2.5 7 9 21 43000 12 3 1 3.33 643.6 4 2
4780 5 14 2 60 304 . . 106 2.1 6 9 21 39000 10.5 1.75 1 . 643.6 3 3
5292 5 14 2 39 177 3 . 106 1.8 9 10 12 38000 10 2.5 1 26.67 336.5 4 0
5293 5 14 2 20 152 3 . 106 2.3 11 24 12 38000 7 1.75 1 13.33 336.5 2 2
4825 5 26 2 . 269 5 6 113 4 9 12 21 59000 15 2.5 1 12 643.6 6 0
4461 5 68 4 15 112 3 2 93 2.5 9 9 15 2000 7 1.75 1 4.17 310.9 2 2
4842 5 68 4 0 146 3 2 100 2.5 8 10 6 2000 7 1.75 1 33.33 310.9 2 2
3624 5 37 2 52 293 5 3 97 2.5 7 7 9 19000 15 2.5 1 6.67 381.9 6 0
4526 5 37 3 0 312 5 4 106 2 9 9 15 17000 9 1.5 1 40 428.9 2 4
3406 5 63 3 0 163 3 3 96 2.5 8 12 24 14000 7 1.75 1 2.78 381.9 2 2
4447 5 63 4 10 171 3 4 93 3 12 18 24 7000 7 1.75 1 8.33 428.9 2 2
5003 5 63 3 25 216 3 6 112 2.5 7 7 11 5000 5.5 1.38 1 33.33 643.6 1 3
5017 5 71 4 30 211 3 4 100 2.5 10 10 15 3000 7 1.75 1 4.17 428.9 2 2
4795 6 50 4 30 213 4 4 112 2.6 9 11 14 27000 8 1.6 1 . 428.9 2 3
4581 6 96 2 0 181 3 6 113 2.5 6 9 9 501000 10 2.5 1 11.11 643.6 4 0
3400 7 49 2 45 201 3 . 108 2.5 6 15 . 59000 10 2.5 1 . 518.9 4 0
35651 7 49 2 5 136 3 . 108 2 4 4 6.8 60000 8.5 2.125 1 . 518.9 3 1
35652 7 49 2 5 136 3 . 108 2 4 4 6.8 51000 7 1.75 1 . 518.9 2 2
4074 7 55 4 0 118 3 3 100 2.5 6 10 10 15000 7 1.75 1 26.67 381.9 2 2
4990 7 55 3 0 181 4 2 106 2.6 8 10 8.8 39000 12.5 2.5 1 30 310.9 5 0
4532 7 73 2 0 113 3 2 114 2.5 8 12 24 46000 10 2.5 1 13.33 310.9 4 0
4260 7 108 4 0 130 3 . 92 . . . . 2000 10 2.5 1 . . 4 0
3058 8 30 3 40 300 6 3 100 2.9 10 24 12 8000 10 1.43 1 10 381.9 2 5
3673 8 34 3 40 315 6 3 140 2 9 12 24 13000 10 1.43 1 5 381.9 2 5
176 8 39 1 15 178 3 3 101 1.6 6 9 12 123000 . . 1 3.33 381.9 . .
3357 8 39 2 40 143 3 3 96 2.3 7 7 20 101000 4 1 1 2.78 381.9 0 4
4144 8 39 2 10 346 5 4 99 1.8 9 12 15 83000 7.5 1.25 1 2 428.9 1 5
4148 8 39 2 0 321 5 4 97 2.5 9 12 18 132000 9 1.5 1 3.33 428.9 2 4

```

```

3937 8 43 2 0 190 3 4 97 2.5 6 6 12 18000 7 1.75 1 5.56 428.9 2 2
4754 8 84 3 30 170 3 4 112 2.5 6 9 12 29000 7 1.75 1 4.17 428.9 2 2
4385 8 106 2 35 276 5 4 106 2.5 9 9 15 27000 10.5 1.75 1 6 428.9 3 3
4575 9 18 2 0 169 3 3 106 2.5 5 7 7 37000 10 2.5 1 16.67 381.9 4 0
5001 9 18 2 10 99 2 3 106 2.5 6 9 18 42000 7.5 2.5 1 15 381.9 3 0
4261 9 33 3 . 169 3 3 116 2 12 18 24 16000 7 1.75 1 10 381.9 2 2
4568 9 33 4 20 246 4 4 113 2 7.5 9 24 1000 8 1.6 1 . 428.9 2 3
5378 9 33 4 25 229 4 3 100 2 6 9 15 4000 12.5 2.5 1 3.13 381.9 5 0
4242 9 91 4 0 301 6 2 93 2.5 9 12 24 1000 13 1.86 1 12.5 310.9 4 3
3949 9 101 3 10 213 4 3 92 2 6 12 24 5000 8 1.6 1 7.5 381.9 2 3
4564 9 101 4 10 181 3 3 93 2.5 11 16 24 3000 10 2.5 1 33.33 381.9 4 0
4566 9 101 4 0 257 4 3 102 1.5 8 6 12 3000 10.5 2.1 1 40.63 381.9 3 3
4462 9 107 4 0 209 4 3 86 2.5 9 24 24 2000 12.5 2.5 1 6.25 381.9 5 0
4741 9 110 3 30 181 3 4 114 3 9 7 10 38000 7 1.75 1 33.33 428.9 2 2
5296 9 110 4 20 205 3 4 100 2.5 6 6 9 5000 7 1.75 1 25 428.9 2 2
4767 10 9 3 30 118 3 2 106 3.5 5 8 12 30000 10 2.5 1 10 310.9 4 0
3273 10 12 2 0 159 3 3 96 2.5 6 24 . 59000 10 2.5 1 2.78 381.9 4 0
4490 5 66 3 . 363 6 4 100 2.5 9 12 . 23000 8.5 1.21 0 0 428.9 1 6
4908 5 76 4 0 378 5 6 100 4 6 8 12 3000 10.5 1.75 0 0 643.6 3 3
4580 6 96 1 0 180 3 6 103 3 6 9 15 591000 10 2.5 0 0 643.6 4 0
4896 6 96 1 41 182 3 4 102 2.5 7 9 12 100000 . . 0 0 428.9 . .
5123 6 92 1 50 312 5 . 95 1.8 5 8 12 175000 15 2.5 0 0 459.9 6 0
4049 7 108 2 37 287 5 4 94 2.5 8 16 24 37000 15 2.5 0 0 428.9 6 0
4968 7 60 3 25 107 2 2 93 2.5 8 10 18 34000 7.5 2.5 0 0 310.9 3 0
5223 7 73 2 38 256 4 4 106 2.5 8 10 24 56000 12.5 2.5 0 0 428.9 5 0
5334 7 73 2 . 193 4 2 106 2 6 9 21 . 12.5 2.5 0 0 310.9 5 0
3259 8 39 3 0 109 3 2 92 2.5 7 12 . 323000 7 1.75 0 0 310.9 2 2
3360 8 39 2 29 137 3 2 96 2.5 6 15 . 108000 5.5 1.38 0 0 310.9 1 3
4183 8 39 2 18 240 4 6 106 3.5 11 19 24 71000 12.5 2.5 0 0 643.6 5 0
4560 8 43 2 0 201 3 6 114 3 12 18 24 19000 7 1.75 0 0 643.6 2 2
4731 8 106 4 15 345 4 6 106 2.5 6 21 . 41000 8 1.6 0 0 643.6 2 3
3898 10 12 2 0 250 3 6 97 2.5 7 18 24 96000 10 2.5 0 0 643.6 4 0
4811 10 16 3 25 178 3 4 114 2.5 9 12 24 90000 7 1.75 0 0 428.9 2 2
5044 10 78 4 5 246 3 6 112 2.5 6 9 21 6000 10 2.5 0 0 643.6 4 0
5089 10 72 2 13 130 3 2 106 2.5 5 8 12 42000 10 2.5 0 0 310.9 4 0
5306 10 103 2 10 136 3 . 95 3 7 9 24 34000 10 2.5 0 0 374.9 4 0
4176 8 39 2 0 260 2 . 116 2.5 12 15 24 95000 6 2 0 0 751.6 2 1
4492 5 66 3 15 125 3 2 100 2.5 6 9 15 11000 7 1.75 0 0 310.9 2 2
3018 5 8 2 5 140 3 3 96 2.5 6 12 21 69000 10 2.5 0 0 381.9 4 0
4094 5 10 2 36 256 4 4 106 3 5 10 12 145000 12.5 2.5 0 0 428.9 5 0
4466 1 11 3 25 216 5 2 112 2.5 7.5 11 24 10000 15 2.5 0 0 310.9 6 0
3803 8 22 2 35 276 4 6 106 3 6 12 21 82000 6.5 1.3 0 0 643.6 1 4
4561 8 22 4 0 250 3 6 112 2.8 5.5 6 8 9000 7 1.75 0 0 643.6 2 2
3316 4 24 1 40 161 3 3 104 2.5 6 10 15 97000 7 1.75 0 0 381.9 2 2
4366 5 27 3 30 332 5 4 100 2.5 10 18 24 14000 12 2 0 0 428.9 4 2
1896 1 41 1 23 214 5 2 108 2.5 6 12 . 45000 15 2.5 0 0 310.9 6 0
3470 7 49 3 5 261 5 4 108 4.5 6.5 21 . 69000 10.5 1.75 0 0 428.9 3 3
3580 7 49 2 15 168 3 4 108 2.5 6 9 24 48000 7 1.75 0 0 428.9 2 2
2896 6 50 4 43 146 3 2 97 2.5 8 18 . 67000 7 1.75 0 0 310.9 2 2
4314 6 50 . 0 321 4 6 106 2.5 6 9 12 58000 8 1.6 0 0 643.6 2 3
3268 10 72 3 0 121 3 2 108 2.5 7 15 24 12000 . . 0 0 310.9 . .
4469 1 74 2 20 196 3 4 100 1.5 6 9 21 19000 10 2.5 0 0 428.9 4 0
3975 4 83 1 3 333 5 . 101 3 7 12 21 40000 15 2.5 0 0 473.9 6 0
4496 4 89 3 . 232 3 6 94 2.5 12 18 24 51000 10 2.5 0 0 643.6 4 0
4237 6 92 1 8 194 4 3 106 2.5 6 12 24 309000 8 1.6 0 0 381.9 2 3
3747 6 96 1 . 335 5 6 101 2.5 9 12 22 705000 15 2.5 0 0 643.6 6 0
4659 6 96 3 6 173 3 6 106 2.5 10 14 24 209000 7 1.75 0 0 643.6 2 2
3793 10 103 2 25 207 3 . 106 1.5 8 4.5 24 31000 . . 0 0 518.9 . .
4401 9 110 4 35 347 5 4 93 2.5 6 8 15 5000 9 1.5 0 0 428.9 2 4

```

3516	8	114	2	15	211	3	.	108	2	5	15	.	48000	7	1.75	0	0	518.9	2	2
1153	1	2	1	28	164	3	4	108	2.5	7	12	24	19000	10	2.5	0	0	428.9	4	0
3510	1	2	1	42	173	3	4	108	2.5	8	24	.	22000	7	1.75	0	0	428.9	2	2
4746	1	32	3	0	221	4	3	93	1.8	6	10	21	11000	12.5	2.5	0	0	381.9	5	0
4764	1	25	2	40	272	5	2	106	2.6	8	9	12	14000	15	2.5	0	0	310.9	6	0
5535	1	74	3	0	180	3	4	93	1.8	8	12	21	6000	10	2.5	0	0	428.9	4	0
3876	2	40	4	35	200	3	4	121	2.5	6	9	12	2000	10	2.5	0	0	428.9	4	0
3890	2	58	3	0	136	3	2	92	1.5	12	17	20	3000	10	2.5	0	0	310.9	4	0
4120	2	1	4	10	337	5	6	93	2.5	12	18	21	4000	12	2	0	0	643.6	4	2
4421	2	105	3	42	254	3	6	100	2.5	9	15	24	7000	10	2.5	0	0	643.6	4	0
3148	3	56	2	40	154	3	3	108	2.5	6	12	.	29000	7	1.75	0	0	381.9	2	2
3319	4	83	3	15	338	5	.	100	3.5	12	18	24	24000	12	2	0	0	518.9	4	2
3341	4	83	1	20	187	3	4	106	2.5	9	12	21	39000	7	1.75	0	0	428.9	2	0
3343	4	83	1	14	151	3	3	106	2.6	9	12	24	63000	10	2.5	0	0	381.9	4	0
3372	4	83	1	13	183	4	3	111	2.5	6	8	12	62000	12.5	2.5	0	0	381.9	5	0
4058	4	48	3	0	144	3	4	118	2.5	9	15	24	183000	10	2.5	0	0	428.9	4	0
4861	4	48	2	12	127	2	4	116	2.5	7	9	11	25000	7.5	2.5	0	0	428.9	3	0
4862	4	48	2	12	128	2	4	112	2.5	7	9	11	25000	7.5	2.5	0	0	428.9	3	0
4863	4	48	2	0	199	2	6	103	2.8	5	6	8	113000	7.5	2.5	0	0	643.6	3	0
5359	4	42	3	20	223	3	6	106	1.8	6	9	21	.	7	1.75	0	0	643.6	2	2
5488	4	42	3	0	170	3	3	106	1.8	7	10	24	.	10	2.5	0	0	381.9	4	0
3548	5	71	3	0	133	3	2	97	2.5	7	12	.	21000	7	1.75	0	0	310.9	2	2
3599	5	37	4	28	214	3	4	98	2.5	9	14	24	2000	10	2.5	0	0	428.9	4	0
4005	5	26	2	0	145	3	4	108	2.5	6	12	24	137000	5.5	1.38	0	0	428.9	1	3
4526	5	37	3	0	312	5	4	106	2	9	15	24	16000	9	1.5	0	0	428.9	2	4
4874	5	27	4	16	169	3	3	112	2	5	8	21	4000	5.5	1.38	0	0	381.9	1	3
5119	5	27	1	13	280	3	6	100	2.5	6	9	12	97000	10	2.5	0	0	643.6	4	0
2944	6	50	3	55	268	4	4	106	2.5	9	12	24	58000	12.5	2.5	0	0	428.9	5	0
2945	6	50	3	55	255	4	4	106	2	10	16	24	58000	12.5	2.5	0	0	428.9	5	0
3028	6	96	.	6	155	4	2	97	2	6	9	12	271000	12.5	2.5	0	0	310.9	5	0
3046	6	50	3	55	162	3	3	96	2.5	6	9	24	87000	7	1.75	0	0	381.9	2	2
3098	6	50	3	8	149	3	3	108	2.5	6	9	12	64000	10	2.5	0	0	381.9	4	0
3746	6	96	1	.	297	5	6	101	2.5	9	15	22	713000	15	2.5	0	0	643.6	6	0
4189	6	36	4	0	232	4	.	93	2.5	18	24	.	2000	8	1.6	0	0	473.9	3	2

## **Appendix E**

J. MYERS, A. NANNI, AND D. STONE

### **PRELIMINARY INVESTIGATION OF THE REVISED DATABASE**

A boxplot is a graphical representation of the distribution of the data in a data set. It can provide information about the center of the data set, the spread of the data, the range in which most of the data falls, and the possibility of outliers. To produce a boxplot the median, the first and third quartiles, the upper and lower inner fences, and the upper and lower outer fences are required. Note that the fences mentioned are function of the interquartile range, which is the difference between the values of the first and third quartiles. The specifics are not defined herein because for the boxplots created the traditional boxplot was modified slightly; the fences were replaced with the minimum and maximum values. Further information can be found in Vining (1998).

The first step is to determine the median of the data set. The median of a data set, “ $\tilde{y}$ ”, is determined by placing the data points in ascending order and then determining the middle value. The location of the median, “ $l_m$ ”, can be calculated by Equation E.1.

$$l_m = \frac{n+1}{2} \quad (\text{E.1})$$

where “ $n$ ” is the number of data points in the data set. If “ $n$ ” is odd then “ $l_m$ ” is an integer and

$$\tilde{y} = y_{(l_m)} \quad (\text{E.2})$$

However, if “ $n$ ” is even then “ $l_m$ ” will contain the fraction  $\frac{1}{2}$ . In this case the calculation of “ $\tilde{y}$ ” will be carried out according to Equation E.3. The median will be the average of the two data points surrounding the location, “ $l_m$ ”.

$$\tilde{y} = \frac{y(l_m - 1/2) + y(l_m + 1/2)}{2} \quad (\text{E.3})$$

The first and third quartiles, “ $Q_1$ ” and “ $Q_3$ ”, respectively, can be determined by first calculating the location of the quartiles, denoted as “ $l_q$ ”.

$$l_q = \begin{cases} \frac{n+3}{4} & \text{if } n \text{ is odd} \\ \frac{n+2}{4} & \text{if } n \text{ is even} \end{cases} \quad (\text{E.4})$$

If “ $l_q$ ” is an integer, the first quartile can be found by counting “ $l_q$ ” data points in from the beginning of the ascending data set and the third quartile can be found by counting in “ $l_q$ ” data points from the end of the ascending data set.

$$\begin{aligned} Q_1 &= y(l_q) \\ Q_3 &= y(n+1-l_q) \end{aligned} \quad (\text{E.5})$$

If “ $l_q$ ” is not an integer, then the quartiles will be the average of the two data points surrounding the location, “ $l_q$ ”.

$$\begin{aligned} Q_1 &= \frac{y(l_q - 1/2) + y(l_q + 1/2)}{2} \\ Q_3 &= \frac{y(n+1-l_q - 1/2) + y(n+1-l_q + 1/2)}{2} \end{aligned} \quad (\text{E.6})$$

The minimum and maximum values are then determined and the values of the median, the first and third quartiles, and the minimum and maximum values are plotted on a horizontal scale as shown in Figure E.

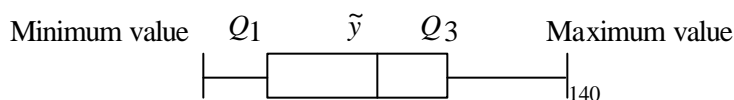
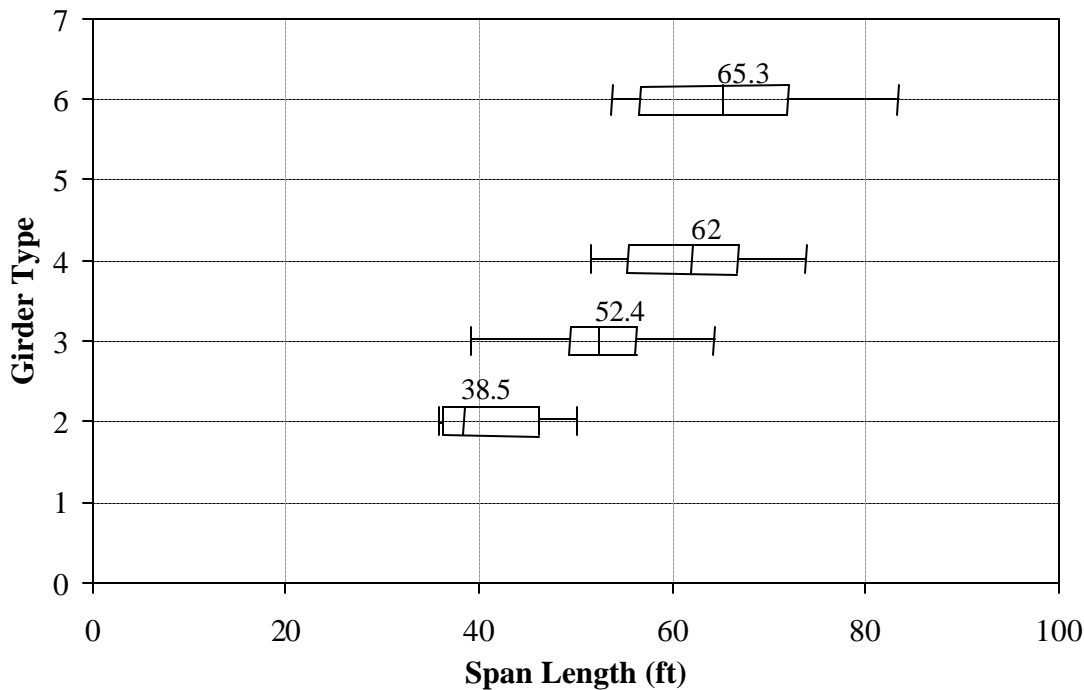


### Figure E.1 Generic Boxplot

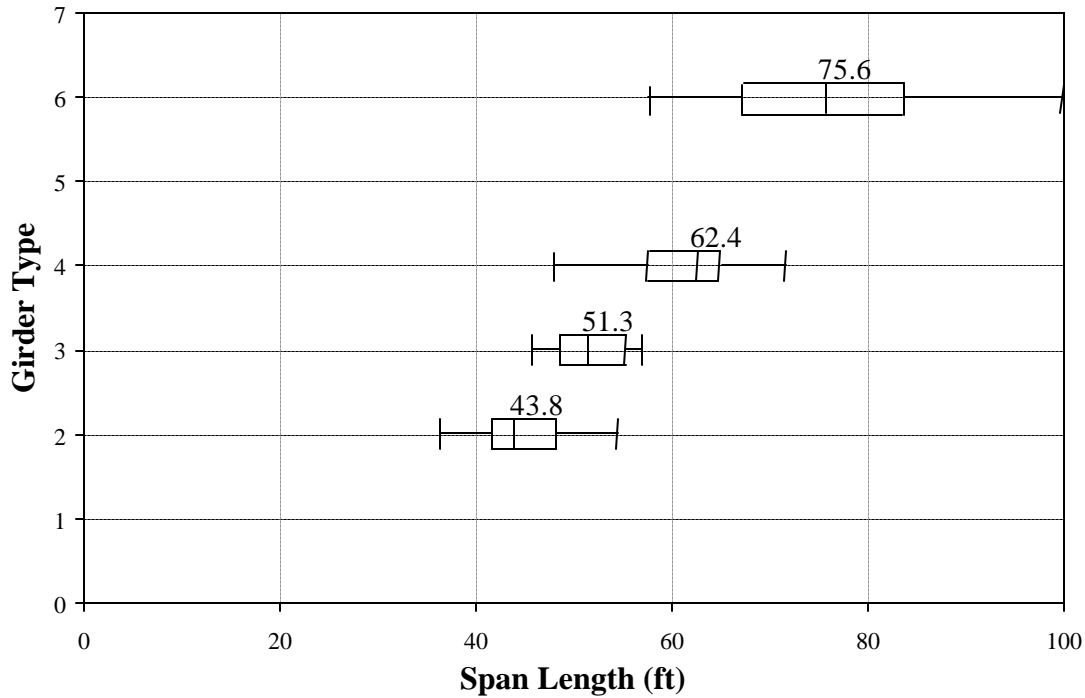
This type of modified boxplot is illustrated in Figures E.2 and E.3. Figure E.2 exhibits the four boxplots, one for each girder type, of the span length of the cracked bridges. Figure E.3 exhibits the four boxplots, one for each girder type, of the span length of the uncracked bridges. In both figures, the number directly above each boxplot is the value of the median of the span length for that girder type.

Figures E.2 and E.3 illustrate that the uncracked bridges tend to have longer span lengths than the cracked bridges. This trend is counter-intuitive, in that, one would expect a longer span to experience higher stresses, due to increases in live and dead load moments, and hence exhibit a higher probability of cracking. Additionally, as expected, as the girder type number increases, indicating a larger size girder, the span length also increases. This is consistent with the MoDOT design guidelines and serviceability requirements.



Note: 1 ft. = 0.3048 m

**Figure E.2 Boxplots of Span Length, by Girder Type, for the Cracked Bridges**



Note: 1 ft. = 0.3048 m

**Figure E.3 Boxplots of Span Length, by Girder Type, for the Uncracked Bridges**

A series of bar charts were created to examine possible trends in the data set. Most try to establish conclusions about the differences or similarities between the cracked and uncracked bridges. Additionally, the number above each bar represents the number of bridges that are included within said classification.

To determine information about the types of girders used in the bridges, Figure E.4 is a representation of the number of bridges by girder type, as a function of cracked status. This would yield conclusions about a potential over/under-design of these bridges. In this case, the distribution in Figure E.4 indicates that no one girder type is solely responsible for a cracked or uncracked bridges. It may be noted that the vertical scale of Figure E.4 is 150, in order to illustrate the relative proportions of each girder type within the entire database.

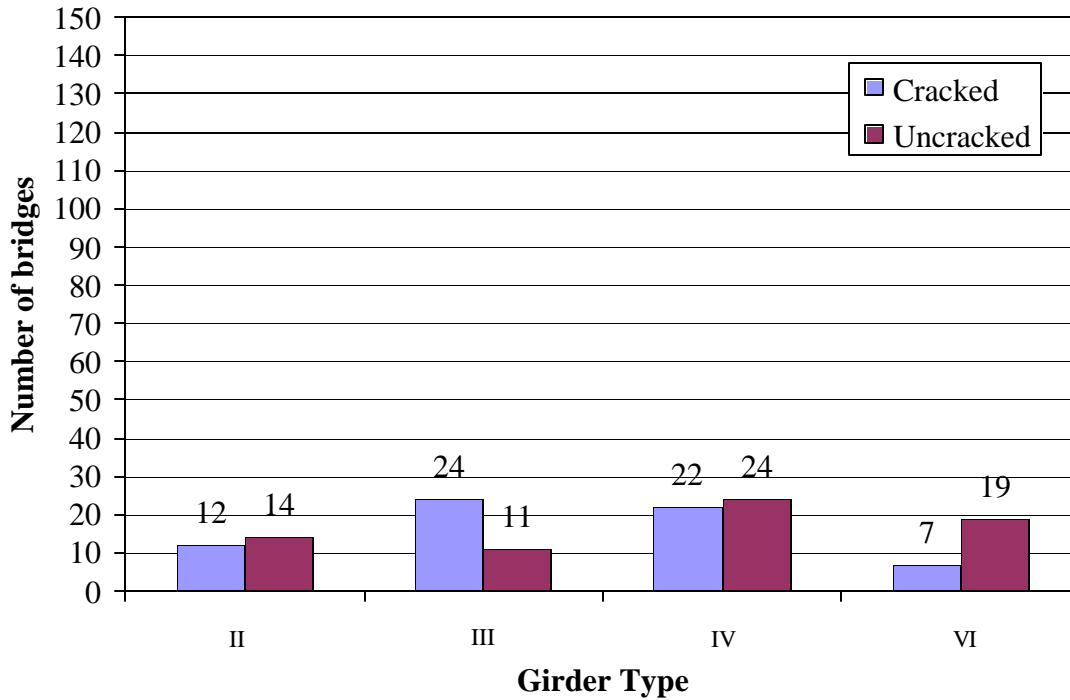


**Figure E.4 Bridges by Girder Type, as a Function of Cracked Status**

Examination of Figure E.4 indicates that girders of Type II and Type IV exhibit roughly a 1:1 proportion of cracked bridges to uncracked bridges. This is in contrast to Type III, which exhibits a larger proportion of cracked girders than uncracked girders, and Type VI, which exhibits a larger proportion of uncracked bridges than cracked bridges. This distribution of girder types by cracked status is reflected in Figures E.5 through E.10, as well.

Figures E.5 and E.6 exhibit the number of bridges by number of spans, for cracked and uncracked bridges, respectively. Figures E.5 and E.6 also exhibit the fact that 3-span bridges are the most common type of continuous PC bridge in Missouri. This may be attributed to span length requirements most often encountered in Missouri.

One variable of interest, in the preliminary analysis, was to determine whether the bridges on one type of route exhibited more cracking than those on another type of route. Figures E.7 and Figure E.8 illustrate the number of bridges by girder type, as a function of route type.

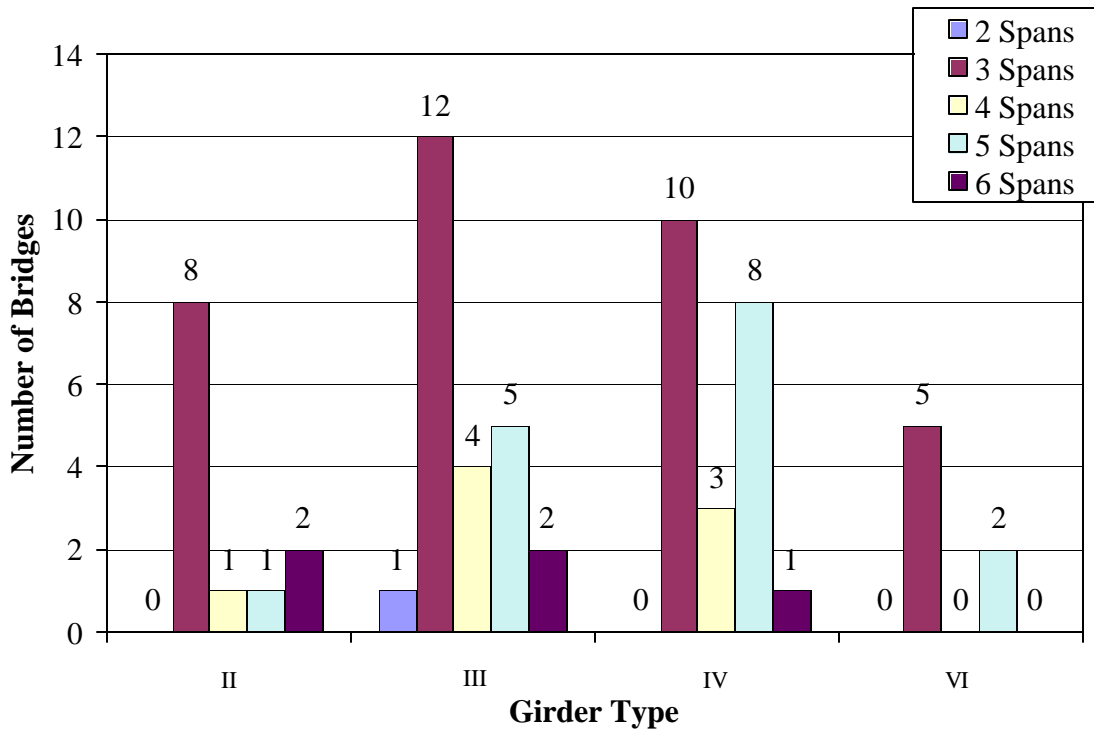


Figure E.5 Cracked Bridges by Girder Type, as a Function of Number of Spans

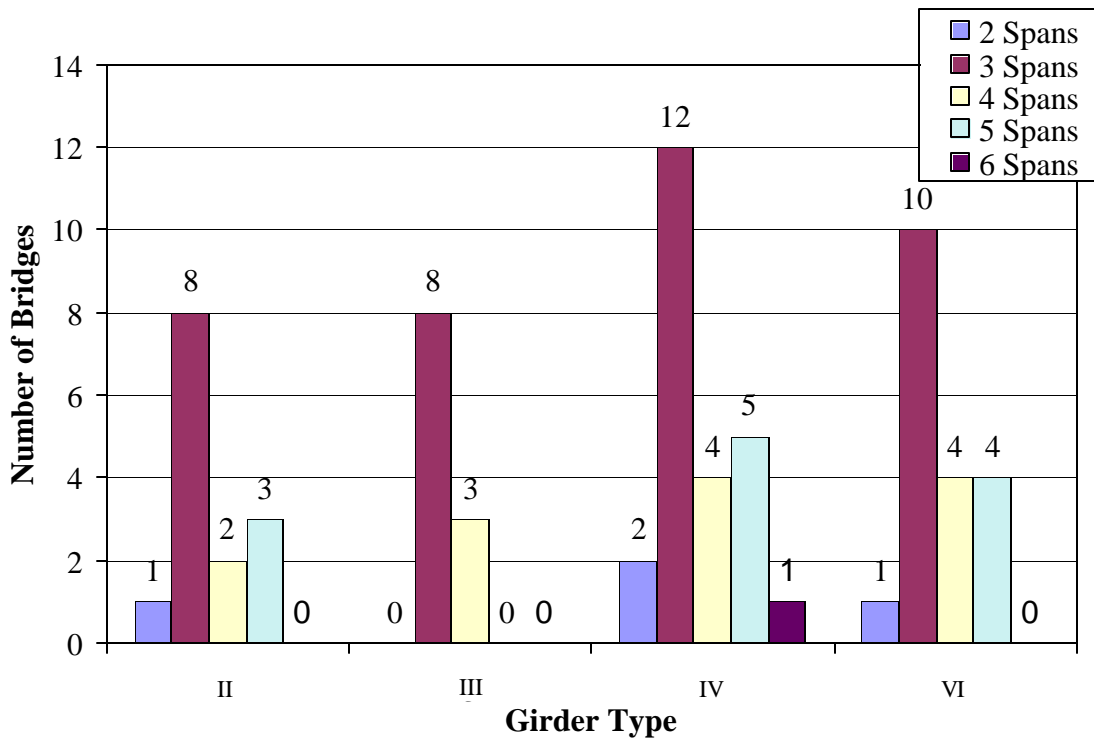
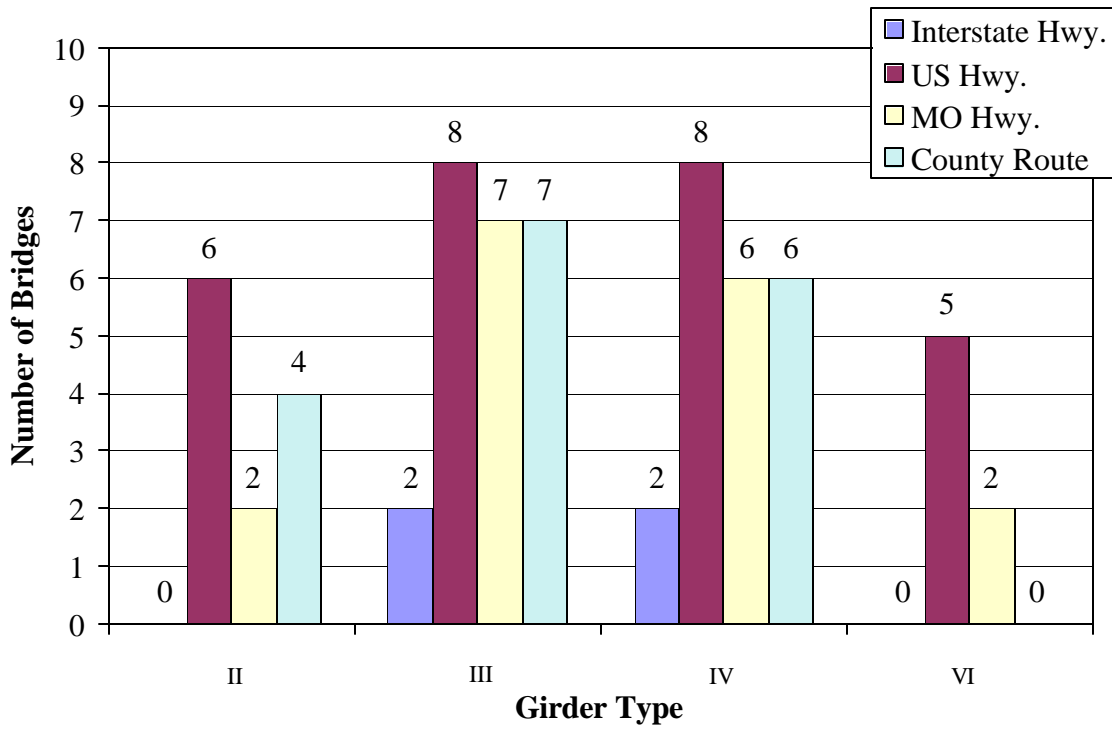
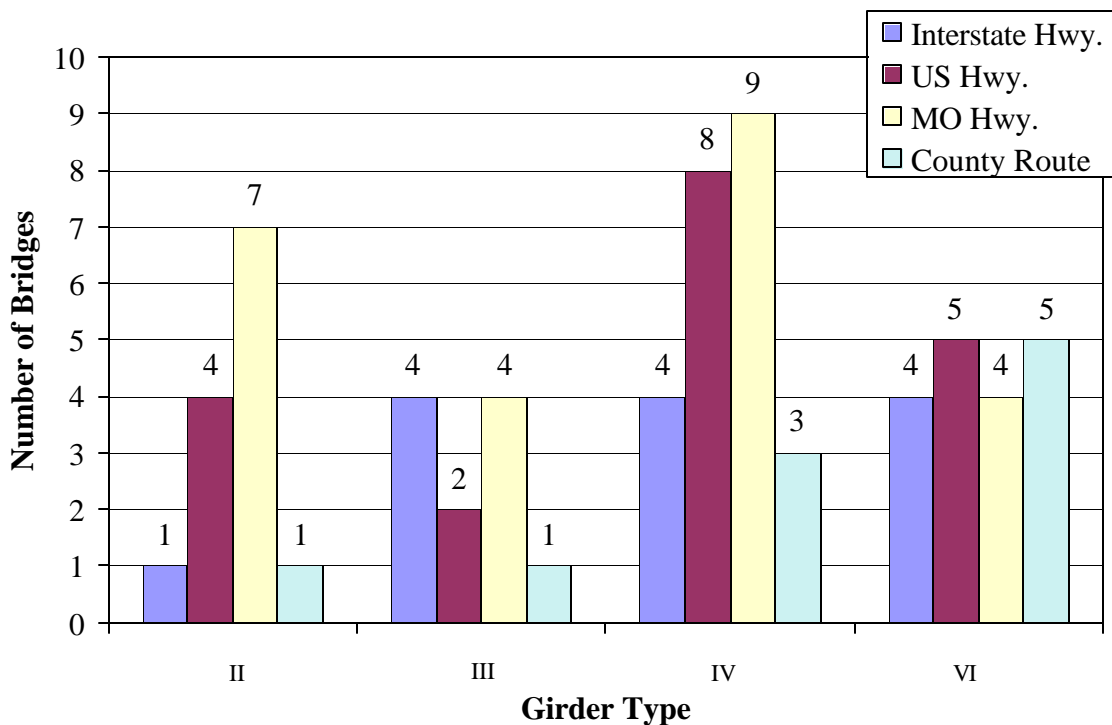


Figure E.6 Uncracked Bridges by Girder Type, as a Function of Number of Spans



**Figure E.7 Cracked Bridges by Girder Type, as a Function of Route Type**

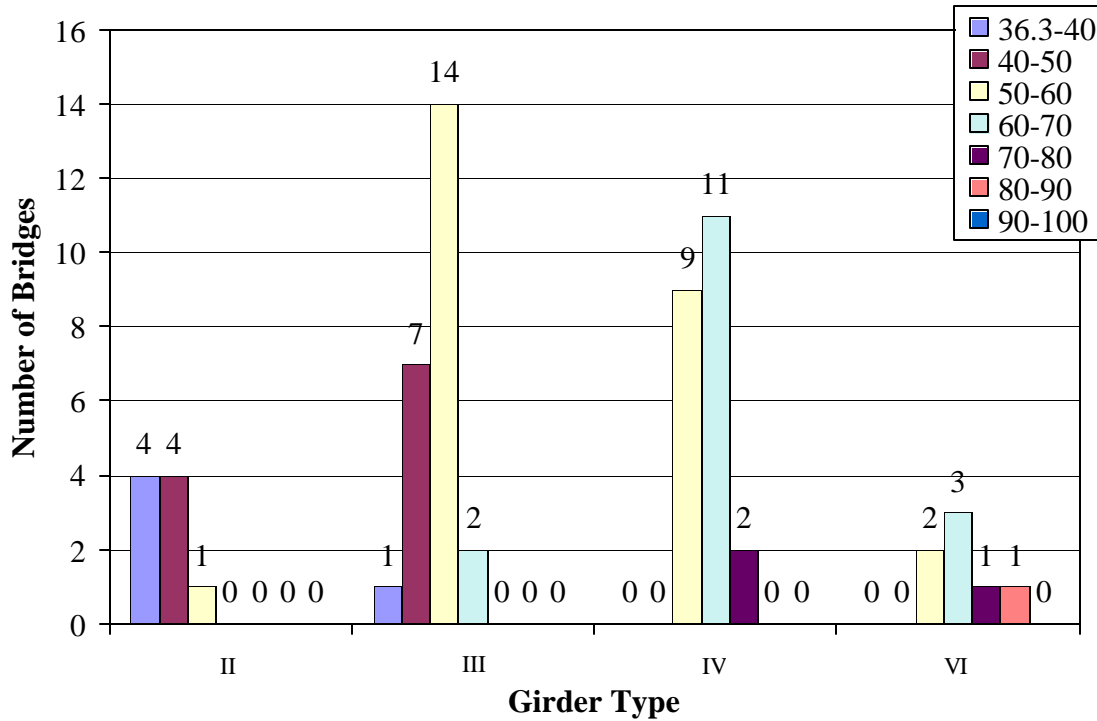
The overall trend exhibited by these two figures indicates that, of the four route types, interstate highways have the smallest proportion of cracked bridges and U.S. highways have the highest proportion of cracked bridges.



**Figure E.8 Uncracked Bridges by Girder Type, as a Function of Route Type**

Plots of the number of bridges by girder type, as a function of span length, can be seen in Figures E.9 and E.10.

The most common span length for the cracked bridges is 50 to 60 feet (15.24 to 18.29 meters) while the most common span length for the uncracked bridges is 60 to 70 feet (18.29 to 21.34 meters). This reiterates the previous trend of shorter span lengths for the cracked bridges and longer span length for the uncracked bridges.



Note: 1 ft. = 0.3048 m

**Figure E.9 Cracked Bridges by Girder Type, as a Function of Span Length**

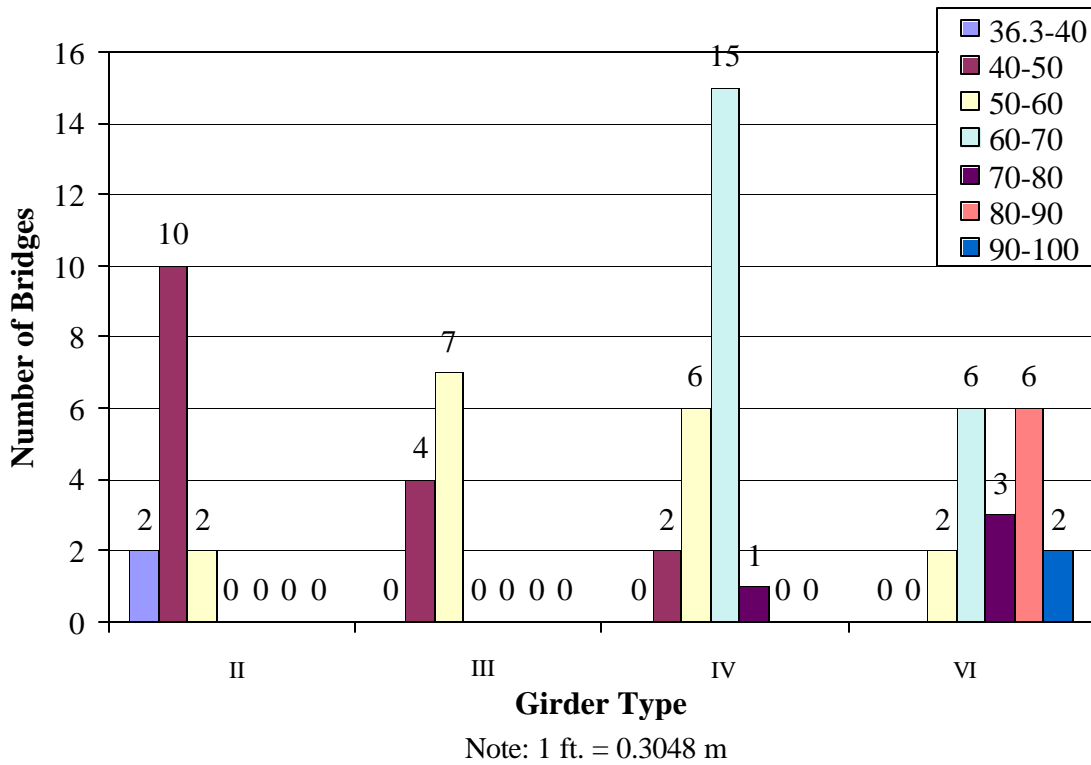


**Figure E.10 Uncracked Bridges by Girder Type, as a Function of Span Length**

In general, the cracked bridges have shorter span lengths than the uncracked bridges. More Type III girders crack than remain uncracked. Type VI girders tend to remain uncracked. Type II and Type IV girders seem to be somewhere in between, with approximately equal proportions of cracked and uncracked bridges. Interstate bridges crack less than the other route types and U.S. highway bridges tend to crack more often. Three span bridges are the most common of the bridges in Missouri utilizing simple span PC I-girder made continuous.

## **APPENDIX F**

J. Myers, A. Nanni, and D. Stone

### **LOGISTIC REGRESSION ANALYSIS**

**PROGRAM FILE:**

```
options ls=72;
data bridge;
infile 'bridge.data';
input id dist co rt skew length spans gtype gspace endspace sec1 sec2
sec3 adt tfs afs crackd percntc garea pfoot sfoot ;
rtd1=0; rtd2=0;
if rt=2 then rtd1=1;
if rt=3 then rtd2=1;
if rt=4 then do; rtd1=1; rtd2=1; end;

if rt=1 then rt1=1; else rt1=0;
if rt=2 then rt2=1; else rt2=0;
if rt=3 then rt3=1; else rt3=0;

if dist<7 then tzone=0; else tzone=1;
if dist=7 then aggzone=0;
if dist=8 then aggzone=0;
if dist=9 then aggzone=0; else aggzone=1;

garea2=garea*garea;
gtd1=0; gtd2=0; if gtype=3 then gtd1=1; if gtype=4 then gtd2=1;
if gtype=6 then do; gtd1=1; gtd2=1; end;
spl=length/spans; garspl=garea*spl;

proc logistic;
model crackd= sec3 spl garea garspl rt1 aggzone/ ctable fast
link=logit;
```

**OUTPUT FILE:**

The LOGISTIC Procedure

Data Set: WORK.BRIDGE  
 Response Variable: CRACKD  
 Response Levels: 2  
 Number of Observations: 134  
 Link Function: Logit

Response Profile

Ordered Value	CRACKD	Count
1	0	64
2	1	70

WARNING: 17 observation(s) were deleted due to missing values for the response or explanatory variables.

Model Fitting Information and Testing Global Null Hypothesis BETA=0

Criterion	Intercept Only	Intercept and Covariates	Chi-Square for Covariates
AIC	187.495	143.852	.
SC	190.393	164.137	.
-2 LOG L Score	185.495	129.852	55.643 with 6 DF (p=0.0001)
	.	.	42.860 with 6 DF (p=0.0001)

Analysis of Maximum Likelihood Estimates

Variable	DF	Parameter Estimate	Standard Error	Wald Chi-Square	Pr > Chi-Square	Standardized Estimate
INTERCPT	1	-0.4793	5.0369	0.0091	0.9242	.
SEC3	1	0.1804	0.0405	19.8278	0.0001	0.611861
SPL	1	-0.0664	0.0835	0.6328	0.4263	-0.492969
GAREA	1	-0.0245	0.0124	3.9195	0.0477	-1.511810
GARSPL	1	0.000342	0.000192	3.1940	0.0739	2.452062
RT1	1	1.8788	0.7220	6.7714	0.0093	0.346044
AGGZONE	1	2.8704	1.1211	6.5554	0.0105	0.470160

The LOGISTIC Procedure

Analysis of  
 Maximum Likelihood  
 Estimates

Variable	Odds Ratio
INTERCPT	.
SEC3	1.198
SPL	0.936
GAREA	0.976
GARSPL	1.000
RT1	6.546
AGGZONE	17.645

Association of Predicted Probabilities and Observed Responses

Concordant = 84.8%	Somers' D = 0.697
Discordant = 15.1%	Gamma = 0.697
Tied = 0.1%	Tau-a = 0.350
(4480 pairs)	c = 0.848

Classification Table

Prob Level	Correct		Incorrect		Percentages				
	Event	Non-Event	Event	Non-Event	Correct	Sensi-tivity	Speci-ficity	False POS	False NEG
0.000	64	0	70	0	47.8	100.0	0.0	52.2	.
0.020	63	4	66	1	50.0	98.4	5.7	51.2	20.0
0.040	63	8	62	1	53.0	98.4	11.4	49.6	11.1
0.060	63	8	62	1	53.0	98.4	11.4	49.6	11.1
0.080	63	10	60	1	54.5	98.4	14.3	48.8	9.1
0.100	63	12	58	1	56.0	98.4	17.1	47.9	7.7
0.120	63	14	56	1	57.5	98.4	20.0	47.1	6.7
0.140	63	17	53	1	59.7	98.4	24.3	45.7	5.6
0.160	61	20	50	3	60.4	95.3	28.6	45.0	13.0
0.180	60	26	44	4	64.2	93.8	37.1	42.3	13.3
0.200	60	30	40	4	67.2	93.8	42.9	40.0	11.8
0.220	60	35	35	4	70.9	93.8	50.0	36.8	10.3
0.240	59	37	33	5	71.6	92.2	52.9	35.9	11.9
0.260	58	39	31	6	72.4	90.6	55.7	34.8	13.3
0.280	56	41	29	8	72.4	87.5	58.6	34.1	16.3
0.300	55	43	27	9	73.1	85.9	61.4	32.9	17.3
0.320	55	45	25	9	74.6	85.9	64.3	31.3	16.7
0.340	54	46	24	10	74.6	84.4	65.7	30.8	17.9
0.360	54	46	24	10	74.6	84.4	65.7	30.8	17.9
0.380	53	46	24	11	73.9	82.8	65.7	31.2	19.3
0.400	53	47	23	11	74.6	82.8	67.1	30.3	19.0
0.420	53	49	21	11	76.1	82.8	70.0	28.4	18.3
0.440	51	52	18	13	76.9	79.7	74.3	26.1	20.0
0.460	51	52	18	13	76.9	79.7	74.3	26.1	20.0
0.480	51	53	17	13	77.6	79.7	75.7	25.0	19.7
0.500	49	54	16	15	76.9	76.6	77.1	24.6	21.7
0.520	48	54	16	16	76.1	75.0	77.1	25.0	22.9
0.540	45	54	16	19	73.9	70.3	77.1	26.2	26.0
0.560	44	54	16	20	73.1	68.8	77.1	26.7	27.0
0.580	43	55	15	21	73.1	67.2	78.6	25.9	27.6
0.600	41	57	13	23	73.1	64.1	81.4	24.1	28.8

0.620	39	57	13	25	71.6	60.9	81.4	25.0	30.5
0.640	38	57	13	26	70.9	59.4	81.4	25.5	31.3
0.660	36	59	11	28	70.9	56.3	84.3	23.4	32.2
0.680	32	59	11	32	67.9	50.0	84.3	25.6	35.2
0.700	30	60	10	34	67.2	46.9	85.7	25.0	36.2
0.720	25	63	7	39	65.7	39.1	90.0	21.9	38.2
0.740	24	65	5	40	66.4	37.5	92.9	17.2	38.1
0.760	24	66	4	40	67.2	37.5	94.3	14.3	37.7
0.780	22	66	4	42	65.7	34.4	94.3	15.4	38.9
0.800	20	67	3	44	64.9	31.3	95.7	13.0	39.6
0.820	17	67	3	47	62.7	26.6	95.7	15.0	41.2
0.840	15	67	3	49	61.2	23.4	95.7	16.7	42.2
0.860	14	68	2	50	61.2	21.9	97.1	12.5	42.4
0.880	13	68	2	51	60.4	20.3	97.1	13.3	42.9
0.900	13	68	2	51	60.4	20.3	97.1	13.3	42.9
0.920	10	68	2	54	58.2	15.6	97.1	16.7	44.3
0.940	8	69	1	56	57.5	12.5	98.6	11.1	44.8
0.960	5	69	1	59	55.2	7.8	98.6	16.7	46.1
0.980	3	69	1	61	53.7	4.7	98.6	25.0	46.9
1.000	0	70	0	64	52.2	0.0	100.0		

## **APPENDIX G**

J. Myers, A. Nanni, and D. Stone

### **BRIDGE MONITORING DATA SHEETS**









## **APPENDIX H**

J. Myers, A. Nanni, and D. Stone

### **ELASTIC ANALYSIS CALCULATIONS FOR THE AASHTO POSITIVE AND NEGATIVE GRADIENTS APPLIED TO A SQUARE CROSS SECTION**

Exact solution of the simply supported square beam  
with AASHTO + and - gradients applied

1. Define the constants

(all units are inches, pounds, and degrees Fahrenheit)

$$\alpha := 6.0 \cdot 10^{-6} \quad c := 6 \quad y_{cg} := 12 - c$$

$$E := 5000000 \quad \text{Area} := 144 \quad I := \frac{12^4}{12} \quad I = 1.728 \cdot 10^3$$

2. Define the thermal gradients

$$y := 0..12$$

$$T_{\text{pos}}(y) := \begin{cases} \frac{(12-0) \cdot y}{8} & \text{if } 0 \leq y \leq 8 \\ \frac{(46-12) \cdot (y-8)}{4} + 12 & \text{otherwise} \end{cases}$$

$$T_{\text{neg}}(y) := \begin{cases} \frac{.5 - (12-0) \cdot y}{8} & \text{if } 0 \leq y \leq 8 \\ \frac{.5 - (46-12) \cdot (y-8)}{4} - 6 & \text{otherwise} \end{cases}$$

3. Define the thermal stresses

$$\sigma_{\text{pos}}(y) := -(E \cdot \alpha \cdot T_{\text{pos}}(y))$$

$$\sigma_{\text{neg}}(y) := -(E \cdot \alpha \cdot T_{\text{neg}}(y))$$

y =	$\sigma_{\text{pos}}(y) =$
0	0
1	-45
2	-90
3	-135
4	-180
5	-225
6	-270
7	-315
8	-360
9	-615
10	-870
11	-1125
12	-1380

y =	$\sigma_{\text{neg}}(y) =$
0	0
1	22.5
2	45
3	67.5
4	90
5	112.5
6	135
7	157.5
8	180
9	307.5
10	435
11	562.5
12	690

### 4. Define the Continuity Stresses

**positive gradient**

$$P_{pos} := \int_0^{12} E \cdot \alpha \cdot T_{pos}(y) \cdot 12 dy \quad P_{pos} = 5.904 \cdot 10^4$$

$$M_{pos} := \int_0^{12} E \cdot \alpha \cdot T_{pos}(y) \cdot (y_{cg} - y) \cdot 12 dy \quad M_{pos} = -1.718 \cdot 10^5$$

$$\sigma_{posf}(y) := \sigma_{pos}(y) + \left( \frac{P_{pos}}{Area} \right) + M_{pos} \cdot \frac{(y_{cg} - y)}{I}$$

**negative gradient**

$$P_{neg} := \int_0^{12} E \cdot \alpha \cdot T_{neg}(y) \cdot 12 dy \quad P_{neg} = -2.952 \cdot 10^4$$

$$M_{neg} := \int_0^{12} E \cdot \alpha \cdot T_{neg}(y) \cdot (y_{cg} - y) \cdot 12 dy \quad M_{neg} = 8.592 \cdot 10^4$$

$$\sigma_{negf}(y) := \sigma_{neg}(y) + \left( \frac{P_{neg}}{Area} \right) + M_{neg} \cdot \frac{(y_{cg} - y)}{I}$$

y =	$\sigma_{posf}(y) =$
0	-186.667
1	-132.222
2	-77.778
3	-23.333
4	31.111
5	85.556
6	140
7	194.444
8	248.889
9	93.333
10	-62.222
11	-217.778
12	-373.333

y =	$\sigma_{negf}(y) =$
0	93.333
1	66.111
2	38.889
3	11.667
4	-15.556
5	-42.778
6	-70
7	-97.222
8	-124.444
9	-46.667
10	31.111
11	108.889
12	186.667

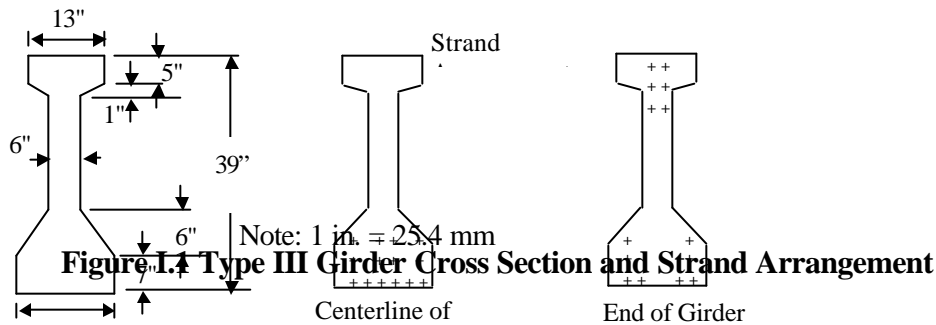
## **APPENDIX I**

J. Myers, A. Nanni, and D. Stone

### **DESIGN EXAMPLE**

## L1 BACKGROUND

The design example was performed on Bridge A4565, which is the cracked bridge that was used for monitoring purposes in this project. The design and construction of the bridge was conducted under project number RS-BRS-1030 (7). Bridge A4565 uses Type III girders; their properties are outlined below.



Preliminary calculations for the design example were supplied by MoDOT. Included in these calculations was information about geometry, loading, moments, and prestress losses. The moments used in the design example were provided by the computer program BR200. The design example stress calculations were performed at the end of the diaphragm on the span (2-3) girders, since this is a location where many cracks were observed. It should be noted that the strand arrangement detailed above is used only for spans (2-3), (3-4), and (4-5), since the design example focused on span (2-3).

Traditionally, the allowable stress values recommended by AASHTO are used to design bridge girders. The allowable concrete stresses at service loads after prestress losses are outlined as follows:

- The allowable compressive stress can be calculated by  $0.40f_c'$ , which, for a 5000-psi concrete (34.45-MPa), is equal to 2000 psi (13.78 MPa).
- The allowable tensile stress can be calculated by  $6\sqrt{f_c'}$ , which, for a 5000-psi (34.45-MPa) concrete, is equal to 424 psi (2.92 MPa).

**I2 DESIGN EXAMPLE CALCULATIONS****Girder Geometry**

Area of a Type III girder (in <sup>2</sup> )	$Area_g := 381.9$
Moment of inertia of a Type III girder (in <sup>4</sup> )	$I_{girder} := 61841$
Composite area of the girder and the deck (93" effective flange width and 8.5" deck thickness) (in <sup>2</sup> )	$Area_{gd} := 1089$

It may be noted that the entire deck thickness of 8.5" was used in this design example. This was done in order to be consistent with AASHTO (1996) and the simplified approach for thermal stress calculations outlined in Section 8.4 of this report. This is contrary to MoDOT design procedure, which would use an effective deck thickness of 7.5" (the entire deck thickness minus 1").

Composite moment of inertia of the girder and the deck (in <sup>4</sup> )	$I_{gd} := 235900$
Length of the girder (CL bearing to CL bearing) (in)	$L := 714$
Distance to end of diaphragm from end of girder (location where the stresses will be checked) (in)	$l := (2 \cdot 12 + 9) - 9 - 4 - 7$ $l = 13$
Center of gravity of the girder (from bottom) (in)	$yc_{gg} := 17.08$
Center of gravity of the strands at the centerline of the girder (from bottom) (in)	$yc_{gsc} := 3.71$
Center of gravity of the strands at the end of the girder (from bottom) (in)	$yc_{gse} := 16.57$
Composite center of gravity (distance from the bottom of the girder) (in)	$cb := 34.07$

**Calculation of Girder Stresses Due to Dead and Live Loads**

Eccentricity varies with location because the tendons are draped. A linear variation is assumed for simplicity.

Maximum eccentricity (in)	$ec_{max} := yc_{gg} - yc_{gsc}$ $ec_{max} = 13.37$
Minimum eccentricity (in)	$ec_{min} := yc_{gg} - yc_{gse}$ $ec_{min} = 0.51$

Determine the eccentricity of the strands at the location being checked.

$$ec := \frac{ec_{max} - ec_{min}}{290.5} \cdot 1 + ec_{min} \quad ec = 1.085$$

The full effective prestress force (transfer length not considered) in span 2 is used in the stress calculations.

Prestressing force (kips)  $P := 356.74$

There are three moments to consider in the stress calculations, the non-composite dead load (the weight of the deck and the girders), the composite dead load (barrier curb and future wearing surface), and the HS20 live load. There are two live load conditions to consider which are outlined by AASHTO. The first is the truck loading and the second is a uniform distributed load over the lane, which is referred to as the lane load.

For these calculations, a linear interpolation was done between the end of the girder and the 0.1\*L location to determine the moments at the face of the diaphragm. These moments are slightly conservative.

Non-composite dead load moment (kip-in)  $M_{dl1} := 285.2$

Composite dead load moment (kip-in)  $M_{dl2} := -1770$

Live load moment, lane loading (kip-in)  $M_{lli} := -4869$

*Sign Convention for Design Example:*

It may be noted that a positive stress denotes tension (+), while a negative stress denotes compression (-).

$$\sigma(y) := \frac{-P}{A_{reag}} + \frac{P \cdot ec \cdot (y - y_{cgg})}{I_{girder}} - M_{dl1} \frac{(y - y_{cgg})}{I_{girder}} - M_{dl2} \frac{y - cb}{I_{gd}} - M_{lli} \frac{y - cb}{I_{gd}}$$

Note that the units of  $\sigma(y)$  are ksi.

$y := 0, 0.5 \dots 39$        $\sigma(0) \cdot 1000 = -1.921 \cdot 10^3$        $y = 0$  inches, bottom of girder

$\sigma(39) \cdot 1000 = -759.204$        $y = 39$  inches, top of girder

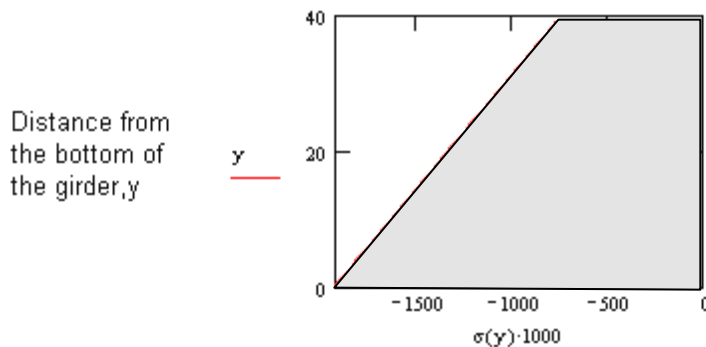


**Figure I.2 Stresses Due to Dead Load, Live Load and Prestressing**

### Calculation of Girder Stresses Due to Thermal Gradients

Define the thermal gradients

$$\text{Modulus of the girders (psi)} \quad E_g := 57000 \cdot \sqrt{5000}$$

$$\text{Modulus of the deck (psi)} \quad E_d := 57000 \cdot \sqrt{4000}$$

Modulus values are based in the design concrete strengths for the deck and girders and are calculated according to AASHTO (1996) Section 8.7.1.

$$\text{Coefficient of thermal expansion (in/in/degree F)} \quad \alpha := 6 \cdot 10^{-6}$$

Coefficient of thermal expansion selected in accordance with AASHTO (1998).

AASHTO Positive Gradient

$$T_{\text{pos}}(y) := \begin{cases} \frac{5 \cdot (8 - y)}{8} & \text{if } 0 \leq y \leq 8 \\ \frac{4 \cdot (y - 8)}{27.5} & \text{if } 8 \leq y \leq 35.5 \\ 4 + (y - 35.5) & \text{if } 35.5 \leq y \leq 43.5 \\ 12 + 34 \cdot \frac{(y - 43.5)}{4} & \text{otherwise} \end{cases}$$

AASHTO Negative Gradient

$$T_{\text{neg}}(y) := \begin{cases} -10 + 4 \cdot \frac{(y)}{4} & \text{if } 0 \leq y \leq 4 \\ -6 + 4 \cdot \frac{(y - 4)}{8} & \text{if } 4 \leq y \leq 12 \\ -2 + 2 \cdot \frac{(y - 12)}{9.375} & \text{if } 12 \leq y \leq 21.375 \\ 0 & \text{if } 21.375 \leq y \leq 26.125 \\ 2 \cdot \frac{(26.125 - y)}{9.375} & \text{if } 26.125 \leq y \leq 35.5 \\ -2 + 4 \cdot \frac{(35.5 - y)}{8} & \text{if } 35.5 \leq y \leq 43.5 \\ -6 + 17 \cdot \frac{(43.5 - y)}{4} & \text{if } 43.5 \leq y \leq 47.5 \end{cases}$$

Define the thermal stresses - fully restrained

Thermal Stresses due to positive gradient, fully restrained (psi)

$$\sigma_{\text{pos}}(y) := \begin{cases} -(E_g \cdot \alpha \cdot T_{\text{pos}}(y)) & \text{if } y \leq 39 \\ -(E_d \cdot \alpha \cdot T_{\text{pos}}(y)) & \text{otherwise} \end{cases}$$

Thermal Stresses due to negative gradient, fully restrained (psi)

$$\sigma_{\text{neg}}(y) := \begin{cases} -(E_g \cdot \alpha \cdot T_{\text{neg}}(y)) & \text{if } y \leq 39 \\ -(E_d \cdot \alpha \cdot T_{\text{neg}}(y)) & \text{otherwise} \end{cases}$$

Define the thermal stresses-unrestrained

Center of gravity of the composite section (deck and girders, measured from the bottom of the girder. (in)  $ycg := cb$

Values for resultant force and moment are from the simplified approach outlined in Section 8.4

Resultant force for positive gradient (lb)	$P_{pos} := 345030$
Resultant force for negative gradient (lb)	$P_{neg} := -191115$
Resultant moment for positive gradient (lb-in)	$M_{pos} := -3076440$
Resultant moment for negative gradient (lb-in)	$M_{neg} := 952320$

Thermal Stresses due to positive gradient, unrestrained (psi)

$$\sigma_{posf}(y) := \sigma_{pos}(y) + \frac{P_{pos}}{A_{reagd}} + M_{pos} \cdot \frac{(ycg - y)}{I_{gd}}$$

Thermal Stresses due to negative gradient, unrestrained (psi)

$$\sigma_{negf}(y) := \sigma_{neg}(y) + \frac{P_{neg}}{A_{reagd}} + M_{neg} \cdot \frac{(ycg - y)}{I_{gd}}$$

**Combination of Girder Stresses**

Combination of loads and positive thermal gradient, fully restrained (psi)

$$\sigma_1(y) := \sigma(y) \cdot 1000 + \sigma_{pos}(y)$$

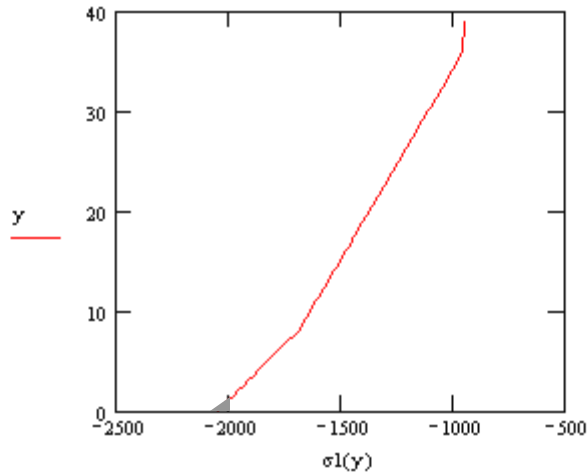


**Figure I.3 Stresses Due to Loading and Positive Thermal Gradient, Fully Restrained**

Combination of loads and positive thermal gradient, unrestrained (psi)

$$\sigma_2(y) := \sigma(y) \cdot 1000 + \sigma_{posf}(y)$$

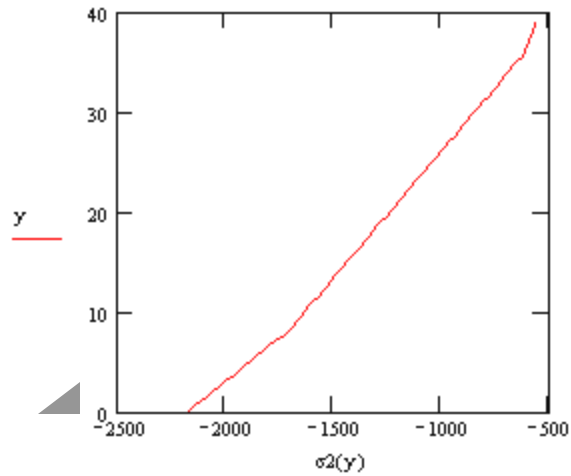


**Figure I.4 Stresses Due to Loading and Positive Thermal Gradient, Unrestrained**

 Exceeds allowable

Combination of loads and negative thermal gradient, fully restrained (psi)

$$\sigma_3(y) := \sigma(y) \cdot 1000 + \sigma_{neg}(y)$$

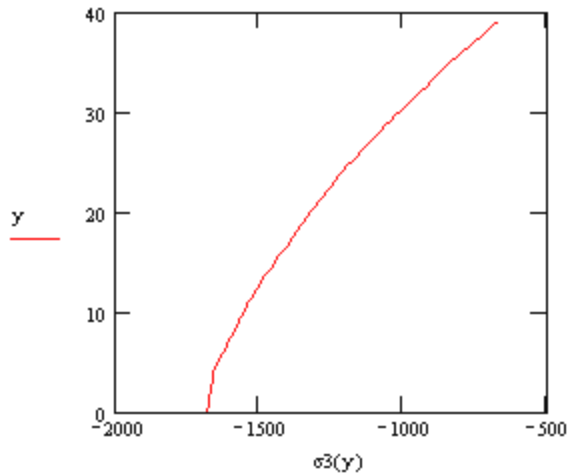


**Figure I.5 Stresses Due to Loading and Negative Thermal Gradient, Fully Restrained**

Combination of loads and negative thermal gradient, unrestrained (psi)

$$\sigma_4(y) := \sigma(y) \cdot 1000 + \sigma_{neg}(y)$$

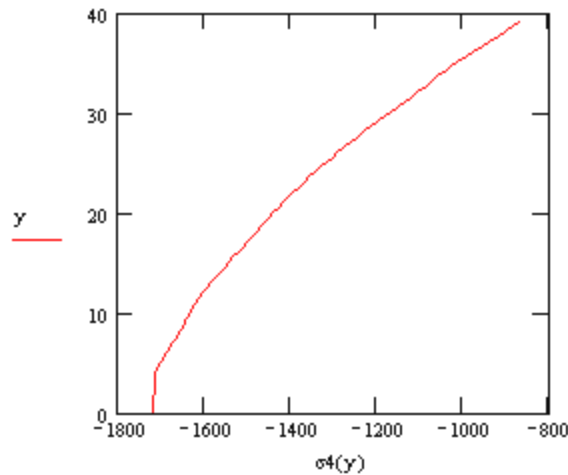


**Figure I.6 Stresses Due to Loading and Negative Thermal Gradient, Unrestrained**

It may be noted that the solid portions of the stress distributions illustrate the regions where the allowable stresses are exceeded. The region where the allowable stress is exceeded is near the bottom of the girder; the allowable compressive stress is exceeded. It may also be noted that a compressive stress in excess of the allowable compressive stress is not a guarantee that cracking will occur.

**I.3 DISCUSSION OF RESULTS**

Additional stress calculations were made at varying points along the length of the span-2 girders. This was done to gain a better understanding of the stress distribution along the length of the girders. Table I.1 outlines the allowable concrete stresses used for the design example. Tables I.2 through I.5 summarize the stresses at the top and bottom of the girder for the conditions of positive live load moment, negative live load moment, and zero live load moment, at the various locations. Tables I.2 and I.3 illustrate the results for the positive gradient in the fully restrained and unrestrained conditions, respectively. Tables I.4 and I.5 illustrate the results for the

negative gradient in the fully restrained and unrestrained conditions, respectively. It may be noted that the shaded cells in Tables I.2 through I.5 indicate that the value exceeds the allowable stress. The nomenclature “f.o.d.” stands for “face of the diaphragm.”

**Table I.1 Allowable Stress Values for Design Example**

Compression	Tension
2000 psi	-424 psi

Note: 1 psi = 6.89 kPa

**Table I.2 Girder Stresses Positive Gradient – Fully Restrained**

		+LL (psi)	-LL (psi)	No LL (psi)
f.o.d.	top	-1064	-940.6	-1042
	bottom	-1187	-2042	-1339
.1*L	top	-1502	-1402	-1479
	bottom	-746.9	-1439	-901.6
.2*L	top	-1816	-1688	-1754
	bottom	-172.8	-1060	-600.5
.3*L	top	-1931	-1783	-1838
	bottom	175.7	-853.7	-472.0

Note: 1 psi = 6.89 kPa, 1 in. = 25.4 mm

**Table I.3 Girder Stresses Positive Gradient – Unrestrained**

		+LL (psi)	-LL (psi)	No LL (psi)
f.o.d.	top	-683.1	-559.5	-661.2
	bottom	-1315	-2170	-1466
.1*L	top	-1121	-1020	-1098
	bottom	-874.4	-1567	-1029
.2*L	top	-1435	-1307	-1373
	bottom	-300.3	-1188	-728.0
.3*L	top	-1550	-1401	-1457
	bottom	48.2	-981.1	-599.5

Note: 1 psi = 6.89 kPa, 1 in. = 25.4 mm

**Table I.4 Girder Stresses Negative Gradient – Fully Restrained**

		+LL (psi)	-LL (psi)	No LL (psi)
f.o.d.	top	-792.2	-668.5	-770.3

	bottom	-824.6	-1679	-976.1
.1*L	top	-1230	-1129	-1207
	bottom	-384.2	-1076	-538.8
.2*L	top	-1544	-1416	-1482
	bottom	190.0	-697.3	-237.7
.3*L	top	-1659	-1510	-1566
	bottom	538.4	-490.9	-109.2

Note: 1 psi = 6.89 kPa, 1 in. = 25.4 mm

**Table I.5 Girder Stresses Negative Gradient – Unrestrained**

		+LL (psi)	-LL (psi)	No LL (psi)
f.o.d.	top	-987.6	-863.9	-965.7
	bottom	-862.6	-1717	-1014
.1*L	top	-1425	-1325	-1403
	bottom	-422.1	-1114	-576.8
.2*L	top	-1740	-1611	-1678
	bottom	152.0	-735.3	-275.7
.3*L	top	-1855	-1706	-1761
	bottom	500.4	-528.9	-147.2

Note: 1 psi = 6.89 kPa, 1 in. = 25.4 mm

The results of the girder stress analyses indicate that there are four locations of the eight investigated where the allowable stresses are exceeded in span 2 of the bridge. Based on these results, the conclusion was made that the design parameters used are insufficient for this bridge structure. While exceedance of the allowable tensile stresses can be accommodated through the use of additional tensile reinforcement or a modification in the tensile reinforcement layout, the exceedance of the allowable compressive stress may warrant a change in the girder type or an increase in the concrete strength. With magnitudes of 0.3 to 1.3 times the stresses due to dead load, live load and prestressing, clearly, thermal stresses must be considered in the design process to avoid an overstress within the member.

**appendix J**

J. MYERS, A. NANNI, AND D. STONE

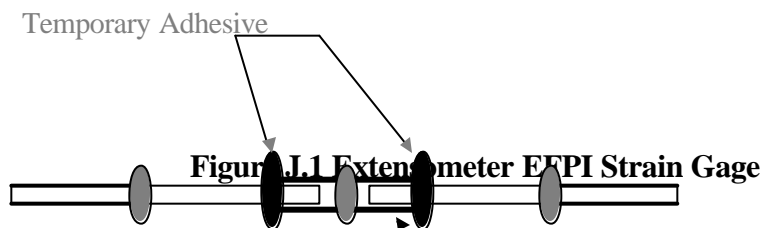
**SUGGESTED BRIDGE MONITORING**

It is clear from the measurements taken at Bridges A4565 and A5736 that the thermal gradients experienced by Missouri bridges have the potential to cause differential upward deflections on the order of 0.30 in (7.62 mm). Furthermore, the thermal stress analyses performed indicate that thermal stresses developed in Missouri bridges are on the order of 0.3 to 1.3 times the stresses developed due to dead load, live load and prestressing. These observations illustrate the potential the thermal gradients have for causing cracking like that experienced by many Missouri bridge structures. To verify the strains experienced due to these thermal stresses, it is proposed that a more in-depth monitoring of the cracked bridge, A4565, be performed. The existence of cracks in the bridge girders and the environmental exposure required for long-term monitoring presents an instrumentation challenge. A pilot study has been performed to validate a potential strain-monitoring instrument.

The extensometer EFPI strain gage, a fiber optic sensor, produced by Luna Innovations was the instrument selected for potential use. The advantages of using the fiber optic gage can be outlined as follows:

- Minimal structural intrusion is necessary for gage application. Only a small groove in the member is necessary for application of the gage. In this application, the groove would be made in a location where the concrete is not contributing to the structure performance of the member, due to the existence of cracks.
- The small size of the gage makes it easy to conceal in a field application where vandalism is often a concern.
- The fiber optic gages have excellent fatigue characteristics. Fatigue of the instrument is a concern for long-term monitoring of bridges due to the nature of loading.

These characteristics lead to selection of this gage. See Figure J.1 for a schematic of a gage.



The strain gage is applied to the member with a permanent adhesive at three locations as outlined in Figure J.1. Once the permanent adhesive has cured the gage is heated to approximately 212°F (100°C) for 2 minutes. This heating will evaporate the temporary adhesive, making the gage capable of sustaining a large amount of deformation. Extreme care is necessary to apply the permanent adhesive to the proper locations. If the permanent adhesive were to be applied at the interface of the fiber and the capillary tube then the gage would not function properly. Figure J.2 displays a picture of the fiber optic gage. The locations of permanent adhesive application are also illustrated in Figure J.2. The relative size of the gage is illustrated to scale with the tip of a pen.

In order to validate the strains read from the fiber optic gage, a more traditional strain measure device (LVDT) was used for comparison.

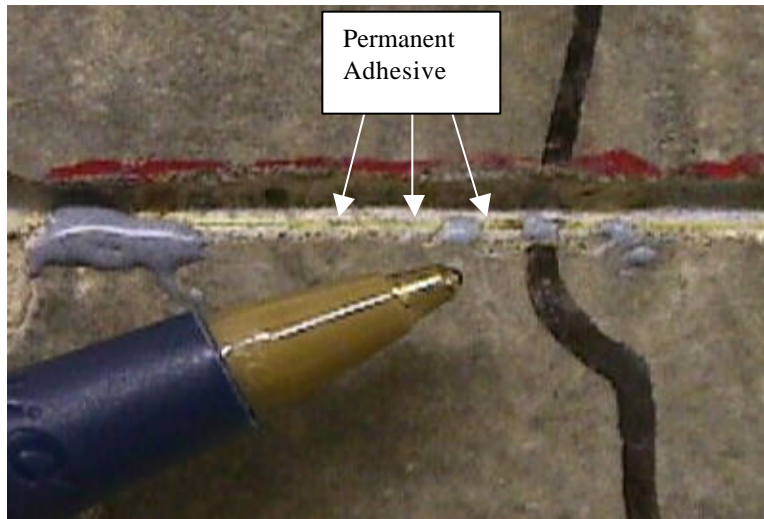


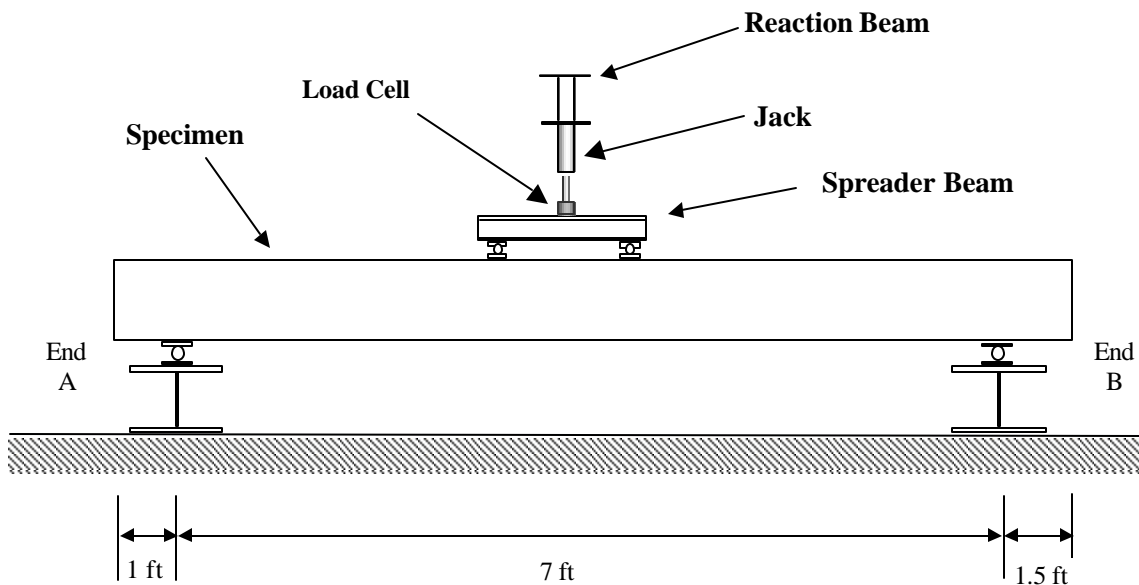
**Figure J.2 Close-up of the Fiber Optic Gage**

The test setup is illustrated in Figure J.3. The member tested was a previously tested prestressed beam of dimensions 6 in. by 12 in. (152.4 mm x 304.8 mm), with a length of approximately 9.5 feet (2.9 meters). Loading was accomplished through the use of a 30-ton (267-kN) jack that was centered 5 feet (1.52 meters) from end “B” of the beam; this was also the location of the monitored crack. The load was applied using four-point loading, with the use of a 2-ft (0.61-m) spreader beam.

The load was applied incrementally and in cycles; so that the behavior of the beam could be monitored as the load increased and the repeatability of the measurements could be verified. Each load increment was 2000 lbs. (8.9 kN), with the cycles outlined as follows:

- Cycle 1 – the member was loaded up to 8000 lb. (35.6 kN) and then unloaded to 2000 lb. (8.9 kN)
- Cycle 2 – the member was loaded up to 20,000 lb. (89 kN) and then unloaded to 10,000 lb. (44.5 kN)
- Cycle 3 – the member was loaded up to 20,000 lb. (89 kN) again and then unloaded completely.

The results of the two deflection measurements can be seen in Figure J.4.



Note: 1 ft. = 0.3048 m

### Figure J.3 Test Setup

The measurements by the fiber optic gage are in good agreement with the readings from the LVDT. The readings from the LVDT are slightly higher than those from the fiber optic gage due to the longer gage length of the LVDT as compared to that of the fiber optic gage. The gage lengths were 4.69 in. (119.1 mm) and 0.21 in. (5.416 mm), respectively. The value of the strains were not compared directly because the LVDT brackets were attached to the beam using an adhesive, rather than a bolt, causing the actual gage length to be unknown. The gage length cited previously is the edge-to-edge distance of the two brackets, however the actual gage length would be somewhere between the distance from one inside edge to the other and the distance from one outside edge to the other.

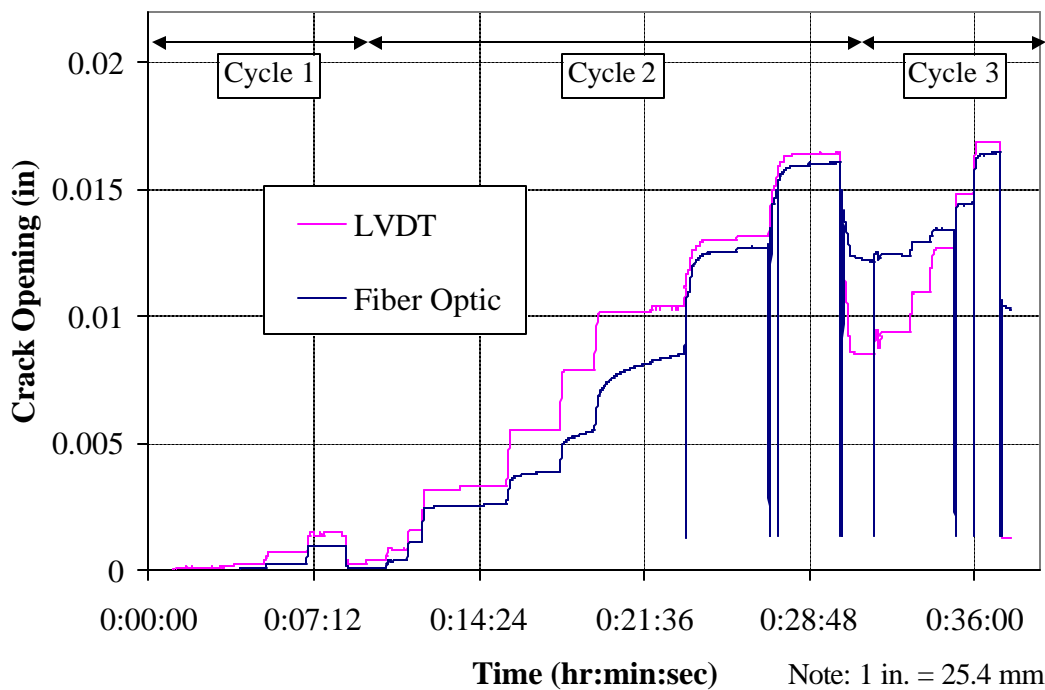


**Figure J.4 Crack Opening Versus Time**

The limitations of this fiber optic gage are its size and the precision with which the permanent adhesive must be applied. Prior to installation the gage is very sensitive and must be handled with care due to the relatively low strength of the temporary adhesive. Also, during installation the permanent adhesive must be applied in very small quantity and at exactly the correct location. These two issues in combination limit the feasibility of effective gage use in some situations. Installation is a significant criterion for use on an existing bridge structure.

Further research is proposed to investigate the alternate use of a fiber optic gage that does not involve the use of temporary adhesive. While this type of gage would have a smaller allowable strain, a suitable gage length can be selected to accommodate for the anticipated strains. The stability of the gage prior to and during application, and the easier application procedure would likely be the controlling factors.

If fiber optic strain gages are selected for long-term monitoring at a bridge, it is recommended that a temperature-measuring device, such as a thermocouple, be integrated into the monitoring program. This would allow for a correlation between the thermal gradient and the measured strain experienced by the bridge girders. A better understanding of the thermal effects and behavior of the members would also result.

